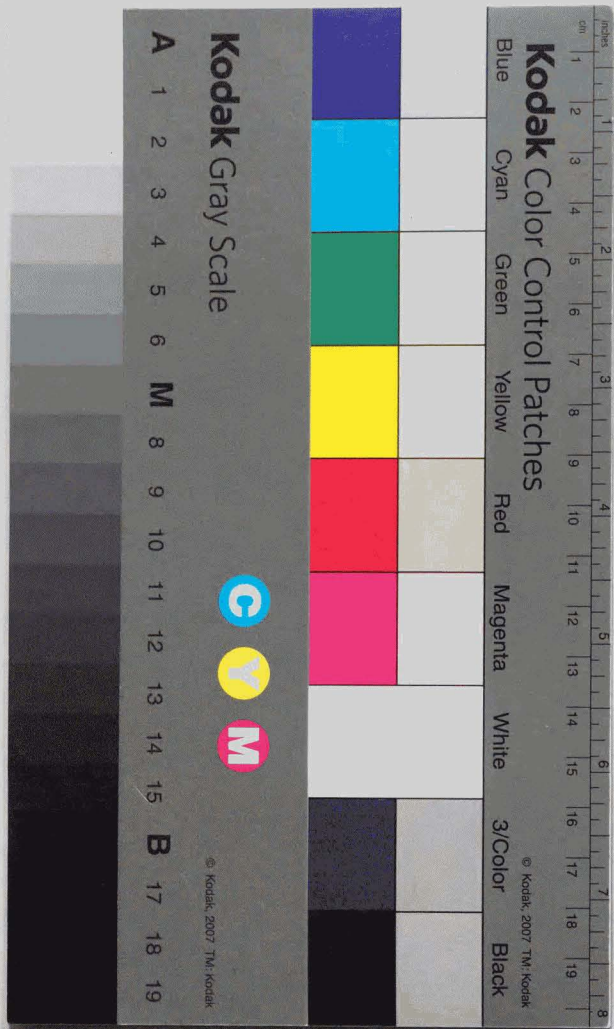DEVELOPMENT AND PRACTICAL APPLICATION OF

PRE-COATED PARALLEL WIRE CABLE

FOR LARGE CABLE-SUPPORTED STRUCTURES

（大規模用構造用被覆平行線ケーブルの開発と実用化に関する研究）

June 1998

TETSUO HOJO

DEVELOPMENT AND PRACTICAL APPLICATION OF

PRE-COATED PARALLEL WIRE CABLE

FOR LARGE CABLE-SUPPORTED STRUCTURES

June   1996

TETSUO   HOJO

ABSTRACT

A remarkable progress has been seen in recent years around the world in the construction of cable—stayed bridges, as well as in suspension bridges. As longer cable—stayed bridges have come to be constructed, the multiple—cable system with mono—strand cables has become popular. Stay cables of such long cable—stayed bridges are required to possess excellent mechanical properties, such as a high static and high fatigue strength, and a superior corrosion protective coat. There were few cables in the past which satisfied those requirements, therefore it was necessary to do a study on them.

This thesis describes the study on the development of a new—type cable for long cable—stayed bridges, and application subjects for large cable—supported structures. Details of the studies are presented respectively.

A slight twist of the wires given to the cable made it possible to coat it with a corrosion protective layer in the manufacturing process and to improve handleability such as installation at the site without damaging the structural performance. It was indicated that the pre—coated parallel wire cable had the same static characteristics (such as the breaking strength and modulus of elasticity) as those of a parallel wire strand, when the twisting angle of a cable was less than 3.5°. It was also shown that the twisting angle had little effect on the time dependent characteristics (such as creep and relaxation) when the twisting angle of a cable was less than 3.5°. Finally, the tensile test was carried out by using full—size cable models and it was confirmed that a pre—coated parallel wire cable with a breaking load of a 3,000 tonf (29,400 kN) class could be put into practical use.

A new fatigue resistant socket having a composite—filler consisting of an epoxy resin and a zinc—copper alloy was developed in order to improve the fatigue strength of a socket. It was confirmed that the socket had a higher fatigue strength of about 25 kgf/mm^2 (245 MPa). It was indicated that the twisting angle had little effect on the fatigue strength of the socket when the twisting angle of a cable was less than 3.5°. Experimental results and analysis indicated that the pre—coated parallel wire cable with the sockets had a bending fatigue strength of about 0.6° and the socket using epoxy resin also had an effect on decreasing the secondary stress at the entrance of a socket. A new method in socket design for a large cable, introducing the concept of rigidity for ultimate strength, was examined.

(1)

As a new protection system against corrosion, an extruded polyethylene coating for a parallel wire cable was developed, which eliminated the need for corrosion protective coating work at the site. A high—density polyethylene was selected as the optimum protective coating material. According to the accelerated weathering test results, it was confirmed that the polyethylene showed no deterioration when 1% carbon black was added. The properties of a polyethylene coated cable were analyzed, and installation characteristics of the cable such as unreeling and clamping were examined using full—size cable models. It was indicated that this protection system was a great advantage in the erection of stay cables of cable—stayed bridges, especially long ones.

In addition to fundamental development, the cable that could be applied to any cable—supported structures was also required to have a higher performance. One of the application subjects was to make the cable colored and durable. The other was to develop aerodynamic measures against cable vibration to lengthen cable—stayed bridge spans. Details of the investigations with respect to these subjects and the results obtained by the study (a fluoropolymer—coated colored cable and a low drag aerodynamically stable cable with an indented pattern), were presented.

A colored cable using a fluoropolymer having outstanding weathering durability was developed. The material properties of the fluoropolymer, especially the weathering durability, were evaluated by using various exposure test methods. It became obvious that the fluoropolymer had excellent weathering durability, which could be estimated to last for more than 100 years if the thickness were 1 mm or more. Structural characteristics of the fluoropolymer—covered cable were examined, and it was indicated that the cable had the same installation properties as those of a polyethylene—coated cable. These characteristics of the fluoropolymer showed that it could be used for various structures and elongated service life and added aesthetic aspects. As a result, a greater freedom of color selection was given to bridge cables that matched the surrounding environment. Finally, it was shown that the colored cable was applied not only to stay cables of long cable—stayed bridges but also to hangers of long suspension bridges.

The vibration problems of a stay cable were surveyed and experimental studies on cable vibration and its suppressing method for a long cable—stayed bridge were discussed. After

examining the aerodynamic characteristics of a cable with a patterned roughness, using wind tunnel tests, a new aerodynamical cable having both a low drag force and a suppression effect on rain vibration was developed. It was found that it had the same drag coefficient of about 0.6 as that of a cable with a smooth surface in any design wind velocity range. It was also found that a cable with a surface roughness had a vibration suppressing effect when the relative surface roughness of 1% of the cable diameter was given discretely on the surface. Suppression effects were analyzed by measurement of the drag coefficient and pressure distribution, indicating that cables with a lumped pattern roughness made it possible to reproduce a supercritical state at a low wind velocity range where rain vibrations occurred. To understand further the aerodynamic characteristics of the surface configuration of the cable, various patterned roughnesses were examined in terms of the Reynolds Numbers. It was found that density and arrangement of lumped roughness were the key factors in controlling the drag characteristics of cables, and that optimization of the drag coefficient—Reynolds number relationship could enable adjusting those two factors.

Responses of stay cables by vortex—induced vibration in natural wind were measured at an actual cable—stayed bridge with a main span of 490 m. The factors affecting this vibration, such as surface roughness and structural damping, were examined by using a wind tunnel test and analysis. It was shown that the response amplitude was estimated at various damping levels, and that the bending angle of a cable, caused by vortex—induced vibration, to be less than 0.1°, which had little effect on the secondary stress and bending fatigue strength of cables.

Cable materials in the future for a super—long cable supported bridge were described. It was shown that the development of cable material was inevitable in order to lengthen a bridge span of a super—long suspension bridge. The present status of cable materials including steel wires and various new materials was surveyed and future problems to overcome were pointed out. As a future prospect, a high strength steel material and a light weight material such as carbon fiber were shown to be possible for use in super—long cable supported bridges.

In conclusion, several ideas for the new—type cable discussed here helped in the lengthening cable—stayed bridge spans, and contributed a great deal to the advancement of cable—supported structures.

CONTENTS

LIST OF TABLES

LIST OF FIGURES

NOTATION

CHAPTERS　1 ～ 5

a	: average internal radius of wire
a, a_i	: twisting angle of wires
A	: effective contact area of zinc$-$copper alloy cone
A_c	: cross sectional area of cable
b	: average external radius of wire
B	: bond strength of alloy
$\varDelta_c$	: creep of cable
d	: diameter of wire
d	: rate of decrease in breaking strength
D_m	: mean diameter of zinc$-$copper alloy cone
$\varDelta D_m$	: change in mean diameter of the zinc$-$copper alloy cone
E	: modulus of elasticity
E_c	: modulus of elasticity of cable
J	: rotational torque
l	: required socket length
L	: cable length
L_c	: supported span length of cable
$\varDelta l_c$	: total elongation of cable
$\varDelta L_e$	: elastic elongation of cable
n_i	: number of wires whose twisting angle is a_i
N	: total number of wires
P	: tension of cable
R	: radius of curvature of wire
R_e	: radius of curvature at epoxy$-$zinc boundary
R_0	: radius of curvature at entrance of socket
$\varDelta R_m$	: change in mean diameter of the socket
$\varDelta_s$	: slippage from both sockets
$\varDelta_{s0}$	: initial slippage from socket
t	: tensile strength of wire
t_m	: mean wall thickness of socket
T	: tensile load of cable
$\varDelta Z$	: slippage of socket metal

R_i : twisting radius of wires

α : relaxation coefficient

α_c : relaxation coefficient of cable

β : creep coefficient

β_c : creep coefficient of cable

δ : space between wires

δ_c : vertical displacement at center of cable

θ : taper angle of socket wall

θ_b : bending angle

ε_c : strain of cable

ε_{c0} : initial strain of cable

ε_e : elastic strain of cable

ε_e' : plastic strain of cable

ε_{e0} : initial elastic strain of cable

ρ : friction angle between socket and alloy cast

σ : stress range

σ_a : allowable stress of socket cone

σ_b : secondary stress

σ_c : stress of cable

σ_m : mean stress of wire

σ_r : radial stress of socket

σ_t : axial stress of cable

σ_u : ultimate strength of wire

σ_z : stress in axial direction of socket

σ_θ : hoop stress of socket

σ_M : internal pressure of socket metal

σ_0 : initial stress of cable

$\varDelta\sigma$: fatigue strength of socket

χ : parameter controlling time dependent property

CHAPTERS 6 ～ 7

A : amplitude of cable vibration

B : width of body

C_d : drag coefficient

C_l : dynamic lift coefficient

C_p : non−dimensional pressure coefficient

D : cable diameter

f_n : natural frequency of cable

L : cable length

m : cable mass per unit length

P_c : consumed energy

P_D : drag force

P_w : input energy

R_e : Reynolds number

S : Strouhal Number

Sc : Scruton Number

u(t) : velocity fluctuation function

U : mean wind velocity

U(t) : wind velocity function

V : wind velocity

V_f : reduced wind velocity

w : unit weight of cable

Y : double amplitude of cable

β : yawing angle of cable

δ : logarithmic decrement of cable

θ : inclined angle of cable

μ : viscosity coefficient

ρ : air density

ν : kinematic viscosity

ω : natural circular frequency

CHAPTER 1 INTRODUCTION

1.1 Progress in Cables of Cable Supported Bridges

Structural members such as cable materials have been used for many bridges for a long time. The Brooklyn Bridge, constructed in 1883, was the first modern suspension bridge to adopt steel wires in its main cables [1]. Since then, the use of parallel steel wires in the main cables of suspension bridges has become common. The tensile strength of the steel wires used in cables has not been improved for more than a half century, remaining at 155–160 kgf/mm ^{2} (1,520–1,569 MPa), since the George Washington Bridge was built in 1931. Size of wires for many suspension bridges were 5 mm in diameter in this half century around the world. The Humber Bridge, constructed in 1981, which has the largest main span of 1410 m at present as shown in Table 1.1, is also one of example. In Japan, steel wires with a tensile strength of 160 kgf/mm ^{2} (1,569 MPa) were used for suspension bridges constructed until completion of the Minami Bisan–Seto Bridge, having a main span of 1100 m, in 1988 [2]. Progress in tensile strength of bridge wire is shown in Fig.1.1.

As the spans increase, the dead load acting on the suspension structure rises. Improved material strength is an effective way to reduce the effect of these rising dead loads, and in this respect the development of cable materials with super–high tensile strength would be a great advantage. For the Akashi Kaikyo Bridge, having a main span of 1990 m, the initial design called for a double–cable system under use of galvanized steel wires of 160 kgf/mm ^{2} [3]. Major efforts have been devoted to the development of super–high strength steel wires, and 180 kgf/mm ^{2} (1,765 MPa) wires allowing for a single–cable system and a consequent structural simplification have been developed [4]. Finally, 180 kgf/mm ^{2} wires were adopted for the main cables of the Akashi Kaikyo Bridge, and it is scheduled to be completed in 1998 [5]. Thus the improvement of cable strength mainly has contributed to elongating the span of suspension bridges.

On the other hand, the history of modern cable–stayed bridges began in the middle of the 1950's. It is comparatively new to the history of the suspension bridges. The Strömsund Bridge was the first modern cable–stayed bridge, constructed in 1956. The Theodor Heuss Bridge was constructed in 1957, with a main span of 280 m, that initiated an impressive development of this type of bridge. Various cable–stayed bridges were built mainly in Germany from the 1960's to the 1970's. Since then, because of economic and aesthetic reasons, cable–stayed bridges have become the most popular bridge type now being

constructed all over the world [6,7,8]. This bridge type varies from short span to long span on the order of 1000 m, which is the range of suspension bridges. Table 1.2 shows the list of long cable—stayed bridges. The improved techniques of structural analysis using computers were greatly effective in lengthening bridge span, and among technical design factors the cables play the most important role in very long cable—stayed bridges.

The cables for steel cable—stayed bridges used to be mostly locked coil ropes. Spiral ropes were adopted in a few cable—stayed bridges. In Japan, like the Katsuse Bridge erected in 1960, mostly locked coil ropes were applied for cable—stayed bridges in the early years [9]. In 1970, shop—fabricated parallel wire strands were used for the Toyosato Bridge, since then the use of parallel wire strands has become common in Japan [10]. As for prestressed concrete cable—stayed bridges, prestressing steel members such as steel wires, steel strands, and steel bars were basically used. Some prestressed concrete cable—stayed bridges adopted locked coil ropes and parallel wire strands.

The selection of a cable type is closely dependent on the design and erection of the cable—stayed bridge. In the design of a cable—stayed bridge, it is considered that a girder be elastically supported by stay cables where they are fixed. In the early days of cable—stayed bridges, the cable supporting interval was considerably long, being 30 to 50m or more. This system required both a large girder section due to a large bending moment between the supporting points and a large cable section consisting of several small—sized ropes. It was also necessary to have a separate anchorage for each rope, which required a large and complicated structure inside the girder to splay and fix them. As spans of cable—stayed bridges increased, these disadvantages had become greater, especially in the fixing procedure of many ropes to the girder. These problems could be solved by adopting a multiple—cable system with mono—strand cables, because it has the following advantages;

a) Girder sections can be designed smaller as supporting intervals become shorter.

b) A mono—strand cable needs no splay saddles, so, anchorage structure can be simplified.

c) Erecting procedure becomes more efficient and economical, because a stay cable also serves as a temporary erection cable.

d) Assembling and corrosion—protecting work at the site can be eliminated if a cable itself has a corrosion protective layer.

Recently, reflecting on the increase in the scale of cable—stayed bridges, the multiple—cable system with mono—strand cables has come to be widely applied around the world for functional reasons such as advantages in economical design, ease of handling at the site, as well as aesthetic reasons [11]. In Japan, all of the recent long cable—stayed bridges adopted this system using the newly developed cable, that is, the pre—coated parallel wire

cable [12]. Fig.1.2 shows the historical change in cables of cable—stayed bridge. The comparison between the two systems is shown in Fig.1.3. The Tatara Bridge, the largest cable—stayed bridge in the world having a main span of 890 m, is now under construction and it is scheduled to be completed in 1999 [13]. The development of new—type cables makes an essential contribution to the advancement of cable—stayed bridges.

1.2 Cable Types of Cable—Stayed Bridges

The stay cables are one of the most important materials of a cable—stayed bridge. In most cases, spiral ropes, locked coil ropes, parallel wire strands and helical wire strands are used for stay cables of cable—stayed bridges. They consist of cylindrically shaped steel wires with a diameter approximately 5 to 7 mm. A 7 mm diameter wire typically is used in parallel wire strands for the stay cables of cable—stayed bridges, while a 5 mm diameter wire is used in the main cables of suspension bridges. Structural characteristics required for the stay cables are as follows [14]; a) High load bearing capacity, b) High and stable modulus of elasticity, c) High fatigue resistance, d) Compact cross—section, e) Ease in corrosion protection, and f) Ease in handling and installation.

The typical types of cables for cable—stayed bridges are shown Fig.1.4 as regard to these characteristics.

A spiral rope has some disadvantages as a stay cable. When the wires of spiral rope are helically stranded, elongation due to the compactness of the strand takes place under the loading. For this reason, the modulus of elasticity of a spiral rope becomes unstable. To eliminate this effect, prestretchings have to be given before it is used. About a half of the breaking strength is generally used for the prestretching load and the loading has to be kept for more than thirty minutes, in a few times [15]. When large sections are required, several spiral ropes are to be bundled into a round or a square shape at the site. A spiral rope, 137mm in diameter, is the largest one ever used for cable—stayed bridges, having a breaking strength of about 1,000 tonf (9,800 kN) [16]. All wires are galvanized for protection against corrosion. It is flexible enough because of the helix. Therefore, there is ease in handling and in installation.

As for a locked coil rope, the lay structure of wires is quite the same as that of a spiral rope except the outer layer consists of wedged shape wires such as a Z—shape. A locked coil rope has the same modulus of elasticity as a spiral rope, and prestretching is also required [15]. As the Z—shaped wires are stranded tightly together, the surface of a locked coil rope

is smooth. Consequently, a locked coil rope has not only the structural advantage that can bear high side pressure at saddles but also a corrosion protection that can be painted easily compared with that of a spiral rope. The largest locked coil rope ever used for cable—stayed bridge is 167 mm in diameter [17]. Concerning handling and installation, it is less flexible than a spiral rope.

The wires of a parallel wire strand are arranged parallel to the cable axis. Accordingly, a parallel wire strand has the same modulus of elasticity and breaking strength as a single galvanized wire. This is an important advantage in designing a cable—stayed bridge. A parallel wire strand is usually fabricated in a regular hexagonal shape with nearly one hundred galvanized wires of 5 mm in diameter, for example 127 wires [18]. When a large section is required, multiple numbers of parallel wire strands are bundled into a cable, and then corrosion—protective work is performed by attaching a plastic covering [19]. Corrosion—protective work at the site causes some inconvenience for a stay cable of cable—stayed bridge.

A parallel wire cable or a parallel strand cable is used for many cable—stayed bridges [20]. Prestressing wire originally has been used for prestressed concrete and consists of bare steel wires of 7mm in diameter or that of seven—wire strands. Their static characteristics are almost the same as a parallel wire strand, but they have considerably larger cross section. They are always covered by a polyethylene tube or a steel pipe for corrosion protection. Cement mortar is usually grouted into the space between the strands and tube or pipe, after all cables are erected. Quality control such as grouting work has to be done under severe scrutiny during the installation at the site. The largest parallel wire cable with a polyethylene tube ever used for cable—stayed bridge consists of 499 wires of 7 mm in diameter [9].

1.3 Problems to Be Discussed

1.3.1 A large—sized fabricated cable

In the early days of cable—stayed bridges, cable systems with relatively few heavy stay cables were usually used. In the few—cable system, a stay cable had to be composed of several ropes or strands. For example, one stay cable of the Theodor Heuss Bridge consisted of 13 locked coil ropes, and of the Toyosato Bridge, 16 parallel wire strands. The few—cable system required a large and complicated anchorage structure to fix an individual rope or strand. And the use of heavy, concentrated stay cables required a local strengthening of the girder. It was also necessary to adjust the tension of each rope or strand during the

anchoring procedure, which was laborious work. Besides all this, several strands had to be assembled into one stay cable after all cables were installed in order to apply corrosion—protection at the site, using temporary scaffolding, like a catwalk.

As longer cable—stayed bridges have come to be constructed in recent years, the multi—cable system has become popular. In the multi—cable system, it is preferable that each stay cable consists of a single prefabricated strand, that is, a mono—strand cable. In the design of a long cable—stayed bridge of multi—cable type with mono—strand cables, a mono—cable is required to possess a breaking strength of more than 2,000 tonf (19,600 kN). In terms of cable length, the cable length should be about 500 m when a cable—stayed bridge has a main span of 1,000 m. For example, the largest cable of the Tatara Bridge was designed to have a breaking strength of 2,400 tonf (23,500 kN) and a length of 465 m.

Requirements for mono—strand cables of a multi—cable system of a long cable—stayed bridge are indicated as follows;

a) It should have a high breaking strength of more than 2,000 tonf (19,600 kN), which is about 3 times higher than that of a conventional rope or strand, such as a locked coil rope or a parallel wire strand.

b) It should have a high and stable modulus of elasticity, consequently, a cable composed of parallel wire is desirable.

c) It should be prefabricated, including a corrosion—protection layer to eliminate corrosion protecting work at the site.

However, the conventional ropes or strands have the following problems to be applied to mono—strand cables of a multi—cable system.

As for helically stranded ropes such as a spiral rope and a locked coil rope, they also have fundamental problem, that is, necessity of prestretching [15]. Even if ignoring it, they would not be applied to a stay cable of a long cable—stayed bridge because of low modulus of elasticity. In the design of a cable—stayed bridge, the stiffness of the bridge is greatly influenced by the modulus of elasticity of a cable as the span increases. Fig.1.5 shows the comparison of the modulus of elasticity related to the cable length between a parallel and a helical strand obtained using Ernst's equation. The figure shows that a higher modulus of elasticity is preferable for a stay cable of a long cable—stayed bridge. This is another reason that helically stranded ropes are undesirable for the long cable—stayed bridges.

A parallel wire strand does not need to be prestretched, but there is another reason that it is not suitable for larger size cables. The individual wires of a parallel wire strand are usually bound by a chemical fibrous tape about 1.5 m apart in length to keep the hexagonal shape.

When it is wound on a reel, it flattens out in order to equalize individual wire lengths in each turn around the reel. The flattening of the strand becomes large enough so as not to be wound on a reel as the number of wires in a strand increases. This property makes it difficult to fabricate a larger size strand. Therefore the standard size of a parallel strand consists of 127 wires and the largest size ever fabricated has been 271 wires of 5 mm in diameter, having a breaking strength of about 800 tonf (7,800 kN).

A parallel wire cable ordinarily has grouted cement mortar layer around the steel cable, that makes a parallel wire cable about 1.2 times heavier than a genuine steel cable having the same breaking strength. When a cable is suspended, the modulus of elasticity of cable decreases due to the sag caused by dead weight. Fig.1.5 shows the comparison related to the cable length between a heavier parallel wire cable with cement mortar and a parallel wire strand consisting of the same number of wires. As shown in Fig.1.5, the modulus of elasticity also suffers a lot from the dead weight of the cable itself in the design of long cable—stayed bridges. Besides, a parallel wire cable has to be twisted once in one turn in order to equalize wire length in each turn while it is wound on a reel, and then twisted off when unreeled at the site. As the length of a cable becomes longer, this additional handling becomes complicated, and in addition, it is undesirable for parallel property of the wire to be kept from the quality control point of view. The maximum size ever used has consisted of 499 wires, having a breaking strength of about 3,000 tonf (29,400 kN), but the length was only 100 m.

A seven—wire strand for prestressing steel members is widely used for cable—stayed bridges [21], which has a breaking strength of about 50 tonf (490 kN) per strand. When a large breaking strength of more than 2,000 tonf (19,600 kN) is required, more than 40 strands are to be bundled into one cable. All strands are adjusted to be the same length one by one at the site by using tensioning equipment. As the length of a cable becomes longer, the adjusting work is apt to be easily affected by wind and temperature. Consequently, a bundled cable consisting of many strands causes concern about the difference in stress among the strands, making it difficult to evaluate the tension of a cable. A fabricated cable has more reliability in this respect.

There were not any conventional ropes or strands that satisfied these requirements, therefore, it was necessary to develop a large—sized fabricated cable having high structural performance.

1.3.2 A cable socket with higher static and fatigue strength

The end terminals of cables are generally anchored by sockets. A socket is designed so as not to decrease the breaking strength of the cable itself. When cables have become larger,

end fittings for larger cables are also required. Under the breaking load of a large cable of more than 2,000 tonf (19,600 kN), the end fitting is about 3 times stronger than that of a parallel wire strand ever used for cable—stayed bridges. But it remains unclear whether the conventional design method for socket guarantees sufficient strength to support a breaking load of a larger cable. So the design method for a large socket has to be examined at the same time in order to realize a large—sized fabricated cable [22].

Stay cables of long cable—stayed bridge are subjected to the fluctuation of the axial stress in cables due to the live load such as vehicles or trains. The fatigue strength of a cable is also determined by the fatigue strength of a socket portion. For this reason, a socket having a higher fatigue strength was absolutely required for stay cables of long cable—stayed bridges.

A zinc—copper alloy cast socket, shown in Fig.1.6, is widely used in Japan, it reduces fatigue strength to less than half that of wires. For example, the fatigue strength of wires for a parallel wire strand having a breaking strength of 160 kgf/mm ^{2} (1,569 MPa) class, is 40—45 kgf/mm ^{2} (392—441 MPa) [1]. When a zinc—copper alloy is cast, the fatigue strength of a cable becomes about 15 kgf/mm ^{2} (147 MPa) [23]. The reduction of fatigue strength is mainly considered to be caused by the heat of the casting metal at the entrance of the socket, requiring a pouring temperature of about 460 ℃. And fretting corrosion occurring between the wires and the cast metal at the entrance of the socket is another reason in decreasing fatigue strength [24,25]. In the case of the socket, these factors have to be eliminated in order to improve fatigue strength.

One solution is to use a cold casting material inside a socket. Cold casting materials composed of epoxy resin, zinc dust and small steel balls are chosen for a higher fatigue socket. It is called a high amplitude (HiAm) socket [26], shown in Fig.1.7. Inside the socket, all wires are provided with button heads through a locking plate at the end of the socket. Some results of fatigue tests have shown that the socket has a fatigue strength of about 25 kgf/mm ^{2} (245 MPa) [27]. This socket is used for various cable—stayed bridges, including concrete ones.

There are some socket types used for post—tensioned concrete cable—stayed bridges [21]. They are anchored by wedges or nuts at the end of the socket strand by strand at the site, and inside the socket epoxy resin or cement mortar is grouted. For example, Freyssinet was used for the Brottone Bridge, Dywidag for the Second Main Bridge, Stronghold for the Luna Bridge, VSL for the Sunshine Skyway Bridge, and SEEE for the Yobuko Bridge. But in the case of the concrete cable—stayed bridges, the dead weight is rather heavier than that of the steel bridges, accordingly the effect of the live load does not need to be taken into account as much as that of the steel bridges. Their fatigue strength is around 15 kgf/mm ^{2} (147

MPa). It is hard to apply these sockets to a fabricated stay cable of long cable—stayed bridges.

Recently, a stay cable of cable—stayed bridges has suffered from bending vibration due to wind [28]. A large amplitude is sometimes observed on a stay cable, which raises a serious problem in the design of a cable, especially a socket. Because this vibration can cause bending fatigue near the cable sockets according to its amplitude, extensive research into the mechanism of vibrations and countermeasures to control the vibrations have been carried out and the effects of such suppressing measures have been observed in some bridges [29]. To judge whether the suppressing measures are required or not, it is desirable to understand the bending fatigue strength of a cable. A few studies have been made concerning the bending fatigue strength of bridge cables. One consisted of bending fatigue tests for helically stranded ropes under the condition of having a buffer device in front of a cable socket [30], and the bending fatigue strength at the socket was not taken into account. Particularly, there are little data concerning an allowable bending fatigue strength of a parallel wire strand, and this important problem has been left unsolved so far. From the above—mentioned point, the bending fatigue strength of a cable related to the bending angle has to be examined.

It was absolutely necessary to develop a new socket having a higher static and fatigue strength for a large cable. And the bending fatigue strength of the socket also had to be examined in order to apply it to long cable—stayed bridges.

1.3.3 Corrosion—protective coat for a large—sized cable

Long cable—stayed bridges require cables with high mechanical properties and excellent corrosion resistance at the same time. They are usually designed to have a longer period of service, for example, more than a period of 100 years. Sometimes the durability of the bridge is greatly influenced by the corrosion protection of the stay cables. According to reports, some stay cables were suffering from corrosion problems. The stay cable of the Köhlbrand Bridge was a typical example [31]. The breaking of wires of locked coil ropes occurred after only 3 years of service, all of them had to be replaced. The reason for a deterioration of stay cables was considered to be caused by a couple of factors, among them the use of ungalvanized wire for a stay cable possibly reduced the durability of the cables.

The fundamental method for protection against corrosion is to galvanize wires [32]. The wires of a helically stranded rope such as a locked coil rope or spiral rope are generally galvanized today. A wire is usually galvanized with a zinc weight of about 300 g/m^2. The surface of a locked coil rope is painted, while a spiral rope depends on only galvanization of individual wires. Corrosion protection by a painting system requires maintenance at short intervals, that is undesirable for a long cable—stayed bridge. Besides, corrosion protection only by galvanization is not considered to be durable enough for a long period, compared with the main cable of a suspension bridge, which has a double corrosion protection system composed of galvanized wires and a wrapping of cable.

The wires used for a parallel wire strand is also galvanized with a zinc weight of about 300 g/m^2. When a parallel wire strand is wound on a drum, it flattens and snakes around the drum. That makes it difficult to apply corrosion protection in a shop. Bundled several parallel wire strands are protected against corrosion by a glass fiber reinforced plastic covering, which is a quite similar to that of the main cable of the Newport Bridge [33]. The plastic covering, shown in Fig.1.8, is performed either by a hand lay—up method or by a prefabricated segment method at the site. Both methods need to be provided with expansion joints on a cable in order to adjust the expanding difference due to change of temperature or live load between a steel cable and the plastic covering. The expansion joint has a disadvantage for corrosion protection because from there water can penetrate the cable, this causes corrosion of cables. Besides, scaffolding is required under all cables in order to install a plastic covering, that is too laborious for cable—stayed bridges of a multi—cable type.

Fig.1.9 shows a corrosion protection system using polyethylene pipe. A pipe made of polyethylene or steel is attached around a parallel wire cable and cement mortar is injected inside the pipe. With this system the wires are generally ungalvanized. This is a similar protective method against corrosion as that used for the prestressed wire of prestressed concrete. A polyethylene pipe can be reeled on a drum, that makes it possible to prefabricate it in a shop, while a steel pipe has to be attached at the site because of its rigidity. For long cable—stayed bridges, a polyethylene pipe is mainly used. As cable length becomes longer, problems related to injection work arise. The injection height depends on the injection material of the cement mortar or the injection pressure. As the height difference for one injection is usually limited to less than 25 m, it requires many injections to complete the corrosion protection work at the site for long stay cables. Stress cracking of polyethylene due to the environment and live load occurs if an excessive hoop stress occurs during the injection procedure. The cracks of polyethylene have been observed in the stay cables of the Luling Bridge [34]. Furthermore, the mortar that is injected may possibly crack off because of a live load or wind induced vibration.

Concerning these problems, a new corrosion—protection system which has the following characteristics is required for a large—sized cable of a multi—cable type;

a) A double corrosion—protection system using galvanized wires is required.

b) It should have excellent weathering durability for a long period.

c) It should be prefabricated in a shop in order to eliminate corrosion—protection work at the site.

d) It should have easy handling characteristics including reeling and unreeling.

1.3.4 A shop—coated and maintenance—free colored cable

In recent years, bridges have come to require aesthetic effects on the surrounding landscape as well as possessing superior mechanical properties and durability. A shop—coated and maintenance—free colored cable, eliminating covering work at the site, is preferable especially for a long cable—stayed bridge.

When polyethylene is used as the protective coating on the surface of a cable, its color is limited to black for preventing degradation by ultraviolet radiation [35]. Polyethylene can be colored other than black by using a coloring pigment. But the weathering resistance of the colored cable using a coloring pigment can not be assured, so that it degrades in the open air in a short period.

A black cable may be colored by wrapping it with a colored tape or covering it with a metal material, for example. These methods, however, involve problems of binding durability for the polyethylene and cover joint contamination, and are not preferred from an aesthetic point of view. For example, a polyvinyl chloride tape used for the stay cables of the Pasco—Kennewick Bridge degraded within three to five years after completion and the tape had to be replaced [31]. Metal coverings made of painted steel pipe or aluminum pipe are commonly attached to the stay cables of prestressed concrete cable—stayed bridges. Painted steel pipes were adopted in the Brotonne Bridge, the Sunshine Skyway Bridge. Colored aluminum pipes were used in the Kanzaki Bridge, and recently coverings made of FRP were used for the Aomori Bridge. Coverings made of a colored polyethylene pipe were applied for the stay cables of the Normandy Bridge. However, they needed installation equipment and time to attach such tapes or coverings along a long cable at the site, and continuous maintenance work is usually required after completion at high position above the deck, that being in the case of a long cable—stayed bridge.

Coloring by painting requires a special working apparatus to ensure uniform adhesive quality because polyethylene is a nonpolar material. It is well known that thermoplastic olefins, in particular polyethylene, are difficult to paint because of a lack of adhesion of the surface. One of the criteria for maximum bond strength between paint and a plastic surface is wettability [36]. Therefore, the surfaces of polyethylene have to be treated to increase wettability prior to application of a surface painting for the attainment of maximum adhesion. In the case of a coloring polyethylene surface by painting, a primer coating was heat—treated on the surface of the polyethylene to improve the bond strength between the paint and the polyethylene. It was the first case to apply the painting system to a polyethylene surface, therefore, a long term durability of the system in the natural environment has to be evaluated. The painting system has only a thin paint thickness of about 100 μ m on the surface of the cable, apt to being damaged during handling. In such cases, laborious repainting work is necessary at the site, because the surfaces need to be heat—treated, using the primer coating again, to obtain the adhesive effect. And long—term maintenance is also required after construction.

A shop—coated and maintenance—free colored cable with excellent weathering durability had to be developed for a stay cable of long cable—stayed bridges. In order to develop a new coloring method, the coloring material properties, the weathering durability, the color change characteristics and the structural properties of the system had to be investigated.

1.3.5 Aerodynamic measures against cable vibration

Stay cables of a cable—stayed bridge are easily vibrated by the wind because of their flexibility, low structural damping and circular cross section. Single—strand cables protected by anti—corrosive coverings (polyethylene for instance) for a cable—stayed bridge of multi—cable type have suffered from the frequent occurrence of vibration. When the vibration occurs in the stay cables, there is a possibility of damage to the cables near the socket. Wind—induced vibration of the stay cable has been understood as vortex—induced vibration, wind—rain—induced vibration (rain vibration) and wake galloping [28,29].

It is well known that the circular section, such as a cable, periodically vibrates because of the shed vortices behind it. The response amplitude is relatively smaller than that of other type vibrations. According to the report [28], vortex—induced vibration was observed in stay cables of some cable—stayed bridges [37]. Depending on the extent of its response amplitude, the vortex—induced vibration of cables is likely to affect the bending fatigue strength of the cables. Therefore, it was essential to quantitatively investigate the response characteristics of vortex—induced vibration for a long cable—stayed bridge.

When two stay cables are closely arranged to the wind such that one cable lies within the wake of the other, the downstream cable may be subjected to the wake galloping. The vibration is mainly governed by the spacing parameter of two cables. On the basis of some experimental results and observations in some cable—stayed bridges, the vibration decreases when the distance between the center of two cables is about four times a cable's diameter, and disappears when it is more than five. And the amplitude of the vibration increases rapidly at a reduced velocity around 20, becoming about twice as large as its diameter. To

suppress the vibration, a wire—connecting method or a spacer with a damper are often used for various cable—stayed bridges [29]. For example, a spacer with a damper was adopted in the Yokohama Bay Bridge [45], a wire—connecting method was used in the Faro Bridge and the Iwagurojima Bridge. As a basic solution, it is desirable to make the distance between the center of two cables more than five times a cable's diameter in the design stage.

Vibrations induced by the combined influence of wind and rain have often been reported in cables having a smooth surface, such as polyethylene, and a diameter between 120 to 200 mm. Rain vibration was observed in the Meiko—Nishi Bridge, then the amplitude of about double the cable's diameter was measured [38]. The vibration is considered to be caused by combined conditions; water rivulets of a cable surface and axial air flow formed along the cable axis [39]. Extensive research into the mechanism of the vibration and measures to control it have been carried out. And the effects of such suppressing measures have been observed in actual bridges. Two main techniques have been used to control rain vibration; one is to install some kind of vibration—damping devices on the cables near the anchor points, or to connect neighboring cables with wires, and the other is to improve the aerodynamic characteristics of cables by introducing a roughness on their surfaces [40]. With the recent demand for a longer cable to suit the increasing span of cable—stayed bridges, there have been certain cases in which it was impossible to obtain a sufficient vibration suppressing effect by using mechanical damping devices; a long cable has a limited fixing point where damping devices are effective. Accordingly, aerodynamic measures are expected to become more important for a stay cable of long cable—stayed bridges. However, there have been a few measures to suppress rain vibration, such as parallel protuberances, helical streaks and V or U groovings [41,42,43].

On the other hand, as a cable—stayed bridge has a longer span, the wind load of stay cables becomes larger and sometimes it is not less than that of the deck. In the design of a long cable—stayed bridge, a smaller drag force of the cable is essentially preferable at a realistic Reynolds number. If this large wind load (the drag force) is able to be decreased, it will be a great help to optimize the whole configuration of the structure. These aerodynamic measures mentioned above, however, cause a greater drag force because they have a larger surface roughness compared with that of a cable having a smooth surface at the design wind velocity [44]. This becomes quite a new subject in the design of a long cable—stayed bridge, not ever being faced.

Therefore, aerodynamic cable sections with better vibration—controlling characteristics and a smaller drag force at the same time had to be developed for long cable—stayed bridges.

1.4 The Purpose of The Study

The purpose of the study consisted of two main points. The first was to develop a new cable which could be applied to a stay cable of long cable—stayed bridges. Stay cables of a long cable—stayed bridge are required to possess excellent mechanical properties, such as high static strength and high fatigue strength, and a superior corrosion protective coat. To meet these requirements, a pre—coated parallel wire cable was developed, which had both a high static and fatigue strength, and had a shop—coated layer. The cable consisted of three major parts; the cable, the socket at both cable ends and a corrosion protective coat. Details of the study are presented respectively.

In addition to fundamental development, the cable that could be applied to any cable—supported structures was also required to have a higher performance. One of the application subjects was to make the cable colored and durable to harmonize with the surrounding environment. The other was to develop aerodynamic measures against cable vibration to lengthen cable—stayed bridge spans. Mentioned above was the application study for the cable. Details of the investigations with respect to these subjects and the results obtained by the study (a fluoropolymer—coated colored cable and a low drag aerodynamically stable cable with an indented pattern), are presented.

The study consists of eight chapters, including this chapter, and summaries of each chapter are presented as follows.

In Chapter 1, the progress in cables for cable—supported bridges and types of cables particularly used in cable—stayed bridges are introduced. It is pointed out that the development of a new—type cable is essentially required to make progress in cable—stayed bridges. Problems of a stay cable caused by elongating the span of a cable—stayed bridge are analyzed and classified into five main subjects; a large—sized fabricated cable, higher static and fatigue strength for a cable socket, corrosion—protective coat for a cable, coloring a cable, and aerodynamic measures against cable vibration. Finally, the purpose and scope of the study is clarified.

In Chapter 2, the basic static characteristics of a newly developed pre—coated parallel wire cable are discussed based on the experimental studies [46]. The wires of the pre—coated parallel wire cable are given a slight twist at a pitch designed to maintain the optimum tensile strength and the modulus of elasticity. From the experimental analysis, the influence of the twisting angle is investigated concerning the static strength and modulus of elasticity, and the

limit of the twisting angle not affecting the static properties is examined. The influence of the twisting angle on the time dependent characteristics, such as creep and relaxation of the pre−coated parallel wire cable, is also investigated [47]. Finally, the tensile test is carried out by using full−size cable models, and static characteristics of a large−sized pre−coated parallel wire cable are shown [12].

In Chapter 3, the experimental studies on the development of the socket for the cable are discussed. First, the mechanical properties of large sockets filled with zinc−copper alloy are studied based on the results of the tensile tests and analysis. The application limit of the conventional design method is studied before examining a new method in socket design for a large cable [22]. Then, fatigue strength and bending fatigue strength of a socket are studied. In this study, the socket cast by zinc−copper alloy and epoxy resin is investigated in order to improve fatigue resistance for a socket [24]. Tensile fatigue tests are also carried out by using cables being twisted by several different angles to examine the influence of the twisting angle on the fatigue strength for the socket. Next, bending fatigue tests are carried out relating to a bending angle to examine the bending fatigue strength that the cable possesses. The effect of the epoxy resin used in the socket is analyzed, then the bending fatigue strength of the pre−coated parallel wire cable is evaluated [25].

In Chapter 4, studies on a corrosion protective layer, which is an important component to maintain the durability of the cable, are discussed [12]. Before polyethylene is applied as the protective coating of the parallel wire cable, its' corrosion−protective performance, mechanical properties and many other characteristics are investigated. The properties of a polyethylene coated cable are analyzed, and installation characteristics of the cable such as unreeling and clamping are examined using full−size cable models. Various data with respect to mechanical properties and installation characteristics obtained by the experiments are shown.

In Chapter 5, a coloring method for a polyethylene−coated black cable is discussed [48,49]. Requirements for material of colored−cable are analyzed in the first place, and the reasons that a fluoropolymer is selected is indicated. The material properties of the fluoropolymer, especially weathering durability [50], are investigated by using various weathering test methods. The weathering durability of the fluoropolymer is estimated using the results obtained by an outdoor natural exposure test, an accelerated outdoor exposure test and an accelerated laboratory test. Further, structural characteristics of the colored cable are examined. It is shown that the colored cable is applied not only to stay cables of long cable−stayed bridges but also to hangers of long suspension bridges.

In Chapter 6, the vibration problems of a stay cable are picked up and experimental studies on cable vibration and its suppressing method for a long cable−stayed bridge are discussed. First, the past works on cable aerodynamics are briefly reviewed [29,51,52]. Fundamental static aerodynamic characteristics of a circular cylinder are introduced and cable vibrations and their various suppression methods are shown.

Next, vibration responses of stay cables by vortex−induced vibration in a natural wind are measured at an actual cable−stayed bridge with a main span of 490 m [53]. The factors affecting this vibration, such as surface roughness and structural damping, are examined by using wind tunnel tests and analysis. It is shown that the response amplitude can be estimated at various damping levels. The effect of the vortex−induced vibration on the bending fatigue strength is evaluated for stay cables of a long cable−stayed bridge with a main span of 1000 m.

Then, aerodynamic measures for a stay cable against rain vibration are investigated using wind tunnel tests [54,55]. A series of experiments are carried out to learn about the formation and behavior of water rivulets on cable surface when rain vibration occurs. Amount and location of water rivulets are measured and analyzed. Various tests under simulated rainfall are carried out in order to investigate the vibration suppressing effects of surface−roughened cables. Various experiments are also carried out concerning the relationship between the surface roughness and aerodynamic properties, such as drag force and pressure distribution. It is pointed out that a super−long cable−stayed bridge needs a cable having not only a suppressing effect but also a low drag force. A low drag aerodynamically stable cable with a patterned surface is experimentally discussed. Finally, to understand the aerodynamic characteristics of the surface configuration of the cable, various patterned roughnesses are examined in terms of a Reynolds Number [56].

In Chapter 7, cable materials in the future for a super−long cable supported bridge are described. It is shown that the development of cable material is inevitable in order to lengthen a bridge span of a super−long suspension bridge [57]. The present status of cable materials including steel wires and new materials (such as carbon fiber) is surveyed, and future problems to overcome are pointed out.

In Chapter 8, the results obtained by each chapter are summarized and concluding remarks are mentioned.

1.5 References

[1] Honshu—Shikoku Bridge Authority, *Examination on Cables of Suspension Bridges* *, 1978, pp.91—100.

[2] M.Matsuzaki, C.Uchikawa and T.Mitamura, Advanced Fabrication and Erection Techniques for Long Suspension Bridge Cables, Proc. of ASCE, Vol.116, 1990, pp.112—130.

[3] Honshu—Shikoku Bridge Authority, Technical Report on Development of High—Strength Galvanized Wire (180 kg/mm ^{2} class) for Bridge Cable *, 1988, pp.6—20.

[4] T.Takahashi, S.Konno, H.Sato, I.Ochiai, Y.Noguchi, O.Serikawa and Y.Tawaraya, Development of High—Strength Galvanized Wire *, Seitetsu Kenkyu, No.332, 1989, pp.53—58.

[5] T.Endo, K.Tada and H.Ohashi, Development of Suspension Bridges: Japanese Experience with Emphasis on the Akasi Kaikyo Bridge, Proc. of Cable—Stayed and Suspension Bridges, Deauville, France, 1994, pp.55—66.

[6] N.J.Gimsing, Cable Supported Bridge, 1983, pp.24—54.

[7] F.Leonhardt and W.Zellner, Past, Present and Future of Cable—Stayed Bridges, Proc. of International Seminar on Cable—Supported Bridges, Yokohama, Japan, 1991, pp.1—33.

[8] T.Naruse, Historical Change of Cable—Stayed Bridges, Bridge and Foundation Engineering, Vol.19, No.8, 1985, pp.11—16.

[9] Japan Society of Civil Engineers, Steel Cable—Stayed Bridges *, 1990, pp.248—249.

[10] M.Ito, Cable—Stayed Bridge in Japan, Proc. of International Seminar on Cable—Supported Bridges, Yokohama, Japan, 1991, pp.341—356.

[11] M.Virlogeux, The Normandie Bridge, France: A New Record for Cable—Stayed Bridges, IABSE SEI Volume 4, November 1994, pp.208—213.

[12] Y.Tawaraya, T.Hojo, Y.Sakamoto, T.Eguchi and I.Tsuchida, Development of NEW PWS for Cable—Stayed Bridges and Its Practical Application, Nippon Steel Technical Report, No.42, 1989, pp.1—11.

[13] T.Endo, T.Iijima, A.Okukawa and M.Ito, The Technical Challenge of A Long Cable—Stayed Bridge; Tatara Bridge, Proc. of International Seminar on Cable—Supported Bridges, Yokohama, Japan, 1991, pp.417—436.

[14] A.Otsuka and K.Yamasaki, Cables for Cable—Stayed Bridges *, Bridge and Foundation Engineering, Vol.19, No.8, 1985, pp.35—43.

[15] Japan Steel Structure Corporation, Standard for Structural Cables *, 1994, pp.12—21.

[16] M.Ohashi, Cables for Cable—Stayed Bridges, Proc. of International Seminar on Cable—Supported Bridges, Yokohama, Japan, 1991, pp.125—150.

[17] D.Westerhoff, R.Freeman and K.Kuwabara, Dao Khanong Cable—Stayed Bridge: Manufacture and Erection of Large Diameter Full Locked Coil Bridge Ropes, Proc. of International Conference on Cable—stayed Bridges, Bangkok, 1987, 1461—1471.

[18] T.Tottori, T.Kawazoe and K.Yoshikawa, Galvanized Cable Wire and Prefabricated Parallel Wire Strand, Nippon Steel Technical Report, No.8, 1976, pp.63—72.

[19] M.Yamada and M.Chinone, Plastic Covering for Bridge Cable *, Seitetsu Kenkyu, No.285, 1975, pp.88—95.

[20] M.Yasuda, T.Takeyama and M.Nozawa, Design and Fabrication of Stay Cables for Iwakorojima Bridge *, Honshi Technical Report, No.39, 1986, pp.12—19.

[21] Prestressed Concrete Association, Cable Members for Prestressed Concrete Bridges *, 1987.

[22] T. Komura, K.Wada, H.Takano and Y.Sakamoto, Study into Mechanical Properties and Design Methods of Large Cable Sockets, Proc. of JSCE No.422, I —14, 1990, pp.133—144.

[23] I.Mitsujima, T.Nishi and T.Shinke, Fatigue Strength of Cable Wire , Kobe Steel Engineering Report, Vol.25, 1978, pp.58—63.

[24] Y.Tawaraya, T.Sugita, S.Konno, H.Otani, T.Hojo and M.Yano, Development of Fatigue—Resistant Sockets, Nippon Steel Technical Report, No.19, 1982, pp.121—132.

[25] Y.Sakamoto, T.Hojo, T.Eguchi and M.Yano, A Study on Secondary Stress and Fatigue Life in Bending of A Pre—Coated Cable for Cable—Stayed Bridge *, Proc. of JSCE Vol.446, I —19, 1992, pp.215—223.

[26] W.Andrä und W.Zellner, Zugglieder aus Paralleldrahtbundeln ünd ihre Verankerung bei hoher Dauerschwellbelastung, Die Bautechnik 46, Hefte 8,9, 1969.

[27] M.Birkenmaier and R.Narayanan, Fatigue Strength of High Tensile Steel Stay Tendons, IABSE Colloquium, Lausanne, 1982, pp.663—672.

[28] National Land Development Technology Research Center, Report on Study of Wind Resistance of Cables in Cable—Stayed Bridges *, 1989, pp.14—34.

[29] Public Works Research Center, Report on Study of Wind Resistance of Cables in Cable—Stayed Bridges *, 1994, pp.78—104.

[30] Y.Kishimoto and H.Takenouchi, Bending Fatigue Test of Bridge Cables *, Honshi Technical Report, Vol.4, No.11, 1980, pp.8—15.

[31] S.Watson and D.Stafford, Cables in Trouble, Civil Engineering, April 1988, pp.38—41.

[32] B.Birdsall, Brighter Future for Stay Cables, Civil Engineering, October 1988, pp.46—49.

[33] J.Durkee and G.Shaw, Plastic Cable Covering, Civil Engineering, February 1966, pp.63—67.

[34] D.Stafford and S.Watson, A Discussion of Critical Corrosion Problems in The Cable

Elements of Stayed Girder Structures, Proc. of International Conference on Cable—stayed Bridges, Bangkok, 1987, pp.1048—1060.

[35] S.Kawawata and M.Kikkawa, Weathering of Some Plastics of Wire and Cable Applications * , Hitachi Hyoron, Vol.9, 1958, pp.63—72.

[36] Nikkan Kogyo Shinbun, Polyethylene Resins * , 1973.

[37] Honshu—Shikoku Bridge Authority, Observation Report of Dynamic Behavior of Cables of The Ikuchi Bridge * , 1991.

[38] Y.Hikami, Rain Vibration of Cables in Cable—Stayed Bridges, Japan Association for Wind Engineering, Vol.27, 1986, pp.17—28.

[39] M.Matsumoto, N.Shiraishi, M.Tsujii and S.Hirai, On Aerodynamic Oscillations of Cables for Cable Stayed Bridges * , Proc. of JSCE Vol.416, I —13, 1990, pp.225—234.

[40] M.Matsumoto, Y.Hikami and M.Kitazawa, Cable Vibration and Its Aerodynamic/Mechanical Control, Proc. of Cable—Stayed and Suspension Bridges, Deauville, France, 1994, pp.439—452.

[41] T.Saito, M.Matsumoto and M.Kitazawa, Rain—Wind Excitation of Cables on The Cable—Stayed Higashi—Kobe Bridge and Cable Vibration Control, Proc. of Cable—Stayed and Suspension Bridges, Deauville, France, 1994, pp.507—514.

[42] O.Flamand, Rain—Induced Vibration of Cables, Proc. of Cable—Stayed and Suspension Bridges, Deauville, France, 1994, pp.523—532.

[43] M.Miyazaki, Unstable Aerodynamic Vibrations and Prevention Methods for Cables in Cable—Stayed Bridges * , Proc. of the 10th Wind Engineering Symposium, 1988, pp.145—150.

[44] T.Miyata, H.Yamada and T.Hojo, Aerodynamic Response of PE Stay Cables with Pattern—Indented Surface, Proc. of International Conference on Cable—Stayed and Suspension Bridges, Deauville, France, 1994, pp.515—522.

[45] K.Wada, S.Eya, H.Touda and H.Takano, Control Methods of Wind—Induced Vibrations for The Yokohama Bay Bridge * , Bridge and Foundation Engineering, Vol.23, No.8, 1989, pp.43—48.

[46] T.Hojo, Y.Sakamoto and T.Eguchi, Structural Characteristics of NEW PWS for Cable—Stayed Bridge, Proc. of IABSE Seminar on Cable—Stayed Bridges, Bangalore, India, 1988, pp. III 13—25.

[47] Y.Sakamoto, T.Eguchi, T.Hojo, T.Komura and K.Wada, Study on Creep and Relaxation of A Pre—Coated Cable for Cable Stayed Bridge * , Bridge and Foundation Engineering, Vol.26, No.3, 1992, pp.27—32.

[48] T.Hojo and I.Tsuchida, Development of Colored Cable for Cable—Stayed Bridges * , Journal of JSCE, Vol.75, No.11, 1990, pp.8—9.

[49] T.Hojo, I.Tsuchida, M.Yano, T.Eguchi and S.Takami, Development of Colored Cable for Suspended Structure, Nippon Steel Technical Report, No.60, 1994, pp.17—23.

[50] T.Hojo, I.Tsuchida and K.Abe, A Study on Weathering Durability of Fluoropolymer * , Proc. of JSCE Vol.480, VI —21, 1993, pp.107—115.

[51] I.Okauchi, M.Ito and T.Miyata, Wind Engineering for Structure, Maruzen, 1977.

[52] E.Simiu and R.H.Scanlan, Wind Effects on Structure, John Wiley &Sons, 1985.

[53] K.Yokoyama, T.Kusakabe, T.Fujiwara and T.Hojo, Experimental Study on Cable Response Caused by Vortex—Induced Vibration * , Proc. of the 12th Wind Engineering Symposium, 1992, pp.279—284.

[54] T.Hojo, Experimental Study on Rain Vibration Characteristics and Suppressing Methods of cables in Cable—Stayed Bridges * , Japan Association for Wind Engineering, Vol.50, 1992, pp.19—26.

[55] T.Miyata, H.Yamada and T.Hojo, Experimental Study on Aerodynamic Characteristics of Cables with Patterned Surfaces, Journal of Structural Engineering, Vol.40A, 1994, pp.1065—1076.

[56] T.Hojo, S.Yamazaki, T.Miyata and H.Yamada, Development of Low Drag Aerodynamically Stable Stay Cable with Patterned Surface Processing * , Bridge and Foundation Engineering, Vol.29, No.6, 1995, pp.27—32.

[57] T.Hojo and M.Akiyama, Cable Materials for Super—Long Suspension bridges, Proc. of International Seminar on Super—Long Suspension Bridges, Tokyo, 1994, pp.52—57.

* Published in Japanese

Table 1.1   World's long suspension bridges

Rank	Name of Bridge	Main Span (m)	Country	Year Completed
1	Akashi—Kaikyo	1990	Japan	1998 (scheduled)
2	Great Belt	1624	Denmark	1996 (scheduled)
3	Humber	1410	U.K.	1981
4	Jiangyin Yangtze River	1385	China	1998 (scheduled)
5	Tsing Ma	1377	Hong Kong	1997 (scheduled)
6	Verrazano Narrows	1298	U.S.A.	1964
7	Golden Gate	1280	U.S.A.	1937
8	Höga Kusten	1210	Sweden	1997 (scheduled)
9	Mackinac	1158	U.S.A.	1957
10	Minami Bisan—Seto	1100	Japan	1988
11	Fatih Sultan Mehmet	1090	Turkey	1988
12	Bosporus	1074	Turkey	1973
13	George Washington	1067	U.S.A.	1931
14	3rd Kurushima	1030	Japan	1999 (scheduled)
15	2nd Kurushima	1020	Japan	1999 (scheduled)
16	25th April	1013	Portugal	1966
17	Forth Road	1006	U.K.	1964
18	Kita Bisan—Seto	990	Japan	1988
19	Severn	988	U.K.	1966
20	Shimotsui—Seto	940	Japan	1988
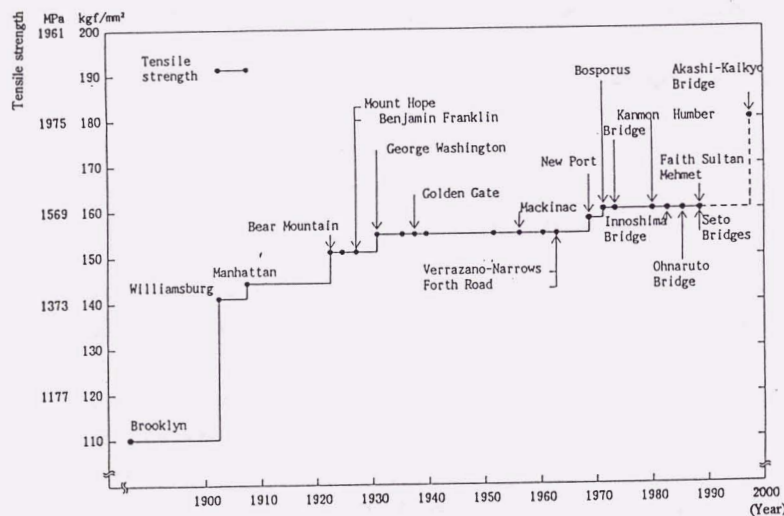
Table 1.2   World's long cable—stayed bridges

Rank	Name of Bridge	Main Span (m)	Country	Year Completed
1	Tatara	890	Japan	1999 (scheduled)
2	Normandy	860	France	1995
3	Yangpu	603	China	1993
4	Meiko—Central	590	Japan	1996 (scheduled)
5	Skarnsundet	530	Norway	1991
6	Tsurumi Tsubasa	510	Japan	1995
7	Ikuchi	490	Japan	1991
8	East Kobe	485	Japan	1994
9	Annacis	465	Canada	1986
10	Yokohama Bay	460	Japan	1989
11	Second Hooghly	457	India	1992
12	Second Severn	456	U.K.	1996 (scheduled)
13	Rama IX	450	Thailand	1984
13	Dartford	450	U.K.	1991
15	Barrios de Luna	440	Spain	1983
16	Kap Shui Mun	430	Hong Kong	1997 (scheduled)
17	Helgeland	425	Norway	1991
18	Nanpu	423	China	1991
19	Iwakurojima	420	Japan	1988
19	Histuishijima	420	Japan	1988

Fig.1.1   Progress in tensile strength of bridge wire
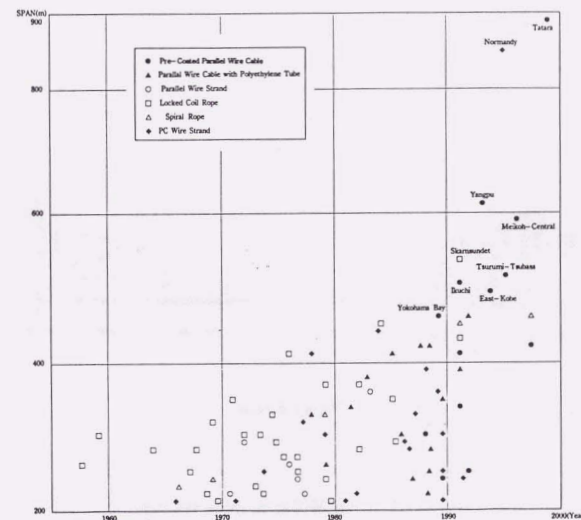
Fig.1.2   Historical change of cable types in cable—stayed bridges
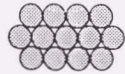
stay cable
13 × locked coil ropes(φ 73)
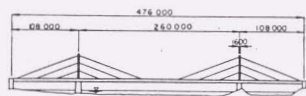
Theodor Heuss Bridge

stay cable
1 × pre—coated parallel wire cable(φ 170)
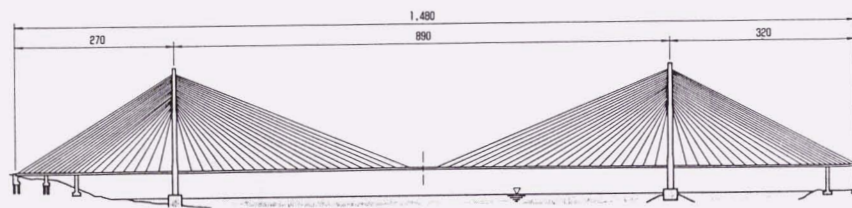
Tatara Bridge

Fig.1.3   Comparison of cable system

| | Pre—Coated Parallel Wire Cable | Conventional cables | | |
		Parallel Wire Strand	Parallel Wire Cable	Locked coil rope
Cable cross section	7mm-dia. galvanized steel wire / Polyethylene	5mm-dia. galvanized steel wire	Polyethylene pipe / 7mm-dia. PC steel wire / Grouting material	Galvanized steel wire
Socket	NS socket: epoxy resin + zinc-copper alloy cast	Ordinary wire socket: zinc-copper alloy cast	HiAm anchor: steel ball + zinc powder + epoxy resin	Ordinary wire socket: zinc-copper alloy cast
Tensile strength (kgf/mm²)	160	160	165	120
Fatigue strength (kgf/mm²)	25-30	About 15	20-25	About 15
Modulus of elasticity (kgf/mm²)	20,000	20,000	20,500	16,000
Corrosion Prevention — Method	Wire galvanizing + polyethylene coating (in the manufacturing plant)	Wire galvanizing + plastic covering (at site)	Polyethylene pipe + grouting (at site)	Wire galvanizing + painting (at site)
Corrosion Prevention — Evaluation	◎	△	○	△
Ease of reeling and transportation	○	○	○	○
Ease of unreeling and field work	◎	△	○	○

1 kgf/mm² = 9.807 MPa

Fig.1.4   Characteristics of various structural cables
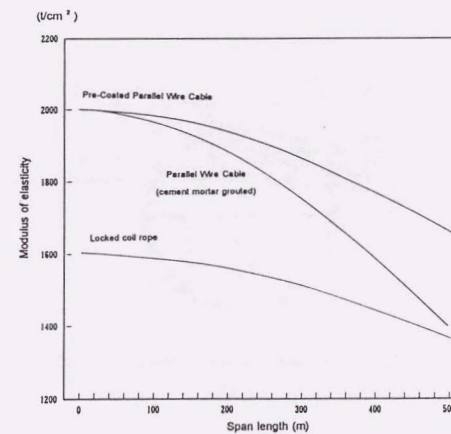
Fig.1.5   Comparison of elastic modulus
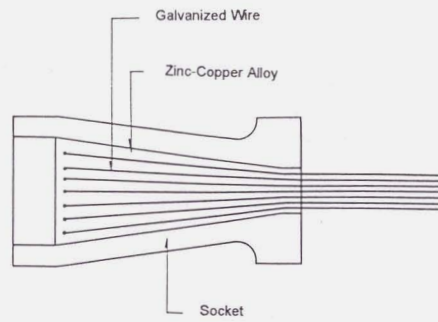
Fig.1.6   Zinc—copper alloy cast socket

Fig.1.8   Plastic covering

Fig.1.7   Steel balls and epoxy resin cast socket
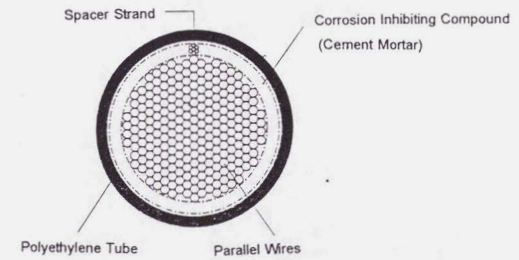
Fig.1.9   Corrosion protection by polyethylene pipe
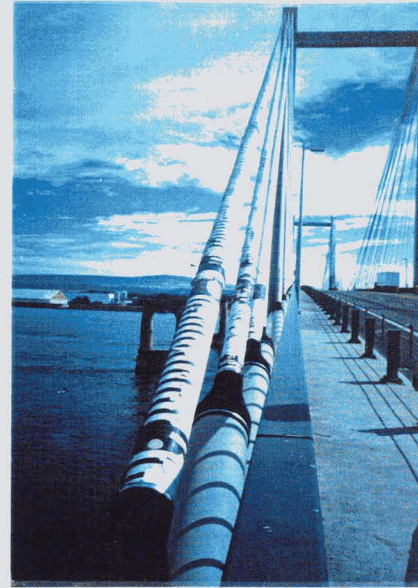
Photo.1.1 Deterioration of wrapped colored—tape

Photo.1.2 Coverings made of colored polyethylene pipe

CHAPTER 2 A LARGE—SIZED FABRICATED CABLE

2.1 Introduction

In the early days of cable—stayed bridges, cable systems with relatively few heavy stay
cables were usually used. In the few—cable system, a stay cable had to be composed of
several ropes or strands. For example, one stay cable of the Theodor Heuss Bridge consisted
of 13 locked coil ropes [1], and of the Toyosato Bridge, 16 parallel wire strands [2]. The
few—cable system required a large and complicated anchorage structure to fix an individual
rope or strand. And the use of heavy, concentrated stay cables required a local strengthening
of the girder. It was also necessary to adjust the tension of each rope or strand during the
anchoring procedure, which was laborious work. Besides all this, several strands had to be
assembled into one stay cable after all cables were installed in order to apply
corrosion—protection at the site, using temporary scaffolding, like a catwalk.

As longer cable—stayed bridges have come to be constructed in recent years, the
multi—cable system has become popular. In the multi—cable system, it is preferable that
each stay cable consists of a single prefabricated strand, that is, a mono—strand cable.
Requirements for mono—strand cables of a multi—cable system of a long cable—stayed bridge
are indicated as follows.

a) It should have a high breaking strength of more than 2,000 tonf (19,600 kN), which is
about 3 times higher than that of a conventional rope or strand, such as a locked coil
rope or a parallel wire strand.

b) It should have a high and stable modulus of elasticity, consequently, a cable composed
of parallel wire is desirable.

c) It should be prefabricated, including a corrosion—protection layer, to eliminate corrosion
protecting work at the site.

At that time, there were few conventional ropes or strands that satisfied these
requirements mentioned above, therefore it was necessary to develop a new type cable.

In this chapter, the basic static characteristics of a newly developed pre—coated parallel
wire cable are discussed based on experimental studies.

First, the material properties of a wire for a pre—coated parallel wire cable are described
after the manufacturing process is briefly introduced.

A slight twist is given to the wires when they are fabricated in order to improve the

handleabilty without seriously damaging the structural performance , that is a pre-coated parallel wire cable (Photo.2.1). The influence of the twisting angle is investigated concerning the static strength and modulus of elasticity, and the limit of the twisting angle not affecting the static properties is examined [3]. The tensile test is carried out by using large-sized cable models. The static characteristics of the pre-coated parallel wire cable are shown based on the tested results [4].

Next, the influence of creep and relaxation is also investigated for a 7 mm diameter wire and a pre-coated parallel wire cable [5]. A creep and relaxation test is carried out using the same device at the same time. Three twisting angles are applied to the test pieces of the pre-coated parallel wire cable in order to investigate the effect of the twisting angle on creep and relaxation. The test results on time dependent characteristics such as creep and relaxation of the pre-coated parallel wire cable are indicated.

2.2 Material Properties of A Wire for A Pre-Coated Parallel Wire Cable

A high-tension galvanized wire of about 5 mm in diameter is usually used for a parallel wire strand for suspension bridges [6]. The diameter of a galvanized wire has remained at about 5 mm from the beginning of the suspension bridge's history up to the Akashi Kaikyo Bridge [7]. The reason may be that a diameter of 5 mm has been empirically considered suitable from a handleability point of view, especially when a air spinning method is employed.

On the other hand, a wire of 7 mm in diameter is usually used for a stay cable of cable-stayed bridges [1]. As for a stay cable of cable-stayed, especially the multiple-cable with mono-strand cable type, it is desirable to use a cable having a greater tensile strength, which can reduce the number of stay cables or the diameter of a cable. A wire of more than 5mm in diameter is required because of the efficiency of its sectional area. Generally speaking, the larger the diameter of a wire, the smaller its tensile strength. Then a high-tension galvanized wire of 7 mm in diameter, which almost has double the sectional area compared to that of one 5 mm, possessing a tensile strength of 160 kgf/mm^2 (1,569 MPa), has been improved beginning in the 1970's, though that of a bare wire has been used for prestressed concrete structures. A galvanized wire of 7 mm in diameter was first adopted for the Iwakurojima Bridge and the Histuishijima Bridge in Japan [8].

A galvanized wire is produced from a piano wire rod by a patenting, drawing and hot galvanizing process [9]. The pre-coated parallel wire cable is composed of a wire of grade SWRS82B specified by JIS G3502 [10]. Table 2.1 shows the chemical composition of the wire

rod.

Patenting is a heat treatment in which the wire rod is isothermally transformed in a lead bath of approximately 530 ° C after it has been heated to approximately 960 ° C in a reheating furnace. A sorbite structure having a high ductility is obtained through these heat treatment process. Then the wire rod is pickled in acid to remove scale, and the film treatment is performed in preparation for cold drawing.

A heat-treated wire rod is passed through the wire-drawing machines six to seven times, drawn from 13 mm in diameter to 6.92 mm. As the drawing ratio of a wire should be preferably 75 to 85% from the toughness and fatigue strength point of view, the diameter of the rod is set to be 13 mm. The strength of the drawn wire is set to 180 to 195 kgf/mm^2 (1,765-1,912 MPa) in expectation of about 10% decrease in strength after galvanization.

In preparation for galvanizing, degrasing, pickling, water rinsing and flux treatment are done to the wire. In the final process in wire production, the wire is dipped into a hot zinc bath heated to 450 ° C and is finished to 7.00 mm in diameter. The zinc weight, thickness and uniformity are most important in the process of galvanizing.

Finally, a wire of 7 mm in diameter is made having a tensile strength higher than 160 kgf/mm^2 (1,569 MPa) and a zinc coating of 300 g/m^2. As toughness is required in addition to strength, a wrapping test and twisting test are specified. Furthermore, straightness is specified as a special requirement for a galvanized wire for a parallel wire cable. Table 2.2 shows the quality required for the galvanized wire. To satisfy the specification for the wire of a stay cable of cable-stayed bridges and to assure a high level of characteristic values, the wire is produced by modern equipment and up-to-date techniques. At the same time, close quality control is performed during each process.

2.3 Static Properties of A Large-Sized Fabricated Cable

2.3.1 Static properties of a pre-coated parallel wire cable

The structure of a pre-coated parallel wire cable is the same as that of a pure parallel wire strand except that the wires are slightly twisted. The twisting pitch of the cable is decided in order to maintain the same mechanical properties as those of a parallel wire strand. The pre-coated parallel wire cable consists of parallel galvanized steel wires of 7 mm in diameter. The cable is polyethylene-coated as a corrosion protective layer in the factory, and then provided with sockets at both ends. Fig.2.1 shows a external view of the

pre-coated parallel wire cable.

Generally speaking, the twisted wire rope is different from a parallel wire strand of the same cross-sectional area in tensile strength, modulus of elasticity and other mechanical properties. This is mainly due to the interaction between contact wires at the crossing points [11]. The difference in lay structure between the pre-coated parallel wire cable and a spiral rope is shown in Fig.2.2. The pre-coated parallel wire cable is twisted with the same pitch, while a spiral rope is twisted with the same angle. Consequently, as for the pre-coated parallel wire cable, all wires never cross over and stay parallel to the neighboring wires along the entire length, though in a spiral rope all wires have crossing points. This lay structure is considered to be the most important factor in contributing to static performance of the pre-coated parallel wire cable.

Fig.2.3 shows the results of a static tensile test conducted on the pre-coated parallel wire cable at different twisting angles [3]. It can be seen that yield strength and breaking strength decrease as the twisting angle exceeds 4°, while they remain almost unchanged when the twisting angle is less than 4°. In the latter case, the breaking load is higher than the specified one. On the other hand, assuming that each individual wire is subject to an equal force, the rate of decrease in the breaking strength of a helical rope, d, can be theoretically calculated by the following equation [12]:

$$d = 1 - \Sigma \; n_i \cdot \cos a_i / N \tag{1}$$

where,　　N : total number of wires

a_i : twisting angle of wires of i-th layer

n_i : number of wires whose twisting angle is　a_i

As for the pre-coated parallel wire cable consisting of 127 wires of 7mm in diameter, the value of d is 0.1% when the twisting angle a is 3.5°, and only about 0.7% even when a is 10°. On the basis of this calculation, coupled with the test results, it can be said that the pre-coated parallel wire cable has a breaking strength comparable to that of a parallel wire strand when the twisting angle is 4° or less.

Fig.2.4 shows the results of an experiment carried out on the pre-coated parallel wire cable's elasticity in comparison with the relevant theoretical values obtained by F.Schleicher and R.H.Knapp [13]. It can be seen that the experimental value is of little difference from the theoretical values of Schleicher and Knapp and that the decrease of the modulus of elasticity is about 0.5 % when the twisting angle is 4°. On the other hand, the values

obtained by the experiment show a somewhat greater decline in modulus of elasticity than the theoretical values. When the twisting angle is less than 4°, however, the experimental lower-side values show nearly the same tendency as the theoretical values. Besides, within this range, the modulus of elasticity of the pre-coated parallel wire cable is well above the design modulus of elasticity of a parallel wire strand, namely 20,000 kgf/mm^2 (196 GPa). Therefore, in practical design, the modulus of elasticity of the pre-coated parallel wire cable can be regarded as the same as that of a pure parallel wire strand.

Based on the experimental values of the tensile strength and modulus of elasticity mentioned above, a standard twisting angle of 3.5° or less has been established for the design of the pre-coated parallel wire cable, within which the deterioration of those characteristics is negligible.

With a twisted cable, a rotational torque occurs when tension is applied to the cable. The rotational torque is far smaller than that of common stranded wire ropes, but it lineally increases with an increasing cable diameter. A rotational torque can be calculated by the following equation:

$$J = (T/N) \; \Sigma \; n_i \cdot R_i \cdot \sin a_i \tag{2}$$

where,　　J : rotational torque

T : tensile load

N : total number of wires

R_i : wire twisting radius

Fig.2.5 shows the results of an experiment carried out on the pre-coated parallel wire cable's torque property. It is clear from this figure that the calculated values agree well with the tested data. The magnitude of this torque is a function of the cable size and the applied tension load [4]. Fig.2.6 shows the relation between the tensile load and rotational torque calculated for a few cables of the pre-coated parallel wire cable. Some measures, including the restraint of rotational torque at the socket, have to be taken according to the tensile load during erection.

2.3.2　Tensile test of large-sized cables

The cable diameter has increased with increasing length of cable-stayed bridges in recent years. The largest cable size used up to the present is composed of 499 galvanized steel wires, 7 mm in diameter. The specified breaking load of the cable is 3,071 tonf (30,116 kN).

Various tensile tests were made for parallel wire strands and pre-coated parallel wire cables composed of about 100 wires of 7 mm in diameter, and their breaking strength and modulus of elasticity and other properties were obtained. The tensile test results of parallel wire stands and pre-coated parallel wire cables are given in Table 2.3. Much remained unclear about the strength characteristics of large cables, which have 4 to 5 times higher breaking strength than that of usual cables. Thus, tensile tests were carried out using the pre-coated parallel wire cable composed of 421 wires of 7 mm in diameter. The pre-coated parallel wire cable being tensile-tested is shown in Photo.2.2. The tensile test was mainly designed to determine the strength characteristics of the large-sized cables, including the modulus of elasticity, wire stress distribution and breaking strength. The specimen was about 4 m long and fitted with sockets at both ends. The tensile test was conducted on a 8,000 tonf (78,400 kN) tensile testing machine at Nippon Steel Corporation.

Table 2.4 shows the tested results. The modulus of elasticity of the tested cable was approximately 2.02×10^4 kgf/mm^2 (198 GPa) and was higher than the designed value of 2.00×10^4 kgf/mm^2 (196 GPa). The stress distribution of the wires in the outermost layer is shown in Fig.2.7. The stress variability in the wires was less than the designated value of each and there was practically an equal stress distribution. The breaking load of the cable was sufficiently higher than that of the specified value. The decline in the breaking strength efficiency was very small, at 1 to 2%. The elongation of the cable at fracture was approximately 5% and was equal to that of individual wires. It was confirmed that static characteristics under design load, such as modulus of elasticity, breaking strength of the cable and stress distribution of wires, were similar to those of usual cables consisting of about 100 wires of 5 mm in diameter. These properties are not considered to decrease with the increase of cable size up to about 500 wires.

2.4 Creep and Relaxation Properties of A Pre-Coated Parallel Wire Cable

2.4.1 Creep and relaxation test of a wire

The creep and relaxation properties of a steel wire are affected by chemical components, heat treatment and process conditioning. They are also affected by experimental conditions such as initial stress or temperature of a wire [11]. The pre-coated parallel wire cable is composed of a wire of grade SWRS82B specified by JIS G3502. Hot stretching or blueing is not done to the wire in the manufacturing process, but the time dependent property of the wire is improved by galvanizing, which has a similar effect as blueing.

In a creep test [5], a constant tensile stress of 64 kg/mm^2 (628 Mpa) was applied to the test piece with a length of 955 mm. Elongation, ΔL_0, between the gauge length, $L_0 = 362$ mm, was measured during 1,000 hours under the temperature of $21 \pm 1°$C. In a relaxation test, the same initial load (T_0) of 2,463 kgf (24,152 N), initial stress of 64 kgf/mm^2, was applied to the same test piece with a length of 955 mm. Decrease of the load (ΔT_0) was measured during 1,000 hours under the temperature of $21 \pm 1°$C and $60 \pm 1°$C, expecting high temperature region at the site.

From the tested result shown in Fig.2.8, the majority of creep ($\Delta L_0 / L_0 \times 100\%$) occurred by about 600 hours, after that the creep increases slightly. The amount of creep after 1,000 hours came up to about 0.005%. The initial elastic strain defining that applied stress, 64 kg/mm^2 (628 MPa), is to be divided by the modulus of elasticity of the wire, 20,000 kg/mm^2 (196 GPa), becomes $3,200 \times 10^{-6}$. When the creep, 0.005%, is expressed by the division of creep strain by elastic strain, the amount of the creep becomes 1.56%. Relaxation ($\Delta T_0 / T_0 \times 100\%$) obtained by the test is shown in Fig.2.9. The majority of relaxation occurred by about 600 hours in either temperature, and the amount of it came up to 1.73% and 2.01% respectively after 1,000 hours. Tested data for a galvanized wire of 7 mm in diameter is almost the same as that of one 5 mm in diameter.

2.4.2 Creep and relaxation test of a pre-coated parallel wire cable

Three test pieces were used in order to investigate the effect of the twisting angle on time dependent properties of the cable. They were made of 55 wires of 7 mm in diameter having a twisting angle of $0°$ (purely parallel), $3.5°$ and $7°$. The test pieces were fixed by the sockets at both ends, in order to examine the creep at the sockets during the test. Pre-compression load of 140 tonf (1,372 kN) was applied to the sockets for 30 minutes. The test condition is shown in Table 2.5.

It is difficult to conduct separately creep test and relaxation test using a large-sized cable because of the restriction of test facility or test period. Therefore, an experimental principle and analytical method [14], that was devised to measure creep and relaxation at the same time, was applied. As temperature condition affects the test a lot, the test piece, including test facility, were placed in the constant temperature room. During the test, tension of the cable, amount of slippage value from the socket, strain of the steel pipe of the facility and temperature were measured. The details of experimental principle and analytical method were stated in Ref.[13], and here the main point is summarized as follows.

Time dependent property including cable and socket is modeled after linear viscous elasticity, as shown in Fig.2.10. The relationship of stress σ_c to strain ε_c can be

expressed by the equation (3).

$$\dot{\sigma}_c + \lambda \sigma_c = E_1 (\dot{\varepsilon}_c + \mu \varepsilon_c)$$ (3)

where, $\mu = E_2 / \eta$

$\lambda = (E_1 + E_2) / \eta$

· : indicating differential calculus operator concerning time

Cable tension can be expressed by the equation (4).

$$P(t) = P_0 [\alpha + (1 - \alpha) \exp(-\chi t)]$$ (4)

where, P_0 : initial tension of the cable

α : relaxation coefficient

χ : controlling parameter of time dependent property

Based on the equations (3) and (4), it is necessary to conduct strain $\varepsilon_c (t)$. Using strain of the steel pipe $\varepsilon_s (t)$ and strain $\varepsilon_c (t)$, the equation (5) can be found.

$$\varepsilon_s (t) + \varepsilon_c (t) = \text{constant}$$ (5)

Laplace transform and inverse Laplace transform are applied to the equation (1) to (3), $\varepsilon_c (t)$ is indicated by the equation (6).

$$\varepsilon_c (t) = \varepsilon_{c0} [\beta + (1 - \beta) \exp(-\chi t)]$$ (6)

where, ε_{c0} : strain of the cable under the initial tension

β : creep coefficient

$E_c A_c$: stiffness of the cable

The relation between tensile load and measuring time, meaning relaxation, is obtained by the test. The relation between strain and measuring time is expressed by the equation (7).

$$\varepsilon_c (t) = \varepsilon_s (t) + \varDelta_s (t) / L$$ (7)

where, ε_s : strain of the steel pipe

$\varDelta_s$: slippage amount from both sockets

L : cable length

Coefficient α and β are determined by the equations (4) and (6) in order to satisfy each other using the least squares method. Both coefficients α and β include the amount of slippage from the socket. Therefore, it is necessary to exclude the effect of the socket portion in order to examine the time dependent property of the cable itself.

Creep coefficient β, as shown in the equation (8), is considered to be the ratio of the initial elongation of the test piece $\varDelta l_{c0}$ to the elongation $\varDelta l_c$, where $\varDelta l_{c0}$ is made by both the amount of initial slippage from the socket $\varDelta_{s0}$ and the elastic elongation of the cable $\varDelta L_e$.

$$\varDelta l_c = (\beta - 1) \varDelta l_{c0} = (\beta - 1)(P_0 L / E_c A_c + \varDelta_{s0})$$ (8)

The elongation $\varDelta l_c$ is considered to be the sum of the elongation by the creep at the cable portion and the amount of slippage form the socket. Creep coefficient of the cable alone, β, can be expressed by the equation (9).

$$\beta_c = (1 + \varDelta l_c' / \varDelta L_e) = 1 + (\varDelta l_{c - \varDelta s}) / \varDelta L_e$$ (9)

Next, relaxation of the cable alone is described. From the definition of relaxation, the sum of the elastic strain and plastic strain is kept constant, and it is equal to the initial elastic strain [15].

$$\varepsilon_e + \varepsilon_e' = \varepsilon_{e0}$$ (10)

where, ε_e : elastic strain

ε_e' : plastic strain

ε_{e0} : initial elastic strain

The equation (11) can be obtained differentiating the equation (10), where ε_e is acquired by differential calculation of (12), that is similar to the equation (6).

$$(d \sigma / dt) / E_c + \varepsilon_e = 0$$ (11)

$$\varepsilon_e (t) = \varepsilon_{e0} [\beta' + (1 - \beta') \exp(-\chi' t)]$$ (12)

Integration is done after substituting the equation (12) into the equation (11). The stress of the cable is given by the equation (13), where σ_0 means the initial stress of the cable. The relaxation coefficient α_c can expressed by the equation (14).

$$\sigma(t) = E_c \varepsilon_{o0}(1 - \beta')[1 - \exp(-\chi' t)] + \sigma_0 \tag{13}$$

$$\alpha_c = (\sigma_0 - \sigma)/\sigma_0 \tag{14}$$

It is confirmed that the value of the relaxation coefficient α_c is almost the same when using the coefficient obtained from the experimental analysis or the tested result of a wire, though coefficient χ is different from the coefficient indicated in the equation (4) or (6) in a strict sense.

The test results on time dependent properties of the cable are shown in Fig.2.11 to 2.13 and Table 2.6. Creep and relaxation of the test piece No.1 became 0.93%, while those of the wire were 1.6% and 1.7% respectively. This is considering that a constant stress condition can not be kept during the test period, therefore causing a decrease of the cable stress compared to that of the wire, because the creep and relaxation properties were tested by the same device at the same time. Further, creep and relaxation properties of the wire are not always the same as that of a cable consisting of 55 wires.

Then, the relative comparison of the time dependent properties among these three test pieces is shown in Fig.2.14. The cable having a twisting angle of 3.5° had the equal time depending property as that of one with a twisting angle of 0°. The amount of creep and relaxation increased rapidly and became doubled when the twisting angle was beyond 7°. According to Ref.[16], the amount of creep of a locked coil rope is about 4.6%, that means creep of a locked coil rope is 5 times as large as that of the pre−coated parallel wire cable, having an equivalent twisting angle to the test piece No.2.

Creep property of the casting material, a zinc−copper alloy, of the socket is affected by the pressure inside the socket. Relation between the pressure and creep strain speed was experimentally examined, the pressure of 5 kgf/mm^2 (49 MPa) was considered to be creep limit for the zinc−copper alloy at the temperature of 50° C.

Creep of the pre−coated parallel wire cable can be estimated by the equation (15), here Δ_c is given by the tested result of the cable, 0.9%, or that of the wire, 1.6%.

$$\text{creep amount} = (2 \Delta_s + \Delta_c)/\Delta L_e \tag{15}$$

where, Δ_c : amount of creep of the cable alone

Δ_s : amount of slippage from the socket

After getting the amount of creep for the cable, relaxation can be calculated by the equations (11) and (12). Powers term of the equation (11) is converged into zero after a long period of time, then the amount of relaxation becomes the same as the creep amount. An estimation of creep and relaxation is made for a cable having a length of 100 m, 200 m and 400 m, using the condition of a stress of 64 kgf/mm^2 (628 MPa) and pressure of 4.5 kgf/mm^2 (44 MPa). The effect of the amount of slippage from the socket becomes smaller as the cable lengthens, because the slippage property is almost constant regardless of the cable length. When the cable length is 400 m, the amount of creep and relaxation is estimated between 1.2 to 1.9% respectively.

2.5 Conclusion

The results obtained by the study in Chapter 2 are summarized as follows.

(1) A newly developed cable, the pre—coated parallel wire cable, had the same static properties as those of a parallel wire strand. The pre—coated parallel wire cable is different from conventionally twisted wire rope, such as a locked coil rope, in its lay structure. The cable has no crossing points in the wires along the entire length, this lay structure is considered to be the key point in contributing to static performance of the pre—coated parallel wire cable. And at the same time, a slight lay given to the cable improves handleability such as reeling on the drum without seriously damaging the structural performance.

(2) The breaking strength and modulus of elasticity were tested for the cable having various twisting angles. It was confirmed experimentally and analytically that these static properties of the cable remained unchanged from the designated value when the twisting angle was less than 3.5°. The breaking strength of the cable is considered to be equal to that of the assembled wires having the same number. And the modulus of elasticity of the cable was more than the designated value of 20,000 kgf/mm^2 (196 GPa), being the same as that of an individual wire.

(3) The rotational torque of the pre—coated parallel wire cable is far smaller than that of common stranded wire ropes, but it is better to take some measures to restrain it during erection.

(4) The amount of creep and relaxation of a galvanized wire of 7 mm in diameter was 1.6% and 1.7% respectively, under the design stress condition of 64 kgf/mm^2 (628 MPa) and at normal temperature. The property of a galvanized wire of 7 mm in diameter was almost the same as that of one 5 mm in diameter.

(5) The amount of creep and relaxation of the pre—coated parallel wire cable became about 1% respectively, a little smaller than that of a wire. Examining the effect of the twisting angle on the creep and relaxation properties of the cable, it was confirmed that a twisting angle of 3.5° for the cable did not affect the time dependent characteristics.

(6) The amount of creep and relaxation of slippage from the socket was investigated at the same time. Taking into consideration the creep and relaxation properties of the casting material, a zinc—copper alloy, the influence of the socket becomes less as the cable lengthens. In the case of a long cable being 400 m in length, the creep and relaxation of the cable are estimated from 1.2% to 1.9% respectively.

2.6 References

[1] N.J.Gimsing, Cable Supported Bridge, 1983, pp.57—69.

[2] Japan Society of Civil Engineers, Steel Cable—Stayed Bridges *, 1990, pp.136.

[3] T.Hojo, Y.Sakamoto and T.Eguchi, Structural Characteristics of NEW PWS for Cable—Stayed Bridges, IABSE Seminar on Cable—Stayed Bridges, Bangalore, India, 1988, pp. III 214—224.

[4] Y.Tawaraya, T.Hojo, Y.Sakamoto, T.Eguchi and I.Tsuchida, Development of NEW PWS for Cable—Stayed Bridges and Its Practical Application, Nippon Steel Technical Report, No.42, 1989, pp.1—11.

[5] Y.Sakamoto, T.Eguchi, T.Hojo, T.Komura and K.Wada, Study on Creep and Relaxation of A Pre—Coated Cable for Cable Stayed Bridges *, Bridge and Foundation Engineering, Vol.26, No.3, 1992, pp.27—32.

[6] Honshu—Shikoku Bridge Authority, Examination on Cables of Suspension Bridges *, 1978, pp.91—100.

[7] T.Endo, K.Tada and H.Ohashi, Development of Suspension Bridges: Japanese Experience with Emphasis on the Akashi Kaikyo Bridge, Proc. of Cable—Stayed and Suspension Bridges, Deauville, France, 1994, pp.55—66.

[8] M.Yasuda, T.Takeyama and M.Nozawa, Design and Fabrication of Stay Cables for The Iwakorojima Bridge *, Honshi Technical Report, No.39, 1986, pp.12—19.

[9] T.Tottori, T.Kawazoe and K.Yoshikawa, Galvanized Cable Wire and Prefabricated Parallel Wire Strand, Nippon Steel Technical Report, No.8, 1976, pp.63—72.

[10] K.Wada, Y.Tawaraya and T.Hojo, Fabrication of Stay Cables for The Yokohama Bay Bridge, Bridge Engineering *, Vol.25, No.10, 1989, pp.7—13.

[11] Nikkan Kogyo Shinbun, Wire Rope Handbook *, 1995.

[12] Y.Tawaraya, T.Hojo, S.Konno and T.Eguchi, Structural Characteristics of NEW PWS for Cable—Stayed Bridges, Nippon Steel Technical Report, No.37, 1988, pp.68—76.

[13] R.H.Knapp, Derivation of A New Stiffness Matrix for Helically Armoured Cables Considering Tension and Torsion, International Journal for Numerical Methods in Engineering, 14, 1979.

[14] E.Watanabe, M.Nagasako, O.Yoshikawa, K.Okumura and M.Kurauchi, Full—Size Creep and Relaxation Tests on Steel Cables, International Conference on Cable—Stayed Bridges, Bangkok, 1987, pp.951—962.

[15] I.Finnie and W.Heller, Creep for Industrial Materials, Corona Publishing, 1980.

[16] Japan Steel Structure Corporation, Design and Construction Criteria for Structural Cables

* , Vol.19, 1983.

* Published in Japanese
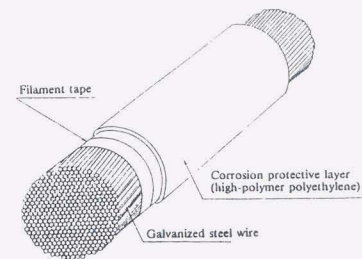
Fig.2.1   View of a pre–coated parallel wire cable

Photo.2.1   A pre–coated parallel wire cable

Table 2.1 Chemical composition of wire rod

unit:%

[SWRS82B]	C	Si	Mn	P	S	Cu
Composition	0.80-0.85	0.12-0.32	0.60-0.90	≤0.025	≤0.025	≤0.20

Table 2.2 Requirements for galvanized wire

		Requirements
Material Quality		Wire Rod : JIS G 3502, SWRS 77B ～ 82B
Size	Wire Diameter	7.00 ± 0.08 mm
	Diameter deviation	0.08 mm or less
Mechanical properties	Tensile Stregth	1,569 MPa ～ 1,765 MPa 160 kg/mm² and over to 180 kg/mm²
	0.7% Proof Stress	1,158 MPa 118 kg/mm² or more
	Elongation	4.0 percent or more
	NOS. of Twists	12 times or more
	Coils	3d × 8 times
Zinc-Coating	Amount applied	300 kg/mm² or more
	Wire Diameter Increase	0.14 mm or less
	Coating Adhesion	5d × 2 times
	External Appearance	No damaging Scratches or defects
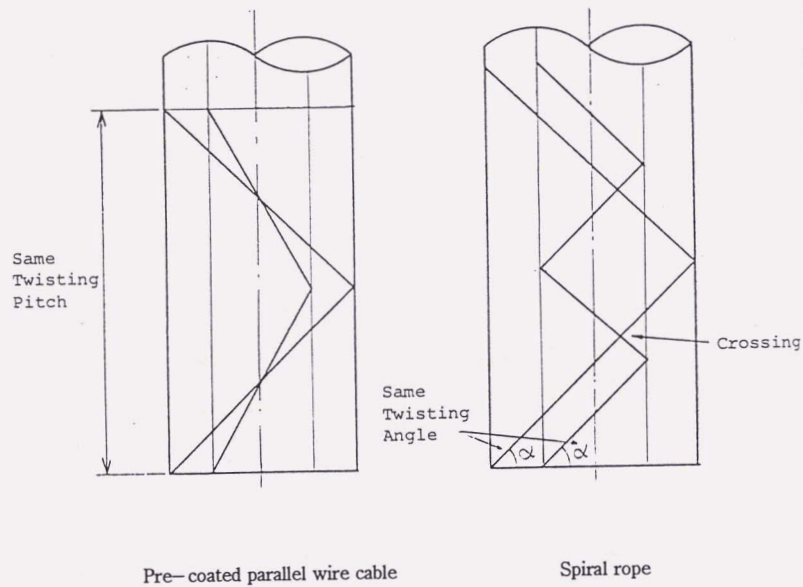
Fig.2.2 Difference in lay structure
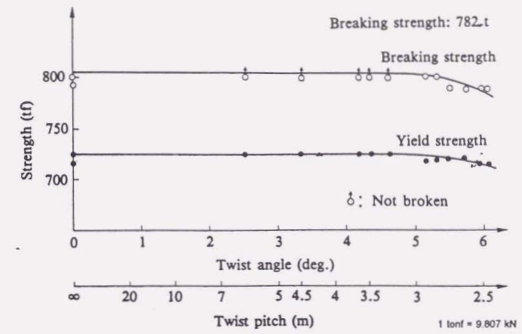
Fig.2.3 Relation between twisting angle and static tensile strength
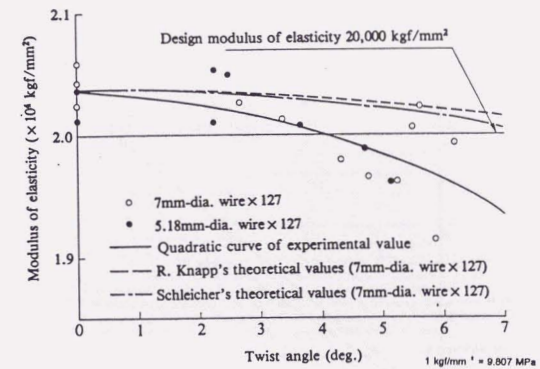
Fig.2.4 Relation between twisting angle and modulus of elasticity
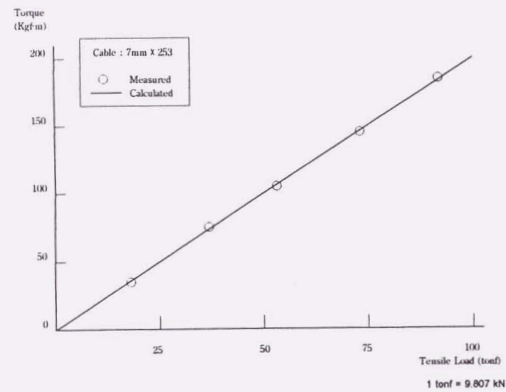
Fig.2.5   Relation between tensile load and rotational torque
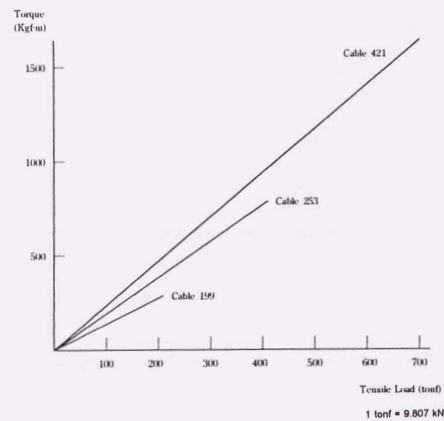
Fig.2.6   Relation between tensile load and calculated rotational torque

Table 2.3   Tensile test results of parallel wire cables

	Cable size (Wire diam in mm × No. of wires) N: No. of specimens	Breaking load A (Specified) (t)	Measured breaking load C (Mean) (t)	C/A	Breaking strength efficiency $\alpha = \dfrac{\text{Measured breaking load}}{\text{Mean tensile strength of wire } \sigma_B \times \text{Cross-sectional area of cable}} \times 100(\%)$	
					σ_B (kgf/mm^2)	$\alpha(\%)$
1	5.04×91(PPWS)N=48	290	304.8	1.05	167	100
2	5.17×127(PPWS)N=2	427	454.0	1.06	168	100
3	5.00×169(PPWS)N=4	520	548.4	1.05	166	99.6
4	5.00×217(PPWS)N=1	682	695	1.02	166	98.3
5	5.00×271(PPWS)N=1	851	892	1.05	168	99.8
6	7.00×91(PPWS)N=1	560	580	1.04	165	100
7	7.00×109(NEW PWS)N=3	671	712.7	1.06	171	99.4
8	7.00×109(NEW PWS)N=6	671	723.0	1.08	173	99.6

1 kgf/mm^2 = 9.807 MPa

1 tonf = 9.807 kN

Table 2.4   Tensile test results of large-sized pre-coated parallel wire cables

	Case 2: 7-mm wire diam × 421 wires	
No.	1	2
Specified breaking load A*¹ (t)	2592	2592
Calculated breaking load B*² (t)	2811	2811
Measured breaking load C (t)	2771	2743
C/A	1.07	1.06
C/B	0.99	0.98
Slippage of front bearing type socket (mm)	8	11
Elongation at fracture*³ (mm)	234	188
Fracture location	Parallel wire section	Parallel wire section

*¹ Specified breaking load: 160 kgf/mm^2 × Cross-sectional area of cable
*² Calculated breaking load: Tensile strength of wire × Cross-sectional area of cable
*³ Elongation at fracture: Elongation of cable under measured breaking load
Slippage of each rear bearing-type socket was approximately 10 mm.

1 tonf = 9.807 kN
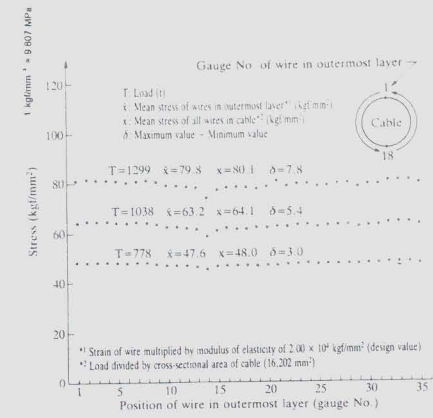
Fig.2.7　Stress distribution of wires in outermost layer
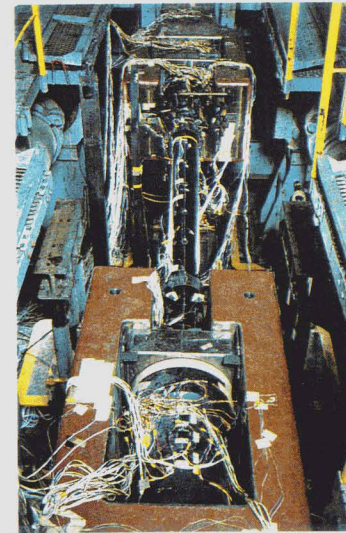
Photo.2.2　Tensile test of a pre−coated parallel wire cable
composed of 421 7mm−dia. wires
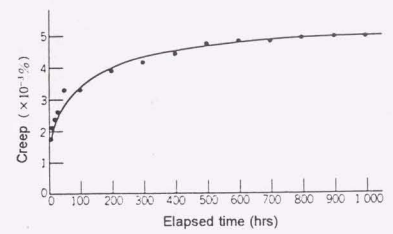
Fig.2.8   Creep of galvanized steel wire 7 mm—dia.
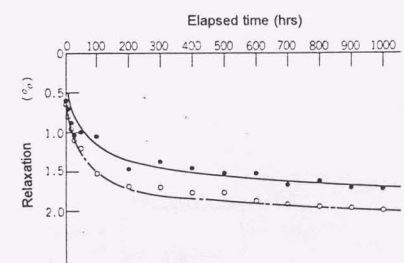
Fig.2.9   Relaxation of galvanized steel wire 7 mm—dia.

Table 2.5 Test specimens and test conditions

	No. 1 θ =0 deg.	No. 2 θ =3.5 deg.	No. 3 θ =7.0 deg.
Initial tension (tf)	131.5	132.4	129.4
Initial stress (kgf/mm^2)	62.1	62.6	61.1
Elastic modulus (kgf/mm^2)	20200	20100	19400
Initial slippage (mm)	2.1	2.2	2.1
α	0.9646	0.9675	0.96
β	1.0321	1.0391	1.0512
κ (/hr)	0.006275	0.006187	0.006112
Total relaxation (%)	3.54	3.25	4
Total creep (%)	3.21	3.91	5.12
Slippage (mm)	0.77	1.01	1.16
Relaxation (%)	0.93	0.93	1.78
Creep(%)	0.93	0.93	1.78

1 kgf/mm² = 9.807 MPa
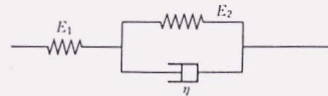
Fig.2.10   Time dependent model for analysis
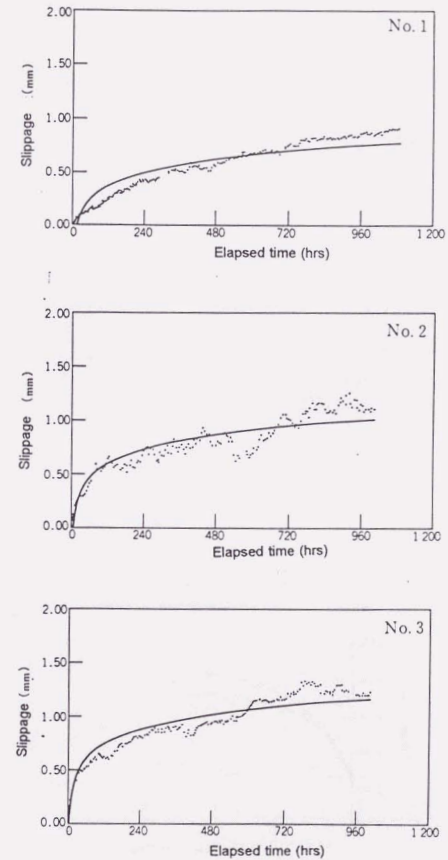
Fig.2.11   Relation between slippage and elapsed time
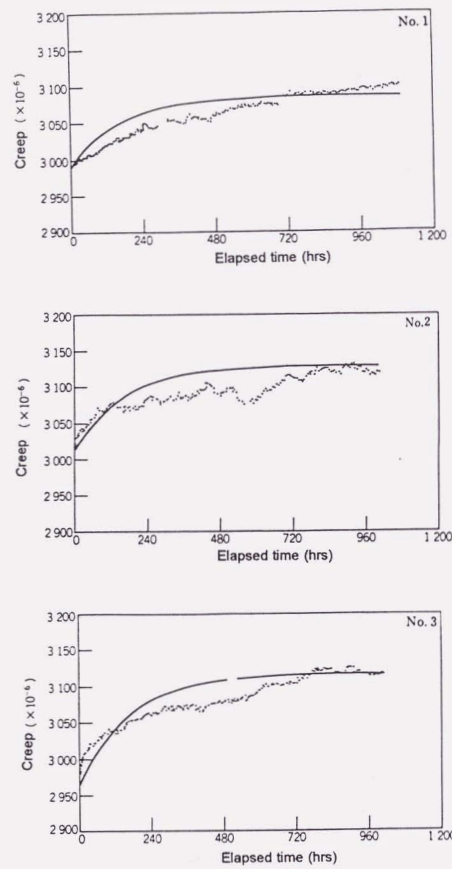
Fig.2.12 Relation between creep and elapsed time

1 tonf = 9.807 kN
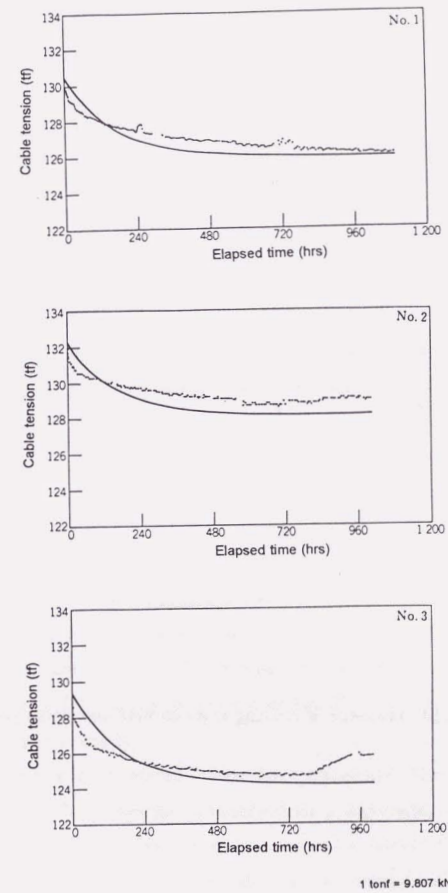
Fig.2.13 Relation between cable tension and elapsed time

Fig.2.14 Influence of twisting angle on time dependent properties

CHAPTER 3   A CABLE SOCKET WITH HIGHER STATIC AND FATIGUE STRENGTH

3.1 Introduction

The end terminals of cables are generally anchored by sockets. A socket is designed so as not to decrease the breaking strength of the cable itself. When cables have become larger, end fittings for larger cables are also required. Under the breaking load of a large cable of more than 2,000 tonf (19,600 kN), the end fitting is about three times stronger than that of a parallel wire strand that has ever been used for cable—stayed bridges. But it remains unclear whether the conventional design method for a socket guarantees sufficient strength to support a breaking load of a larger cable. Therefore, the design method for a large socket had to be examined in order to realize a large—sized fabricated cable.

Stay cables of long cable—stayed bridge are subjected to the fluctuation of the axial stress in cables due to the live load, such as vehicles or trains. The tensile fatigue strength of a cable is also determined by the fatigue strength of a socket portion. For this reason, a socket having a higher fatigue strength is absolutely required for stay cables of long cable—stayed bridges. A zinc—copper alloy cast socket is widely used in Japan. The fatigue strength of wires for a parallel wire strand, having a breaking strength of 160 kgf/mm^2 (1,569 MPa) class, is 40—45 kgf/mm^2 (392—441 MPa) [1]. When a zinc—copper alloy is cast, the fatigue strength of a strand becomes about 15 kgf/mm^2 (147 MPa) [2]. The reduction of fatigue strength is mainly considered to be caused by the heat of casting metal at the entrance of the socket, requiring a pouring temperature of about 460 ° C. And fretting corrosion occurring between the wires and cast metal at the entrance of the socket is another reason in decreasing fatigue strength [3]. In the case of the socket, these factors had to be eliminated in order to improve fatigue strength.

Recently, a stay cable of cable—stayed bridges has suffered from bending vibration due to wind [4]. A large amplitude is sometimes observed on a stay cable, which would raise a serious problem to the design of a cable, especially a socket. Countermeasures to control the vibration have been carried out, because this vibration can cause bending fatigue near the cable sockets according to its amplitude. It is desirable to understand the bending fatigue strength of bridge cables in order to judge whether the suppressing measures are required or not. Particularly, there were little data concerning an allowable bending fatigue strength of a parallel wire strand, and this important matter has been left unsolved so far. Therefore, the
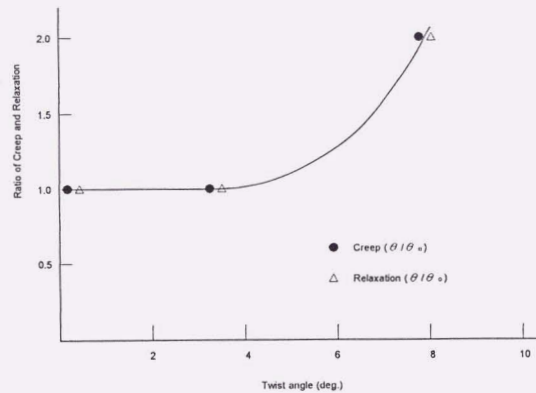
bending fatigue strength of a cable related to the bending angle had to be examined.

It was absolutely necessary to develop a new socket having a higher static and fatigue strength for a large cable. And the bending fatigue strength of the socket also had to be examined in order to apply it to long cable—stayed bridges.

In this chapter, a new design method for a socket and the end fitting of the pre—coated parallel wire cable are discussed and the tested results of a newly developed socket are described.

First, the design method applied to a conventional socket cast with zinc—copper alloy is described [3]. To examine a design method for a large scale socket, tensile tests of a large sized cable are carried out [5]. It is indicated that the breaking strength of the cable is affected by the thickness of the socket wall, and a new design method for a large socket is examined taking into consideration the ultimate strength [6].

Next, the fatigue strength of a socket is studied. Fundamental data for fatigue strength of a cable are examined using galvanized steel wires of 7 mm in diameter [7], and the fatigue strength of the galvanized steel wire is shown compared with that of one 5 mm in diameter. After analyzing the factors that affect fatigue strength of the socket, a new design method to improve fatigue strength is presented [3]. It is shown that a new socket is cast by a composite—filler of epoxy resin and zinc—copper alloy, and that wire configuration in the socket is required in order to determine the radius of curvature of the wire and the space between the wires. Fatigue tests are conducted using a newly developed socket. Based on the tested results, it is shown that the socket has a higher fatigue strength than that of a conventional one. Fatigue tests are also carried out using cables being twisted by several different angles, the effect of the twisting angle on the fatigue strength of the socket is investigated [8].

Then, the bending fatigue properties of the socket relating to the bending angle are examined using bending fatigue tests of the cable [9]. Through the bending fatigue tests, secondary stress at the entrance of the socket is compared with that of a conventional socket, and the effect of epoxy resin cast in the entrance of the socket is studied. The bending fatigue tests are carried out at three million cycles at most, and locations along the cable where wires break in the test pieces are investigated. Finally, based on the tested results, the bending fatigue strength at the socket of the cable is presented.

3.2 A New Design Method for A Large—Sized Socket

3.2.1 Design method for conventional socket

The design method applied to conventional sockets cast with zinc—copper alloy is given as follows [10]:

a) Bond length must be sufficient to prevent extraction of a single wire.

$$l = t \cdot d / 4B \tag{1}$$

where,   d : diameter of wire

t : tensile strength of wire

B : bond strength of alloy

l : required socket length

b) The maximum pressure, σ_M, must not be greater than the allowable compressive stress determined primarily from the creep properties.

$$\sigma_M = T \cdot \cos\rho / A \cdot \sin(\theta + \rho) \tag{2}$$

where,   T : design load of the cable

A : effective contact area of the zinc—copper alloy cone

θ : taper angle of socket wall

ρ : friction angle between the socket and alloy cast

c) The tensile stress of the socket, shown in Fig.3.1, is not greater than the allowable stress.

$$\sigma_\theta = \sigma_M (b^2 + a^2) / (b^2 - a^2) \tag{3}$$

where, σ_M : internal pressure

a : average internal radius

b : average external radius

The design method was applied to conventional sockets for small—diameter cables such as the parallel wire strand of suspension bridges, and no particular problems occurred so far. However, the following two limitations of the conventional design were considered when it was applied to large sockets.

A three-axis stress acts on the socket cone, consisting not only of a hoop stress but also of a radial stress and a stress in the direction of the cable axis. Therefore, it is inadequate to check the stress using only the equation (3). If the combined stress due to the three components is evaluated using a formula of combined stress, it is often found that the total stress is beyond the allowable stress even though the hoop stress is within limits.

The conventional method of design does not take into account the strength required under ultimate conditions. As long as the design method aims to guarantee against breakage, it is necessary to consider the ultimate strength beyond the elastic range, but the conventional method of elastic design lacks consideration of this point.

3.2.2 Tensile test on large-sized sockets

The tensile breaking test of the cable was carried out mainly to examine the strength characteristics of the large-sized socket [5]. The pre-coated parallel wire cable used in the test consisted of 421 wires of 7 mm in diameter, the same specimens as already mentioned in paragraph 2.3.2. Cables in each case were fixed by three types of sockets shown in Table 3.1. In Cases 1 and 2, thin walled front-bearing sockets designed by the conventional method were used. The front-bearing type socket of Case 3 had an increased wall thickness, as compared with that of Cases 1 and 2. The wall thickness of the rear-bearing type sockets in both Cases was determined by checking the local stress at the corner using the Finite Element Method.

Table 3.2 shows the tested results including the cable breaking load, the position and the elongation of the cable failure. In Cases 1 and 2, a thin walled front-bearing socket and a rear-bearing socket were used, satisfying the specific value, but these were within a small margin of the lower limit. Slippage in the thin walled front-bearing sockets was about 50 mm. In addition, the failures were concentrated in a particular location near the entrance of the socket only in the thin walled front-bearing type and this breakage pattern has not been seen in conventional small-sized sockets before. The efficiency of the cable breaking strength was reduced by 4%.

On the contrary, in Cases 3 and 4, of thick walled front-bearing sockets, slippage in the socket was about 10 mm and the efficiency of the cable breaking strength was only reduced by 1 to 2%. The breakage point of the cable was scattered along the portion where the wires were parallel in the cable. There was no breakage concentration at any particular location in the socket, unlike in Cases 1 and 2.

The elongation of the cable at the breaking load was 2.8 to 3.5% in Cases 1 and 2, (where a thin walled front-bearing socket was used), which was about half the elongation of the wire,

5 to 6%, and below its specified value of 4%. On the other hand, in Cases 3 and 4, (where a thick walled front-bearing socket was tested), the elongation was 5.5 to 6.8%, which was equal to that of individual wires, and satisfied the specified value.

3.2.3 Discussion on design method for a large-sized socket

Under the breaking load, most of the thin walled front-bearing sockets became plastic up to the outer surface, and expanded by a few millimeters (or increased in radius) [5]. These factors were considered responsible for the increase in the slippage of the zinc-copper alloy cone, concentration of fracture within the socket, and a decrease of about 4% in the breaking strength efficiency. After the test, the thin walled socket was dismantled and the cable failure position was investigated. The wires were found to have been deformed locally where the fracture was concentrated. The wires in the region were considered to have reached a critical strain to be broken, while the elongation of the cable at rapture was thought to have declined by 2 to 3% compared with that of the single wire.

When thick walled front-bearing and rear-bearing sockets were used, the stress in the socket was mostly under the yield stress despite the localized plasticization of the socket, and the socket deformation was a very small 0.2 to 0.3 mm. Thus, the slippage of the zinc-copper alloy cone was a small 10 mm, and the breaking strength efficiency was high. The static strength characteristics of the cable under the breaking load were governed by the rigidity of the socket (defined as t_m/D_m described later). If the socket had some degree of rigidity under the breaking load, it could be expected to have a breaking strength efficiency comparable to those experimental results in Table 3.3.

It was presumed from the tensile test results that the zinc-copper alloy cone slippage, breaking strength efficiency and fracture pattern were closely related to each other. To examine the relationship, a model test was conducted paying attention to socket rigidity. The model test results helped to confirm the phenomena that the slippage of the zinc-copper alloy cone increased with a thin walled or low rigidity socket at the failure of the cable, that the fracture was concentrated in the socket, and that the breaking strength efficiency decreased with increasing slippage ΔZ. The relationship between breaking strength efficiency and slippage is shown in Fig.3.2.

Based on the above-mentioned phenomena, the slippage of the zinc-copper alloy cone was elasto-plastically analyzed to the analytical flow shown in Fig.3.3. The relationship between the slippage of the zinc-copper alloy cone and the type and rigidity of the socket is shown t_m/D_m (defined as the mean wall thickness of the socket, t_m, divided by the mean diameter of the zinc-copper alloy cone D_m). The slippage of the zinc-copper alloy cone

was considered as the sum of a component due to the deformation of the socket and a component due to the compressive deformation of the zinc−copper alloy cone. In Fig.3.3, $\triangle D_m$ is the change in the mean diameter of the zinc−copper alloy cone in a given position, $\triangle R_m$ is the change in the mean diameter of the socket in the same position, and θ is the taper angle of the inside wall of the socket. The analyzed results closely agreed with the test results as shown in Fig.3.4 and confirmed being effective to calculate the slippage according to the flow indicated Fig.3.3.

The theoretical analysis results of three types of sockets are shown in Fig.3.5. With the socket material used in the tensile test, it can be estimated that the slippage of the zinc−copper alloy cone steeply increases and the breaking strength efficiency of the cable decreases when socket rigidity (t_m/D_m) of the front−bearing socket falls below 0.22 to 0.23. The t_m/D_m ratio is 0.165 for front−bearing socket in Cases 1 and 2 in the tensile test. This means that the breaking strength efficiency of the cable largely depends upon socket rigidity, and that the conventional elastic design method did not suffice for larger sockets.

The rear−bearing of a socket had a small zinc−copper alloy slippage in the same way as in the tensile test and was sensitive to the relationship between the socket rigidity and zinc−copper alloy slippage. The back−fixed socket was lower in rigidity than that of the front−bearing type, and did not appreciably decline in zinc−copper alloy slippage. This is probably because the rear−bearing type of socket has positive axial and hoop stress, being favorable yield conditon compared with the front−bearing socket. Consequently deformation of the socket is small.

3.2.4 A new design method for a large−sized socket

The analyzed results indicate that it is particularly important to design the socket with adequate rigidity when the front−bearing type socket is used [6]. If a conventional method of the allowable stress against the design load alone is applied to that of a large socket, the breaking strength efficiency of the cable decrease as noted above. Thus, it is necessary to introduce a new design method that can estimate the ultimate state of the socket considering the slippage of a zinc−copper alloy cone and socket deformation under the breaking load of the cable.

A new proposed method of design for socket cone requires two steps of verification, following a) and b), to overcome the limitation associated with the conventional design method previously mentioned. In this new method, the length of the alloy cone is calculated by the conventional method. A new method is shown as follows:

a) Checking the stress at the cable design load

The cable design load means the load obtained by multiplying the cross−sectional area of the cable by the allowable stress of each wire. While a conventional design method considers only the hoop stress, this new method takes into account the axial stress, the radial stress occurring in the socket and the hoop stress, as shown in Fig.3.6, thus checking the combined stress using the equations (4) and (5).

$$\sigma_{eq} = \frac{1}{\sqrt{2}} \sqrt{(\sigma_r - \sigma_\theta)^2 + (\sigma_\theta - \sigma_z)^2 + (\sigma_z - \sigma_r)^2} \tag{4}$$

where, σ_r : radial stress

σ_θ : hoop stress

σ_z : stress in the axial direction

$$\sigma_{eq} \leqq \sigma_a \tag{5}$$

where, σ_a : allowable stress of the socket cone

b) Checking the socket rigidity at the ultimate strength

The ultimate strength means the condition defined by the specified value of the cable breaking load. In order to restrict the amount of slippage in the zinc−copper alloy cone at the ultimate strength to a small value, the concept of socket rigidity t_m/D_m is introduced. This check can be done using Fig.3.7, which is obtained by the analysis. And the socket rigidity should not fall below the required value at the yield stress (specified value) of the socket materials.

3.3 Fatigue Strength of A New Fatigue−Resistant Socket

3.3.1 Fatigue strength of a 7 mm galvanized wire

To examine the fatigue properties of galvanized wires of 7 mm in diameter, fatigue tests were carried out using the wires specified by HBS, having a tensile strength of 160 kgf/mm^2 (1,569 MPa)[11]. Fig.3.8 shows typical test results for the wires varying the stress ratio (R= $\sigma_{min}/\sigma_{max}$), the higher the stress ratio, the lower the stress range.

Referring to this figure, it can be considered that endurance fatigue limit of the wire is more than about 40 kgf/mm^2 (392 MPa), if the stress ratio, R, is less than 0.7. Under the

condition of minimum stress of 50 kgf/mm ^{2} (490 MPa), endurance stress amplitude, $\Delta \sigma$, is about 42 kgf/mm ^{2} (412 MPa). It is indicated that the fatigue strength of a galvanized wire of 7 mm in diameter has the same fatigue strength as that of one 5mm in diameter.

In order to compare HBS with the actual fatigue strength of the wire, the Goodman Diagram is shown in Fig.3.9. From the figure, it is recognized that the actual wire is expected to exhibit a much higher fatigue strength than the defined one.

3.3.2 Fatigue strength of zinc−cast sockets

Zinc−copper cast sockets are widely used for parallel wire strands of suspension bridges and for other ropes such as locked coil ropes and helically stranded ropes [10]. A zinc−copper alloy is used as the casting material because the alloy is considered most suitable for the following reasons; 1) It is excellent in creep and mechanical properties, 2) It has good adhesion to steel wires, and 3) It is relatively easy to cast, but its melting point is high.

Fatigue of sockets means that the cable has been subjected to a certain fluctuation of stress [1,12,13], the cable undergoes fatigue failure at the socket. As a result of the fundamental research so far carried out, the following findings have been obtained as to the factors of the fatigue of sockets. These factors are considered correlated.

a) Influence of fretting corrosion

Fretting corrosion is a special frictional phenomenon that occurs in areas undergoing very small reciprocating friction or a repetition of friction when a metal surface is pressed against another metal or nonmetal surface. Corrosion occurs and oxide metal powder adheres to the contact surfaces. Further, fatigue failures may occur under some stress conditions. Side pressures act on the front side of the socket due to the bending of the wires, and fretting corrosion occurs between the wires or between the wires and the cast metal [14]. This reduces fatigue strength (see Fig.3.10, 3.11 and 3.12).

b) Influence of bending

The results of the fatigue tests reveal that wire breakage occurred mainly in the bends of the wires at the entrance of the socket. The fatigue strength decreased as the bending curvature of the wire became smaller, and many wires broke when the radius curvature of the wire was 250 mm or less (in the case of a wire of 5 mm in diameter). Secondary stress was generated in the wires due to bending, and the side pressure increased. The decrease in fatigue strength was considered to be caused by these reasons.

c) Influence of temperature

Casting was carried out at a temperature of 460 $^\circ$ C $\pm$ 10 $^\circ$ C in order to cast the alloy into small spaces between the wires in the socket, that decreased fatigue strength due to the effect of temperature, as shown in Fig.3.13.

From the mentioned above, fatigue−resistant sockets were required to have the following characteristics, and the composite−filler type socket shown in Fig.3.14 was found to be excellent. The main features are as follows;

1) The filling material should be high in fretting corrosion resistance. An epoxy resin of good castability was selected so that even the entrance of the socket with only small spaces between the wires could be filled with the resin.

2) By increasing the radius of curvature of the wires in the entrance of the socket, stress concentration on the wires should be prevented and, at the same time, side pressure should be reduced.

3) The influence of temperature should be avoided at the entrance of the socket which is subjected to the stress concentration of the wires.

4) The wires should be fitted by the conventional zinc−copper alloy, because it is a reliable material judging from the applied results.

3.3.3 A new design method for a fatigue−resistant socket

In designing this composite−filler type socket, it is necessary first to find an equation of wire configuration, and then to determine the radius of curvature of the wire, the space between the wires, using this equation [3]. Therefore, the following examinations can be conducted.

(1) Equation of wire configuration

The curvature of the wires in the socket was given using two forming plates. The equation of wire configuration for the wires bent as illustrated in Fig.3.15, is given as follows.

$$\text{Curvature,} \quad y = C_1 x^3/6 + C_2 x^2 + C_3 x + C_4 \tag{6}$$

Span E to F	Span F to G
$x_1 = 0$ and $y_1 = 0$	$x_2 = 0$ and $y_2 = \delta$
$x_1 = 0$ and $y_1' = 0$	$x_2 = b$ and $y_2 = \delta$
$x_1 = a$ and $y_1 = \delta$	$x_2 = b$ and $y_2'' = 0$

Continuous condition

$x_1 = a, \quad x_2 = 0$ and $y_1' = y_2'$

$x_1 = a, \quad x_2 = 0$ and $y_1'' = y_2''$

From the above, the equation of wire configuration between E and F is given by

$$y = \frac{\delta}{a^2(3a+4b)} \left(3(3a+2b) - \frac{2}{a}(3a+b)x \right) x^2 \tag{7}$$

(2) Radius of curvature of wire

The radius of curvature of the wire is determined from (1) above.

$$\frac{dy}{dx} = \frac{6\delta}{a^2(3a+4b)} \left((3a+2b) - \frac{1}{a}(3a+b)x \right) x \tag{8}$$

$$\frac{d^2y}{dx^2} = \frac{6\delta}{a^2(3a+4b)} \left((3a+2b) - \frac{2}{a}(3a+b)x \right) \tag{9}$$

The radius of curvature, R, is given by

$$R = \frac{\left[1 + \left(\frac{6\delta}{a^2(3a+4b)} \right)^2 \left((3a+2b) - \frac{1}{a}(3a+b)x \right)^2 x^2 \right]^{3/2}}{\left| \frac{6\delta}{a^2(3a+4b)} \left((3a+2b) - \frac{2}{a}(3a+b)x \right) \right|} \tag{10}$$

From $dy^2/dx^2 = 0$, the inflection point is given by the following equation:

$$x_c = \frac{a(3a+2b)}{2(3a+b)} \tag{11}$$

(3) Radius of curvature at the entrance of socket

The radius of curvature is minimal at the entrance of the socket (starting point of bending). From $x = 0$,

$$R_0 = \frac{a^2(3a+4b)}{6\delta(3a+2b)} \tag{12}$$

(4) x−coordinate having an arbitrary radius of curvature

The position in the x−coordinate having an arbitrary radius of curvature is determined by solving the following equation:

$$\left[1 + \left(\frac{6\delta}{a^2(3a+4b)} \right)^2 \left((3a+2b) - \frac{1}{a}(3a+b)x \right)^2 x^2 \right]^{3/2}$$
$$- R_e \left| \frac{6\delta}{a^2(3a+4b)} \left((3a+2b) - \frac{2}{a}(3a+b)x \right) \right| = 0 \tag{13}$$

The socket length and epoxy−filled length can be calculated using these equations discussed above, following steps are adopted; 1) Calculate the socket length using condition of strength, 2) Check the configuration of wires which have the net spaces more than 1.5 mm, and 3) Check the radius of cuvature at the epoxy−filled point.

The cast length is determined by calculation of the stress of the cast metal, and then, the net spaces between wires, $\triangle y$, is examined by calculation of the wire configuration. Here the narrowest space between wires that permits sufficient penetration of zinc−copper alloy and ensures sufficient bond is empirically set at 1.5 mm or more. The epoxy resin is filled into the region $\triangle y$ being 1.5mm or less. Next, the epoxy−filled length is checked by determining a position that satisfies the radius of curvature, R, at the entrance of the socket. From the results of fundamental experiments, the radius of curvature at the entrance of the socket, R_0, and that of epoxy−zinc boundary part, R_e, are fixed as follows:

$$R_0/d \geq 100 \tag{14}$$
$$R_e/d \geq 200 \tag{15}$$

where,   R : radius of curvature (mm)

d : diameter of wire (mm)

3.3.4 Fatigue strength of a new fatigue—resistant socket

Some factors, such as effects of wire socketing, wire bundling and wire length errors, can be considered to reduce the fatigue strength of a cable [13,14]. Among them, wire socketing is considered the greatest factor affecting the fatigue strength of a cable. To examine the fatigue strength of the composite—filler socket, the tensile fatigue tests were conducted using the pre—coated parallel wire cable of various sizes, including purely parallel ones. The main tested results are shown in Table 3.4. All tested data are indicated in Fig.3.16, where non—dimensional stress range, S, is used [17]. S is given as follows:

$$S= (\sigma / \sigma_u)\{1-(\sigma_m/ \sigma_u)^2 \}$$ (16)

where, σ : stress range
           σ_u : ultimate strength
           σ_m : mean stress

The tested results explain the following fatigue properties of the socket. First, fatigue strength of the socket, $\Delta\sigma$, can be estimated from 20 to 30 kgf/mm^2 (196—294 MPa), being about a half of that of a galvanized wire, however, it was higher than that of a conventional socket. Secondly, ruptured parts of the wires were not concentrated at the entrance of the socket but scattered along the portion where wires were parallel in the cable. The chances of the first wire rupture can occur equally both in the cable and in the socket section, this means that the socket section has a fatigue strength no less than that of the cable section. There was little effect of twisting angle on the fatigue strength of the cable when it is less than 4 degrees.

Analyzing the data of the first wire rupture and that of non—rupture, S—N curve for the socket can be described by the following equations:

$$\log N= 10.56- 3.35 \cdot \log \Delta\sigma \qquad (N \leq 1.08 \times 10^6)$$ (17)
$$\Delta\sigma = 22.4 \qquad\qquad (N > 1.08 \times 10^6)$$ (18)

Consequently, the fatigue endurance limit for the socket, $\Delta\sigma$, can be estimated at 22.4 kgf/mm^2 (220 MPa). And based on the tested results, 5% probability of rupture for the socket can be calculated 31.3 kgf/mm^2 (307 MPa), which is considered sufficient from a practical point of view.

3.4 Bending Fatigue Strength of A New Fatigue—Resistant Socket

3.4.1 Outline of the bending fatigue test

To examine the bending fatigue properties of the pre—coated parallel wire cable with the new socket, bending fatigue tests were carried out. The specimens used for the test are shown in Fig.3.17 and Table 3.5. The composite—filler sockets, cast epoxy resin and zinc—copper alloy, were fixed to the end of all cables, except for specimen No.9. Using specimen No.9, effects of the epoxy resin in the socket on the secondary stress and bending fatigue strength were investigated, then one side was filled with only the zinc—copper alloy.

In the testing process, the strain gauges were attached to the surface of the cable in order to measure secondary stress of the wires caused by bending deformation, and a static bending test was conducted before the bending fatigue test. While the cable tension was given initially, the secondary stress and vertical displacement of the cable by the bending deformation were measured during the test. The relationship between the vertical displacement and the bending angle was defined as the next equation. The bending fatigue test conditions are shown in Table 3.6.

$$\theta_b = \tan^{-1}\{ \delta_c /(L_c /2)\}$$ (19)

where, θ_b : bending angle
           δ_c : vertical displacement at the center of the cable
           L_c : supported span length of the cable

3.4.2 Secondary stress of the cable

When vertical displacement is given to a cable, axial stress by axial force occurs, and additional axial stress by vertical displacement, a bending stress by the cable's bending and by wire's bending in the cable occur [11,18,19]. The total strain was measured, which consisted of above mentioned components. The strain generated by additional tension is considered to be an average strain in the cable. In this test, secondary stress was calculated by multiplying the difference between the average strain of the cable obtained after bending and the upper or lower side strain of the cable by modulus of elasticity of the wire, 20,000 kgf/mm^2 (196 GPa). But residual stress caused by wire slippage in the bending cable was neglected.

The secondary stress distribution along the cable is shown in Fig.3.18. The epoxy resin in the socket had a great influence on the secondary stress of the cable. When a socket was filled with the epoxy resin, the maximum secondary stress occurred at the entrance of the

socket, and it decreased as it approached the boundary of the zinc—copper alloy. In the case of a socket without epoxy resin, the maximum secondary stress occurred at the boundary of the zinc—copper alloy. And the maximum stress in the cable was greater than that of the epoxy filled socket, for example it was about 1.4 times as much as that of the epoxy filled one. This reason was that the epoxy resin in the socket was considered to be supported elastically by the wire displacement. It was found that the secondary stress in the cable at a distance of 1 m from the socket disappeared and it could be neglected.

The relationship between the secondary stress and bending angle is shown in Fig.3.19. The secondary stress calculated from the Wyatt method, regarding a cable as a round bar, is given by the equation (20). And from the equation obtained by a least squares method based on the tested results, the secondary stress can be expressed by the equation (21).

$$\sigma = 2\theta_b \sqrt{E\theta_t} \tag{20}$$

where, σ_b : secondary stress

θ_b : bending angle (rad)

E : modulus of elasticity : 20,000 kgf/mm^2 (196 GPa)

σ_t : axial stress

$$\sigma = 19.2 \cdot \theta_b \tag{21}$$

where, σ_b : secondary stress

θ_b : bending angle (rad)

The secondary stress calculated from the equation (21) gives a rather small value compared to that of the equation (20). It can be explained as follows. The equation (20) regards a cable as a round bar that neglects wire slippage, but in an actual cable, it can not be neglected, and that the boundary condition of the equation (20) is different from the elastic support using epoxy resin. The equation (21) is considered to be sufficient for the pre—coated parallel wire cable with the composite filler socket from a practical point of view.

Fig.3.20 shows the relationship between measured and calculated values of the cable vertical displacement for various cable tension. The displacement of the cable was analyzed using the finite deformation theory. The bending rigidity of the cable was only about 15 to 20% of that of a round bar having the same diameter.

3.4.3 Bending fatigue strength of the socket

The bending fatigue test results are shown in Fig.3.21. From the figure, the cable with sockets can be estimated to have a bending fatigue strength of $\pm\,0.6\,°$ at two to three million cycles.

The S—N curve for the socket is indicated in Fig.3.22, (non—dimensional stress range S is used), because the influence of the initial tensile stress can be eliminated. In the figure, the same definition is used as that of the tensile fatigue test except for the definition of average stress, σ_m, expressing the sum of the initial tensile stress and additional tensile stress when bent.

The bending fatigue endurance limit of the socket became 0.18 of the non—dimensional stress range. This is just between the S value of 0.131 and 0.225, which are similar results to the tensile fatigue test of the socket. The bending fatigue strength of the socket seems to be related to the tensile fatigue strength. A further study is required to discuss the correlation between them.

After the bending fatigue test, the breaking point of the cable was surveyed. For specimens No.2 and 5, the wire broke at the center of the cable, (clamping point), while for the others it occurred inside the socket. It was considered that unusual side pressure affected the clamping point, which caused the wire breakage in specimens No.2 and 5. In the case of the tensile fatigue test, wires ruptured scattered along the cable entirely, but for the bending fatigue test, rupturing was concentrated inside the socket, being 20 to 50 mm from the entrance of the socket. The wire breakage occurred mainly at the upper and lower side of the cable section. The wire rupturing was concentrated at the boundary of the zinc—copper alloy, where the maximum secondary stress in the wire occurred.

In the bending fatigue test the maximum secondary stress occurred inside the socket near the entrance, while in the static bending test, it occurred at the boundary of the zinc—copper alloy. The reason for this difference is considered as follows. The cable near the socket was fastened and restrained by a polyethylene coating, as will be mentioned in the next chapter. When repeated displacement was given to the cable, the temperature of the polyethylene coating on the cable increased, causing a decrease in the fastening force in the polyethylene coating. As a result, the maximum secondary stress occurred in the epoxy resin inside the socket, which had a higher modulus of elasticity. The relationship between the breaking point and the place where the maximum secondary stress occurred was analyzed using the Finite Element Method, proving the tested result.

3.5 Conclusion

The results obtained by the study in Chapter 3 are summarized as follows.

(1) A new design method for a large—sized socket was developed. When a socket becomes larger in size, the design method applied to a conventional socket comes to be insufficient, because various stress conditions and the rigidity of the socket cone are not taken into account. It is required to consider the combined stress such as the axial stress and the radial stress in addition to the hoop stress, and to check the socket rigidity at the ultimate strength in order not to decrease the breaking strength efficiency of the cable.

(2) The tensile test was carried out using a large—sized cable consisting of 421 wires of 7 mm in diameter to examine the design method. The result of the tensile tests confirmed that the large—sized cable had the same breaking efficiency at the socket as the small ones had, when the new design method was adopted. Thus, the new design method made it possible to put a large—sized cable with a socket having a breaking strength of more than 3,000 tonf (29,400 kN) to practical use.

(3) A new fatigue—resistant socket having a composite—filler consisting of an epoxy resin and zinc—copper was developed. It was required to control the wire configuration in the socket and to fill it with a good castability material in order to eliminate the affecting factors that decrease the fatigue strength of the conventional socket, such as influence of fretting, bending and casting temperature

(4) The tensile fatigue tests were conducted to examine the fatigue strength of the pre—coated parallel wire cable with the new socket, including purely parallel ones. It was found that the socket had a higher fatigue strength of about 25 kgf/mm^2 (245 MPa), and that there was little influence of the twisting angle on the fatigue strength of the cable when it was less than 3.5 degrees.

(5) It was found that a socket using an epoxy resin had the effect of decreasing the secondary stress at the entrance of the socket compared with that of the conventional socket cast by a zinc—copper alloy. In the case of the socket, the maximum secondary stress occurred at the entrance of the socket, but it was only about 60% of that of the conventional one.

(6) Judging from the bending fatigue tests, the cable with the sockets can be estimated to have a bending fatigue strength of ± 0.6 ° at two to three million cycles. The bending fatigue endurance limit of the socket was considered to be 0.18 of a non—dimensional stress range, which was about the same value of that of the tensile fatigue strength.

3.6 References

[1] Honshu—Shikoku Bridge Authority, Examination on Cables of Suspension Bridges * , 1978, pp.91—100.

[2] I.Mitsujima, T.Nishi and T.Shinke, Fatigue Strength of Cable Wire , Kobe Steel Engineering Report, Vol.25, 1978, pp.58—63.

[3] Y.Tawaraya, T.Sugita, S.Konno, H.Otani, T.Hojo and M.Yano, Development of Fatigue—Resistant Sockets, Nippon Steel Technical Report, No.19, 1982, pp.121—132.

[4] National Land Development Technology Research Center, Report on Study of Wind Resistance of Cables in Cable—Stayed Bridges * , 1989, pp.14—34.

[5] Y.Tawaraya, T.Hojo, Y.Sakamoto, T.Eguchi and I.Tsuchida, Development of NEW PWS for Cable—Stayed Bridges and Its Practical Application, Nippon Steel Technical Report, No.42, 1989, pp.1—11.

[6] T.Komura, K.Wada, H.Takano and Y.Sakamoto, Study into Mechanical Properties and Design Method of Large Cable Sockets, Proc. of JSCE No.422, I —14, 1990, pp.133—144.

[7] Nippon Steel Corporation, Test Report on 7mm Galvanized Wire for Cable—Stayed Bridges * , 1980.

[8] T.Hojo, Y.Sakamoto and T.Eguchi, Structural Characteristics of NEW PWS for Cable—Stayed Bridge, Proc. of IABSE Seminar on Cable—Stayed Bridges, Bangalore, India, 1988, pp. III 13—25.

[9] Y.Sakamoto, T.Hojo, T.Eguchi and M.Yano, A Study on Secondary Stress and Fatigue Life in Bending of A Pre—Coated Cable for Cable—Stayed Bridge * , Proc. of JSCE Vol.446, I —19, 1992, pp.215—223.

[10] Japan Steel Structure Corporation, Standard of Cable Materials for Structures * , Vol.19, 1978.

[11] M.Yasuda, T.Takeyama and M.Nozawa, Design and Fabrication of Stay Cables for The Iwakurojima Bridge * , Honshi Technical Report, No.39, 1986, pp.12—19.

[12] K.Hironaka and Y.Ohishi, Fatigue Properties of Parallel Wire Strand(1) * , Proc. of JSCE Annual Conference, I —328, 1977, pp.629—630.

[13] K.Hironaka and Y.Ohishi, Fatigue Properties of Parallel Wire Strand(2) * , Proc. of JSCE Annual Conference, I —92, 1978, pp.176—177.

[14] V.G.Rehm, Draft—Fachzeitschrift, No.4, 1977.

[15] A.Matsukawa, M.Kamei, Y.Fukui and Y.Sasaki, Fatigue Analysis of Parallel Wire Strand Cable under Consideration of Influencing Factors * , Journal of Structural Engineering, Vol.31A, 1985, pp.327—340.

[16] A.Matsukawa, M.Kamei, T.Mizoguchi and Y.Sasaki, Fatigue Analysis of Parallel Wire Strand Cables Based on the Statistical Theory of Extremes *, Journal of Structural Engineering, Vol.32A, 1986, pp.619—630.

[17] S.Nakamura and H.Hosokawa, A Study on the Fatigue Design of Parallel Wire Strands on Cable—Stayed Bridges, Proc. of JSCE, No.410, I —12, 1989, pp.157—166.

[18] T.A.Wyatt, Secondary Stress in Parallel Wire Suspension Cable, ASCE, ST7, 1960, pp.37—59.

[19] Y.Tanaka, H.Nagai, T.Haraguchi and S.Komatsu, The Secondary Bending Stress of Parallel Wire Cables *, Journal of Structural Engineering, Vol.35A, 1989, pp.15—25.

* Published in Japanese
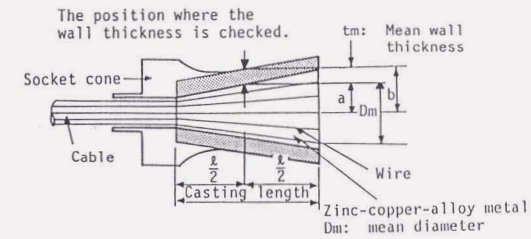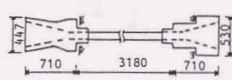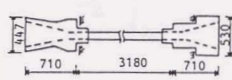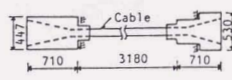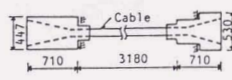
Fig.3.1 Typical dimensions of socket

Table 3.1 Socket types used in the test

Note: Material quality of socket; S45C　　　　　　　　　　　(Unit: mm)

Table 3.2   Breaking test results

Case		1	2	3	4
Tensile strength of wire		167.0 kgf/mm²	167.0 kgf/mm²	173.5 kgf/mm²	173.5 kgf/mm²
Breaking load	Specified value A*	2,592 tf	2,592 tf	2,592 tf	2,592 tf
	Calculated value B**	2,706 tf	2,706 tf	2,811 tf	2,811 tf
	Measured value C	2,610 tf	2,598 tf	2,771 tf	2,743 tf
C/A		1.01	1.00	1.07	1.06
C/B		0.96	0.96	0.99	0.98
Slippage	Front-bearing type socket	48 mm	56 mm	8 mm	11 mm
	Rear-bearing type socket	11 mm	8 mm	8 mm	7 mm
Failure position		Concentrated on the front face of zinc-copper alloy	Concentrated on the front face of zinc-copper alloy	Parallel section of wires	Parallel section of wires
Elongation of cable at breaking load		3.5%	2.8%	6.8%	5.5%

Notes: *; 160.0 kgf/mm²(1,569 MPa) x cross-sectional area of cable
       **; tensile strength of wire x cross-sectional area of cable

1 tf = 9.807 KN
1 kgf/mm²= 9.807 MPa

Fig.3.2   Relation between braking strength efficiency and slippage

Table 3.3   Results of breaking tests

Test specimen N: Number of specimens	Breaking load A (specified value) (tf)	Measured breaking load C (mean) (tf)	C/A	$\alpha = \dfrac{\text{Measured breaking load}}{\sigma_B \times \begin{array}{c}\text{Cross-sectional}\\\text{area of cable}\end{array}} \times 100(\%)$ where, σ_B : tensile strength of wire (mean value)	
				σ_B (kgf/mm²)	α (%)
5.04 x 91 N=48	290	304.8	1.05	167	100
5.17 x 127 N=2	427	454.0	1.06	168	100
5.00 x 169 N=4	520	548.4	1.05	166	99.6
5.00 x 217 N=1	682	695	1.02	166	98.3
5.00 x 271 N=1	851	892	1.05	168	99.8
7.00 x 91 N=1	560	580	1.04	165	100
7.00 x 109 N=3	671	712.7	1.06	171	99.4
7.00 x 109 N=6	671	723.0	1.08	173	99.6

1 tf=9.807 kN,   1 kgf/mm²=9.807 MPa

Fig.3.3   Analytical flow for slippage of zinc—copper alloy cone
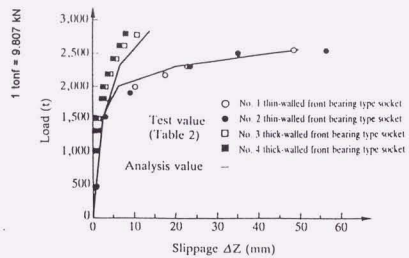
Fig.3.4 Analyzed results of slippage

Fig.3.6 Position for checking stress and rigidity

Fig.3.5 Relation between socket rigidity and slippage
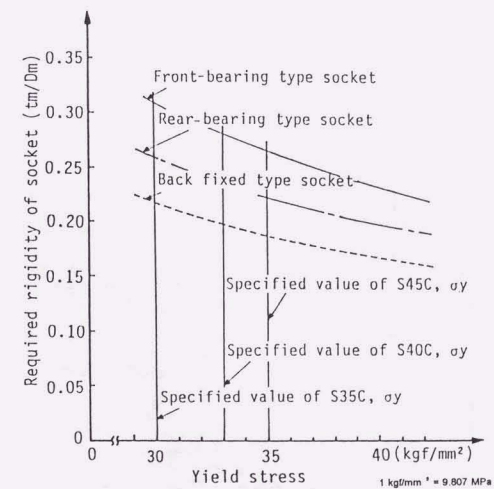
Fig.3.7 Relation between yield strength and required socket rigidity
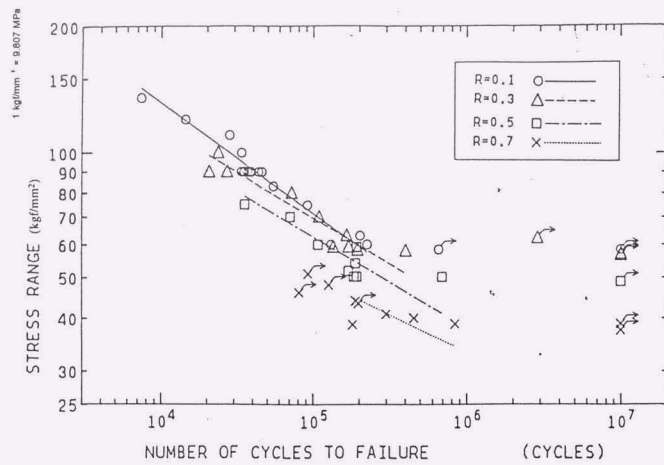
Fig.3.8　Fatigue strength of a 7 mm galvanized wire
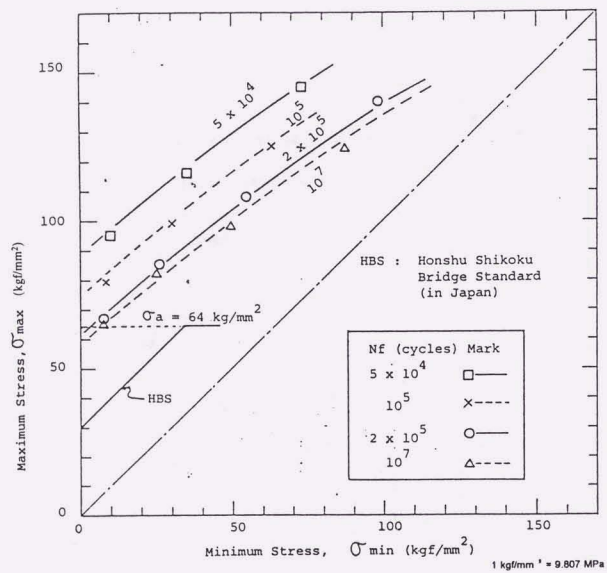
Fig.3.9　Goodman Diagram for a 7 mm galvanized wire
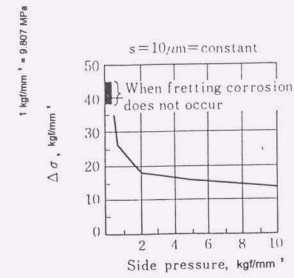
Fig.3.10　Relation between side pressure and fatigue strength
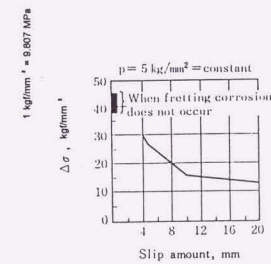
Fig.3.11　Relation between slippage and fatigue strength
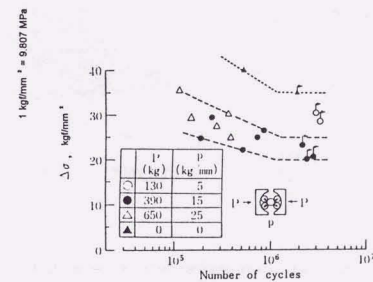
Fig.3.12　Relation between side pressure and fatigue strength

$1\ kgf/mm^2 = 9.807\ MPa$
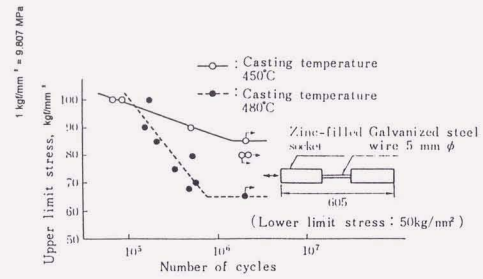
Fig.3.13 Influence of temperature on fatigue strength

Fig.3.15 Wire configuration in the socket

Fig.3.14 Composite—filler type socket

Table 3.4 Tensile fatigue test results

No.of wires	stress ranges	mean stress	S	cycles (x10⁴)	percentage of broken wires and broken parts
139	196	529	.141	200	0.7% inside socket
139	196	529	.141	500	0%
139	245	505	.174	225	2.2% inside socket
139	294	480	.207	100	6.6% inside/outside socket
139	294	480	.207	103	8.6% inside socket
127•	196	529	.141	504	0%
127•	196	529	.141	206	0%
127•	245	505	.174	210	2.4% inside socket
127•	245	505	.174	244	2.4% inside socket
127•	343	456	.239	52	1.6% outside socket
91•	294	480	.207	200	1.1% outside socket

• Indicates test data carried out previously[1]
Wires are all 7 mm diameter. Unit of stresses is MPa
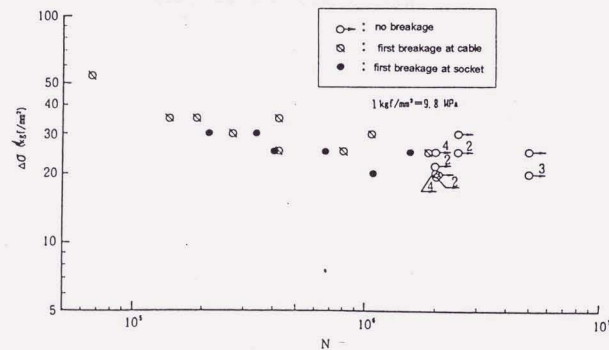
Fig.3.16 Tensile fatigue test results

Table 3.5 Dimensions of specimens for bending fatigue test

Specimen No.	Cable size	Sectional area (mm²)	Lo (mm)	Lc (mm)	Ls (mm)	L₁ (mm)	Do (mm)	Ds (mm)
1	7 × 31	1193	1640	2380	370	272	54	256
2	7 × 31	1193	1640	2380	370	272	54	256
3	7 × 85	3271	5426	6000	450	287	81	280
4	7 × 139	5349	5426	6000	532	287	106	280
5	7 × 139	5349	5426	6000	532	287	106	280
6	7 × 139	5349	5426	6000	532	287	106	280
7	7 × 139	5349	5426	6000	532	287	106	280
8	7 × 139	5349	5426	6000	532	287	106	280
9	7 × 139	5349	5426	6000	532	287	106	280
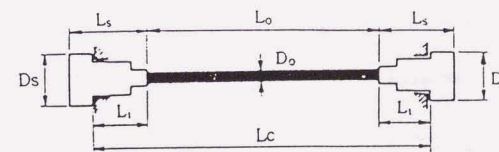
Fig.3.17 Specimen for bending fatigue test

Table 3.6 Bending fatigue test conditions

Specimen No.	Cable tension (t f)	Cable stress (kgf/mm²)	Vertical disp. (mm)	Bending angle (deg.)	Test speed (Hz)
1	76.4	64.0	± 8.0	± 0.5	6.0
2	76.4	64.0	± 8.0	± 0.5	6.0
3	307	93.8	± 31.5	± 0.6	1.7
4	285	53.3	± 63.0	± 1.2	0.9
5	300	56.1	± 42.0	± 0.8	1.4
6	300	56.1	± 31.5	± 0.6	1.5
7	305	57.0	± 52.5	± 1.0	1.0
8	320	59.8	± 37.0	± 0.7	1.6
9	305	57.0	± 73.5	± 1.4	0.8

1 tf = 9.807 KN
1 kgf/mm² = 9.807 MPa

Fig.3.19 Relation between secondary stress and bending angle

Fig.3.18 Secondary stress distribution
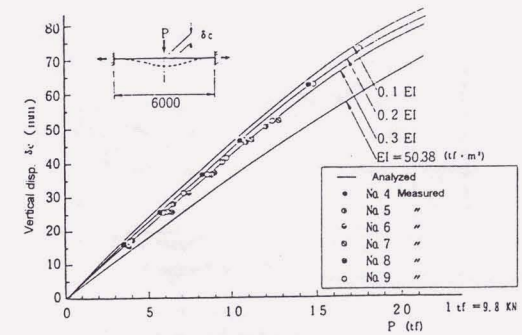
Fig.3.20 Bending rigidity of a cable

Fig.3.21　Bending fatigue test results

Fig.3.22　Bending fatigue strength

CHAPTER 4　CORROSION−PROTECTIVE COAT FOR A LARGE−SIZED CABLE

4.1　Introduction

Long cable−stayed bridges require cables with high mechanical properties and excellent corrosion resistance at the same time. A long cable−stayed bridge is usually designed to have a longer period of service, for example, more than a period of 100 years. Corrosion protection for a stay cable is considered to be one of the most important factors in the durability of cable−stayed bridges [1]. The corrosion protection system of a stay cable depends on cable types. A painting system is used for a locked coil rope, a plastic covering for a parallel wire strand, and a polyethylene with mortar injection for a parallel wire cable. These systems have several problems when applied to a stay cable of a long cable−stayed bridge of a multi−cable type.

The fundamental method for protection against corrosion is to galvanize wires [2]. The wires of a helically stranded rope such as a locked coil rope are generally galvanized today, since the use of an ungalvanized wire for a stay cable reduced the durability of the cables [1]. A wire of a locked coil rope is galvanized with a zinc weight of about 300 g/m ^{2}. The surface of a locked coil rope is usually painted. However, corrosion protection by painting requires maintenance at short intervals, that is undesirable for a long cable−stayed bridge of a multi−cable type.

Parallel wire strands are protected against corrosion by a glass fiber reinforced plastic covering after installation, which is quite similar to that of the main cable of suspension bridges [3]. When a parallel wire strand is wound on a drum, it flattens and snakes around the drum. That makes it difficult to apply corrosion protection in a shop. This system needs expansion joints on a cable in order to adjust the expanding difference due to change of temperature or live load between a steel cable and the plastic covering. The expansion joint has a disadvantage for corrosion protection, because water can penetrate the cable from the joint part, this causes corrosion of cables. Besides, scaffolding is required under all cables in order to install a plastic covering at the site, that is too laborious for a long cable−stayed bridge of a multi−cable type.

A pipe made of polyethylene or steel is attached around a parallel wire cable and cement mortar is injected inside the pipe. With this system the wires are generally ungalvanized. This is a similar protective method against corrosion as that used for the prestressed wire of
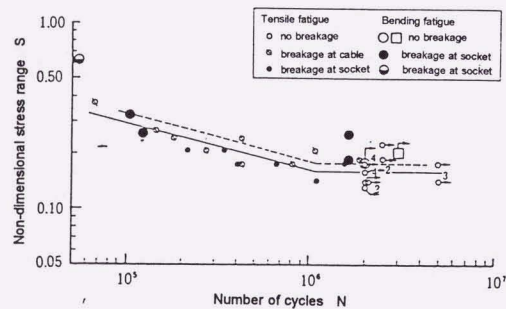
prestressed concrete. A polyethylene pipe can be reeled on a drum, that makes it possible to prefabricate it in the shop. As cable length becomes longer, problems related to injection work arise. The injection height depends on the injection material of the cement mortar or the injection pressure. As the height difference for one injection is usually limited to less than 25 m, it requires many injections to complete the corrosion protection work at the site for long stay cables. Stress cracking of polyethylene due to the environment and live load occurs if an excessive hoop stress occurs during the injection procedure [4]. Furthermore, the mortar that is injected may possibly crack off because of a live load or wind induced vibration.

Concerning these problems, a new corrosion protection system which has the following characteristics is required for a large—sized cable of a multi—cable type;

   a) A double corrosion system using galvanized wires is required.

   b) It should have excellent weathering durability for a long period.

   c) It should be prefabricated in a shop in order to eliminate corrosion—protecting work at the site.

   d) It should have easy handling characteristics including reeling and unreeling.

In this chapter, studies on a corrosion protective layer of a pre—coated parallel wire cable are discussed.

The parallel wire cable is extrusion—coated with polyethylene as a protection against corrosion (Photo 4.1). First, the physical properties of polyethylene coating for the cable are described [5]. The mechanical properties such as tensile strength and modulus of elasticity are measured for various temperatures, because polyethylene is a temperature dependent material [6,7]. Polyethylene is a polymeric material, subject to the effect of environmental factors, environmental stress cracking resistance is also checked. The weathering durability of polyethylene is analyzed using an accelerated weathering test in relation to the amount of carbon black addition.

The structural properties of a polyethylene—coated cable are investigated, because the coated polyethylene has an extrusion—induced shrinkage stress in it. The friction force caused by shrinkage stress is analyzed using a full—sized specimen. End treatment of the polyethylene—coated cable is also tested to examine the corrosion protective system at the socket. Then, installation characteristics of a polyethylene—coated cable such as unreeling and clamping are examined to establish the usage of the cable [8]. Various data with respect to installation characteristics are shown [9].

4.2 Material Properties of Polyethylene for A Pre—Coated Parallel Wire Cable

4.2.1 Physical properties of polyethylene

The wires of the cable are coated with $300g/m^2$ of zinc as a primary protection against corrosion [2,10,11]. Considering the severe environments, the surface of the cable is extrusion coated with polyethylene to improve resistance against corrosion.

Polyethylene is extensively used as the protective coating of electrical wires and cables [12]. It is a kind of thermoplastic and visco—elastic material. Material of this type changes in performance with a slight change in molecular weight and molecular structure, and it is susceptible to temperature and other environmental conditions with the use of additives. It has to be accurately characterized in order to apply it to a stay cable. High—density polyethylene that meets the requirements of JIS K6748 Class—3 Grade—1 was selected as the optimum protective coating material for the cable. The physical properties of high—density polyethylene are given in Table 4.1.

To study the strength characteristics of the polyethylene coating, specimens were cut from the coated polyethylene of the cable and the temperature dependent properties of tensile yield strength and tensile strength were tested. The results are given in Fig.4.1. The tensile modulus of elasticity, shown in Fig.4.2, is determined over an elongation range of 0 to 1%. No difference of mechanical properties was found between high—density polyethylene in the virgin state and those specimens cut from the coated polyethylene of the cable. The tested data, shown in Fig.4.1 and Fig.4.2, are used for the mechanical properties required for the design of the end terminal of the cable.

Polyethylene, a polymeric material, is subject to the effects of water, ultraviolet radiation and other environmental factors. Those indicate a possibility of lessening fracture strength and thus developing cracks on the surface, which lead to a brittle failure after some time. In the case of the cable, the shrinkage stress remaining in the coated polyethylene integrates the coat with the internal strand. The cable is also subjected to stress developed under a live load, such as elongation due to tension applied to the coated polyethylene or temperature change in the coated polyethylene.

A thorough study was made for the environmental stress cracking resistance of high—density polyethylene by considering stress concentration due to eccentricity and damage, because it was applied to bridges having a long service period. As a result, a high—density polyethylene, that has been satisfactorily performed for over 1,000 hours of testing by the method specified in JIS K6760, was selected as coating material for the cable. Approximately 500 hours of crack—free testing are said to correspond to 30 ∼ 50 years of

environmental stress cracking resistance, although a clear correlation has not been established between the test time and the actual service period.

4.2.2 Weathering durability of high−density polyethylene

The protective coating of the cable is a principally high−density polyethylene, which is uniformly blended with carbon black to improve its weathering durability [13,14]. The effect of added carbon black to high−density polyethylene was measured in an accelerated weathering test conducted with a weatherometer. The results are shown in Fig.4.4. High−density polyethylene deteriorates with decreased retained elongation within 1,000 hours when the carbon black addition was 0 to 1%. When the carbon black addition was 1% or more, no deterioration was observed even after 5,000 hours, suggesting that good weathering durability over a long period can be expected.

According to the above−mentioned results of the accelerated weathering test, 2.5 ± 0.5% of carbon black was blended into the coated high−density polyethylene to maintain a long period of service. A polyethylene coating thickness of about 1 mm is sufficient from the viewpoint of weathering durability, but the coating thickness was set over a range of 5 to 10 mm according to the cable size considering the case of winding on reels and handling during erection.

4.3 Structural Properties of Polyethylene−Coated Cable

4.3.1 Friction force of polyethylene−coating

The cable and polyethylene coating are considered to expand and contract relatively to each other because they are different in material and the polyethylene coating has extrusion−induced shrinkage stress in it. Because of the shrink stress in the polyethylene coating of the cable, a full−sized specimen of a polyethylene−coated cable, shown in Fig.4.5, was tested to examine the change in the shrinkage (shrinkback) of the polyethylene coating. The polyethylene coating was cut away in a ring at the mid point of the specimen and the increase in the opening of the ring was measured over about 500 hours. The specimen was marked from the ring toward either end as shown in Fig.4.5, and shrinkback of the polyethylene coating was determined from the change in these marked intervals. The opening of the ring reached 6.5 mm after about 300 hours and it did not increase thereafter. The slipped length of the polyethylene relative to the cable was 1.5 to 2 m, judging from the change in the marked interval on the surface of the cable. The polyethylene coating and

cable were considered to expand and contract integrally with each other over the most of the total length.

The friction force developed between the cable and polyethylene coating by the shrinkage stress present in the coating was considered the main cause of the state mentioned above. Accordingly, the friction test shown in Fig.4.6 was conducted. The friction force was found to decrease exponentially with increasing temperature. This is presumably because polyethylene is a highly temperature−dependent material and the change in the circumferential shrinkage stress of the polyethylene is sensitive to temperature. No.5, 6 and 7 in Fig.4.6 refer to the sequence of No.4 test repeated to investigate the effect of temperature hysteresis. The frictional force was shown to recover to normal as the temperature fell.

The expansion and contraction of the polyethylene−coated cable and the factors involved were studied in a relatively short time under the constant environmental conditions discussed above. In view of the change with time of properties and service environment of the cable, the frictional force is expected to decrease more than shown in Fig.4.6, and the relative expansion and contraction of the polyethylene coating at the end are expected to increase more. The end termination of a polyethylene−coated cable described next is designed to retain sufficient strength even when the frictional force is completely lost after a long period of service.

4.3.2 End termination of a polyethylene−coated cable

The end termination of the cable is the point where the polyethylene coating and socket contact each other. This area constitutes a discontinuity in the corrosion protective system of the cable and has to be protected against water infiltration and other corrosive agents.

The cable−socket connection is sealed by a sleeve of heat−shrinkable polyethylene that is heated to shrink tightly onto the connection, as shown in Fig.4.7. This area must be water−resistant for corrosion protection and also be strong and stretchable against the axial force of the polyethylene coating. The heat−shrinkable polyethylene sleeve and polyethylene coating are provided with a sufficient length of adhesion to each other. In addition, the socket is provided on the outside surface with a projection of such a shape and size that stress concentration can be minimized and that the heat−shrinkable polyethylene sleeve can be completely prevented from slipping off the socket.

When the dead load and live load tension of the cable at the reference temperature of 20 ° C and the axial force generated in the polyethylene coating by heat variation are both directly transferred to the heat−shrinkable type polyethylene sleeve, then the axial stress is

calculated. The thickness of the polyethylene sleeve is designed so that its tensile yield strength is sufficiently higher than its axial stress. It was verified by various tests that the socket structure designed as described above had sufficient strength, stretchability and water resistance.

The stretching test result is shown in Fig.4.8. The heat—shrinkable polyethylene sleeve did not slide on the socket or polyethylene coating, and exhibited enough elongation where it was expected to stretch. The maximum load reached twice as high as the designed tension and thus it was confirmed that it had sufficient strength. The test result using a full—sized cable specimen shows that the heat—shrinkable polyethylene sleeve stretched where it was designed to do so.

Water immersion tests with and without a pressure of 1 atmosphere were conducted for six months to confirm water resistance. The connection point was found to have sufficient water resistance as no water infiltration was observed at the adhesive joint between the heat—shrinkable polyethylene sleeve and polyethylene coating.

4.3.3 Installation properties of a polyethylene—coated cable

When a polyethylene—coated cable is lifted or cable socket is put into a tower or main girder, the bending radius of the cable is likely to decrease locally. A bending test, shown in Fig 4.8, was carried out to examine the flexibility and other bending characteristics of the cable.

The test results are shown in Fig.4.9. The coated polyethylene showed no abnormal deformation such as buckling when it was bent up to the degree that the value of D/d (cable bending diameter/cable diameter) was 6.8. After the bending load was removed, the coated polyethylene returned to its original condition, leaving no harmful deformation. Thus, the coated polyethylene having a design thickness was bearable enough for bending loads likely to be applied during fabrication or installation. The bending stiffness of the pre—coated parallel wire cable measured from the relationship between load and bending stiffness is about 15% of the value when the entire cross section is effective.

It is necessary to examine the unreeling characteristics of a polyethylene coated cable in order to plan the erection equipment for the cable. An unreeling test was therefore performed using a full—sized polyethylene coated cable, composed of 421 wires, 7 mm in diameter (Photo.4.2). According to the test results, a force of 5 tonf (49 kN) was required to pull a large—sized cable from the reel and the unreeler needed a braking capacity of at least 5 tonf—m to prevent the cable from forming a loop of the reel. Since the cable has a high rigidity, it is desirable to prevent damage to the coated polyethylene of the cable by

synchronizing unreeling and pulling so that the movement of the cable in the reel can be minimized.

As the cable was unreeled from the reel, it swung off the line 500 to 600 mm. This deviation can be properly accommodated if rollers, about 1 m wide, were installed at intervals of 5 to 7.5 m. The swaying of the cable virtually disappeared when slight tension was applied to the unreeled cable, leaving no trace at all when the cable was erected. There may be cases where the layout of erection equipment requires a change in the direction of the cable unreeling. If the angle of the cable deflection is limited to 10 degrees or so, providing a vertical roller at an appropriate point, a solution to any unreeling problem involved was proved.

The coated polyethylene has to be gripped when the cable is unreeled or lifted for installation. The polyethylene coated cable requires a special clamp that positively transfers the pull force to the cable without damaging the coated polyethylene. After various tests, the design method of the clamp for the polyethylene coated cable was obtained. It is required to use a surface pressure of 50 kgf/mm^2 (490 MPa) and coefficient of friction of 0.15 for a design value. Table 4.2 shows the measured coefficients of friction between the polyethylene and clamp. One major advantage of the pre—coated parallel wire cable is that it can be handled like common wire ropes when suitable clamps are used.

In some cases, devices are attached to the cable to prevent cable vibration after installation. In this point, a creep test was conducted to study any long—term property of the polyethylene coated cable. The test results are shown in Fig.4.10. It was found that the creep property of clamped polyethylene coated cable showed generally the same trend as properties of polyethylene itself. Namely, the bolt axial force decreased by about 50% a day. According to the regression line based on measured values for 100 days, it is estimated that the residual axial force will be about 30% one year later, and about 25% 10 years later. Therefore, when the cable is clamped permanently, it is necessary to take into account its long—term property at the design stage.

4.4 Conclusion

The results obtained by the study in Chapter 4 are summarized as follows.

(1) A new protection system against corrosion using extruded polyethylene coating for a parallel wire cable was developed. The extrusion process was applied directly to the bundled cable in the manufacturing plant, that eliminated the need of corrosion protective coating work at the site. This protection system is considered to be a great advantage in the erection of stay cables of cable—stayed bridges, especially long ones.

(2) A high—density polyethylene of JIS K6748 Class—3 Grade—1 was selected as the optimum protective coating material for the cable after examining its corrosion—protective performance, mechanical properties and many other characteristics.

(3) To adopt polyethylene as a corrosion—protective layer, the weathering resistance of polyethylene was investigated in the first place. According to the accelerated weathering test results, it was confirmed that high—density polyethylene showed no deterioration after 5,000 hours when 1% carbon black was added. So, the parallel wire cable was covered with a high—density polyethylene blended with $2.5 \pm 0.5\%$ of carbon black.

(4) The mechanical properties of polyethylene were accurately studied by using cut specimens from the coating, and no significant difference of the properties was found compared to those of the virgin state. Environment stress cracking resistance of the polyethylene was also assured by the ESCR test of 500 hours.

(5) The structural properties of polyethylene coating were investigated and the relation between the coated polyethylene and the cable was analyzed. It was found that the friction force developed between the cable and polyethylene coating by the shrinkage stress present in the coating was considered the main cause of the coating system.

(6) The cable—socket connection was sealed by a sleeve of heat—shrinkable polyethylene that was heated to shrink tightly onto the connection. It was confirmed that the end termination of the cable using the heat—shrinkable polyethylene sleeve had sufficient protection against corrosion and prevented slippage off the socket.

(7) The installation properties of a polyethylene—coated cable were investigated to establish the usage of the cable. Various practical data with respect to installation properties, such as unreeling and clamping, were obtained.

4.5 References

[1] S.Watson and D.Stafford, Cables in Trouble, Civil Engineering, April 1988, pp.38—39.

[2] B.Birdsall, Brighter Future for Stay Cables, Civil Engineering, October 1988, pp.46—49.

[3] J.Durkee and G.Shaw, Plastic Cable Covering, Civil Engineering, February 1966, pp.63—67.

[4] D.Stafford and S.Watson, A Discussion of Critical Corrosion Problems in The Cable Elements of Stayed Girder Structures, Proc. of International Conference on Cable—stayed Bridges, Bangkok, 1987, pp.1048—1060.

[5] Y.Tawaraya, T.Hojo, Y.Sakamoto, T.Eguchi and I.Tsuchida, Development of NEW PWS for Cable—Stayed Bridges and Its Practical Application, Nippon Steel Technical Report, No.42, 1989, pp.1—11.

[6] Nikkan Kogyo Shinbun, Polyethylene Resins *, 1973.

[7] S.Okuda, Material Properties of Polyethylene, Material Testing *, Vol.8, No.73, 1960, pp.764—772.

[8] T.Hojo, Y.Sakamoto and T.Eguchi, Structural Characteristics of NEW PWS for Cable—Stayed Bridges, Proc. of IABSE Seminar on Cable—Stayed Bridges, Bangalore, India, 1988, pp. III 13—25.

[9] Y.Tawaraya, T.Hojo, S.Konno and T.Eguchi, Structural Characteristics of NEW PWS for Cable—Stayed Bridges, Nippon Steel Technical Report, No.37, 1987, pp.68—76.

[10] M.Yasuda, T.Takeyama and M.Nozawa, Design and Fabrication of Stay Cables for The Iwakorojima Bridge *, Honshi Technical Report, No.39, 1986, pp.12—19.

[11] K.Wada, Y.Tawaraya and T.Hojo, Fabrication of Stay Cables for The Yokohama Bay Bridge *, Bridge Engineering, Vol.25, No.10, 1989, pp.7—13.

[12] S.Kawawata and M.Kikkawa, Weathering of Some Plastics of Wire and Cable Applications *, Hitachi Hyoron, Vol.9, 1965, pp.63—72.

[13] Honshu—Shikoku Bridge Authority, Report on Fabrication, Transportation and Erection of Stay Cables for Cable—Stayed Bridge *, 1982.

[14] Institute of Electrical Engineers of Japan, Degradation of Polymers *, Corona Publishing, 1960.

* Published in Japanese
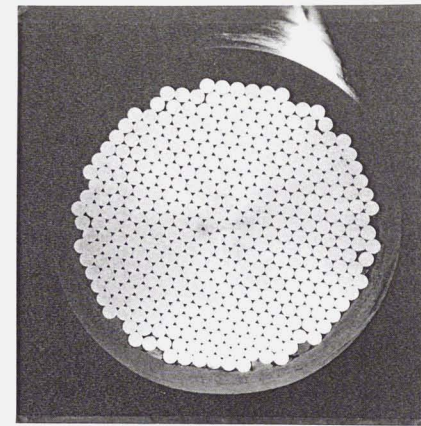
Photo.4.1   Cross section of a pre—coated parallel wire cable

Table 4.1   Physical properties of polyethylene

Porperty		Value
Density	(g/cm³)	$\geqq 0.942$
Melt flow rate	(g/10 min)	< 0.4
Tensile strength	(kgf/cm²)	$\geqq 200$
Elongation at tensile fracture	(%)	$\geqq 300$
Durometer hardness	(H_DD)	$\geqq 60$
Vicat softening point	(°C)	$\geqq 115$

1 kgf/cm² = 0.098 MPa
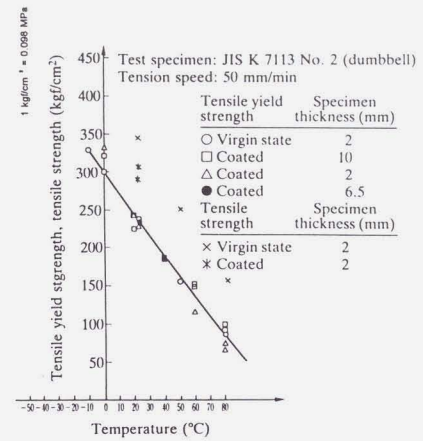
Fig.4.1 Effect of temperature on tensile yield strength of HDPE
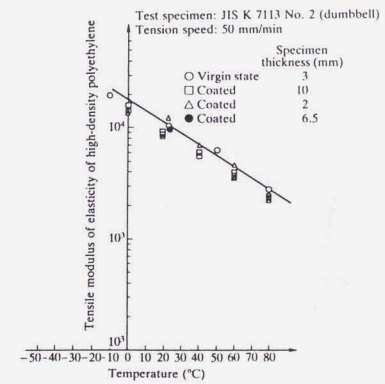
Fig.4.2 Tensile modulus of elasticity of HDPE
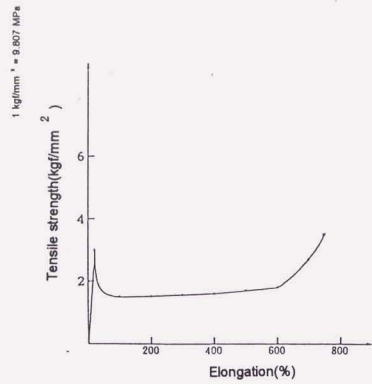
Fig.4.3 Stress—strain curve of polyethylene
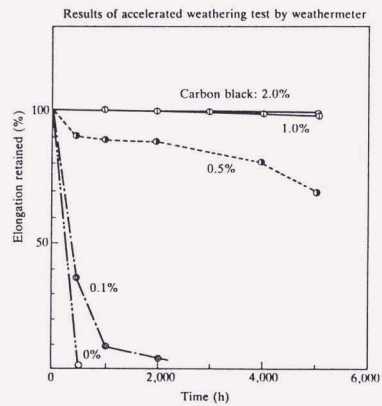
Fig.4.4 Effect of carbon black on weathering resistance of HDPE
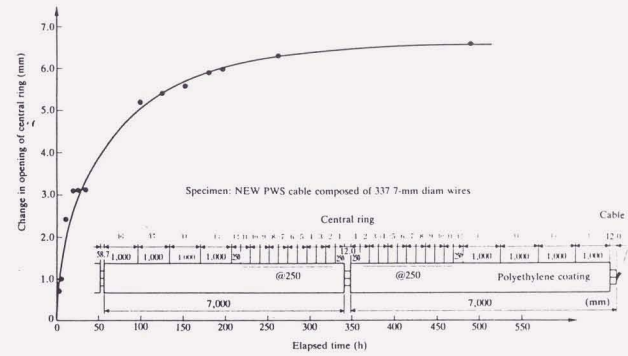
Fig.4.5 Shrinkback of polyethylene coating
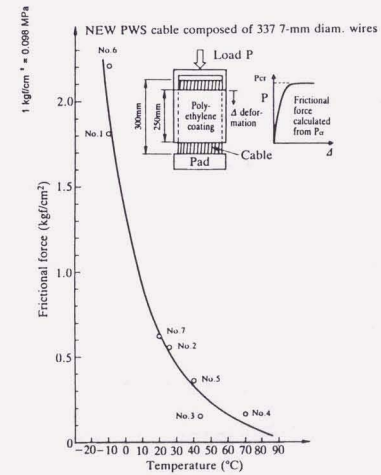
Fig.4.6 Frictional force of polyethylene
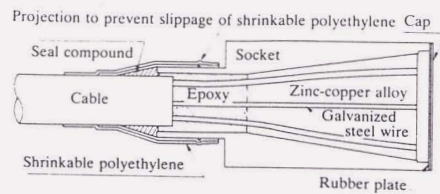
Fig.4.7   End termination of pre—coated parallel wire cable
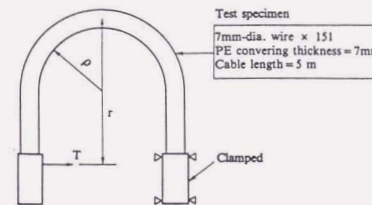
Fig.4.9   Bending test for polyethylene—coated cable

Table 4.2   Friction coefficient of polyethylene—coated cable

Load T (kgf)	Distance between loaded point and cable center r (mm)	Bending moment applied to cable center M (t·m)	Cable radius of curvature ρ (cm)	2 × radius of curvature /cable diameter
2,150	896.7	1.93	60.8	11.3
2,070	1,289.3	2.67	42.5	7.9
2,170	1,339.6	2.91	40.0	7.4
2,750	1,400.0	3.85	36.9	6.8
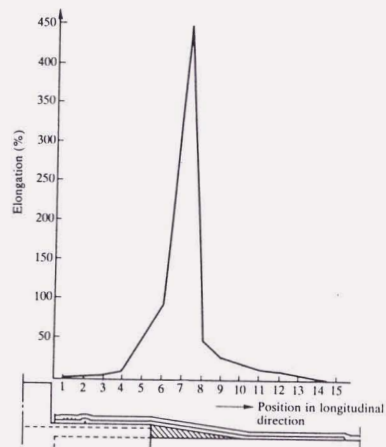
Fig.4.8   Elongation of heat—shrinkable polyethylene for end termination

NEW PWS (7mm-dia. wire × 295, PE covering thickness = 10 mm)

High-tension bolt

Clamps (hot dip galvanized)

200mm   200mm

Cable tension = 0
(clamp temperature maintained at 60°C ± 4°C)

○ Without neoprene rubber (surface pressure about 170 kgf/cm²)
△ With neoprene rubber (surface pressure about 105 kgf/cm²)
— · — Polyethylene physical properties
σ_0: Bolt initial axial force
σ : Bolt axial force

$\sigma/\sigma_0 = \log 2.5997 t^{-0.0353}$

Fig.4.10   Creep characteristics of polyethylene—coated cable

Photo.4.2   Unreeling test of a pre—coated parallel wire cable

CHAPTER 5 SHOP–COATED AND MAINTENANCE–FREE
COLORED CABLE

5.1 Introduction

In recent years, bridges have come to require aesthetic effects on the surrounding landscape as well as possessing superior mechanical properties and durability. A shop–coated and maintenance–free colored cable, eliminating covering work at the site, is preferable especially for a long cable–stayed bridge.

When polyethylene is used as the protective coating on the surface of a cable, its color is limited to black to prevent degradation by ultraviolet radiation [1]. Polyethylene can be colored other than black by using a coloring pigment. But the weathering resistance of the colored cable using a coloring pigment can not be assured, so that it degrades in the open air in a short period.

A black cable may be colored by wrapping it with a colored tape or covering it with a metal material, for example. These methods, however, involve problems of binding durability for the polyethylene and cover joint contamination, and are not preferred from an aesthetic point of view. Metal coverings made of painted steel pipe or aluminum pipe are commonly attached to the stay cables of prestressed concrete cable–stayed bridges. Recently, coverings made of FRP or a colored polyethylene pipe were applied for some stay cables. However, they need installation equipment and time to attach such tapes or coverings along a long cable at the site. Besides, continuous maintenance work is usually required after completion at a high position above the deck.

Coloring by painting requires a special working apparatus to ensure uniform adhesive quality because polyethylene is a nonpolar material. It is well known that thermoplastic olefins, in particular polyethylene, are difficult to paint because of a lack of adhesion of the surface [2]. In the case of a coloring polyethylene surface by painting, a primer coating was heat–treated on the surface of the polyethylene to improve the bond strength between the paint and the polyethylene. The painting system has only a thin paint thickness of about 100 μ m on the surface of the cable, apt to being damaged during handling. In such cases, laborious repainting work is necessary at the site, because the surfaces need to be heat–treated, using the primer coating again, to obtain the adhesive effect. And long–term maintenance is also required after construction.

A shop–coated and maintenance–free colored cable with excellent weathering resistance

has to be developed for a stay cable of long cable—stayed bridges. In order to develop a new coloring method, the coloring material properties, the weathering durability, the color change characteristics and the structural properties of the system had to be investigated.

In this chapter, a coloring method for the polyethylene—coated black cable is discussed and a newly developed colored cable using fluoropolymer is presented [3,4].

Requirements for material of colored cable are analyzed first, and characteristics of various polymers are compared. Excellent properties of fluoropolymer are pointed out, then general features of fluoropolymers are introduced. The basic mechanical properties of the fluoropolymer, which is used for the surface layer of a colored cable, are investigated. The specification with respect to the material properties of the fluoropolymer for the cable is presented.

Weathering deterioration of polymers is discussed by the relationship between the solar radiation energy and intermolecular binding energy [5]. Weathering tests are carried out to evaluate the weathering durability of the fluoropolymer by various test methods including the latest accelerated outdoor exposure test. The detailed data of the tensile strength and elongation retention of the fluoropolymer after the test are shown. Based on the obtained data, the weathering durability of the fluoropolymer is estimated.

Color change and fading characteristics of the fluoropolymer are measured at the same time to examine changes in its appearance. It is shown that the color tone variation greatly depends on the weathering resistant property of pigments added to the fluoropolymer, and that colored fluoropolymer can work with a minimum of discoloration and fading over a long period of service. Another visual degradation due to the deposition of air pollutants is also examined using exposed specimens in the Tokyo industrial area.

In addition, structural properties of a fluoropolymer—coated cable such as bending, clamping and damage resistance are investigated. An adhesion method is examined to increase the adhesive strength between fluoropolymer and polyethylene, then handleablity of the fluoropolymer—coated cable is shown. The external damage durability and repairability are also discussed.

Finally, it is shown that the fluoropolymer—coated colored cable is applied not only to stay cables of cable—stayed bridges but also to hangers of long suspension bridges.

5.2 Material Properties of Colored—Fluoropolymer for A Pre—Coated Parallel Wire Cable

5.2.1 Requirements for material of a colored—cable

The material to put color on the surface of the cable had to be selected under the following requirements [3];

　　a) It should have excellent weathering resistance and durability.

　　b) It should have high mechanical strength.

　　c) It should allow the extrusion coating process.

To meet these requirements, a fluoropolymer was selected among various materials, shown in Table 5.1 [6,7]. Recently, high durability and high functionality have come to be required for materials in many industrial fields. Fluoropolymer has been used as a material having weathering resistance, heat resistance, chemical resistance and non—tackiness and moldability [8]. Fluoropolymer excels particularly in weathering resistance among other properties. This outstanding property led to its application to bridge cables.

The colored cable has a conventional polyethylene coating with additional peripheral surface layer of a thin colored fluoropolymer. It is possible to coat the cable using only a fluoropolymer, but a double cooating system was chosen considering the economical reason. A cross section of the colored cable is shown in Fig.5.1 and Photo.5.1.

5.2.2 Properties of fluoropolymer

Eight types of fluoropolymer, shown in Table 5.2, are currently used in various fields [7]. Tetra—fluoroethylene (TEF) and chlorotri—fluoroethylene (CTFE) were developed first. TEF exhibits excellent heat resistance, chemical resistance and electric non—conductance because of its strong intermolecular binding energy. But it has a high viscosity at a melting temperature of 330 ° C or more, therefore it is inferior to other fluoropolymers in moldability such as melting extrusion. CTFE has a lower melting temperature compared to that of TEF, and at the same time it has disadvantages in deterioration of heat resistance and chemical resistance when it is molded.

Next, a polymer of tetra—fluoroethylene/ hexa—fluoroethylene (FEP) was developed in order to improve moldability of those polymers. It has almost the same quality as TEF except moldability. Then, polyvinylidene—fluoride (PVDF) and polyvynil—fluoride (PVF) were also developed, which can be made by a single polymerization. PVDF has a comparatively lower melting temperature (high moldability), and superior mechanical properties among the other fluoropolymers. It also has good chemical resistance, except for

some chlorine or ketone such as acetone. PVF can only be used as a film, because it decomposes at the molding temperature. Therefore, it is not applied for coating of the cable.

Polyvinylidene fluoride (PVDF), a fluoropolymer with superior mechanical strength and an optimum extrusion coating property, was selected as the outer coating material of the colored cable taking into account of the following points.

The basic mechanical properties of PVDF were investigated before using it as the outer material of the colored cable. The temperature dependent properties are shown in Fig.5.2. From the figure, it is clear that the fluoropolymer has a slightly higher tensile breaking strength than the high−density polyethylene (HDPE), but the temperature dependence of its tensile breaking strength is almost the same as that of HDPE [9]. It has the highest mechanical properties such as tensile strength and hardness among fluoropolymers, that makes it the most suitable covering material for the cable. The stress−strain curves of PVDF and HDPE are shown in Fig.5.3.

PVDF has superior moldability because of its low melting point compared to the other fluoropolymers. It can be extruded at a temperature of about 200 ° C, that is almost the same extruding process condition as that of the high−density polyethylene.

The weathering resistance of PVDF is excellent, like those of the other fluoropolymers. Its weathering resistance was already confirmed [10] using a thin film for 17 years of natural outdoor exposure test. Based on the actual results, it is considered that the fluoropolymer is a reliable material to apply to the outer layer of the cable.

As for thermal property, PVDF has a limited oxygen index of 44%, this means it is a self−extinguishing polymer, and does not burn in the air. It passed the burnability test specified by ASTM E84 (UL9). This is a distinguished characteristic of the fluoropolymer compared to any of polyethylene, which can easily burn in the air. It is decomposed into a carbide and gas component such as fluorine or hydrogen at a temperature of 350 ° C. It is necessary to pay attention to color change from a coloring point of view when it is used in a condition of high temperature over the melting point for a long time.

The outer fluoropolymer coating is applied by the same melting extrusion coating process as the inner polyethylene coating. Therefore, residual stress remains in the coating. Elongation by introduced tension and by change of a temperature add some stress to the cable structure. Aging under such a stressed state suddenly initiates cracks in polymers, which propagate through the polymer and eventually lead to its brittlenss. From this viewpoint, the fluoropolymer must be investigated also for environment stress cracking resistance. This property of fluoropolymer was tested by referring to the constant−strain method in JIS K6760. The ESCR test results confirmed that the fluoropolymer developed no cracking at all

after 1,000 hours and that it was as satisfactory as polyethylene so far as environment stress cracking resistance was concerned.

Fluoropolymer has been in use for such a short period in the construction field that its material standardization is still to be established. Accordingly, its properties for use in a colored cable were set to meet those of HDPE shown in Table 5.3 by referring to the specification of JIS K6896, Polytetra−fluoroethylene Powder for Molding and Extrusion Materials and so forth.

5.3 Weathering Resistance of Colored−Fluoropolymer

5.3.1 Discussion on Weathering Deterioration of Polymers

Generally speaking, polymers gradually deteriorate when they are used outdoors for a long term, suffering from the various natural climatic environments. The primary elements that contribute to deterioration are: solar radiation, particularly the ultraviolet rays, moisture as dew, humidity, rain, and temperature. These factors, combined together, degrade weathering resistance, among them, ultraviolet wavelengths are considered to be the greatest cause that contributes to deterioration of polymers. The reason can be explained by the relationship between solar radiation energy and intermolecular binding energy.

The solar radiation energy arriving on the earth, E, can be expressed by the following equation: $E = hc / \lambda$ (where, h: a constant of Pranct, c: light speed, λ : wave length) [11]. Consequently, energy per light quantum increases as wave length becomes shorter. Short wavelengths such as ultraviolet wavelengths ($300 \sim 400$ nm) affect deterioration of polymer a lot. They have an energy of $71 \sim 95$ kcal/mol, which is equal to the binding energy of some polymers. When ultraviolet radiation is absorbed by polymers, it can break up their intermolecular binding, causing deterioration.

In the case of polyvinyl chloride (PVC), for example, the main structure of intermolecular binding energy (C−C bond: 85 kcal/mol) is smaller than that of ultraviolet wavelengths (300 ∼ 400 nm), and solar radiation has sufficient energy to break the intermolecular binding of PVC easily. On the other hand, the main structure of binding energy of fluoropolymer (C−F bond: about 116 kal/mol) is much greater than that of ultraviolet wavelengths. Therefore, the fluoropolymer is stable enough against ultraviolet radiation. Fig.5.4 shows the relationship between solar energy and intermolecular binding energy.

Fig.5.5 shows the light transmittance of fluoropolymer (PVDF) for various thicknesses. It is found that non−colored PVDF does not have absorbing wavelengths in the range of

ultraviolet rays. Compared to PVC, for instance, which has absorbing wavelengths of about 320 nm, it is clear that PVDF is a material that hardly deteriorates. From the figure, it is found that light transmittance of the fluoropolymer decreases as the thickness of the film increases. When a white pigment of 1~2% is mixed into the fluoropolymer, the fluoropolymer of a thickness of 0.15 mm is not penetrated by a wavelength of 300 nm. In this way, light transmittance of the fluoropolymer greatly depends upon the concealability of fluoropolymer such as thickness or color pigment. This indicates that a colored fluoropolymer can protect its undercoat layer from ultraviolet rays if it has a thickness of about 1 mm.

5.3.2 Weathering test methods

A weathering test is designed to evaluate the service and appearance durability of materials against weather conditions, such as outdoor light (ultraviolet radiation in particular), heat and rain. It is classified into two categories, a natural outdoor exposure test and an accelerated exposure test (Fig.5.6).

By the natural exposure test method, specimens is exposed in a natural environment. It provides reliable data, but it takes a long time to complete. The conventional accelerated exposure test method uses various artificial light sources in the laboratory to simulate the natural environment [12], and is simple to perform. The outdoor accelerated exposure test (EMMAQUA test [13]), concentrating sunlight on specimens by mirrors, can evaluate the weathering resistance of specimens within a short period of time, and is often used to evaluate new materials.

The EMMAQUA employs Fresnel–reflecting solar concentrators that use ten flat mirrors to uniformly focus natural sunlight onto specimens mounted in the target plane. High quality first–surface mirrors provide an intensity of approximately eight suns with the spectral balance of natural sunlight in terms of ultraviolet integrity. The test machine, whose optical design is shown in Fig.5.7, is summarized as a follow the sun rack with mirrors positioned at tangents to an imaginary parabolic trough. The test machine's axis is oriented in a north–south direction, with the north elevation having the capability for periodic altitude adjustment. The target board, located at the focal line of the mirrors, lies under a wind tunnel along which a deflector directs cooling air across the specimens. An oscillating nozzle assembly is employed to spray the specimens with deionized water in accordance with established schedules.

Solar radiation consists nominally of 5% ultraviolet light extending from 300 to 400 nm wavelength, visible light from 400 to 700 nm, and infrared radiation from 700 to 3,000 nm wavelength. In the EMMAQUA test, ultraviolet beam radiance is computed by integrating

the solar spectra in the interval 300 to 385 nm wavelength on a daily basis. The total energy amount of ultraviolet wavelengths per year measured by the EMMAQUA becomes 1,600 MJ/m^2, which is about 5 times as much as that of the natural exposure in Florida. One year's EMMAQUA test is almost equivalent to 5 ~ 7 years natural exposure test in Japan. Therefore, it is possible to evaluate weathering resistance using natural sunlight in a short period.

The fluoropolymer is examined by the natural exposure test method that is most reliable in weathering resistance evaluation. The colored fluoropolymer used in the colored cable has been investigated for about two years by the accelerated outdoor exposure test method to ensure approximately the same evaluation period as the conventional natural exposure test method. The weathering resistance of fluoropolymer is also studied by the latest accelerated laboratory test method.

(1) Natural exposure test

The results of the natural exposure tests on fluoropolymer resins are indicated in Ref.[3]. According to it, these tests were conducted in the United States. Polyvinylidene fluoride (PVDF), polytetra–fluoroethylene (PTFE) and tetra/hexa–fluoroethylene (FEP) were used for test materials. The natural film of PVDF, having a thickness of 0.20 mm, was used as a test piece. It was exposed in Miami for 17 years. The natural film of PTFE and FEP, having a thickness of 0.13 mm and 0.25 mm respectively, were exposed in Miami and Flint for 20 years.

Fig.5.8 shows the tensile strength retention of the fluoropolymer after the natural exposure tests. Test pieces were continuously exposed for 17 and 20 years respectively, and indicated no particular change in strength. This proved that PVDF, PTFE and FEP did not suffer any weather aging when exposed to such natural environment factors as sunlight, rain and gas over at least 17 or 20 years. The test being natural exposure, the weathering resistance exhibited by the test materials can be taken to represent their performance in an actual outdoor service. Taking into account the thickness of the tested film, 0.20 mm for PVDF, weathering durability can be estimated for more than 100 years if the fluoropolymer has a thickness of 1 mm or more.

It is thus presumed that fluoropolymer resins will not deteriorate semipermanently under natural sunlight if their coating thickness were 1 mm or more. The largest factor in the excellent weathering resistance of fluoropolymer is considered to be its extremely high intermolecular binding energy.

(2) Accelerated outdoor exposure test

The accelerated outdoor exposure test concentrates sunlight on the specimen surface with a reflecting concentrator system consisting of 10 plane mirrors [13]. The test can be performed while keeping the ultraviolet spectral balance of the sunlight. The test machines are installed in the Arizonan desert region near Phoenix that is one of the most severe weather areas in the United States.

The colored fluoropolymer was tested using this test machines. White colored PVDF sheet, having a 1 mm thickness, was used for the test pieces. Deionized water was sprayed on to the specimens three minutes at night. The highest temperature of the surface of the specimens was at 58 ° C in summer, and the lowest at 17 ° C in winter. The test was conducted according to ASTM G90 and D4364.

Fig. 5.9 shows the tensile strength and elongation retention of specimens measured after the accelerated outdoor exposure test. The test results are shown in Table 5.4 and Fig.5.10. The two data exhibit no evident deterioration at the ultraviolet radiation dose 4,000 MJ/m ^{2}, which is equivalent to exposure for about 12 years in the Arizonan desert region in the United States. In Japan, the ultraviolet radiation dose differs from place to place ranging from 180 to 240 MJ/m ^{2} per year (in the wavelength range of 300 to 400 nm) according to Ref.[13,14]. If the ultraviolet radiation dose were put at 210 MJ/m ^{2} for an average area, the results of the accelerated outdoor exposure test would correspond to about 19 years of natural weathering in Japan. When corrected for the difference between ultraviolet measurement regions in the United States and Japan by referring to the past data [15], the test results are presumed to correspond to at least 22 to 23 years of natural weathering in Japan.

The state of weathering aging can be judged from structural deterioration as well as from the change of mechanical strength. A white colored fluoropolymer was observed by an electron microscope after the accelerated outdoor exposure test. As shown in Photo.5.3, a few traces of pigment, breaking away from the fluoropolymer, were found on the surface of it, but the surface structure itself was sound enough. On the other hand, the PVC exposed panel using the accelerated exposure test (see 4.5.5) showed deterioration on the surface structure. The result confirmed that the test specimens of fluoropolymer had undergone no chemical degradation at all.

This test was carried out using 1 mm thick white colored fluoropolymer specimens under conditions close to the actual conditions of use, unlike the past natural exposure tests that used uncolored and thin fluoropolymer specimens. The test results confirmed that the colored fluoropolymer would suffer practically no weathering aging for more than 20 years.

(3) Accelerated laboratory test

There are three testing type methods for accelerated laboratory test according to the light source used: a sunshine carbon arc, an ultraviolet carbon arc and a xenon arc. They do not always represent natural sunlight, because their spectral distributions are different from those of solar radiation. But, it is relatively possible to evaluate weathering resistance of materials.

To investigate the weathering resistance of fluoropolymer (PVDF), a sunshine carbon arc type weatherometer accelerated test was conducted with polyvinyl chloride (PVC) used as a control. Fig.5.11 shows the elongation retention of fluoropolymer and PVC measured after the accelerated test. While the PVC degraded in a short time, the fluoropolymer showed no appreciable change in elongation retention after 5,000 hours and demonstrated as high weathering resistance as polyethylene.

A testing machine capable of accelerating natural weathering to a high degree, called QUV (super accelerated weathering test machine) has been recently developed [16]. QUV is claimed to accelerate natural weathering by a factor of about 10 as compared with the sunshine carbon arc weatherometer. Using the QUV testing machine, fluoropolymer (PVDF) was subjected to the accelerated exposure test and observed as to surface change. While the PVC resin used as a control began to degrade in 170 hours, and had its surface structure destroyed in 240 hours, the fluoropolymer exhibited no particular degradation even after 10,000 hours.

The accelerated laboratory test were conducted over the range feasible at present. The fluoropolymer revealed no apparent deterioration and proved its satisfactory weathering resistance as evident from the exposure test results mentioned previously.

The various exposure test results demonstrated that the fluoropolymer coating applied to the colored cable was free from weathering aging for at least 20 years, and had a weathering durability equal to or greater than that of the polyethylene coating conventionally applied to bridge cables.

An evaluation method for weathering resistance is not standardized yet in a strict sense, because it depends greatly upon testing methods and testing conditions. In this study, the weathering resistance of fluoropolymer could be judged based on the reliable natural exposure test data, however it took a long period of time. So, it is desirable to make an evaluation of weathering durability of new materials in a short term. An evaluation method for weathering resistance concerning the relationship between outdoor exposure test and accelerated laboratory test is the subject for a future study.

5.4 Color Change and Fading Characteristics of Colored—Fluoropolymer

5.4.1 Color change and fading test method

In recent years, bridges have come to be required to have aesthetic effects on the surrounding landscape. Structural members used for bridges, having a long service life outdoors, are required to have superior weathering resistance, and excellent durability in appearance at the same time.

When a fluoropolymer is used as a colored coating, a change in its appearance, through discoloration and fading, and its stain resistance as well as weathering durability are important governing factors in the durability of the surface structure. The change of appearance through discoloring and fading is usually judged by changes in color tone and gloss. These properties are expressed by numerical values of visual factors.

The difference of color tone before and after the test was measured by a color difference meter and indicated by the color difference Δ E, according to the Lab system of the color difference representation method specified in JIS Z8730. The gloss variation was measured by a gloss meter as gloss difference (60 ° specular reflectance) before and after the test and was determined by the specular glossiness measuring method specified in JIS Z8741. A quantitative evaluation may not always be valid, but it serves to indicate discoloration and fading due to exposure and stain in the air. In the test, the discoloration and fading characteristics of fluoropolymer were examined by the accelerated outdoor exposure test method, EMMAQUA.

5.4.2 Discoloration and fading characteristics

Fig.5.12 shows the test results on changes in color tone. Test pieces of colored fluoropolymer (PVDF), being 50 mm in width, 130 mm in length and 1mm in thickness, were used. The color tone variation practically depended on the weathering resistant property of pigments added to the fluoropolymer. Generally inorganic pigments are less liable to change in color and tone than that of organic ones. The present test measured the red, blue, green, gray, yellow and white colors. An organic pigment was used only for the red color.

From Fig.5.12, it is evident that the red color suddenly changed at an ultraviolet radiation dose of about 2,000 MJ/m ^{2} and had the largest color variability among the tested colors. This was probably due to the use of the organic pigment, which was in line with the general tendency. Each of the other colors had a very small color difference Δ E of less than 3 at the ultraviolet radiation dose of 2,500 MJ/m ^{2} and was very stable. According to JIS D0205, a standard for discoloration and fading, it can be judged not to deteriorate. If these results are utilized to design pigments and stable color tone, colored fluoropolymers can work with a minimum of discoloration and fading over a long period of service.

The surface of the red—colored fluoropolymer, showing the largest change in color, was rubbed by a paper file in order to examine depth distribution of color—changed portion. After a few polishing, the original red color appeared. It can be presumed that color change is not caused by deterioration of a fluoropolymer itself but by the added pigment part of the surface alone.

Fig.5.13 shows the measured results of changes in gloss. As evident from Fig.4.23, the colored fluoropolymer changed little in gloss after 2,500 MJ/m ^{2} of ultraviolet radiation, and demonstrated a very stable gloss retention of more than 90%. Even though the red color had the greatest tone change, its gloss retention was no lower than the gloss retention in other colors. Because the gloss change depended chiefly on material properties, and the fluoropolymer itself was superior in weathering resistance and gloss retention. Judging from JIS D0205, a standard for gloss retention, the colored fluoropolymer, keeping a gloss retention of more than 80%, can keep its original gloss for more than 10 years.

5.4.3 Stain resistance

Another factor of visual degradation is apparent change and fading in color due to the deposition of air pollutants. The staining property widely varies with environmental condition and is difficult to evenly evaluate. The colored fluoropolymer resins were exposed and tested for the change of color tone in a Tokyo industrial area known for a highly staining environment.

Test pieces of colored fluoropolymer, being 20 mm in width, 50 mm in length and 1 mm in thickness, were used. Five typical colors, discoloring slightly, were chosen for the specimens. The exposed specimens were measured by a color difference meter for 15 months. At the end of the exposure test, the surface of the specimens were measured after washing by water.

Almost all the colored fluoropolymer resins were stained to a saturation point in three months of exposure, but they remained without any appreciable color tone. The rate of tone change varied from color to color, and the apparent color difference Δ E ranged from about 3 to 12, as shown in Fig.5.14. Dark brown colors were relatively low in the rate of tone change. Similar data obtained in coastal and mountain regions are not presumed to surpass these data of the Tokyo industrial area.

Once the stains were cleaned, little or no more tone change was observed, and the color difference Δ E fell to about 1 or close to the original value. Fluoropolymer resins were so

high in non—tackiness and chemical resistance that their contaminants could be easily removed by cleaning. The stain remained on their surface and hardly penetrated into their bulk. When a colored fluoropolymer changes in appearance due to environmental staining, it can be restored to the original condition with ease by washing or other measures. This indicates that a colored fluoropolymer coating is extremely advantageous over painting and other coloring systems in long term maintenance.

5.5 Structural Properties of A Fluoropolymer—Coated Cable

5.5.1 Adhesive properties of fluoropolymer and polyethylene

A colored cable consists of a double layer: a fluoropolymer is coated onto the coated polyethylene. A fluoropolymer is extruded by the same process as a polyethylene, and the shrinkage stress remaining in the coated fluoropolymer integrates the coating with the internal polyethylene.

The friction force of fluoropolymer coating was measured by the same way as polyethylene coating was tested. It was found that the fluoropolymer coating had a friction force at only one third compared to that of polyethylene, and it had a lower temperature dependent property than that of polyethylene, as shown in Fig.5.15. The two layers are not adhered by the ordinary extrusion process. But it is desirable that the two layers are adhered to each other from a fabrication and installation point of view. If a thin fluoropolymer is coated in a non—adherent condition to the polyethylene, some restrictions on handling such as bending or clamping are needed because it suffers damage as crinkling or peeling. Then, an adhesion method was required to be developed to increase the adhesive force between the two layers.

As a fluoropolymer originally has non—tackiness, a primer composition for the fluoropolymer has been newly developed [14]. The peeling strength between the two layers was measured given various test conditions such as surface temperature and concentration of the primer composition. According to the test results, processing conditions were established: a primer composition was painted on the surface of polyethylene, and then it was heated to $70 \sim 80\,°C$ by infrared light before the fluoropolymer was extruded. Fig.5.15 shows the relationship between the surface temperature of polyethylene and adhesion strength obtained by the tests. The thickness of colored fluoropolymer was determined to be 2 mm from an extrudablity point of view.

5.5.2 Installation properties of fluoropolymer—coated cable

The colored cable is coated in two layers. The inner layer is of polyethylene, and the outer is of fluoropolymer. The fluoropolymer can be sufficiently colored to a thickness of about 1 mm, but the coating thickness must be determined from the consideration of bendability during fabrication, installation, and external damage resistance as well.

To examine the bending properties of the colored fluoropolymer coating, three sizes of colored cables were tested, as shown in Photo.5.4. The dimension of the tested cable is shown in Table 5.5. When the colored cables were bent to a D/d (cable bend diameter versus cable outside diameter) of about 10, they showed no deformation such as buckling. When unloaded, they returned to the original condition and retained no harmful deformation. If the fluoropolymer coating thickness were about 2 mm, the colored cable could be successfully bent to a D/d ratio of about 18 during fabrication and installation, which was the same as that of the polyethylene—coated cable.

A cable may be clamped during installation or to prevent vibration after installation. The clamp design needs to determine the coefficient of friction between the colored cable and the clamp.

The colored cable was fit with a clamp and slippage was measured by changing the clamping contact pressure in the axial direction. When the pressure was from 30 to 100 kgf/cm^2 (2.9—9.8 MPa), the coefficient of friction calculated from the maximum slip load was 0.16 to 0.25, which were approximately equal to that for polyethylene—coated cables (Table 5.6). A rubber sleeve was considered effective in ensuring the desired coefficient of friction between the clamp and the fluoropolymer coating as well as in protecting the surface of the fluoropolymer coating.

To examine its external damage resistance, the colored cable was put to a drop weight test according to JIS C3005 (impact test). The colored cable was composed of 55 wires of 7 mm in diameter, coated with 7 mm of polyethylene and 2 mm of fluoropolymer, and had 76 mm in outside diameter. The fluoropolymer coating did not rupture when tested with a drop weight of 20 kgf (196 N) and drop height of 2 m.

The colored cable was evaluated for progressive damage by assuming that it sustained some damage during installation. A 300 mm long colored cable specimen was cut with a notch 1mm in depth (a half of the coating thickness) or 2 mm in depth (penetration) and 50 mm in length, then put to a thermal shock test between $-20\,°C$ and $+80\,°C$. After 100 cycles (8 hours per cycle), the colored cable showed no external damage propagation and was proved to have sufficiently high external damage durability.

The colored cables are shipped in a packaged condition for protection, but are subject to

damage by pulling and unreeling during installation. Their repairability was also studied. A fluoropolymer's melting point is sightly higher than that of a polyethylene, but any damage in the fluoropolymer coating could be easily repaired by applying a piece of the same fluoropolymer while heating with a hot—air fan. To verify the quality of colored cable repairs, totally and partly repaired colored cable specimens were subjected to a thermal cycling test. The test that consisted of 100 cycles (8 hours per cycle) between $-20\,^\circ$C and $+80\,^\circ$C, revealed no abnormality in repairs. This confirmed the effectiveness of the repairing method.

5.6 Main Applications of the Pre—Coated Parallel Wire Cable

The pre—coated parallel wire cable has been used in many bridges due to its superior strength, easy installation and excellent aesthetic aspects. The numbers of bridges employing the cable have become more than 80, including 15 colored ones. The cable is mainly applied to a stay cable of long cable—stayed bridges such as the Tatara Bridge, and sometimes to a tension member of nielsen bridges.

Recently, a pre—coated parallel wire cable with pin—connected supports has been designed for a hanger system of long suspension bridges. Helically stranded ropes have been used for hanger cables of suspension bridges up to now, but they need periodic maintenance. They are bent and taken into the saddle of cable bands. When tension is applied to helically stranded ropes, the painting of the surface is apt to crack. Water penetration from those cracks causes troubles in maintenance. Therefore, re—painting is absolutely required for the use of helically stranded ropes.

On the other hand, a pre—coated parallel wire cable is almost maintenance free due to its durability. This is the main reason that the pre—coated parallel wire cable has been applied for many bridges. Besides, it can be colored using a fluoropolymer, having excellent weathering durability. Based on the many results applied to cable—stayed bridges, the fluoropolymer—coated parallel wire cable is also applied for hangers of long suspension bridges: the Akashi Kaikyo Bridge, the 1st Kurushima Bridge, the 2nd Kurushima Bridge and the 3rd Kurushima Bridge.

Table 5.7 shows the main applications of the pre—coated parallel wire cable, including the colored one.

5.7 Conclusion

The results obtained by the study in Chapter 5 are summarized as follows.

(1) A colored cable consisting of a double layer (a colored fluoropolymer is coated onto the coated polyethylene) was developed. The fluoropolymer, having outstanding weathering durability, can elongate service life of the cable and add aesthetic aspects. As a result, a greater freedom of color selection was given to bridges cables that matched the surrounding environment.

(2) Requirements for material of colored cable were analyzed, and characteristics of various fluoropolymers were compared. Polyvinylidene fluoride (PVDF) was selected as the outer coating material of the colored cable because of its superior mechanical strength and optimum extrusion property. The specification with respect to the material properties of the fluoropolymer for the colored cable was determined referring to that of the polyethylene.

(3) Weathering deterioration of polymers was discussed by the relationship between the solar radiation energy and intermolecular binding energy. It became obvious that the fluoropolymer was superior to other plastics, especially in weathering durability because of its strong binding energy in molecular structures. Judging from the natural exposure test of the film and not showing deterioration for a period of about 20 years, the weathering durability of the fluoropolymer could be estimated to last for more than 100 years if the thickness were 1 mm or more.

(4) An outdoor accelerated exposure test was carried out and the results assured that the colored fluoropolymer had excellent weathering resistant and durability with regard to color change and gloss retention. When colored fluoropolymer changed in appearance due to environmental staining, it could be restored to the original condition with ease, for example by washing, because of the characteristics such as non—tackiness and chemical resistance.

(5) An adhesion method was examined to increase the adhesive strength between the fluoropolymer and the polyethylene, then the structural properties of the cable, such as bending, clamping and damage resistance were investigated. It was confirmed that the cable can be handled the same way as that of a polyethylene—coated cable if suitable devices were used.

(6) These characteristics of the colored cable showed that it could be used for various structures. It was shown that the fluoropolymer—coated colored cable was applied not only to stay cables of long cable—stayed bridges but also to hangers of long suspension bridges.

5.8 References

[1] S.Kawawata and M.Kikkawa, Weathering of Some Plastics of Wire and Cable Applications[*], Hitachi Hyoron, Vol.9, 1965, pp.63−72.

[2] Nikkan Kogyo Shinbun, Polyethylene Resins[*], 1973.

[3] T.Hojo, I.Tsuchida, M.Yano, T.Eguchi and S.Takami, Development of Color Cable for Suspended Structure, Nippon Steel Technical Report, No.60, 1994, pp.17−23.

[4] T.Hojo and I.Tsuchida, Development of Color Cable for Cable−Stayed Bridges[*], Journal of JSCE, Vol.75, No.11, 1990, pp.8−9.

[5] T.Hojo, I.Tsuchida and K.Abe, A Study on Weathering Durability of Fluoropolymer[*], Proc. of JSCE Vol.480, VI −21, 1993, pp.107−115.

[6] Japan Fluoropolymers Industry Association, Fluoropolymers[*], 1970.

[7] A.Nireki, Chemistry of Fluorine, Maruzen[*], 1988, pp.103−113.

[8] Du Pont−Mitsui Fluorochemicals, Teflon Application Handbook[*], 1984.

[9] Y.Tawaraya, T.Hojo, Y.Sakamoto, T.Eguchi and I.Tsuchida, Development of NEW PWS for Cable−Stayed Bridges and Its Practical Application, Nippon Steel Technical Report, No.42, 1989, pp.1−11.

[10] K.Abe, Properties and Applications of Polyvinylidene Fluoride (Kynar)[*], Plastic Age, No.30, 1984, pp.1−7.

[11] Institute of Electrical Engineers of Japan, Degradation of Polymers[*], Corona Publishing, 1960.

[12] I.Onishi, Estimation for Deterioration and Reliability of Polymers[*], Material Life, Vol.12, No.4, 1990, pp.213−220.

[13] G.Zelaut and J.Robbins, Accelerated Outdoor Exposure Testing of Coil Coating by the EMMAQUA Test Method, ECCA Annual Congress, 1984.

[14] G.Zelaut, M.Rupp and T.Anderson, Ultraviolet Radiation as a Timing Technique for Outdoor Weathering of Materials, Society of Automotive Engineers Technical Paper Series, 850348, 1985, pp.1−8.

[15] A.Nireki and K.Tomiita, Proposal for Solar Radiation Dosage in Ultraviolet Regions in Japan[*], Journal of Structural and Construction Engineering, No.381, 1987, pp.17−25.

[16] Y.Kijima, Super Accelerated Weathering Test of Plastic Materials[*], Plastic Age, No.33, 1987, pp.143−148.
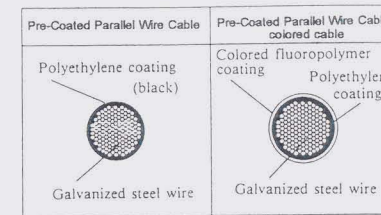
[*] Published in Japanese

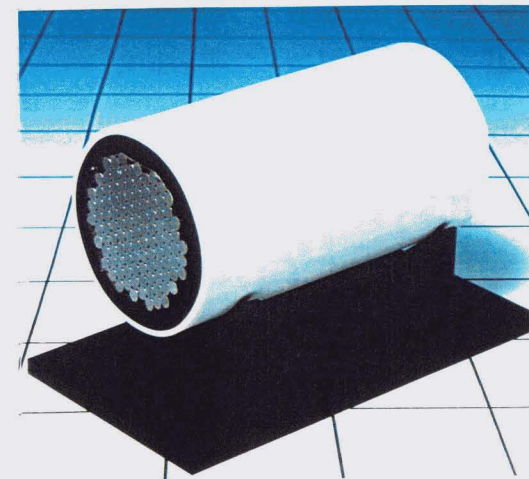Fig.5.1 Structure of colored fluoropolymer coated cable

Photo.5.1 Cross section of colored fluoropolymer coated cable

Table 5.1 Comparison of properties of fluoropolymer with other polymers

Property	Fluoropolymer	Nylon 6	Polypropylene	Polyvinyl chloride
Specific gravity	1.7-2.2	1.13	0.90	1.35-1.45
Tensile strength (kgf/cm^2)	140-460	720-820	200-400	350-620
Elongation (%)	100-400	25-320	600-800	2-40
Weather resistance	○	×	×	×
Heat resistance (°C)	150-260	80-120	100-120	60
Chemical resistance	○	×	△	△
Non-tackiness	○	×	○	×
Moldability	○	○	○	○

1 kgf/mm² = 9.807 MPa

Table 5.2 Comparison of various fluoropolymers

	PTFE	FEP	PFA	PVDF	PCTFE	ETFE	ECTFE	PVF
Density (g/cm³)	2.14-2.20	2.12-2.17	2.12-2.17	1.75-1.78	2.03-2.20	1.70	1.68-1.69	1.38
Tensile Strength (kgf/cm²)	140-350	190-220	280-300	250-510	314-420	460	420	300-400
Elongation (%)	200-400	250-330	300	460-980	80-250	100-400	200-300	150-200
Melting Point (°C)	327	275	310	156-178	220	270	230-245	200-210
Heat Resistance (°C)	260	200	260	150	177	150	165	110
Moldability (Extrusion)	×	○	△	○	×	×	×	×

1 kgf/cm² = 0.098 MPa

1 kgf/cm² = 0.098 MPa
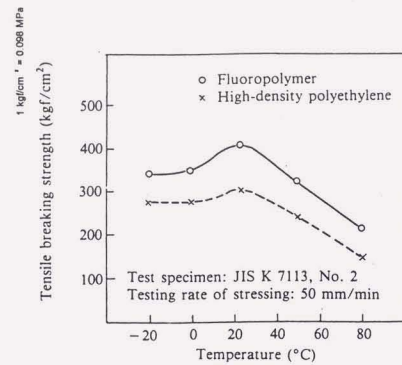
Fig.5.2   Tensile breaking strength of fluoropolymer
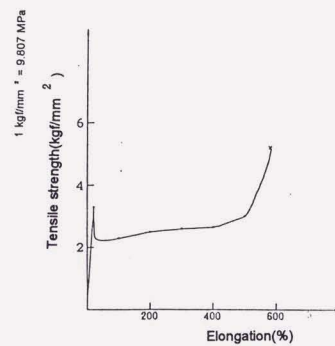
Fig.5.3   Stress−strain curve of fluoropolymer

Table 5.3   Physical properties of fluoropolymer

Property	fluoropolymer	polyethylene (JIS K 6748 Class 3 Grade 1)
Density (g/cm³)	≥ 1.7	≥ 0.942
Tensile strength (kgf/cm²)	≥ 300	≥ 200
Elongation (%)	≥ 200	≥ 300

1 kgf/cm² = 0.098 MPa
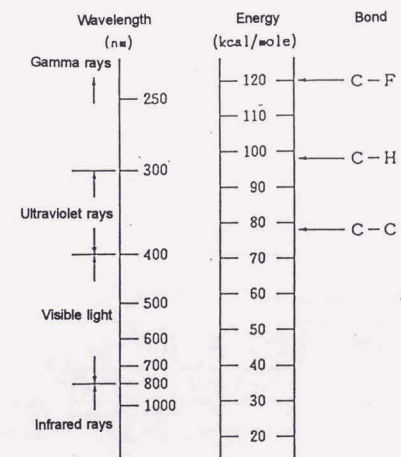
Fig.5.4 Relation between solar energy and intermolecular binding energy

Fig.5.5 Light transmittance of fluoropolymer (PVDF)
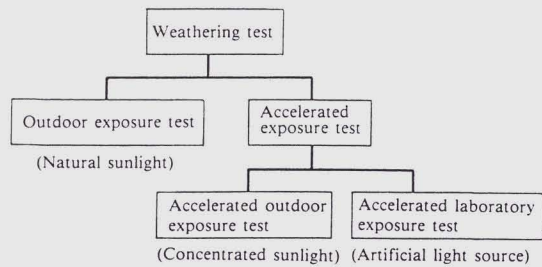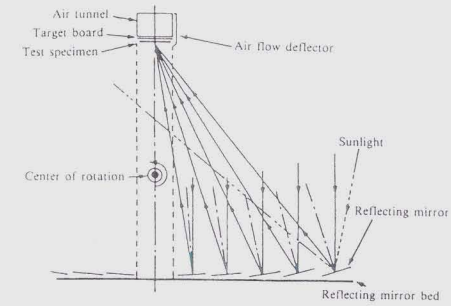
Fig.5.7 Reflecting light concentrator of EMMAQUA testing machine

Fig.5.6 Weathering test methods

Photo.5.2 Accelerated outdoor exposure test (EMMAQUA)
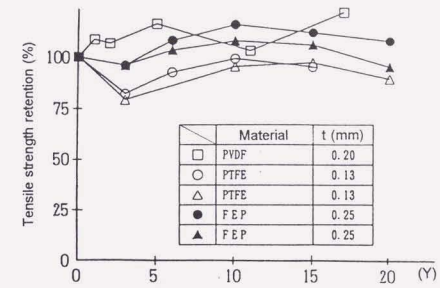
Fig.5.8   Natural sunlight exposure test results of fluoropolymer
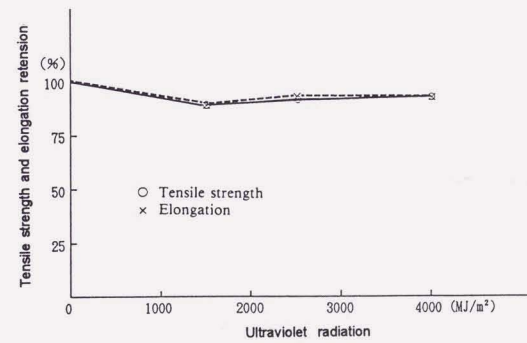
Fig.5.9   Accelerated outdoor exposure test results of fluoropolymer

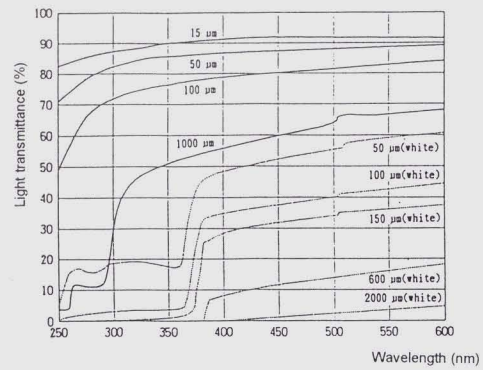Table 5.4 Accelerated outdoor exposure test results

Ultraviolet Radiation Date / Tensile Property	Unexposed Control	1540 MJ/m²	2464 MJ/m²	4042 MJ/m²
	1991. 4. 5	1991. 8. 29	1992. 6. 15	1993. 8. 4
Yield Stress (PSI)	3863	4026	4120	4107
Standard Deviation (PSI)	43	94	79	44
Yield Strain (%)	8.0	9.0	9.0	8.0
Standard Deviation (%)	0.4	0.5	0.6	0.3
Tensile Stress (PSI)	6825	6228	6171	6440
Standard Deviation (PSI)	488	408	687	805
Tensile Strain (%)	465.0	432.2	421.3	435.2
Standard Deviation (%)	25.8	23.8	48.5	53.4
Modulus (PSI)	106595	106830	102662	126764
Standard Deviation (PSI)	4529	6233	4715	4666
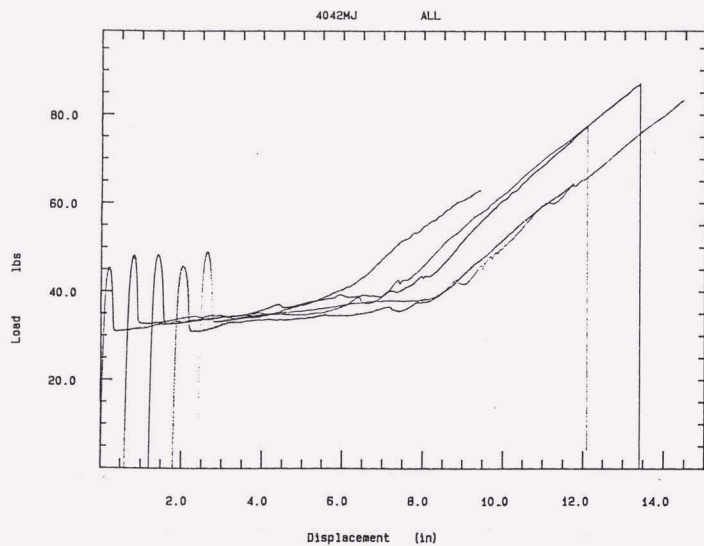
Fig.5.10　Tensile test results of fluoropolymer (PVDF)

Fluoropolymer (PVDF)

control panel　　　　exposed panel
(EMMAQUA 2500MJ/m²)

PVC

control panel　　　　exposed panel
(QUV 240 HR.)
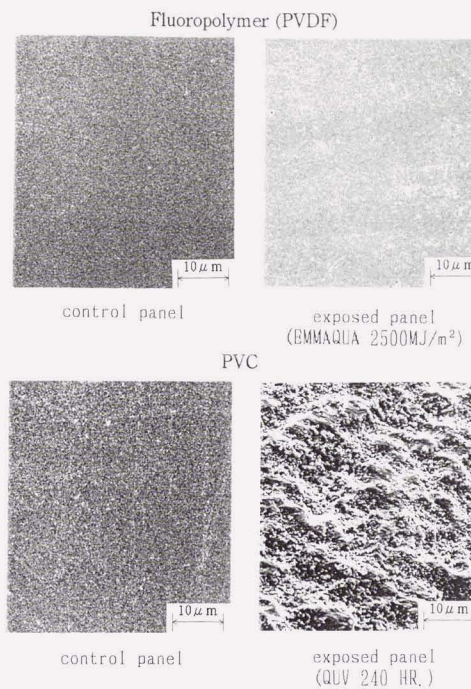
Photo.5 3　Surface of fluoropolymer and PVC observed by electron microscope (✕ 1000)
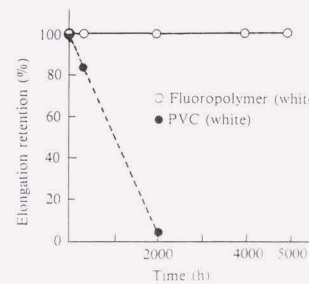
Fig.5.11　Accelerated laboratory test results of fluoropolymer
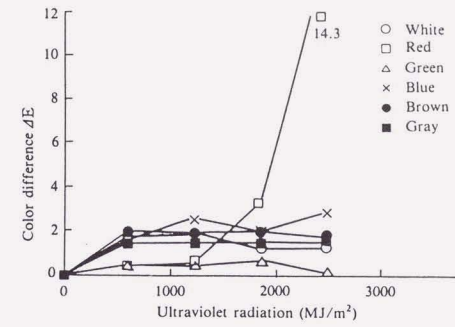
Fig.5.12　Discoloration and fading characteristics of colored fluoropolymer
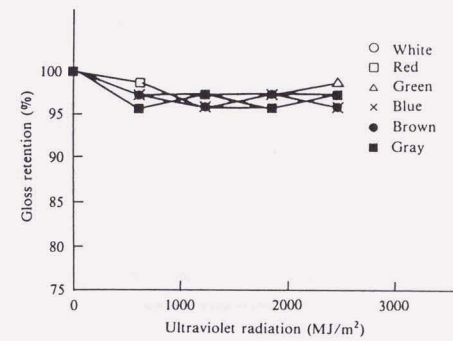
Fig.5.13　Gloss change of colored fluoropolymer
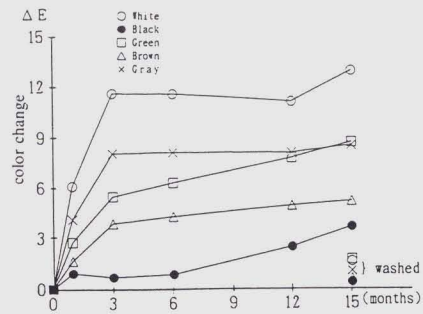
Fig.5.14　Environmental color change in industrial area
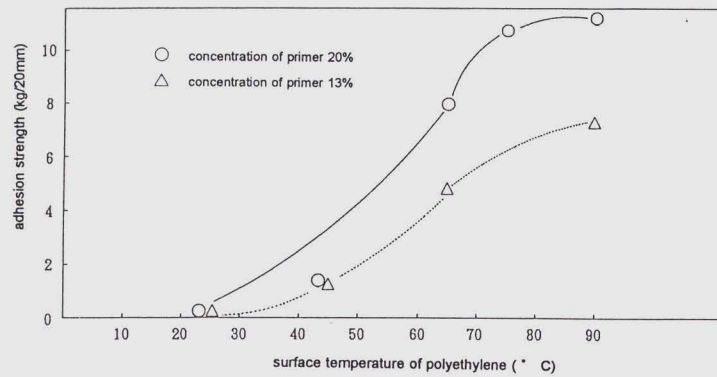
Fig.5.15　Relation between surface temperature and adhesion strength
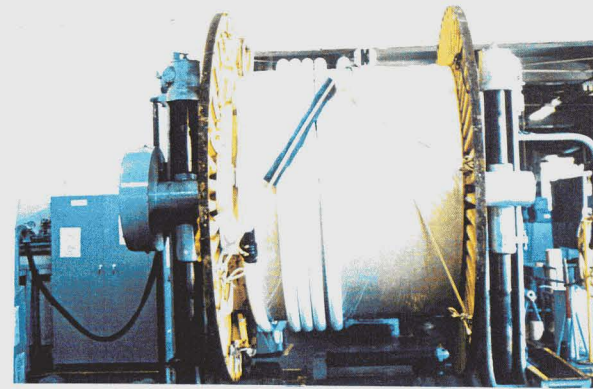
Photo.5.4　Bending test for colored cable

Table 5.5　Test dimension of colored cable

Item	Cable size		
	31 wires in 7-mmφ each	55 wires in 7-mmφ each	139 wires in 7-mmφ each
Strand diameter (mm)	44	58	92
Polyethylene coating thickness (mm)	7	7	9
Cable outside diameter d (mm)	58	72	110
Fluoropolymer coating thickness (mm)	1.1	1.1	1.3
Maximum bend diameter D (mm)	440	580	1070

Table 5.6　Coefficient of friction of colored cable

Specimen	Contact pressure (kgf/cm^2)	Maximum load (tf)	Coefficient of friction μ	Remarks (rubber sleeve)
No. 1	32.9	10.8	0.25	Yes
No. 2	50.2	15.5	0.23	Yes
No. 3	94.3	20.2	0.16	Yes

1 kgf/cm^2 = 0.098 MPa
1 tonf = 9.807 kN

Table 5.7 Main results of pre—coated parallel wire cable fabrications

Name of Bridge	Bridge Type	Main Span (m)	Cable Size	Year Completed	Remarks
Nagaragawa	Nielsen	137	ϕ 5× 91	1985	
Toda Park	Cable-Stayed	134	ϕ 7×223	1987	
Utsumi	Nielsen	220	ϕ 5× 85	1987	
Sugawarashirokita	Cable-Stayed	238	ϕ 7×163	1988	
Araishinbashi	Nielsen	160	ϕ 7×109	1988	
Nishihaga	Cable-Stayed	116	ϕ 7×223	1989	
Yokohama Bay	Cable-Stayed	460	ϕ 7×421	1989	
Hattabara	Cable-Stayed	144	ϕ 7×127	1990	
Ikuchi	Cable-Stayed	490	ϕ 7×241	1990	
Nakajimagawa	Nielsen	156	ϕ 7×187	1990	※
Sakitama	Cable-Stayed	190	ϕ 7×397	1991	
Heisei	Cable-Stayed	125	ϕ 7×421	1991	
Shinhamadera	Nielsen	254	ϕ 7× 73	1991	
Usui	Cable-Stayed	110	ϕ 7×241	1991	
Karnali	Cable-Stayed	325	ϕ 7×199	1991	
Tokimeki	Cable-Stayed	100	ϕ 7×199	1993	※
Toyomi	Cable-Stayed	150	ϕ 7×283	1993	※
Tatsumi-unga	Cable-Stayed	115	ϕ 7×121	1993	※
Iwatsu	Cable-Stayed	175	ϕ 7×199	1993	
Haneda Skyarch	Arch Type	103	ϕ 7×199	1993	
Gouto	Nielsen	140	ϕ 7× 91	1994	※
Onneyu	Nielsen	140	ϕ 7× 55	1994	※
Yuge	Cable-Stayed	150	ϕ 7×139	1994	
Tsurumi Tsubasa	Cable-Stayed	510	ϕ 7×499	1995	
Meiko-Central	Cable-Stayed	590	ϕ 7×397	(1996)	※
Akashi Kaikyo	Suspension	1990	ϕ 7× 85	(1998)	※
Tatara	Cable-Stayed	890	ϕ 7×367	(1999)	
1st Kurishima	Suspension	600	ϕ 5×139	(1999)	※
2nd Kurushima	Suspension	1020	ϕ 5×139	(1999)	※
3rd Kurushima	Suspension	1030	ϕ 5×139	(1999)	※

※ Colored Cable

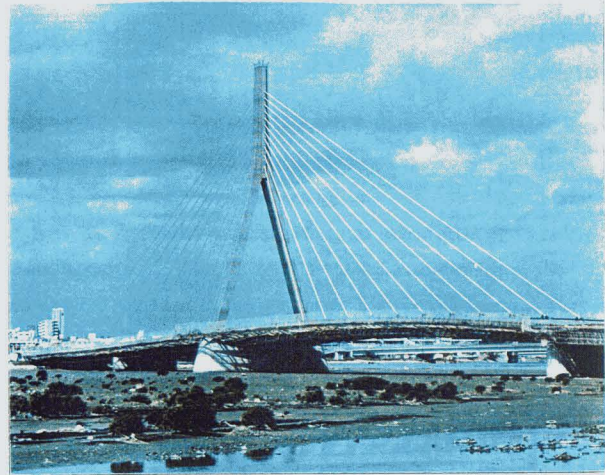Photo.5.5   Yokohama Bay Bridge

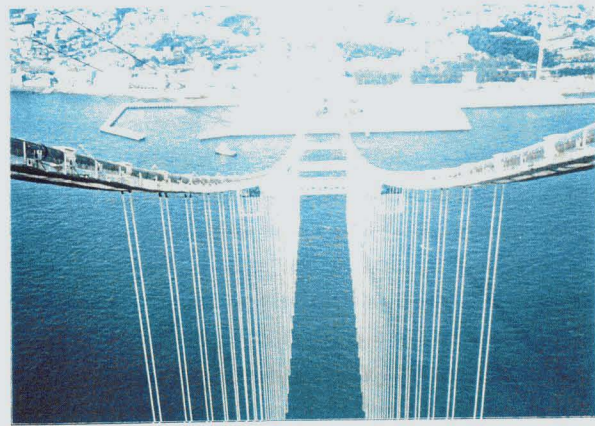Photo.5.6   Tsurumi Tsubasa Bridge

Photo.5.7　Toyomi Bridge

Photo.5.8　Akashi Kaikyo Bridge
(Under construction)

CHAPTER 6   AERODYNAMIC MEASURES AGAINST CABLE VIBRATION

6.1 Introduction

Stay cables of a cable—stayed bridge are easily vibrated by the wind because of their flexibility, low structural damping and circular cross section. Single—strand cables protected by anti—corrosive coverings (polyethylene for instance) for cable—stayed bridges of multi—cable type have suffered from the frequent occurrence of vibration. When the vibration occurs in the stay cables, there is a possibility of damage to the cables near the socket. Wind—induced vibration of the stay cable has been understood as vortex—induced vibration, wind—rain—induced vibration (rain vibration) and wake galloping [1,2].

It is well known that the circular section, such as a cable, periodically vibrates because of the shed vortices behind it. The response amplitude is relatively smaller than that of other type vibrations. According to the report [1], vortex—induced vibration is observed in stay cables of some cable—stayed bridges [3]. Depending on the extent of its response amplitude, the vortex—induced vibration of cables is likely to affect the bending fatigue strength of the cables. Therefore, it is essential to quantitatively investigate the response characteristics of vortex—induced vibration for a long cable—stayed bridge.

Vibrations induced by the combined influence of wind and rain have often been reported in cables having a smooth surface, such as polyethylene, and a diameter between 120 to 200 mm. Rain vibration was observed in the Meiko—Nishi Bridge, then the amplitude of about double the cable's diameter was measured [4]. The vibration is considered to be caused by combined conditions; water rivulets of a cable surface and axial air flow formed along the cable axis [5]. Extensive research into the mechanism of the vibration and measures to control it have been carried out. And the effects of such suppressing measures have been observed in actual bridges. Two main techniques have been used to control rain vibration; one is to install some kind of vibration—damping devices on the cables near the anchor points, or to connect neighboring cables with wires, and the other is to improve the aerodynamic characteristics of cables by introducing a roughness on their surfaces [6]. With the recent demand for a longer cable to suit the increasing span of cable—stayed bridges, there have been certain cases in which it was impossible to obtain a sufficient vibration suppressing effect by using mechanical damping devices; a long cable has a limited fixing point where damping devices are effective. Accordingly, aerodynamic measures are expected to become more important for a stay cable of long cable—stayed bridges. However, there have been a few

measures to suppress rain vibration, such as parallel protuberances, helical streaks and V or U groovings [7,8,9].

On the other hand, as a cable–stayed bridge has a longer span, the wind load of stay cables becomes larger and sometimes it is not less than that of the deck. In the design of a long cable–stayed bridge, a smaller drag force of the cable is essentially preferable at a realistic Reynolds number. If this large wind load (the drag force) is able to be decreased, it will be a great help to optimize the whole configuration of the structure. These aerodynamic measures mentioned above, however, cause a greater drag force, because they have a larger surface roughness compared with that of a cable having a smooth surface at the design wind velocity [10]. This becomes quite a new subject in the design of a long cable–stayed bridge, not ever being faced.

Therefore, aerodynamic cable sections with better vibration–controlling characteristics and a smaller drag force at the same time must be developed for stay cables of a long cable–stayed bridge.

In this chapter, dynamic behavior of a stay cable in cable–stayed bridge is described and newly developed countermeasures against cable vibration are discussed based on the results of wind tunnel tests.

First, the past works on cable aerodynamics are briefly reviewed. Fundamental static aerodynamic characteristics of a circular cylinder are introduced and it is pointed out that a circular cylinder is very sensitive to the Reynolds number and the surface roughness in a flow [11,12,13]. Cable vibrations such as rain vibration, vortex–induced vibration and wake galloping, and their various suppressing methods, including aerodynamic measures, are shown [1,2]. It is indicated that a stay cable for long cable–stayed bridges is required to have not only a suppression effect but also a lower drag force at the same time [14,15].

Next, cable responses by vortex–induced vibration in natural wind are observed in a long cable–stayed bridge, and the characteristics of the vibration are analyzed [3,16]. The factors affecting the vibration such as surface roughness and structural damping are examined by using a wind tunnel test and analysis. A wind tunnel test is carried out for the cables having various surface roughnesses. Using an energy–balance analysis, the response amplitude of the cable is estimated at various damping levels. Based on the results obtained by the estimation, the bending angle of a long cable is calculated and the bending fatigue strength of the cable is examined.

Then, the aerodynamic measures against rain vibration are studied by using wind tunnel tests in order to develop a new cable having a suppression effect and a lower drag force at the

same time [10,17,18,19]. Various experiments are carried out concerning the relationship between the surface roughness and aerodynamic properties, such as drag force. Static characteristics of various cables with uniform, indented and embossed patterned surfaces are examined within the design wind velocity range. The model cables having the same dimension, especially diameters, as practical ones have, are used for the test. A series of experiments are carried out to learn about the formation and behavior of water rivulets on cable surface when rain vibration occurs. Through the tests, location and volume of water rivulets are surveyed. Various tests under simulated rainfall are carried out in order to investigate the vibration suppressing effects of surface–roughened cables. Pressure distribution of the cables is also measured to analyze the flow around the cable. Then, the patterns and distribution of surface roughness are discussed by spectral analysis.

It is pointed out that a super–long cable–stayed bridge needs a cable having not only a suppressing effect but also a low drag force [14,15]. A low drag aerodynamically stable cable with a patterned surface is experimentally discussed. Finally, to understand the aerodynamic characteristics of the surface configuration of the cable, various patterned roughnesses are examined in terms of a Reynolds Number.

6.2 Brief Review of Past Work

6.2.1 Flow around a circular cylinder

The flow around a circular cylinder and the drag force on it have been studied for a long time. It is well–known that its aerodynamic characteristics are affected by not only the Reynolds numbers but also by surface roughness and turbulence flow [20,21]. It is explained as follows from a viewpoint of fluid mechanics.

(1) Influence of Reynolds number

According to Bernoulli's theorem, the net pressure caused by a fluid flow creates an inertial force on the fluid elements enclosed by a volume, and is of the order of $\rho U^2 D^2$. On the other hand, a viscosity–related force on the element is of the order of μUD, where ρ is fluid density, U is flow velocity, D is typical surface dimension, and μ is viscosity coefficient. The ratio of inertia to viscous force, which is the Reynolds number, is given by

$$R_e = \rho U^2 D^2 / \mu UD = \rho UD / \mu = UD / \nu \qquad (1)$$

where $\nu = \mu / \rho$, is called the kinematic viscosity, being $1.5 \times 10^{-5} \, \mathrm{m}^2/\mathrm{s}$ at a temperature of $20°$ C. As for the structural members of bridges, R_e number is of the order of 10^5 to 10^7 under a natural wind. When R_e numbers become large, inertia effects predominate, meaning that the viscous effects can be neglected. Then the concept of boundary layer is introduced.

In a large R_e number range, there exists a thin flow around a body, called a boundary layer, where frictional stress is produced because of velocity gradients on the surface. Boundary layer separation occurs if fluid particles in the boundary layer are sufficiently decelerated by inertial forces so that the flow near the surface reverses. As a result, the flow around the body in a large R_e number range is classified into the next three categories: region I, where the flow is completely laminar, region II, where the thin boundary layer is produced, and region III, where the separation layers generate vortices. These relationships are shown in Fig.6.1 [11].

In the case of a circular cylinder, the flow past greatly depends on the R_e numbers, as shown in Fig.6.2 [11]. In the engineering field, the characteristics in R_e numbers more than 10^5, being in subcritical range and supercritical range, have been a main theme of research. In a subcritical range, a flow stream up to the separation point is laminar, and then transition to turbulent flow occurs in the wake. Beyond a R_e number of 2×10^5, the wake narrows considerably and vortex shedding appears much more random. In a supercritical range, the separation bubble disappears and transition to turbulent separation occurs without being accompanied by flow separation. A boundary point between a subcritical range and a supercritical range is called a critical R_e number.

The relationship between drag coefficient, C_d, of a circular cylinder with a smooth surface in a uniform flow and the R_e number is indicated in Fig.6.3. As it is clear from the figure, drag coefficients of a circular cylinder are remarkably affected by the R_e numbers. In a subcritical range, C_d remains almost 1.2, and it drops sharply in a R_e number of 2×10^5 to 4×10^5. C_d increases moderately up to about 0.7 in an ultracritical range. Taking the R_e numbers' effect into consideration, the drag coefficient is determined to be 1.2 below the critical R_e number, and 0.7 beyond it by the specification of the Honshu–Shikoku Bridge Standard in Japan.

These phenomena can be explained by the pressure distribution around a circular cylinder. Fig.6.4 shows a typical distribution of the mean pressure coefficient for a circular cylinder in a smooth flow as a function of an angular position [22]. The non–dimensional pressure coefficient is defined by the following equation.

$$C_p = (P - P_\infty) / (\rho U^2 / 2) \qquad (2)$$

where U is flow velocity and $P - P_\infty$ represents the pressure difference between local and distant upstream pressure P_∞. The integration of the pressures over the body surface results in a net force, being a drag force for a circular cylinder.

The circular cylinder has the maximum pressure at the stagnation point, $\theta = 0$, and the minimum at $\theta = 70 \sim 80$ [23]. From there the pressure increases gradually. When the R_e numbers are within the range of 1×10^5 (case a), the pressure around the separation point is the weakest, therefore, the drag coefficients become the highest, being about 1.2. In a R_e numbers range of $3 \sim 4 \times 10^5$ (case c), when the pressure around the separation point is the strongest, the drag coefficients go down to the lowest, about 0.3.

(2) Influence of surface roughness

The surface roughness also has a great effect on the drag coefficient of a circular cylinder around a critical R_e number range, since changes in drag coefficient are dominated by the location of a separation point. The surface roughness causes a shift in a separation point along a body where the section is circular, and this accelerates the transition into a turbulent flow range. Generally speaking, when uniform roughness is given to a circular cylinder, a critical R_e number shifts to a lower R_e number range. The minimum drag coefficient at the critical R_e number increases as surface roughness becomes greater, and it also increases beyond the critical R_e number. Fig.6.5 shows the influence of surface roughness on drag coefficient in terms of relative surface roughness k/D, where k is the average grain size of sand and D is the diameter of the circular cylinder [24].

When roughness partially is given to the surface of a circular cylinder, the flow around it is greatly affected by the location or distribution of roughness as well as the R_e numbers. The influences of the location and distribution of roughness on the drag coefficient are shown in Fig.6.6 [12]. In any case, partial roughness also can affect acceleration of the transition from the laminar flow into the turbulent flow, as a result the critical R_e number decreases. It is found that the drag coefficient doesn't increase so much beyond the critical R_e number range, having almost the same value of that of a circular cylinder without any roughness. But if a partial roughness is distributed to a wider area around the separation point, for example $\theta = 50° \sim 130°$, the drag coefficient immediately increases and approaches to 1.0, indicating the same characteristics as that of a circular cylinder with uniform roughness. It is estimated that the difference is caused by the movement of the separation point, consequently the location and distribution of roughness also have a great influence on the flow near the

separation point.   The relation between them is the subject for a future study.

6.2.2   Dynamic behavior of a cable

Dynamic behavior of a stay cable in cable−stayed bridges is classified into three categories: vortex−induced vibration, rain vibration and wake galloping.   They are briefly explained as follows.

(1) Vortex−induced vibration

When the wind blows across a circular cylinder such as a cable, alternating vortices are shed from the cylinder and form a vortex trail downstream, as shown in Fig.6.7 [11].   The vibration caused by vortex shedding occurs when the wind velocity is such that the vortex shedding frequency, f_s, corresponds to a natural frequency of the cable, f_n.   The frequency of the shed vortices f_s, the mean wind velocity U and the cable diameter D can be expressed as the Strouhal Number.

$$S = f_s D/U \tag{3}$$

The Strouhal Number of a cable greatly depends upon the R_e number.   The relation of the Strouhal Number to the R_e number is shown in Fig.6.8 [24].   The Strouhal Number is approximately 0.18 in the subcritical range where the vortex−induced vibration is usually observed, and the critical wind velocity can be estimated as $U_{cr} = 5.5 f_n D$.

Under the action of vortex shedding, the cable vibrates periodically at the frequency of f_s.   Near the frequency of f_s, greater cable movement is induced and the cable begins to interact strongly with the flow, then the natural frequency of the cable, f_n, controls the vortex shedding.   This phenomenon is commonly known as lock−in, as shown in Fig.6.9 [24].   It is a characteristic of the vortex−induced vibration that has a strong nonlinearity of aerodynamic force being dependent on the response amplitude and is considered as a kind of self−excited vibration.

The response amplitude of the vibration is sensitive to the mass−damping parameter, the Scruton Number, S_c,

$$S_c = 2m \, \delta / \rho \, D^2 \tag{4}$$

where, m is cable mass per unit length, δ is logarithmic decrement and ρ is air density. Fig.6.10 shows a typical example of a response amplitude for a circular cylinder [25].   The response amplitude practically decreases to a low level when the Scruton Number is beyond 20.

According to Ref. [1], the vortex−induced vibrations occurred in stay−cables of various cable−stayed bridges.   It was found that the vibration was observed in a low wind velocity range with high order modes.   There seemed to be a tendency for the vibration to occur more frequently as a cable has become longer.   However, the exciting force is very small, and it can be suppressed when structural damping of 0.01～0.015 in logarithmic decrement is added to the cables.

(2) Rain vibration

Vibrations induced by the combined effects of rain and wind, named rain vibration, have often been observed in stay cables.   Rain vibration is caused by water rivulets forming on the cable surface giving it an aerodynamically unstable shape, as shown in Fig.6.11.   Rain vibration was first observed in the Meiko−Nishi Bridge, and the phenomenon was subsequently confirmed by a wind tunnel investigation.   Fig.6.12 shows the measured example of the rain vibration on the Meiko−Nishi Bridge [4].   The stay cables of the bridge were covered by polyethylene, having a diameter of 125～165 mm.   And they were 65 to 200 m in length.   Only the cables that sloped downward in the wind direction vibrated.

After that, rain vibration was observed in various cable−stayed bridges such as the Hitsuishijima Bridge, the Iwakurojima Bridge, the Aratsu Bridge and the Tenpozan Bridge [1,2,26,27].   The characteristics of rain vibration based on the observations in actual bridges are shown in Fig.6.13(a)～(c) [2].   Based on the field observation data, rain vibration characteristics of the stay cables are summarized as follows.

a) Vibrations occur at low frequency modes such as 1st to 3rd mode, within a frequency of 3 Hz.

b) Vibrations are recognized   under the wind velocity is more than 6 m/s,   or the reduced wind velocity more than 20.

c) Vibrations frequently occur in the cables with a vibration node length of about 50 m.

d) The cables that slope downward in the wind direction frequently vibrate.

e) Vibrations occur in cables having a smooth surface such as polyethylene.

f) Vibrations can be suppressed when the Scruton Number is more than 60.

Extensive research into the mechanism of rain vibration has been carried out by using a wind tunnel test.   Referring to [4], it is pointed out that vibration is caused by the combined factors, water rivulets formed on the surface of the cable and an axial flow generated near the inclined cable.

It is considered that water rivulets either on the upper or lower side of the cable play the key role in inducing rain vibration. Many experiments using wind tunnel tests with simulated rainfall and analysis were carried out to investigate the fundamental behavior of water rivulets on cable surfaces [17,28,29]. The cable response of a wind tunnel test under a simulated rainfall using a two-dimensional model is shown in Fig.6.14 [4]. The cable attitude to the wind, a yawing angle β, and an inclined angle θ, are defined as shown Fig.6.15.

When water was sprayed on the cable, a vibration with a large amplitude occurred at a higher wind velocity range than that of a vortex-induced vibration range. It was found that upper rivulets were formed on the surface of the cable while vibrating. This is a typical example that indicates that the vibration is caused by the existence of water rivulets on the surface of the cable, giving it an aerodynamically unstable shape. A paper pointed out, based on the test results, that a specified location or width of water rivulets were necessary for vibration to occur. The reasons for the unstable vibration could be considered that it is a kind of galloping caused by a negative lift coefficient, similar in behavior to power cables, or of a self-exciting vibration caused by water pulsation on the surface [30]. But, the phenomena can not be simply explained by these.

The other factor considered to induce vibration is an axial flow generated near the inclined or yawed cable [5,31]. Fig.6.16 shows the relationship between the wind velocity and the yawing angle of the cable [31]. It was found that the velocity of the axial flow depended upon the yawing angle and that wind velocity of the axial flow along the cable, V_a, increased as the yawing angle became larger. When the yawing angle, β, was 45°, the wind velocity of the axial flow reached up to 90% of the wind velocity. And aerodynamic response characteristics of the inclined cable were almost the same as those of the yawed cable. Thus, it is considered that the inclined cable fundamentally has aerodynamic instability, generating the vibration. Therefore, it is regarded that the vibration is caused by these complicatedly mixed factors such as the water rivulets and the axial flow.

It is reported that the additional damping requirement to suppress vibration is at most 0.02 in logarithmic decrement, and that the turbulent flow reduces the response of the vibration.

(3) Wake galloping

When two stay cables are closely arranged in parallel, the downstream cable may be excited by the wake of the upstream cable, it is called wake galloping [1,2]. The vibration is explained in Fig.6.17. The vibration was observed in some bridges such as the Hitsuishijima Bridge, the Iwakurojima Bridge and the Yobuko Bridge [1,2]. Vibration occurs usually at the first mode, in the reduced velocity of more than 20. It is reported that vibration occurred when the wind direction was about 0° to 45° from a transverse direction to the bridge axis and the amplitude grew as the wind velocity increased. The amplitude observed was about twice as much as that of the cable diameter.

It is considered that the spacing of the two cables is a dominant parameter of vibration. The tested results of the influence of the distance between the cables on vibration amplitude are shown in Fig.6.18 [32]. Vibration occurs within the space ratio of five. It is considered that a vibration can be suppressed when the distance between the center of the two cables is more than about five times that of the cables' diameter. However, so-called wake induced vibration appears again when the distance between the cables is increased, becoming 10 to 20 times that of the cables' diameter.

According to a wind tunnel test, a vibration is caused by an accelerated flow generated on the upper or lower surface of the downstream cable. This accelerated flow plays a key role in the occurrence of wake galloping. The flow patterns for various cable position are shown in Fig.6.19 [33]. Vibration is also investigated using a flow visualization analysis. It is pointed out that a vibration is caused by the relative location of each cable, that periodically changes the flow condition at the two adjacent cables and that it is a kind of self-excited vibration.

It is generally considered that logarithmic damping of 0.05 is required to suppress a vibration and that turbulence has little influence on the vibration.

6.2.3 Countermeasures against cable vibrations

Various techniques have been used in actual cable-stayed bridges to control cable vibrations. They are classified into two main categories: one is structural countermeasures, the other is aerodynamic ones, being introduced as follows.

(1) Structural countermeasures

  1) Installing damping devices

This method is to install some kind of vibration-damping devices on the cables near the cable anchor points in order to increase structural damping of the cables. This countermeasure is now widely used for various cable-stayed bridges to suppress vibrations, especially rain vibration. It is considered that additional damping as the Scruton Number of more than 60 is required to suppress rain vibration.

The dampers are usually attached on the deck near the cable anchor points. They are placed to suppress not only vertical vibration but also horizontal vibration. There are two types of dampers being used: namely, oil-damper and viscous-shearing damper.

Oil-dampers are widely adopted around the world: the Brotonne Bridge and the Normandy Bridge in France, the West Gate Bridge in Australia, the Sunshine Skyway Bridge in the U.S.A., the Aratsu Bridge and the Tenpozan Bridge in Japan. An example of an oil-damper used in the Brotonne Bridge is shown in Photo.6.1. Viscous-shearing dampers have been recently developed in Japan, and used for the Sakitama Bridge, the Tomei-Ashigara Bridge and a few other bridges in Japan [6,34], as shown in Photo.6.2.

The spacer-damper is used for the Yokohama Bay Bridge, as shown in Fig.6.20 [35]. A damper is built in the spacer which connects the cables to each other, and a damping effect is obtained when the downstream cable vibrates, utilizing the damping force of the downstream cable. A rubber is sometimes used as a buffer device near the anchor point of the cable to prevent any bending of the cable. It is reported that rubber increased the damping of the cable a little, logarithmic damping of 0.01, in the 1st Kemi Bridge. A rubber-damper having higher damping effect is now being developed.

Damping effects can be estimated by analytical calculation. The mode damping ratio ξ ($= \delta /2 \pi$) of a cable with a damper is theoretically given,

$$\xi /(x_c /L) = \pi^2 (C/mL \omega)i(x_c /L) \tag{5}$$

where, x_c is a point where a damper is attached, L is a cable length, m is a unit weight, ω is a first mode frequency and i is a mode order. The equation indicates that a damping effect is a function of an attached point ratio, x_c /L, and is greatly affected by a length of a cable, as shown in Fig.6.21 [36].

In the case of a long stay cable, it is required to have a large value of x_c in order to get a sufficient damping effect, that means a damper is attached more than a few meters above the deck. But, there is a limit to the places where additional damping devices can be installed, because it is desirable that dampers are attached near or below the handrails or guardrails on the deck, from the structural, economical and also aesthetic points of view. Therefore, there are certain cases in which it is impossible to obtain a sufficient damping effect by dampers.

2) Tying the cables with wires

This method is to tie stay cables with wires in order to suppress the vibration mechanically [37,38], as shown in Fig.6.22.

The system is adopted in the Meiko-Nishi Bridge, the Hitsuishijima Bridge, the Iwakurojima Bridge and the Yobuko Bridge in Japan, and the Faro Bridge in Denmark and the Damespoint Bridge in the U.S.A. Stay cables are usually tied by more than two wires made of stainless steel. Sometimes, the system is used together with spacers or dampers. It is necessary to pay attention to the strength of the wire itself, because a large force occurs in the wire when the cables vibrate. In fact, there are some cases in which the wire was broken or loosened.

This method expects the mass effect, the damping effect and the frequency effect [2]. These effects are briefly explained as follows. The cables are vibrated with other cables by tying wires, as a result the mass of the cables relatively increases, giving a suppressing effect.

When the cables are vibrated with wires, a large force, namely strain, occurs in the wires. That increases the damping of the cable-wire system by dissipating the hysteresis energy of the wires. Points to which special attention should be paid are that the damping effect is dominated by many factors such as the material of the wire, elongation property of the wire and the arrangement of the wire.

The tying wires divide a stay cable length into two or more sub-spans, increasing the frequency level of the cable. More than two wires are usually used, because the frequency of a cable does not increase so much by using only one wire.

But, it is considered that the suppressing effect, especially for rain vibration, can not be quantitatively estimated at present because the mechanism of a vibration is unclear. This is the subject for a future study.

(2) Aerodynamic countermeasures

The other method is to improve the aerodynamic characteristics of cables by giving deformation on their surfaces, this is called aerodynamic countermeasures. Extensive research concerning the suppressing measures of cable vibrations, especially rain vibration, has been carried out, and a few countermeasures are adopted in actual cable-stayed bridges [2].

In the East-Kobe Bridge, parallel protuberances were applied to the surface of the stay cables covered with polyethylene. The projections are 5 mm in height, 11 mm in width, and are attached at a pitch of 30 ° on the circumference, as shown in Fig.6.23 [6]. The cables are 140 mm in diameter. Helical streaks were added on the surface of the stay cables in the Normandy Bridge. The streaks are 3 mm in height, and are put at a pitch of 60 mm on a polyethylene pipe, as shown in Fig.6.24 [8]. U shaped groovings were cut on the surface of the stay cables coated by polyethylene, in the Yuge Bridge. The groovings are 2 mm in depth, and are cut at a pitch of 10 ° on the circumference, shown in Fig.6.25 [39].

Except the above mentioned, various aerodynamic countermeasures are proposed through wind tunnel tests. They are of a helical wire method, V grooving method, transverse

scraping method [17], twisted hexagonal section method and octagonal section method [9].

It is considered that the countermeasures are to control aerodynamically the cause of a vibration. The mechanism of the suppressing effects is investigated and analyzed as follows.

The first one is considered to be the shape effects: that is to prevent formation of any stable water rivulets on the surface by changing the cable surface. It is possible to control the separation point by changing the shape, disturbing the air pressure distribution balanced on the cable surface. Because when rain vibration occurs, water rivulets are formed at a specified position, being balanced between water gravity, water surface tension and air pressure force on the surface of the cable. The parallel protuberances and the helical streaks are examples being applied to this mechanism [40].

Another considered is the surface roughness effects. As mentioned before, a flow around a cable greatly depends upon the Reynolds Number. The roughness given to the surface of the cable causes a shift of the separation point, and that makes it possible to reproduce a supercritical state at a wind where rain vibration occurs. As a result, a peak negative pressure caused by the surface roughness suppresses the formation of water rivulets on the cable. U or V groovings are considered to be based on this mechanism [39].

The other one is considered to be the water repellent effects. It is clear from the tested results that the occurrence of vibration is affected by water volume flowing along the surface of the cable. The water volume on the cable depends upon the surface condition of the covered materials such as polyethylene. It is possible to increase the water repellence of the polyethylene cable surface by scraping it or by coating it with highly water-repellent substances such as a fluoropolymer. This mechanism is applied to the transverse scraping method.

Aerodynamic countermeasures mentioned above, such as parallel protuberances or U groovings, are apt to cause a greater drag force at the design wind velocity than that of a smooth surface. In the design of a long cable-stayed bridge, a smaller drag force is essentially preferable, then these aerodynamic methods having a large drag force can not be applied to a long cable-stayed bridge. Therefore, it was quite necessary to investigate any aerodynamic countermeasure to develop a cable section with a smaller drag force and better vibration suppressing effects at the same time.

6.3　A Study on Cable Response Caused by Vortex-Induced Vibration

6.3.1　Field observation of vortex-induced vibration in a long cable-stayed bridge

During the constructing stage of the Ikuchi Bridge, vortex-induced vibration was frequently observed, although rain vibration did not occur. Field observation of the cable behavior was conducted to obtain data on vortex-induced vibration in the bridge [16]. The Ikuchi Bridge is a long cable-stayed bridge consisting of a multiple type with mono-strand cables, having a main span of 490 m, as shown in Fig.6.26. It was completed in 1991. Table 6.1 shows the main dimension of the stay cables.

The observation was carried out before and after an elastic rubber was attached near the anchor point of the cables in order to confirm the suppressing effect of the rubber. The elastic rubber was originally installed as a buffer device to relieve any secondary stress of the cable near the anchor point, but at the same time, it was expected to increase the damping of the cable. The structural damping, natural frequency and amplitude of the cable were measured within a wind velocity of 2 m/s by using an acceleration meter fixed on the cable. Measurements were also carried out when the cable was vibrated by the wind.

The vibration frequently occurred at a low wind velocity of 10 m/s or below, and the vibration could be recognized as a vortex-induced vibration in view of the frequency [3]. Fig.6.27 shows an example of the observation results of the cable, being 113 m in length and 136 mm in diameter. Table 6.2 shows the maximum amplitude of each mode. As measurements were taken at locations approximately two meters above the girder, the double amplitude shown in Table 6.2 are the values obtained by converting the measured amplitude into the maximum amplitude of each mode. The intensity of turbulence in the direction of the main stream was less than $10 \sim 15\%$ for the most part, and the mean intensity, with a wind velocity around 10 m/s, was about 10%.

The structural dampings of the cables were obtained from the first through fourth modes as shown in Table 6.3. Depending on the condition in which the respective vibration modes were measured, the logarithmic decrement of the cable varied in the range of 0.001 to 0.006, averaging to be approximately 0.003. This value was nearly the same as the previously measured value [34,41]. After an elastic buffer was installed, the structural dampings of the cables increased to a range of 0.012 to 0.020, averaging approximately 0.015, and as a result, the amplitude decreased. It was found that the elastic rubber had a suppressing effect on the vortex-induced vibration.

6.3.2 Aerodynamic characteristics of cable with surface roughness

(1) Wind tunnel test overview

As the cable response caused by vortex—induced vibration is closely related to the surface roughness of the cable and structural damping, these factors were examined and analyzed through a wind tunnel test. The wind tunnel test was conducted in the Public Works Research Institute of the Ministry of Construction.

The cable models used were identical in diameter to the actual stay cables, and their aluminum tube was coated with the same polyethylene that is now used for the bridge cables. The surface roughness of the bridge cables ranges between 3 and 30 μ m. The additional model surfaces were covered with thermally melted polyethylene particles to artificially create the surface roughness of 100 to 1500 μ m in order to examine the effect of surface roughness. Its surface roughness was represented by the mean roughness R_z on the roughness curve and measured using a contact type surface roughness tester. Fig.6.28 shows an example of the surface roughness measured. In this figure, the same roughness was distributed in a very similar pattern, therefore no specific attention was given to the shape of the roughness. In the case of the roughness being more than 200 μ m, the mean roughness was indicated by reading from an enlarged photograph of the cross section.

The cable models weighed about 1/6 to 1/7 of the bridge cable weight due to the limitation of the testing facility, so the Scruton number was approximately 2.5. At the time of resonance vibrations, the Reynolds number was approximately 2.5×10^{4}, and the frequency was about 4 H z, which was close to the frequency of the bridge. Table 6.4 shows the cable model dimensions which were used for the tests, and they are shown in Photo. 6.3.

(2) Test results

Fig.6.29 shows the effect of the surface roughness on the vortex—induced vibration amplitude. Except for model A6, which had an extremely different surface roughness, the relationship between the wind velocity and the amplitude was nearly identical, including the maximum amplitude. An insignificant difference in developing the amplitude was that each cable was probably subject to nearly the same aerodynamic force. Also, there was no significant difference observed at models A1 through A3, in the relationship between the surface roughness and the drag coefficient as shown in Fig.6.30. Therefore, for stay cables of a cable—stayed bridge, the difference in the surface roughness would hardly affect the vortex—induced vibration amplitude when the ratio of the surface roughness to the diameter, k/D, is less than 0.01 in a Reynolds number range where the vortex—induced vibration usually occurs.

Many stay cables for cable—stayed bridges have a cylindrical section and are coated with polyethylene. Their surface roughness is within the range of 30 μ m, namely being that of models A1 and A2. Depending on the bridge, the frequency of vortex—induced vibration differs. This may be due to the difference in the cable surface roughness. But, the test result indicated that the difference in the intensity of the turbulence, the characteristics of wind property (such as wind directions) and structural characteristics (such as structural damping) were the main reasons that affected vortex—induced vibration amplitude, when the surface roughness of the cable was less than 100 μ m. A further detailed study would be necessary to clarify the effect of vibration on turbulence or on the range where the drag coefficient suddenly changes.

Fig.6.31 shows the relationship between the drag coefficient and the surface roughness for various Reynolds number ranges. It is found that a decrease in the drag coefficient, which was seen in the supercritical range, was observed as the surface roughness increased. Compared to a decrease of a cylinder with a smooth surface in the supercritical range, the decrease of the cable models was less than that of the smooth surface, and the drag coefficient recovered again as wind velocity increased. The results suggest that the flow had a pattern between the subcritical and supercritical range, although the surface roughness of the cable affected both the separation point and re—attachment of the flow.

The test was carried out on a finer surface roughness area than that of previous tests, and it was learned that the drag coefficient was slightly affected even though the roughness ratio was in the order of 10^{-4} to 10^{-5}. When the roughness ratio was in the range of 10^{-2} to 10^{-3}, the results agreed with those of the previous studies.

To examine the effect of structural damping, tests were carried out by changing the damping using cable model A1. As shown in Fig.6.32, the results indicated that the tendency of the amplitude varied inversely with that of the structural damping, except in a low damping range. Fig.6.33 shows the relationship between the Strouhal number and the structural damping. The reciprocal of a reduced wind velocity at which the maximum amplitude occurred approached 0.2, and that can be regarded as the Strouhal number of a circular cylinder, with an increasing structural damping.

The test was conducted using light cable models, therefore it is further necessary to investigate the relationship between the actual bridge cable and vortex—induced vibration amplitude. The non—dimensional amplitude of the Ikuchi Bridge was 0.08 to 0.1, which was nearly the same as the amplitude that occurred in the wind tunnel test with a structural damping of 0.01. The non—dimensional mass of the cable (m/ ρ D ^{2}) in which

vortex—induced vibration was observed, was 6.5 times greater. This presumably indicates that the structural damping was near 0.002 to 0.003, suggesting that there would be many values smaller than those achieved through the test. This proves that the results match the assumption, the vortex—induced vibration amplitude is virtually inverse proportionately to the Scruton number.

6.3.3 Discussion on cable response caused by vortex—induced vibration

(1) Estimation of cable response caused by vortex—induced vibration

In order to estimate the amplitude of vortex—induced vibration more quantitatively, influence of damping was analysed using the energy—balance method [42]. The energy—balance analysis method is to obtain the cable amplitude from the balance between the wind—input energy and the consumed energy of the cable. This method is known to achieve a reliable value empirically with respect to power transmission cables, therefore it was applied to the calculation.

Input energy P_w is calculated using Slethei's equation, an empirical equation which has been applied to the analysis of the vibration of power transmission. This equation assumes the dynamic lift coefficient in order to calculate the input energy. In the case of this analysis, the dynamic lift coefficient allows for amplitude dependence. The equation is given,

$$P_w = 16.2C_1 f^3 D^4 [Y_0/D + 0.6(Y_0/D)^2] \quad (W/m) \tag{6}$$
$$C_1 = 1.7/[1 + 0.07(1 - U)^2]$$

where, C_1 : dynamic lift coefficient

f : frequency (Hz)

D : cable diameter (m)

Y_0 : double amplitude (m)

U : fD/0.2 (m/s)

Fig.6.34 shows the relationship between the input energy and the amplitude, and Fig.6.35 the amplitude and frequency of the measured data.

As for the consumed energy P_c, it was calculated on the assumption that P_c was in proportion to the damping, although P_c often uses experimental values achieved through the vibration test of an actual cable, because it differs according to the tensile force working on the cable or cable types.

$$P_c = 4\pi^2 f^3 w Y_0 L \delta \tag{7}$$

where, w : unit weight of the cable

L : cable length

δ : logarithmic decrement

Fig.6.36 shows the calculated results and the measured values. In the figure, the calculated balance amplitude can be achieved by obtaining the input energy (broken line) and the consumed energy (solid line), taking the amplitude and energy as axes until they concur. In this analysis, a structural damping (logarithmic decrement) of 0.003 was used.

Furthermore, the effects of damping were examined in a similar manner by calculating the amplitude of 0.01, 0.015 and 0.02 given as a logarithmic decrement. Fig.6.37 shows the relationship between the frequency and the amplitude in each damping. Based on the measured values, this method would be able to estimate the peak amplitude of vibration, except for low modes. Concerning the added damping effect on reducing the amplitude of vibration, it is considered to be well correlated with the calculated value, since the peak amplitude, after the buffer devices had been installed to the cable, was approximately 4 mm at most. The experimental equation based on the analysis method, except for low modes, can be expressed as follows:

$$Y = 10^{-0.073x} \times 0.17/\delta \tag{8}$$

where, x : frequency (Hz)

Y : double amplitude (m)

δ : logarithmic decrement

As the experimental equation was based on the results of only one observation example, it is necessary, in a strict sense of the word, to make corrections, taking into consideration the effect of turbulence and geographical features. Also the accumulation of measured data obtained under the conditions with different cable dimensions is required, and therefore these are the subject for a future study.

(2) Influence of vibration on the bending fatigue strength of cables

The amplitude of vortex—induced vibration was calculated using the experimental equation in order to examine the influence of cable anchors on the secondary stress and bending

fatigue strength.

The response amplitudes of vortex—induced vibrations of the fourth through sixth modes were estimated in terms of cables having lengths of 50 to 500 meters. The results are shown in Fig.6.38. The amplitudes were calculated for the cable, composed of 301 wires, each being 7 mm in diameter, the logarithmic decrement of δ =0.003 and cable tensions T=0.3T $_B$. The amplitudes gradually increased in proportion as the cables became longer, and there is a possibility that the maximum amplitude of the cables 400 to 500 m long (η /D), approximately equal 0.15.

From Fig.6.39, it is found that the bending angles relatively decreased as the cables lengthened. With a cable length of 100 meters or so, its maximum bending angle was 0.06 °. Therefore, the maximum bending angle using for the design would be considered 0.1 °. According to the previous study, the secondary stress was 2 kgf/mm ^{2} (20 MPa), when the bending angle was 0.1. Also for bending fatigue strength of the cable, the secondary stress was smaller than bending fatigue limit of $\pm$ 0.6 ° [43]. Both static and bending fatigue can be judged as problem free for the amplitude caused by vortex—induced vibration.

6.4 Experimental Discussion on Rain Vibration of Cable with Surface Roughness

6.4.1 Fundamental characteristics of rain vibration

First, a series of experiments were carried out to learn about the formation and behavior of water rivulets on cables when rain vibrations occurred. Then, the relationship between rain vibration and location or volume of water rivulets was examined through the tests, indicated as follows.

(1) Outline of the experiment

Fig.6.40 shows the general view of the wind tunnel test. The test model, being 3 m in length, was set up and supported vertically by springs. Piano wires were used to keep the cable to face the wind direction and the cable axis direction, allowing it to vibrate along a vertical direction only. Referring to the results of previous research reports, the cable was placed to have an inclined angle θ =45 ° and a yawing angle β =45 °. The wind tunnel used in the experiment was a Gettingen type wind tunnel with a height of 2,000 mm and a width of 1,200 mm. There was no correction made for the experimental results, although the blockage ratio (wind tunnel mouth area to cross—sectional area of the cable model) was a rather large 14%.

To simulate rainfall, a spray water nozzle (water volume Q $_1$) and a supply water nozzle (water volume Q $_2$) were used. As pointed out Ref.[17], the outcome of this type of experiment greatly depends on the placement of water nozzle. Special care must be taken when the nozzle is placed in the middle of the air flow, since the existence of the nozzle itself delicately affects the vibration response of the cable, and this is why a great deal of care was taken to determine the optimum location for the nozzle before the experiment. Namely, the nozzle was put in place and static air forces on the cable model without rainfall were measured in order to survey the influence of the nozzle. The placement of the nozzle was examined in rainfall condition to find a location not disturbing local air flow and allowing the nozzle to keep a steady rainfall. As a result, the nozzle was determined to be at a position a=400 mm and b=70 mm from the cable, as shown in Fig.6.41.

The most important objective of the rain vibration experiments was to learn about water rivulets forming along the surface of the cable. The location of the water rivulets was judged by the markings drawn along the surface of the cable. A television camera was also used to record and analyze the formation and behavior of water rivulets. The volume of the water rivulets was measured by the quantity of water which flowed off the end of the cable.

A steel pipe covered with a polyethylene, in the same way as an actual bridge cable, was used in the experiment. The model cable weighed 21 kgf/m (206 N/m), having a natural frequency of 1.8 Hz, a 0.003 in logarithmic decrement. Considering that a Scruton number of 2.3 was only one—fifth of that of an actual cable, the model cable used in the experiment was extremely light and sensitive to vibration. The dimensions of the model used in the experiment are shown in Table 6.5.

(2) Results of the experiment

1) Vibration characteristics

The test results of the polyethylene—coated model cable, caused by a spray water nozzle, are shown in Fig.6.42. Vibration of a velocity—restricted type occurred when water was sprayed from the nozzle onto the model cable, while there was no vibration observed without rain.

The vibration thus observed was clearly the result of the wind and rain. The vibrations of a velocity—restricted type occurred at wind velocity of between 9 m/s and 13 m/s, being a Reynolds numbers of 0.9 ~ 1.3 X 10 ^{5}. It reached the maximum amplitude when the quantity of simulated rain became 0.8 liters/minute. Quantities of rain greater than this resulted in less amplitude and a narrowing of the range of wind velocity in which rain vibration occurred. It is considered that the volume of water flowing along the surface of the cable affected the

occurrence of the vibration, since no vibration was observed at a water volume of 2.0 lit./min.

Observing the surface of the vibrating cable, the stable streams of water flowed down the upper and lower surfaces of the cable along its axis. Comparing this to what has been learned from the observation of actual bridges and various wind tunnel tests, the range of wind velocity in which rain vibration occurred in this experiment closely resembled the previous data [1,2]. Thus, it was considered that the conditions leading to rain vibration have been properly reproduced.

The supply water was designed to correspond to the flow of water along the cable from its upper end. It was simulated here through the use of a nozzle supplying water on the cable at one point only from outside the wind flow. The stable streams of water flowed down along the upper and lower surfaces of the cable and vibration of velocity—restricted type occurred at wind velocity of between 9 m/s and 13 m/s. This was quite the same result as those gained from the spray nozzle. Since the effects of the supply nozzle seemed to be equivalent to that of the spray nozzle, all subsequent experiments were conducted using the spray nozzle alone.

2) Analysis on water rivulets

In order to learn about the formation and behavior of the water rivulets flowing along the upper and lower surface of the cable, measurements for amount of water in these rivulets as well as their location and width were carried out. The volume of water in these rivulets was measured by placing a bucket at the end of the cable to catch the water as it flowed down along the upper and lower surfaces of the cable and dripped down from the cable's end.

Fig.6.43 shows the volume of water measured from the rivulets running down the upper and lower surfaces of the cable during the experiment. From these measurements, it was observed that a vibration of velocity—restricted type occurred when the volume of water was below 0.6 lit./min., a quantity which corresponded to roughly 40 to 60 % of the water sprayed down on the cable during the experiment. At a high wind velocity range, water was blown away by the wind, and at a wind velocity of 20 m/s, the supplementary ratio fell as low as 30% and vibration no longer occurred.

The inertia of the vibrating cable together with the wind force caused the water rivulets fluctuating along the upper surface of the cable to spiral around the circumference of the cable as they flowed downward. On the other hand, the water flowed down along the cable axis and the flow velocity grew faster, when there was no vibration or the amount of water was too much.

Fig 6.44 shows a comparison of the volume of the water caught on the upper and lower surfaces of the cable. The figure indicates that the volume of water in the rivulets flowing along the upper surface was less than that of the lower one. It is considered that the location of the rivulets shifted downward of the circumference of the cable, preventing water rivulets from being blown away by the wind, together with the effects of gravity.

Fig.6.45 shows the location and width of the water rivulets which formed along the upper and lower surfaces of the cable as determined with respect to the markings drawn on the cable beforehand. A summary of the location and width of the water rivulets forming on the cable is shown in Fig.6.46 through Fig.6.49.

As shown in Fig.6.46 and Fig.6.47, water rivulets on the upper surface of the cable formed suddenly when the wind reached a velocity of about 10 m/s, and continued to form steadily at a higher wind velocity range. Since the water rivulets flowing down the lower surface of the cable existed at all tested wind velocities, it is considered that the upper water rivulets is one of the causes of rain vibration. These phenomena agreed well with the results of previous research. It was found that the center of the upper water rivulets was located at $\theta = 45°\sim 60°$, and that it shifted downward as wind velocity increased.

Fig.6.48 and Fig.6.49 show the measured width of the water rivulets flowing along the cable surface. At a wind velocity range where rain vibration occurred, the width of the water rivulets flowing along the upper surface was greater than that of the lower one, and $\Delta\theta \leqq 20°$. Referring to the ratio of the upper flow to the lower, the depth of the upper water rivulets seemed to be approximately one—third to one—fifth of that of the lower one.

Fig.6.50 shows the relationship between the water volume and the logarithmic decrement of the cable. It was found that rain vibration didn't occur when there was too much rain or when the wind velocity was too high. This indicates that rain vibration only occurred when the water flowing along the cable met certain conditions. When the width of the water flow increased or its depth decreased, the balance created by the wind and water on the surface of the cable was disturbed and rain vibration tended not to occur under these circumstances. Through the experiment, the behavior of the water rivulets was understood, but a qualitative analysis remains a problem for future research.

6.4.2 Experimental discussion on suppressing effect of surface—roughened cable

(1) Aerodynamic properties of cables with surface roughness

To understand the effects of surface roughness on aerodynamic properties, a three—component test was carried out [18,19]. Aluminum pipes with the same diameter and with a polyethylene coating as those used in actual bridge cables were used as cable models. To clarify the effects of surface roughness, models with different shapes and distributions

were prepared.

As shown in Fig.6.51, a grid—like roughness was applied over the whole surface of models B1 to B3, and this roughness was described in terms of the depth of the grid. As shown in Fig.6.52 and Fig.6.53, the circular concave and convex patterns were added discretely to the surface of models C2 and C3, and the roughness was described in terms of the depth of the concavities or the height of the convex sections. Table 6.6 shows the experimental parameters for these cable models.

Experiments were implemented on models B in a low—speed wind tunnel 2.0 m in section height and 1 m in width, the same wind tunnel previously mentioned in section 6.3.2. Measurements were made up to a wind velocity of about 25 m/s, equivalent to a Reynolds number of about 2.2×10^5. Experiments on models C were carried out in a large—scale circulating wind tunnel with a 3.0 m section height and 2.0 m width at Sumitomo Heavy Industries Co.,Ltd. These measurements were extended up to almost the designed wind velocity assumed for actual bridges, or about 55 m/s, where the Reynolds number was 5.5×10^5. The ratio of wind tunnel mouth area to cross—sectional area of the model, known as the blockage ratio, was less than 7% for models B, and 5% for models C. Since the geometrical ratio of the model to the end plate had a critical effect on measurements, two—dimensionality was assured by providing a sufficiently large end plate.

Fig.6.54 shows the drag coefficient of models B_1 through B_3, which were given approximately the same degree of surface roughness as models A_4 through A_6, as mentioned in section 6.3.2, but in a grid —like pattern. The critical Reynolds number of models with this grid—like roughness decreased as the relative surface roughness increased, as with models A_1 through A_6 having a uniform surface roughness. However, the drag characteristics were different from those of models A; the drag coefficient increased gradually with increasing wind velocity. The critical Reynolds number of model B3, where the grid—like surface roughness was about 1% of the diameter, was about 6×10^4 and the drag coefficient was about 0.9 at a Reynolds number of 2.2×10^5.

Fig.6.55 shows the drag coefficient of models C2 and C3, which had approximately the same degree of surface roughness as models A6 (see Fig.6.31) and B3 but applied discretely. Experimental results of model C1, which had the same smooth surface as A1, agreed well with the previous study illustrated in Fig.6.3. Both C2 and C3 had the same behavior; the critical Reynolds number and drag coefficient were 1×10^5 and 0.6, respectively. Within the range of measurements up to a Reynolds number of about 5.5×10^5, equivalent to a wind velocity of about 55m/s, the drag coefficient remained approximately constant.

Thus, as noted in a previous study, the shape and distribution of surface roughness as well

as size had a strong influence on the drag characteristics of circular sections, because they changed the flow separation on the surface. The experiments described above indicate that the models having a discrete roughness have less drag force than that having a uniform roughness in the critical range and almost the same C_D value in the supercritical range up to a Reynolds number of 5.5×10^5. It was also proved that almost equivalent drag coefficients can be obtained with discrete roughness patterns as with smooth surfaces within the design wind velocity range. The effects of the shape and distribution pattern of surface roughness are described later.

(2) Experiment on suppressing effects of surface—roughened cables

In order to learn the vibration suppressing effects of surface roughness, vibration tests under simulated rainfall were carried out [18,19]. Fig.6.56 shows the wind tunnel apparatus used.

Models C1 through C3, each 3 m in length, were used for the test. The models were freely supported on a spring in a direction perpendicular to the cable axis, and fixed with piano wire in the direction of the cable axis. The model weight was 19.8 kgf (194 N), a natural frequency of about 1.8 Hz, the structural damping (logarithmic decrement) ranged from 0.003 to 0.004, and the Scruton number ranged from 1.7 to 2.3. Table 6.7 shows the experimental parameters for each cable. Cable models were set up with an inclined angle, θ, of $45°$, and a yawing angle, β, of $45°$ during experiments with rainfall, and an inclined angle, θ, of $45°$, and a yawing angle, β, of $135°$ during experiments without rainfall. These experiments were done in a Eiffel type wind tunnel having a 2.5 m height and 1.5 m width and equipped with a water nozzle. To simulate water rivulets, water was supplied from a point near the higher end of the model cable.

Fig.6.57 shows the vibration response characteristics of cable model C1 at a water volume of 0.8, 1.4, and 2.0 lit./min. Except for a vortex—induced vibration in the low wind velocity range, vibration didn't arise during the no—rainfall experiments on model C1 with a smooth surface. With simulated rainfall at a water volume of 0.8 and 1.4 lit./min., vibrations occurred at wind velocity of about 9 to 12 m/s and higher, respectively. This is a characteristic already proven by past experiments.

Fig.6.58 shows the damping characteristics of cables at a vibration amplitude ratio, A/D, of 0.1. Of the three water volumes studied, Fig.6.58 clarifies that the wind velocity range within which rain vibration occurred was the greatest and that negative damping was the highest with a water volume of 0.8 lit./min.

Fig.6.59 shows the V–A–δ curve for model C1. The maximum logarithmic decrement

for this cable model was about minus 0.07. In the experiment, measurements were continued up to a non−dimensional amplitude, A/D, of 1.0. Within this range, unstable vibrations occurred when the reduced wind velocity, V/(fD), exceeded about 40.

For models C2 and C3 with roughened surfaces, on the other hand, no rain vibrations occurred, as shown in Fig.6.60. This indicates that cables with such sectional forms had vibration suppressing effects. It was ascertained that no rain vibrations occurred in models C2 and C3 at other volume under the same experimental conditions as for model C1, although Fig.6.60 shows only the results at a water volume of 0.8 lit./min.

Fig.6.61 and 6.62 show the measured location and width of rivulets that formed on the upper surfaces of models C1, C2 and C3 at a distance of 2.2 m from the end of the cable models. The location of the rivulets was surveyed by reference to markings drawn around the surface of the cables. On the upper surface of model C1, which had a smooth surface, rivulets started forming at the same time as rain vibration occurred, or at a wind velocity of about 9 m/s, indicating that rivulets were one of the factors leading to rain vibration.

In the case of models C2 and C3, which had patterned surfaces, the location of rivulets on the upper surface shifted downstream in comparison with model C1. The rivulets on models C2 and C3, having a vibration suppressing effect, were located at an angle θ of $80°$ and $70°$, respectively. Although the rivulets on the upper surface of model C1 were located at an angle θ of about $60°$, the same location as noted in a previous study. The width of the rivulets, $\Delta\theta$, in the case of models C2 and C3 was about half that of model C1. These phenomena can probably be explained by the fact that surface roughness created small concave and convex patterns on the surface, increasing the apparent Reynolds number, and moving the separation point backward. This tendency was particularly marked in model C2, with the greatest vibration suppressing effects, where no rivulets formed on the upper surface at wind velocity in excess of 13 m/s.

In the case of models C2 and C3, which had roughened surfaces, water flowed along the concave and convex patterns in a way clearly different from the flows in model C1. In contrast with the stable boundaries between rivulets on the smooth surface of model C1, the boundaries in models C2 and C3 were unstable. It appeared that a stable formation of rivulets can be restrained by adopting a pattern of concavities and convexities as in models C2 and C3. Photo.6.4 and 6.5 show rivulets on the upper surface of the cable models.

To ascertain the vibration suppressing effects of cables with roughened surfaces, vibration tests without rainfall were conducted. The purpose of this test was to confirm the possibility of unstable cable vibrations when no rain was falling, even if no rivulets formed during rainfall, as reported previously.

Fig.6.63 shows the damping characteristics of models C1 and C2. For smooth surface model C1, unstable vibrations arose at a wind velocity of about 20 m/s. With model C2, which had the roughened surface, stability was seen throughout the wind velocity range, indicating that there was a suppressing effect even without rainfall.

(3) Pressure distribution of cables with surface roughness

Cables with a discretely roughened surface had different aerodynamic and vibration suppressing characteristics from those with smooth surfaces. Accordingly, their characteristics were analyzed in terms of pressure distribution. Cable models were set up with an inclined angle, θ, of $0°$, and a yawing angle, β, of $90°$.

Measurements of the pressure distribution around cable models were made by reading pressure at each of the 36 pressure−measuring taps embedded in models C1 and C2, being circumferentially at intervals of $10°$. These measurement points were connected to a pressure converter through vinyl tubes. Ultra−high−sensitivity strain−gauge−type differential pressure meters were used for the measurements. The reference static pressure was measured using a Pitot tube installed in a wind tunnel itself.

Fig.6.64 shows the measured pressure coefficient for model C1. This shows the same characteristics as those obtained in a previous experiments. That is, in the subcritical range, the location of the separation point, θ, was about $80°$ for a Reynolds number of about 0.9×10^5, and the pressure coefficient on the rear surface was almost constant, showing that thorough flow separation took place at the rear surface. The separation point θ was defined as transferring point where C_D curve turned from upward to level. In the supercritical range at a Reynolds number of about 5.5×10^5, the separation point moved backward to an angle θ of about $100°$, and the static pressure on the rear surface was restored because of turbulent mixing, a narrower wake width, and so on.

On the other hand, with model C2, no difference in pressure coefficient at a Reynolds number of about 0.9×10^5 and 5.3×10^5 was noted, as shown in Fig.6.65. The separation point in this case was located at an angle θ of about $110°$. This proves that model C2 had already entered the supercritical range at a wind velocity of about 10 m/s, which agreed well with the results of drag coefficient measurements.

These results indicate that roughening the cable surface makes it possible to reproduce the supercritical state at wind velocities where rain vibrations occur. For models with smooth surfaces, no evident negative pressure peak was observed within the range of wind velocities at which rain vibrations occurred. By contrast, with model C2, a negative pressure peak was observed at an angle θ of about $80°$ in the supercritical range. This negative pressure

suppressed the formation of rivulets on the upper surface; such rivulets were one of the causes of rain vibration. Pressure distribution measurements indicated that discrete roughness is estimated to suppress rain vibration by forming a negative pressure where water rivulets occur. The pressure distribution around an inclined cable remains a problem for future research.

6.4.3 Analysis of cable surface patterns

In general, surface roughness is defined in terms of Rz, the average peak—to valley height, but this method fails to take the distribution of surface roughness into consideration. In this analysis, as a way to understand not only the degree but also the distribution of surface roughness, the surface patterns of cable models were analyzed in greater detail. The surface patterns of models A, B and C were modeled numerically as a) surface patterns in the form of sine waves, b) surface patterns with periodic rectangular waveforms, and c) surface patterns with waveforms consisting of a random step function. The arithmetic mean deviation of the roughness and the Fourier spectra were obtained for each. Expressing a surface waveform in terms of f(x), the average arithmetic mean deviation of the roughness, Ra, is given by the following equation:

$$Ra = \frac{1}{l} \int_0^l |f(x)| \, dx \qquad (9)$$

Ra is calculated using an evaluating length, l, of 400 mm.

In spectral analysis, the intensity of a waveform is often defined by the energy spectrum, or $|x(f)|^2$. However, in this analysis of spatial surface waveforms , the Fourier spectrum x(f) was used. The appearance of cable models B3 and C2 used in the analysis were previously shown in Fig.6.51 and Fig.6.52 respectively.

Table 6.8 and Fig.6.66 show the results of analyzing typical surface patterns. By considering Ra, it was possible to gain an understanding of the average height of surface roughness on each side of the line while taking the concave and convex patterns into account. Accordingly, the surface roughness was uniformly distributed, the characteristics of the surface pattern could be expressed more precisely in terms of the average arithmetic mean deviation of the roughness than in terms of the apparent relative surface roughness, k/D.

As is clear from Fig.6.66, the Fourier spectrum is dominated by a certain wavelength, L, which means that, in the case of a non—uniform distribution of surface roughness, the surface pattern is a repetition of certain patterns at certain intervals, corresponding to the dominant

wave number (or inverse wavelength). That is, the amount of spread surface roughness can be considered small when the repeated dominant wave number is small. The distribution of surface roughness can be found by calculating the dominant wave number.

It is shown that the surface patterns adopted for cables used in this study had almost the same degree of relative surface roughness, but different average roughness height and surface roughness spread. The rough qualitative agreement with the measurements means that this analytical approach can be considered adequate, although this analytical method could not be correlated with the relationship between surface pattern and aerodynamic characteristics. A further quantitative study of the relationship between surface roughness (average and distribution) and aerodynamic characteristics will be required, preferably using wind tunnel tests, numerical analysis, and so on.

6.5 Development of A Low Drag Aerodynamically Stable Stay Cable with A Patterned Surface

6.5.1 Importance and idea of low drag cables

The combination of a very slim deck and a multiple cable system has been standard geometry in recent long cable—stayed bridges. From a viewpoint of the wind load contribution, an increasing importance of the wind load of cables in the structural design is evident. For example, considering a super—long cable—stayed bridge, having a main span of 1,000 m or more, the wind loading of the cable system can become larger than that of the deck. The relation between the span length and the wind load ratio (drag force on the cable to the deck) is shown in Fig.6.67, calculation based on conventional geometry [14,15]. It is found that the structural design of a super—long cable—stayed bridge greatly depends upon the drag coefficient of the cable. If this large wind load (the drag force) is capable of being decreased, it will be a great help in optimizing the whole configuration of the structure. Therefore, development of not only an aerodynamically stable but also a low drag cable is of great importance for a super—long cable—stayed bridge.

It is well known that the drag characteristics of a cable are affected by a Reynolds number, and their behavior highly depends on the surface roughness, as mentioned in section 6.2. Assuming the typical sized stay cables and their design wind velocity, their Reynolds numbers range from the subcritical range to the supercritical range (1×10^5 to 5×10^5). In a supercritical range, the drag coefficient for a cable without a surface roughness is about 1.2, and it sharply drops to about 0.5 at a Reynolds number of 2×10^5 to 4×10^5 , where

transition from laminar to turbulent flow in the separated flow around the cable occurs. The drag coefficient gradually increases with increasing wind velocity beyond the critical Reynolds number. On the other hand, when the roughness, for example, 1% of its diameter, is given to a cable, the critical Reynolds number becomes 6×10^4, and the drag coefficient increases to about 1.0.

In order to minimize the drag coefficient in the design wind velocity range, the drag characteristics in the supercritical range are required to be almost the same as those of a critical Reynolds number. Therefore, it is considered that a cable be required to have a smooth surface part, keeping the characteristics of a smooth surface cable, and have a partially roughened surface at the same time, reproducing a turbulent separation flow. This is the fundamental idea in establishing low drag force cables by surface modification under the idea of separation flow control. As for rain vibration, it is considered that water rivulets can be restrained by a given surface roughness, controlling the flow around the cable.

6.5.2 Experimental discussion on cables with low drag and suppressing effect

Cable models with smooth and improved surfaces were wind-tunnel tested to investigate the aerodynamic characteristics of the drag force and the vibration suppressing effect. The test was carried out using the same experimental apparatus as tested in section 6.4.

(1) Aerodynamic characteristics of a cable with a pattern indented surface

Table 6.9 shows the dimensions of the cable models used in the test. The surface configurations are illustrated in Fig.6.68. The surface of the low drag cables had a smooth part and partially lumped indented roughness features, which were grouped. Cables with less drag proposed here were only two, but there seemed to be quite a few possibilities of low drag circular cylinders with a combination surface of smooth and lumped patterns. Their relative surface roughnesses, k/D, were 0.002% for the normal cable and 1.1% for the improved cables. This 1.1% relative roughness was not a small roughness with reference to the drag coefficient behavior. The drag coefficient of this type of cable was estimated to be about 0.8 at a critical Reynolds number of a low wind velocity range, and it would increase to more than 1.0 at a high wind velocity range, if it behaved as a circular cylinder with a uniform roughness.

Fig.6.69 shows the drag coefficients of the models. The measurement was carried out up to a Reynolds number of about 5.8×10^5, which was equivalent to a wind velocity of about 55 m/s. The critical Reynolds numbers were about 1×10^5, and their drag coefficients were about 0.6, which were almost constant beyond the critical Reynolds number until the

maximum wind velocity was measured. The drag coefficients beyond the critical Reynolds number seemed to be almost constant with a very slight increase. From the test results, it is understood that the drag coefficient of the cables was lowest at a critical Reynolds number and it increased very slightly in the design wind velocity range, having the same characteristics of those of model C2. Therefore, the results indicated that low drag characteristics of the cable could be obtained by changing the flow pattern around the cable from that of a circular cylinder, which was affected by a Reynolds number.

The mean pressure distribution of the cable with an indented pattern is shown in Fig.6.70. The improved cable model shows a very similar pressure coefficient distribution at Reynolds numbers of 1×10^5 and 3×10^5, and that the separation point is located at an angle of about $110°$, having quite the same characteristics as those of model C2 tested previously. This proves that the pressure distribution of this cable model, as well as cable model C2, already entered the supercritical range at a Reynolds number of about 1×10^5, which agreed with the results of the drag coefficient measurements.

(2) Vibration characteristics of a cable with a pattern indented surface

Vibration tests were carried out under the condition shown in Table 6.10. Measured responses were calibrated by their Scruton numbers. Cable models were set up with an inclined angle, θ, of $20°$ and a yawing angle, β, of $45°$ for the experiment with rainfall, and with an inclined angle, θ, of $0°$ and a yawing angle, β, of $30°$ for the experiment without rainfall, in consideration for a long cable-stayed bridge.

Fig.6.71 and Fig.6.72 show the V-A-δ curves and the vibration response of the cable during rainfall. In the case of the cable having a smooth surface with a frequency of 0.73Hz, large vibrations occurred at a wind velocity of more than about 10 m/s, having the same tendency as the one in the previous experiments. And the vibration occurred at a wind velocity of about 5 m/s as the frequency decreased to 0.45Hz, observed for the first time in these experiments, including the previous ones. As for the cable having a pattern indented surface, vibration was also observed at a wind velocity of about 5 m/s, though the exciting force was weak. It was found that the vibration that occurred in the low wind velocity range had frequency dependent characteristics, being similar to those of the cable with a smooth surface. But, no significant vibration occurred in the high wind velocity range more than 10 m/s, showing sufficient vibration suppressing effects. Water rivulets flowing on the surface of the cable seemed to be controlled by the indented patterns. In this experiment, vibration tests were carried out using cables having a low Scruton number, and were more easily vibrated compared with the actual cables with a high Scruton number. Considering the

Scruton numbers of the actual cables, more than ten times larger than those of the tested models, it can be estimated that the amplitude would be reduced to a negligibly low level. The V–A–δ curves and the vibration response for the Scruton number of 21 are shown in Fig.6.73 and 6.74. It was also found that the response was reduced to a low level when the wind had a turbulent flow, for example, a turbulence intensity of about 10%, as shown in Fig.6.75.

To confirm the vibration suppressing effects of a cable with a pattern indented surface, vibration tests without rainfall were conducted. As shown in Fig.6.76, when the cable had a Scruton number of 2, vibration occurred at a wind velocity of more than 10 m/s, and it became larger as the wind velocity increased. But, considering the Scruton number of the actual cables, the response could be reduced to a low level under a limited wind velocity range. When the damping was increased to 0.02 in logarithmic decrement, it was also observed that the response decreased to a satisfactory amplitude.

Finally, a pattern indented surface of cable model D1, shown in Fig.6.68, was applied to the stay cables of the Tatara Bridge, the largest cable–stayed bridge in the world.

6.5.3 Control of drag force by roughness distribution

A cable with pattern indented surfaces has a low drag force and stable characteristics beyond a critical Reynolds number range, however, the relationship between the pattern on the surface and drag force characteristics has not been clearly understood yet. Then, to investigate the relationship in detail, drag force characteristics of cable models with parametric distributed lumped roughness were measured.

(1) Experimental condition

The test was carried out using the wind tunnel at Yokohama National University, having a height of 1,800 mm and a width of 1,800 mm. The test model had a diameter of 82 mm, taking into consideration the blockage ratio. An indented lumped roughness consisting of eight dots was applied to the surface of the cable models, each having the same configuration except density, as shown in Fig.6.77. Namely, each cable model had the same indented area ratio when it had the same arrangement in circumferential direction. The diameter of one dot was 4 mm, and depth 1 mm, being about 1% of the depth of the diameter of the cable. The cable had the same pitched lumped roughness in longitudinal direction every 100 mm by staggered arrangement, although it had three types of arrangement in circumferential direction. The measurements were conducted up to the maximum wind tunnel velocity of 36 m/s, corresponding to a Reynolds numbers of 2×10^5.

(2) Variation of drag force characteristics by patterned roughness

The results are summarized in Fig.6.78. The drag force characteristics of a cable with a dense–dot pattern of coarse pitch arrangement tended to be similar to those of a cable with a smooth surface. On the other hand, the drag force characteristics of a cable with a coarse–dot pattern of dense pitch arrangement were similar to those of a cable with the same roughness parameter k/D. The pitch of the roughness pattern seemed to have a more important contribution to the drag force characteristics. Even when a cable had the same number of roughness dots on the surface, the dense–dot arrangement of the roughness pattern seemed to result in a higher critical Reynolds number and also it decreased the drag coefficient at a critical Reynolds number. Beyond a critical Reynolds number range, most of the tested patterned roughness cables showed a sign of almost the same constant tendency of drag coefficient as those of the cable models mentioned before. Therefore, it is considered possible to adjust the density and arrangement of the dots in the patterned roughness to optimize the drag coefficient–Reynolds number relationship.

Fig.6.79 shows a comparison of pressure distributions at two sections in the roughness pattern (A) and in the smooth surface (B) of a cable model with a medium roughness pattern at a 45° pitch. The pressure distribution at position A in the roughness changed quickly as the Reynolds number increased, while pressure distribution at position B kept an almost identical pattern even in a high Reynolds number range. The pressure distribution of position B at a higher Reynolds number was close to the same typical figure seen in a supercritical range. The results indicate that a cable with a lumped distributed roughness showed a special characteristic of the separation, which was not uniform along the cable axis but was a combination of both the laminar and turbulent separation. The drag force characteristics of the cable were easily understood by the results of the pressure distribution measurements.

6.6 Conclusion

The results obtained by the study in Chapter 6 are summarized as follows.

(1) A new aerodynamically measured cable having both a low drag force and suppression effects on rain vibration was developed. Through wind tunnel tests, it was confirmed that an indented pattern with a relative surface roughness of 1% of the diameter applied discretely on the cable surface had such aerodynamic characteristics.

(2) The drag coefficient of the cable with a discrete surface roughness was lower than that of cables with the same degree of uniform surface roughness. The drag coefficients of the cables with a relative surface roughness of about 1% of their diameter were about 0.6, which was just about the same as those with a smooth surface, for a Reynolds number of 5.5×10^5 (which is in the design wind velocity range). It was found that density and arrangement of lumped roughness were the key factors in controlling the drag characteristics of cables and that it was possible to adjust those two factors to optimize the drag coefficient—Reynolds number relationship.

(3) Through rainfall experiments, it was confirmed that the cables with a relative surface roughness of about 1% of their diameter had rain vibration suppressing effects in a high wind velocity range. The vibration observed in the test in a low wind velocity range around 5 m/s could be reduced negligibly to a low level in the actual bridges, considering the Scruton numbers of the actual cables or the turbulent flow at the site. Through experiments without rainfall, it was found that a limited—type vibration could be suppressed to a low level when damping was added to the cables.

(4) Measurement of the pressure distribution showed that cables with a lumped patterned roughness made it possible to reproduce a supercritical state for a greater wind velocity range. It was considered that the lumped patterned roughness changed the flow around the cable, causing a combining of the laminar separation and the turbulent separation. The drag force characteristics of the cables were well explained by the results of the pressure distribution measurement.

(5) The behavior of vortex—induced vibration of the cables of a long cable—stayed bridge in a natural wind was obtained. It was found that the vortex—induced vibration responses were predominant in the fourth through sixth vibration modes, and that the maximum amplitude of vibration, η /D, approximately equalled 0.1.

(6) With the surface roughness of the cables, k/D, being about 0.01, it was evident that the surface roughness of the cables hardly affected the cables amplitude caused by the vibration.

It was confirmed that the response caused by the vortex—induced vibration was almost inversely proportional to the Scruton number. The effects of the response amplitude and the additional damping were able to be estimated analytically.

(7) The bending angle of a stay cable of long cable—stayed bridges caused by the vortex—induced vibration can be estimated to be less than $\pm$ 0.1 °. It was found that the vibration had little effect on the bending fatigue strength of the pre—coated parallel wire cable.

(8) In this study mentioned above, wind induced vibrations of a single cable were mainly dealt with. Concerning cable vibrations, the dynamic behavior of a cable structure caused by the wind is one of the problems to be examined. As a representative example of cable structures, an investigation into dynamic behavior of a catwalk for suspension bridges under a natural wind is summarized in the Appendix.

6.7 APPENDIX DYNAMIC BEHAVIOR OF A CABLE STRUCTURE

6.7.1 Introduction

The main wind−induced vibration of cable structures, such as cable nets, is considered to be gust response due to gusts of natural wind. It is rare that self−excited vibration types occur because cable structures are basically composed of an open section, and they are quite stable to the wind. As a representative example of cable structures, an investigation into dynamic behavior of a catwalk under a natural wind is indicated here [44,45].

A catwalk, suspended scaffolding, is an important cable structure for the erection of the main cables of a suspension bridge, as shown in Fig.6.80. It consists of several wire ropes, wire netting and transverse beams for a floor frame [46]. The width of a catwalk, for example, is about 4 m in the case of a long suspension bridge with a main span of 1,000 m. Storm ropes and hanger ropes are usually used to minimize any deformation due to live loads, such as a wind load working on the floor frame, and to increase dynamic stability against vibration, such as man−induced vibration by worker footsteps [47,48]. To find the aerodynamic characteristics of a catwalk, wind tunnel tests are carried out for a couple of typical catwalk cross sections, and the field observation results for wind responses of an actual catwalk are analyzed.

6.7.2 Aerodynamic characteristics of a catwalk

A series of wind tunnel tests for catwalk models were conducted and aerodynamic coefficients for catwalks were measured. The specifications of the models used in the tests are shown in Table 6.11. As shown in Fig.6.81, the test results indicated that lift and aerodynamic moment coefficients were quite small, and the slope of both curvatures for the attack angle was also small. It was found that changes in width of the catwalk resulted in very little change in drag coefficient, therefore floor size contributed very little to the drag force.

Further measurements were performed in order to determine the amount of the drag force applied to each part in accordance with changes in width of a cross section. The results of these measurements are shown in Table 6.12. An experimental model for the test is shown in Fig.6.82. The drag coefficient caused by the front side of the catwalk was roughly 1.3, the rear side 0.65 and the floor 0.1. An experimental equation obtained by the results is expressed as follows.

$$P_D = 1/2 \; \rho \; U^2 C_D A$$
$$= 1/2 \; \rho \; U^2 \{ \; 1.3 \; (1.0+0.5) \; H \; \phi_S \; + 0.1B \; \phi_F \; \} \tag{1}$$

where H is the height of a side handrail, ϕ_S is the solidity ratio of a side handrail, B is the width of the floor frame and ϕ_F is the solidity ratio of the floor frame.

To examine the dynamic characteristics of a catwalk, free vibration tests were carried out using model IV in Table 6.1. Vertical, torsional and lateral vibration characteristics were investigated. In addition to tests using the original model, tests were also conducted by changing the solidity ratio of the floor area to analyze the effects of the shape of the cross section.

The results of the tests are summarized as follows;

a) The cross section of the catwalk had excellent stability against wind. The model tested showed no sign of unstable vibration up to the maximum wind velocity in the wind tunnel (equivalent to an actual wind velocity of 75 m/s).

b) Aerodynamic damping characteristics were evaluated by using the quasi−steady theory with regard to vertical and lateral vibrations, shown in Fig.6.83.

c) When the solidity ratio of the floor of the catwalk greatly increased, especially to more than 80%, self−excited vibrations occurred.

6.7.3 Gust response of a catwalk

The vibration responses of a catwalk under a natural wind in the Hirado Bridge were measured and analyzed. The catwalk of the Hirado Bridge had a main span of 462 m and a floor width of 2.5 m. The solidity ratio for the floor frame was about 28%, for the side handrails, about 20%.

Gust response of the catwalk was analyzed based on Ref.[49]. The standard deviation of the lateral vibration at the span center of the Hirado Bridge catwalk, due to the drag force, was numerically calculated. The outline of the analysis is briefly introduced as follows.

a) Power spectrum density of the fluctuating wind load

Wind velocity is expressed using a mean wind velocity and time−dependent component:

$$U(t) = U + u(t) \tag{2}$$

where,   U(t): wind velocity

         U : mean wind velocity

         u(t): velocity fluctuation

The power spectrum of the velocity fluctuation based on measured values or Hino's spectrum is given [50]:

$$\frac{fSu(f)}{u^2} = A \frac{Lf/U}{\{1+(Lf/U)^2\}^{5/6}}$$ (3)

$$L = \sqrt{1.5/(f/U)}$$

$$A = \text{constant}$$

$$\frac{fSu(f)}{u^2} = 0.238 \frac{f/\beta}{\{1+(f/\beta)^2\}^{5/6}}$$ (4)

$$u^2 = 6K_r U_{10}^2$$

$$\beta = 1.169 \times 10^{-3} \frac{U_{10}\alpha}{\sqrt{k_r}} \times \left(\frac{Z}{10}\right)^{(2m\alpha-1)}$$

where, $m=2$, $\alpha=1/7$, $K_r=0.0025$, $Z=45$

The power spectrum for the fluctuating drag force is expressed as follows:

$$S_P(f) = 4P^2 |\chi_1(f)|^2 Su(f)/U^2$$ (5)

$$|\chi_1(f)|^2 = \frac{1}{1+(2Df/U)^{4/3}}$$

Wind load $P(x,t)$ can be expressed by using a load $Pr(t)$ that causes an r−th vibration and an r−th vibration mode shape $\phi_r(x)$.

$$P(t,x) = \sum_r P_r(t) \phi_r(x)$$ (6)

$$P_r(t) = \frac{1}{N_r} \int_0^l P(t,x) \phi_r(x) dx$$

$$N_r = \int_0^l \phi_r^2(x) dx$$

The power spectrum density for an r−th load can be given using the Fourier transform:

$$S_{Pr}(f) = \frac{1}{N_r^2} \int_0^l \int_0^l S_P(x_1,x_2:f) \phi_r(x_1) \phi_r(x_2) dx_1 dx_2$$ (7)

$$S_P(x_1,x_2:f) = S_P(f) R_u(x_1,x_2:f)$$

where $S_P(x_1,x_2:f)$ represents a cross spectrum of the fluctuating drag force working on x_1 and x_2 of the x−axis.

b) Response spectrum

The motion of the structure is described by the equation:

$$M_r \frac{d^2 y_r}{dt^2} + C_r \frac{dy_r}{dt} + K_r y_r = P_r(t)$$ (8)

where M_r is the generalized mass, C_r is the generalized damping constant, K_r is the generalized stiffness of the structure and $P_r(t)$ is the time−dependent generalized load acting on the structure.

The response spectrum for an r−th mode is:

$$Sy = \frac{|H_r(f)|^2}{K_r^2} S_{Pr}(f)$$ (9)

$$K_r = \{(2\pi f_r)^2 M_r\}$$

$$|H_r(f)|^2 = \{[1-(f/f_r)^2]^2 + 4\zeta_r(f/f_r)^2\}^{-1}$$

$$\zeta = \zeta_0 + \zeta_a = \frac{1}{2\pi}\left(0.03 + \frac{\rho UBC_D}{2Mf_r}\right)$$

where ζ is the damping ratio including both structural and aerodynamic damping.

The power spectrum density for response can be given using equations above:

$$S(x, f) = \sum_r Sy_r(f) \phi_r^2(x) \tag{10}$$

$$= \sum_r \frac{\phi_r^2(x)}{K_r^2} |H_r(f)|^2 |J_r(f)|^2 S_p(f)$$

$$|J_r(f)|^2 = \frac{1}{N_r^2} \int_0^l \int_0^l Ru(x_1, x_2 : f) \phi_r(x_1) \phi_r(x_2) dx_1 dx_2$$

$$Ru(x_1, x_2 : f) = \exp\{(-kf1|x_1 - x_2|)/U1\}$$

Then, the standard deviation of the random vibration, σ (R.M.S.), due to buffeting can be obtained by the following equation:

$$\sigma^2(x) = 2 \int_0^\infty S(x, f) df \tag{11}$$

c) Results of analysis

The calculation took into account the second mode, the following natural frequency and vibration mode that were used:

$$f_1 = 0.109 \text{ Hz}, \quad \phi_1(x) = \sin(\pi/l)x + 0.009\sin(3\pi/l)x \tag{12}$$

$$f_2 = 0.299 \text{ Hz}, \quad \phi_2(x) = 0.165\sin(\pi/l)x + \sin(3\pi/l)x \tag{13}$$

The power spectrum of the fluctuating wind at the three points along the catwalk (the center of the span and both tower tops) is shown in Fig.6.84. The Y axis of these figures shows the power spectrum divided by a mean square value and normalized by multiplying this by the frequency, while the X axis shows the frequency of the measured wind velocity divided by an average wind velocity.

Fig.6.85 shows the power spectrum of the displacement at the center of the span. The Y axis shows the power spectrum divided by a mean square value and normalized by multiplying this by the frequency, while the X axis shows the frequency. From the figure, it was understood that the catwalk was subject to static lateral deformation accompanied by the first mode vibration when it was subjected to a natural wind.

Calculated and measured values for the R.M.S. of vibration response are shown in Fig.6.86. Calculation was performed for two cases of turbulence intensity, 8% and 12%, considering the measured values shown in Table 6.13. It was found that the maximum R.M.S. of the catwalk response displacement was almost equal to that of the calculation with an intensity of approximately 12%. Thus it yields an important conclusion from the standpoint of design.

Therefore, it is indicated that it is possible to estimate quite closely the gust response amplitude of a cable structure like a catwalk by this method.

6.7 References

[1] National Land Development Technology Research Center, Report on Study of Wind Resistance of Cables in Cable—Stayed Bridges * , 1989, pp.14—34.

[2] Public Works Research Center, Report on Study of Wind Resistance of Cables in Cable—Stayed Bridges * , 1994, pp.78—104.

[3] K.Yokoyama, T.Kusakabe, T.Fujiwara and T.Hojo, Experimental Study on Cable Response Caused by Vortex—Induced Vibration * , Proc. of the 12th Wind Engineering Symposium, 1992, pp.279—284.

[4] Y.Hikami, Rain Vibration of Cables in Cable—Stayed Bridges, Japan Association for Wind Engineering * , Vol.27, 1986, pp.17—28.

[5] M.Matsumoto, N.Shiraishi, M.Tsujii and S.Hirai, On Aerodynamic Oscillations of Cables for Cable Stayed Bridges * , Proc. of JSCE Vol.416, I —13, 1990, pp.225—234.

[6] M.Matsumoto, Y.Hikami and M.Kitazawa, Cable—Vibration and Its Aerodynamic /Mechanical Control, Proc. of Cable—Stayed and Suspension Bridges, Deauville, France, 1994, pp.439—452.

[7] T.Saito, M.Matsumoto and M.Kitazawa, Rain—Wind Excitation of Cables on The Cable—Stayed Higashi—Kobe Bridge and Cable Vibration Control, Proc. of Cable—Stayed and Suspension Bridges, Deauville, France, 1994, pp.507—514.

[8] O.Flamand, Rain—Wind Induced Vibration of Cables, Proc. of Cable—Stayed and Suspension Bridges, Deauville, France, 1994, pp.523—532.

[9] M.Miyazaki, Aerodynamic Vibration of Bridge Cables and Preventive Methods * , Proc. of the 10th Wind Engineering Symposium, 1988, pp.145—150.

[10] T.Miyata, H.Yamada and T.Hojo, Aerodynamic Response of PE Stay Cables with Pattern—Indented Surface, Proc. of Cable—Stayed and Suspension Bridges, Deauville, France, 1994, pp.515—522.

[11] I.Okauchi, M.Ito and T.Miyata, Wind Engineering for Structure * , Maruzen, 1977.

[12] A.Okajima and Y.Nakamura, Flow around Cylinder with Surface Roughness in a High Reynolds Number Range * , Report of Applied Mechanics Laboratory, Kusyu University, No.40, 1973, pp.387—400.

[13] E.Achenbach, Influence of Surface Roughness on the Cross—Flow Around A Circular Cylinder, Journal of Fluid Mechanics, Vol.46, 1971, pp.321—335.

[14] T.Hojo, S.Yamazaki, T.Miyata and H.Yamada, Development of Low Drag Aerodynamically Stable Stay Cable with Patterned Surface Processing * , Bridge and Foundation Engineering, Vol.29, No.6, 1995, pp.27—32.

[15] T.Miyata, H.Yamada, T.Hojo and S.Yamazaki, On Aerodynamically Stable PE—Stay Cables with Decreased Drag Force by Introduction of Newly Developed Lumped Surface Roughness, Proc. of International Symposium on Cable Dynamics, 1995, pp.481—488.

[16] Honshu—Shikoku Bridge Authority, Observation Report of Dynamic Behavior of Cables of The Ikuchi Bridge * , 1991.

[17] T.Hojo, Experimental Study on Rain Vibration Characteristics and Suppressing Method of cables in Cable—Stayed Bridges * , Journal of Wind Engineering, No.50, 1992, pp.19—26.

[18] T.Miyata, H.Yamada and T.Hojo, Experimental Study on Aerodynamic Characteristics of Cables with Patterned Surfaces * , Bridge and Foundation Engineering, Vol.27, No.9, 1993, pp.30—36.

[19] T.Miyata, H.Yamada and T.Hojo, Experimental Study on Aerodynamic Characteristics of Cables with Patterned Surfaces, Journal of Structural Engineering, Vol.40A, 1994, pp.1065—1076.

[20] Y.Uematsu, M.Yamada and M.Kikuchi, Observation of the Flow Around Rough—Walled Two—Dimensional Circular Cylinders Using Infrared Thermography * , Journal of Wind Engineering, No.43, 1990, pp.9—21.

[21] Y.Uematsu, M.Yamada and K.Ishii, Aerodynamics of A Circular Cylinder of Finite Length (Part 2 Wind Tunnel Experiments) * , Journal of Wind Engineering, No.34, 1988, pp.27—43.

[22] H.Nakaguchi and H.Honma, Fluid Mechanics * , Chijin Syokan, 1987, pp.122—128.

[23] T.Adachi, K.Matsuuchi, S.Matsuda and T.Kawai, On the Force and Vortex Shedding on a Circular Cylinder from Subcritical up to Transcritical Reynolds Numbers * , Proc. of Japan Society of Mechanical Engineers, Vol.51, No.461, 1985, pp.295—299.

[24] E.Simiu and R.H.Scanlan, Wind Effects on Structure, John Wiley &Sons, 1985

[25] Japan Society of Civil Engineers, Vibration Handbook, 1985, pp.378—381.

[26] K.Yoshimura, C.Tanaka, N.Sasaki, S.Nakaya and S.Hiki, Rain—Wind Induced Vibration of the Cables of The Aratsu Bridge, Proc. of the 10th Wind Engineering Symposium, 1989, pp.127—132.

[27] Y.Miyasaka, J.Nanso, M.Nanjo, H.Kado and T.Ishitobi, Suppression Method for Cable Vibration of The Tenpozan Bridge * , Bridge and Foundation Engineering, Vol.26, No.4, 1993, pp.27—36.

[28] H.Teramoto, Y.Fujino, M.Ito and T.Asaeda, Cross—Sectional Shape of Water Flow on Cable in Wind * , Journal of Wind Engineering, No.32, 1987, pp.45—46.

[29] M.Matsumoto, N.Shiraishi, M.Kitazawa, Y.Kim and M.Tsujii, On Rain—Wind Induced Vibration of the Cables * , Proc. of the 10th Wind Engineering Symposium, 1988, pp.133—138.

[30] Y.Fujino, H.Yamaguchi and M.Ito, Galloping Oscillations of Figure—8 Overhead

Telecommunication Cables, Proc. of the 8th Wind Engineering Symposium, 1984, pp.221−226.

[31] M.Matsumoto, N.Shiraishi, H.Shirato, S.Hirai, Y.Sano and K.Katsura, Study on Two Main Causes of Rain Vibration in Cable−Stayed Bridges, Proc. of the 11th Wind Engineering Symposium, 1990, pp.263−268.

[32] M.Matsumoto, N.Shiraishi, H.Shirato, Aerodynamic Behavior of Cables of Cable−Stayed Bridges, Asia Pacific Symposium on Wind Engineering Ⅱ, 1986.

[33] H.P.Ruscheweyh, Aeroelastic Interference Effects Between Slender Structures, Journal of Engineering and Industrial Aerodynamics, No.14, 1983.

[34] M.Yoneda, Control of Wind−Induced Vibrations of Stay Cables for Cable−Stayed Bridges *, Vibration Control Colloquium Part A, JSCE, 1993, pp.21−40.

[35] K.Wada, H.Higashida, S.Eya, and H.Takano, Control Methods of Wind−Induced Vibrations for The Yokohama Bay Bridge *, Bridge and Foundation Engineering, Vol.23, No.8, 1989, pp.43−48.

[36] Y.Fujino, B.Pacheco and A.Sulekh, Evaluation of Damping for Stay−Cables with Damper *, Bridge and Foundation Engineering, Vol.26, No.4, 1992, pp.41−45.

[37] K.Yokoyama, T.Kusakabe and H.Sekiya, Study on Suppression Effects of Cable Cross Ties for Stay Cables *, Proc. of the 12th Wind Engineering Symposium, 1992, pp.285−290.

[38] T.Miyata, Design Considerations for Wind Effects on Long−Span Cable−Stayed Bridges, International Seminar on Cable−Stayed Bridges, Yokohama, Japan 1991, pp.235−256.

[39] M.Miyazaki, Y.Saito and Y.Suzuki, Aerodynamic measure for Stay Cables of Cable−Stayed Bridges *, The 48th Annual Conference of JSCE, Ⅰ−318, 1993, pp.784−785.

[40] T.Kinoshita, H.Nakanishi and K.Sugii, Countermeasures of Rain−Wind Induced Vibration of Cables in Cable−Stayed Bridges *, Journal of Structural Engineering, Vol.370A, 1991, pp.1001−1009.

[41] M.Yoneda, K.Maeda and S.Iseki, Damping Added Effects of Viscous Shearing Type Damper Newly Developed for Suppression of Vibration *, Proc. of the 11th Wind Engineering Symposium, 1990, pp.85−90.

[42] Electrical Institute of Japan, Breeze−Induced Vibration of Power Transmission Lines *, Electrical Institute of Japan Report Ⅱ, No.2, 1982, pp.39−57.

[43] Y.Sakamoto, T.Hojo, T.Eguchi and M.Yano, A Study on Secondary Stress and Fatigue Life in Bending of A Pre−Coated Cable for Cable−Stayed Bridge *, Proc. of JSCE, Vol.446, Ⅰ −19, 1992, pp.215−223.

[44] M.Ito, T.Miyata, T.Sugita and T.Hojo, Wind−Resistance Study of Catwalk for Long Suspension Bridge *, Proc. of the 4th Wind Engineering Symposium, 1976, pp.231−238.

[45] T.Hojo, M.Ito and T.Miyata, Wind−Resistant Study on Catwalk *, The 31st Annual Conference of JSCE, Ⅰ−29, 1976, pp.373−374.

[46] S.Tsuyama, T.Sugita, I.Koga and T.Hojo, Catwalk for Long Suspension Bridge, Nippon Steel Technical Report, No.8, 1976, pp.90−104.

[47] T.Hojo, S.Yamazaki and H.Yamaguchi, Experimental Study on Countermeasure for Man−Induced Vibration of Catwalk without Storm System *, Journal of Structural Engineering, Vol.41A, 1995, pp.763−770.

[48] T.Hojo, S.Yamazaki and H.Yamaguchi, Experimental Study on Countermeasure for Man−Induced Vibration of Suspension Structure, Proc. of International Symposium on Cable Dynamics, 1995, pp.461−468.

[49] A.G.Davenport, Buffeting of A Suspension Bridge by Storm Wind, Proc. of ASCE, Journal of Structural Division, Vol.88, ST3, 1962, pp.233−267.

[50] Honshu−Shikoku Bridge Authority, Wind−proof Design Standards for The Honshu−Shikoku Bridges *, 1976.

* Published in Japanese

Fig.6.1　Flow around a body

(a) 　$R_e < 3 \sim 6$

(b) 　$3 \sim 6 < R_e < 40$

(c) 　$40 < R_e < 150$

(d) 　$300 < R_e < 3.8 \times 10^5$

(e) 　$3.8 \times 10^5 < R_e < 8 \times 10^6$

(f) 　$R_e > 8 \times 10^6$
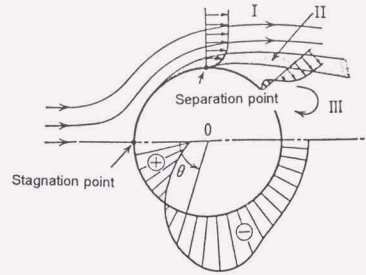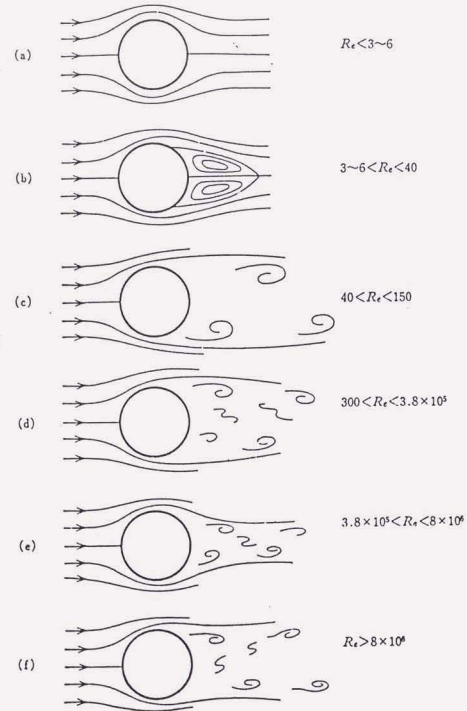
Fig.6.2　Flow past a circular cylinder
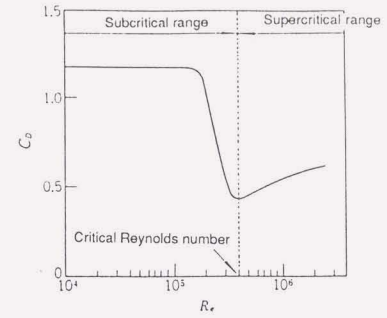
Fig.6.3　Relationship between the drag coefficient of
a circular cylinder and the Reynolds number

—— Laminar flow　　　▽　Laminar flow separation point

—— Turbulant flow　　　▼　Turbulant flow separation point
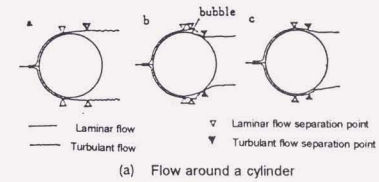
(a)　Flow around a cylinder
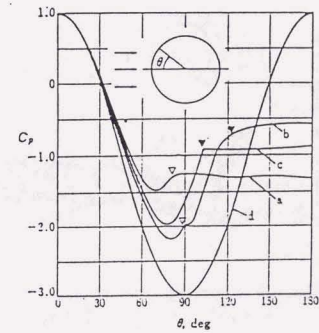
(b)　Pressure distribution

Fig.6.4　Mean pressure coefficient of a circular cylinder
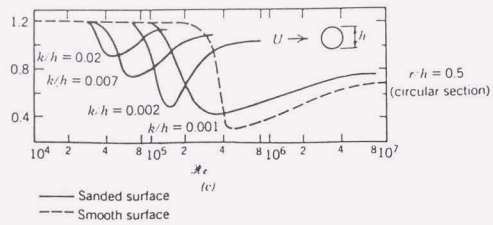
Fig.6.5　Influence of uniform surface roughness on
drag coefficient of a circular cylinder
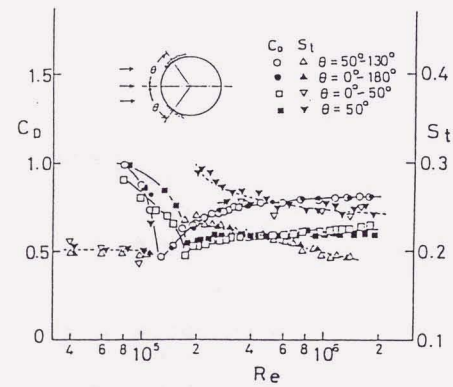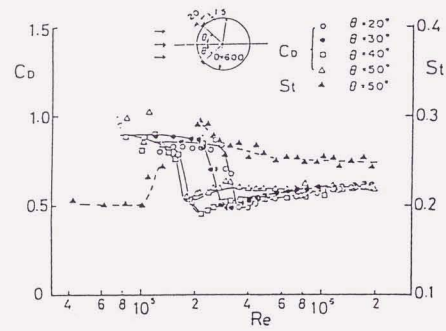
Fig.6.6　Influence of distribution and location of
roughness on drag coefficient
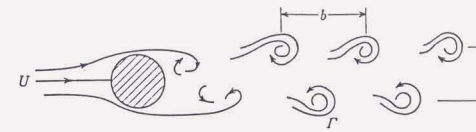
Fig.6.7　Karman vortex trail
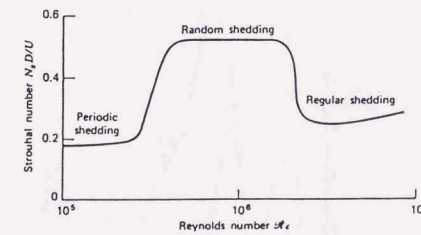
Fig.6.8　Relation of Strouhal number to Reynolds number
for a circular cylinder
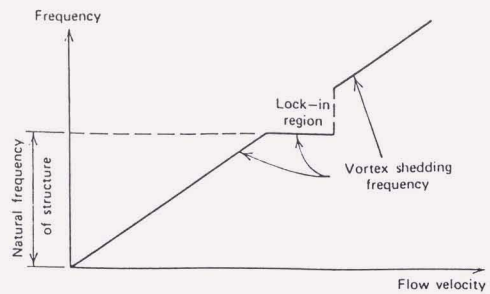
Fig.6.9   Effect of lock−in upon vortex shedding
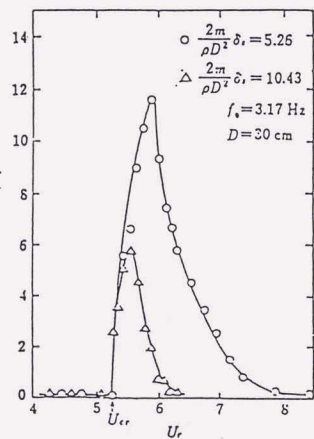
Fig.6.10   Response amplitude of a circular cylinder
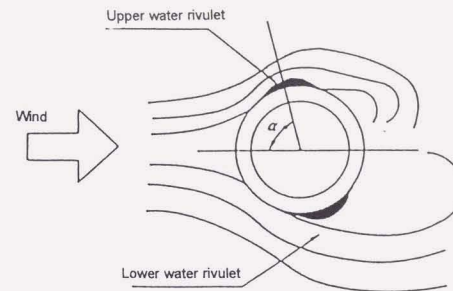
Fig.6.11   Water rivulets forming on a cable surface
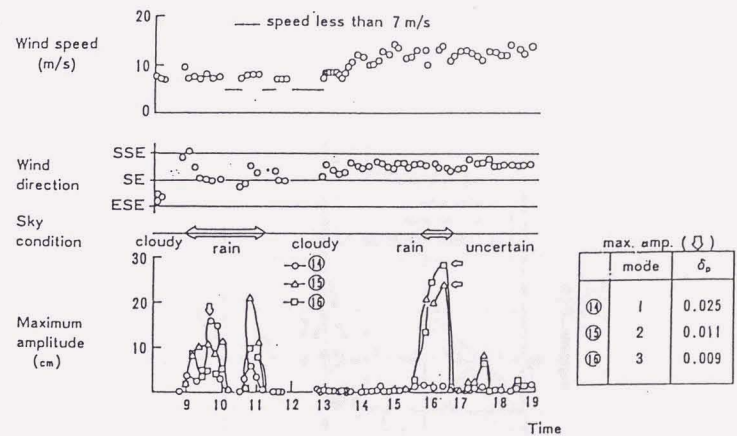
Fig.6.12   Rain vibration measured in the Meiko−Nishi Bridge

(a)

5.4 ↑ 6.6

○ Meiko-Nishi Bridge
△ Aratsu Bridge
◇ Tenpozan Bridge
● Tenpozan Bridge (contd.)

Amplitude y／D

Mode n

(b)

5.4 ↑ 6.6

○ Meiko-Nishi Bridge
△ Aratsu Bridge
◇ Tenpozan Bridge
● Tenpozan Bridge (contd.)

Amplitude y／D

Frequency f（Hz）

(c)

6.6 ↑ 5.4

○ Meiko-Nishi Bridge
△ Aratsu Bridge
◇ Tenpozan Bridge
● Tenpozan Bridge (contd.)

Amplitude y／D
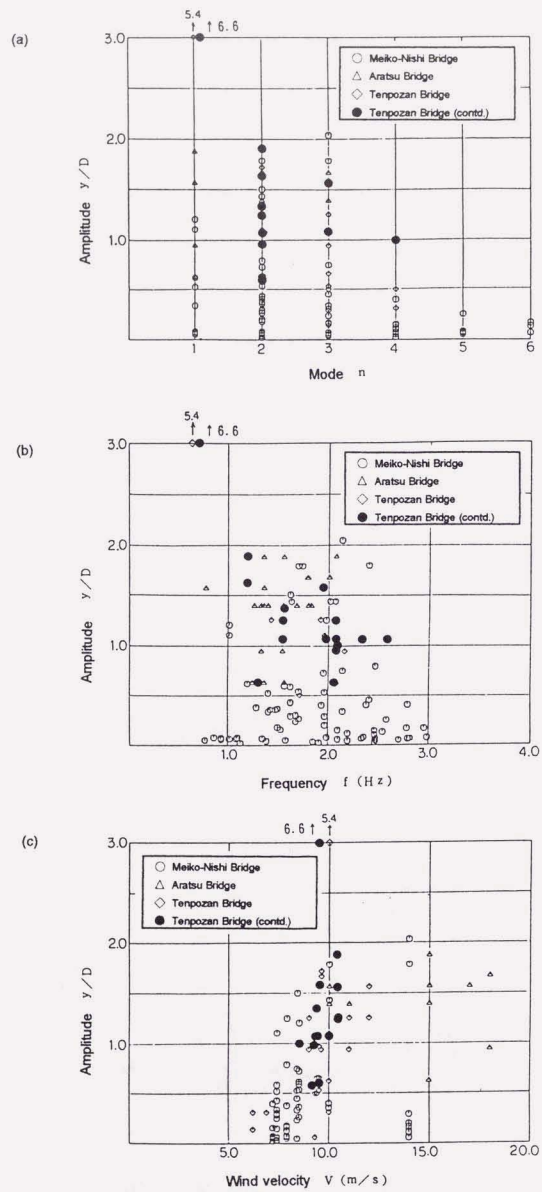
Wind velocity V（m／s）

Fig.6.13   Rain vibration characteristics observed in cable—stayed bridges

– 183 –

With rain

$\beta = 45°$
$\theta = 45°$

Amplitude （mm）

Without rain
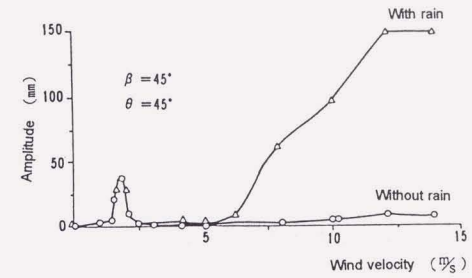
Wind velocity （m／s）

Fig.6.14   Cable response in wind tunnel with simulated rainfall

Wind

β θ
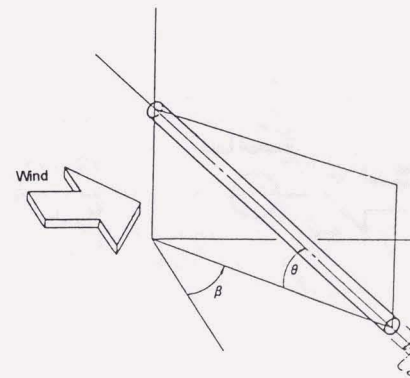
Fig.6.15   Cable attitude

– 184 –
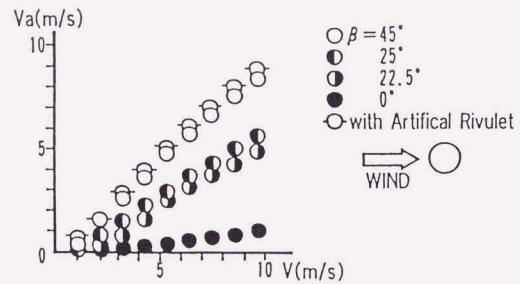
Fig.6.16 Relation between wind velocity of axial flow and yawing angle
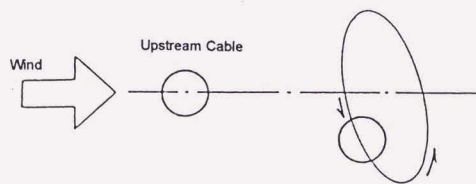
Fig.6.17 Wake galloping
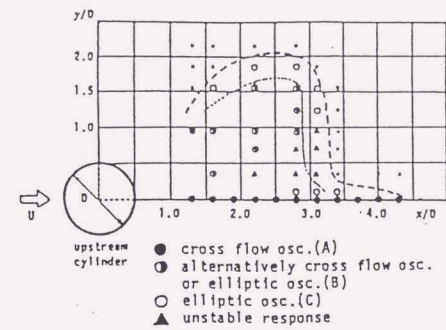
Fig.6.18 Influence of distance between two cables on vibration amplitude

Flow patterns for various X/D (L/D = 3)..
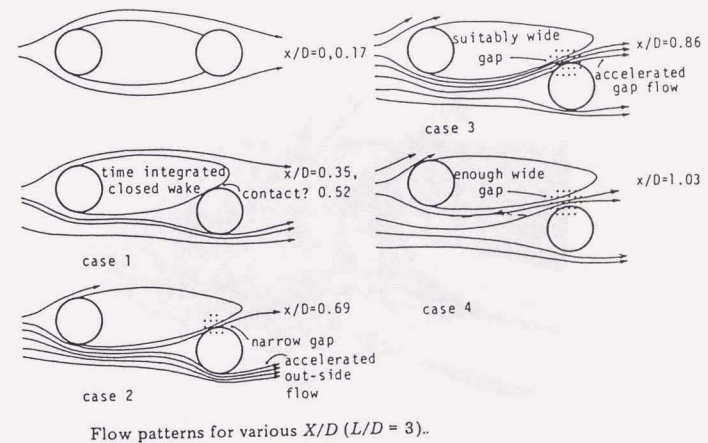
Fig.6.19 Flow patterns for various cable position x/D(L/D=3)

Photo.6.1   Oil—damper of the Brotonne Bridge
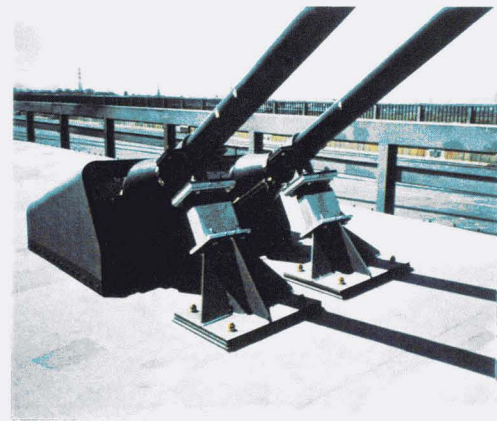
Photo.6.2   Viscous—shearing damper of the Sakitama Bridge
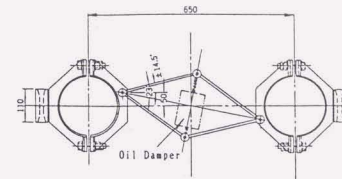
Fig.6.20 Spacer—damper of the Yokohama Bay Bridge
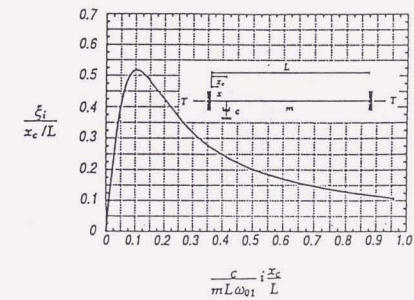
Fig.6.21 Modal damping curve of cable with damper
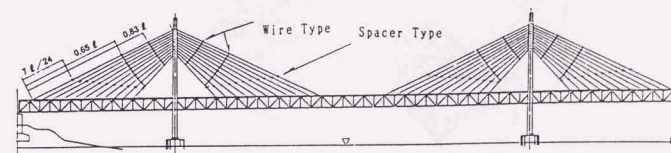
Fig.6.22 Tying wires of the Iwakurojima Bridge
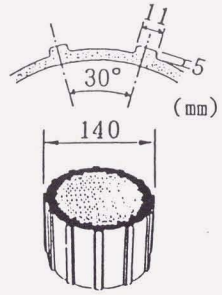
Fig.6.23 Cable with axial protuberance of the East—Kobe Bridge
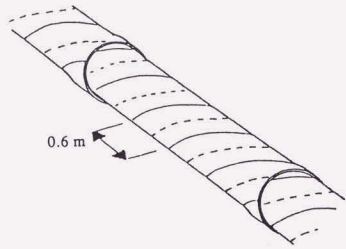
Fig.6.24 Cable with helical streak of the Normandy Bridge
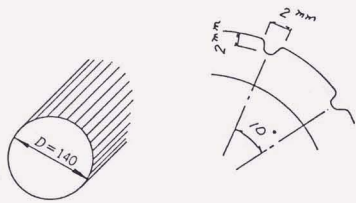
Fig.6.25 Cable with U—shaped grooving of the Yuge Bridge
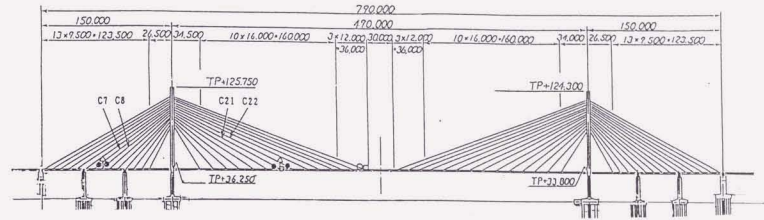
Fig.6.26 General view of the Ikuchi Bridge
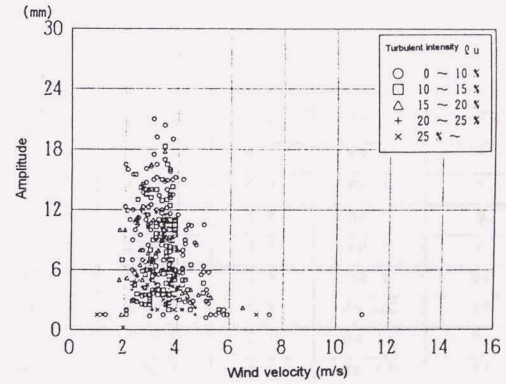
Fig.6.27 Measurement results of cable vibration

Table 6.1 Cable dimensions of the Ikuchi Bridge

		Cable parameter
Cable length	ℓ (m)	53-246
Cable diameter	D (mm)	119-139
Cable weight	M (kgf/m)	55-77
Cable tension	T (kN)	1,765-3,923

Table 6.2 Observation results of cable vibration

Dimension number	Frequency (Hz)	Wind velocity (m/s)	Measured amplitude (m)	Double amplitude (m)
1	0.95	0.7	0.003	0.0189
2	1.90	1.3	0.006	0.0191
3	2.85	2.0	0.010	0.0217
4	3.80	2.5	0.015	0.0252
5	4.75	3.2	0.020	0.0280
6	5.70	3.9	0.021	0.0257
7	6.65	4.5	0.023	0.0256
8	7.60	5.2	0.019	0.0199
9	8.55	5.8	0.009	0.0091
10	9.50	6.4	0.008	0.0080
11	10.45	7.2	0.009	0.0092
12	11.40	8.5	0.006	0.0064
13	12.35	9.6	0.004	0.0046

Table 6.3 Structural damping of cables

Vibration mode	Cable No.7	Cable No.8
1st (without elastic buffer)	0.00015-0.00321	0.00087-0.00520
(with elastic buffer)	0.0176	0.01468
2nd (without elastic buffer)	0.00079-0.00704	0.00041-0.00226
(with elastic buffer)	0.01611-0.01745	0.01715-0.01877
3rd (without elastic buffer)	0.00102-0.00445	0.00286-0.00567
(with elastic buffer)	0.01596-0.01660	0.01383-0.01815
4th (without elastic buffer)	0.00058-0.00118	0.00214
(with elastic buffer)	0.01266-0.01997	0.01619-0.02121

※ Logarithmic decrement
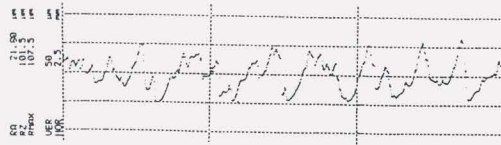
Fig.6.28 Measurement example of cable surface roughness

Table 6.4 Dimensions of cable models

Model designation	Diameter (m)	Surface roughness (μm)	Coefficient of roughness (k/D)
A1	0.1315	3	2.3×10^{-3}
A2	0.1220	30	2.5×10^{-4}
A3	0.1315	100	7.6×10^{-4}
A4	0.1235	200	1.6×10^{-3}
A5	0.1240	600	4.8×10^{-3}
A6	0.1275	1500	1.2×10^{-2}

A 1

A 6

A 2

B 1

A 3

B 2

A 4

B 3

A 5
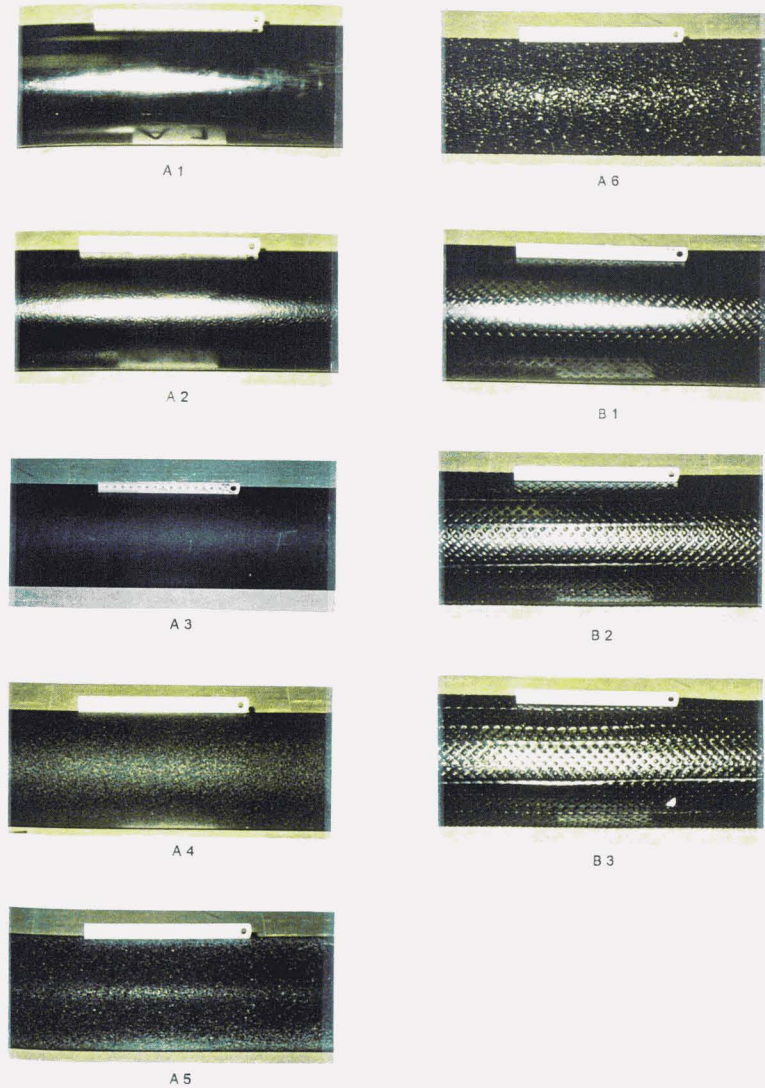
Photo.6.3 Cable models used
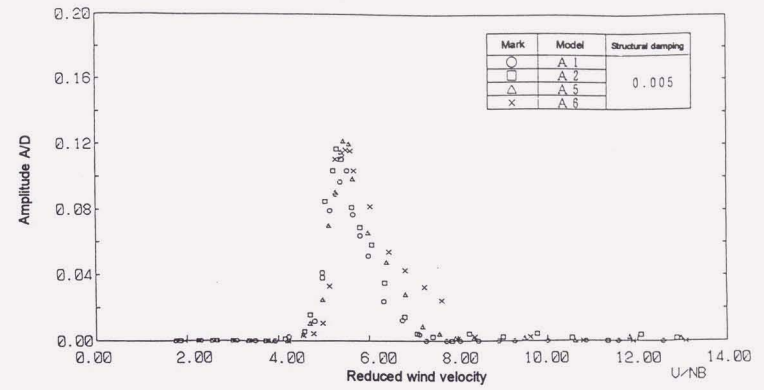
Fig.6.29 Effect of surface roughness on vibration amplitude
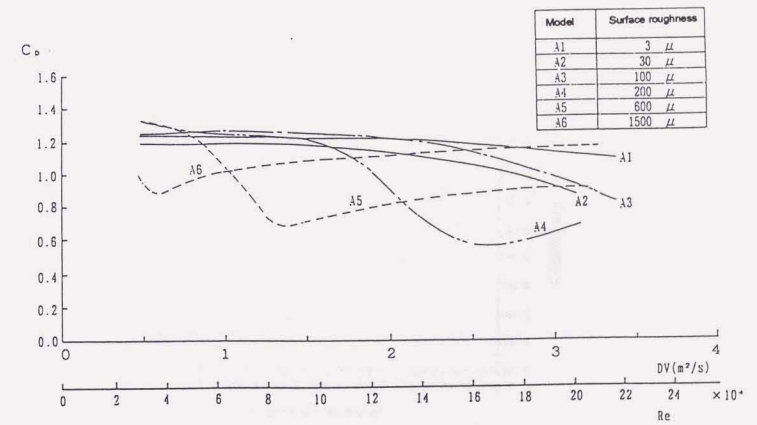
Fig.6.30 Relation between surface roughness and drag coefficient
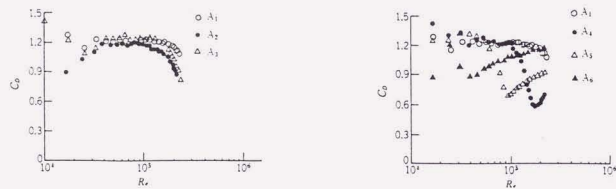
Fig.6.31 Relation between drag coefficient and Reynolds number
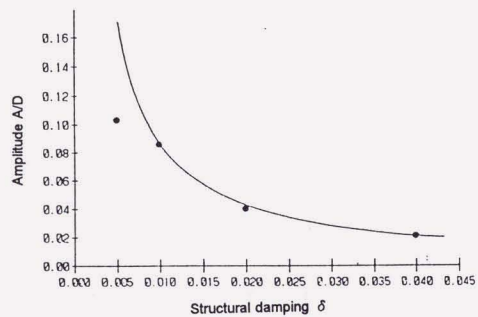
Fig.6.32 Structural damping and vibration amplitude
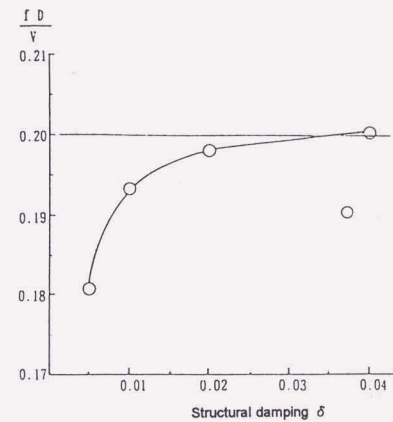
Fig.6.33 Structural damping and Strouhal number
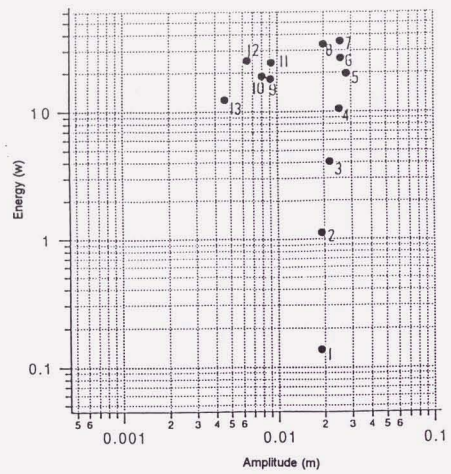
C7E

Fig.6.34　Relation between input energy and amplitude

Fig.6.36　Measured and calculated responses

C7E

Fig.6.35　Relation between amplitude and frequency
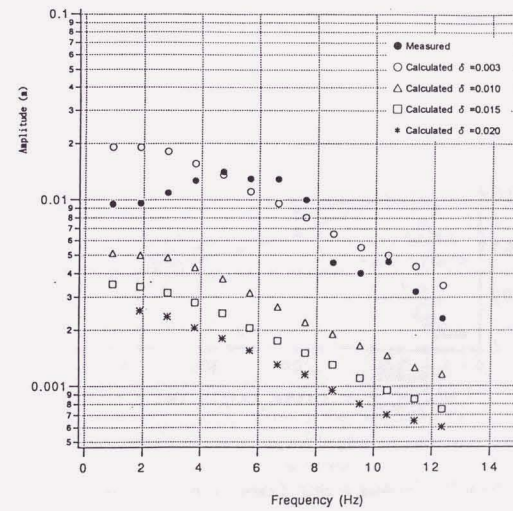
Fig.6.37　Effect of added damping
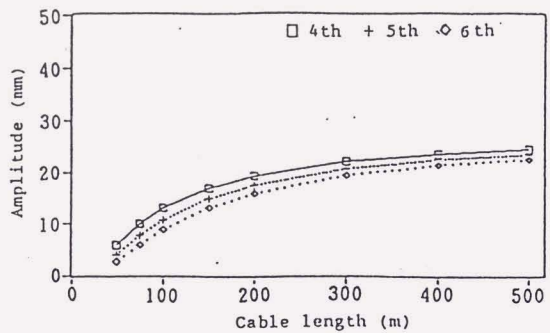
Fig.6.38 Estimated response amplitude
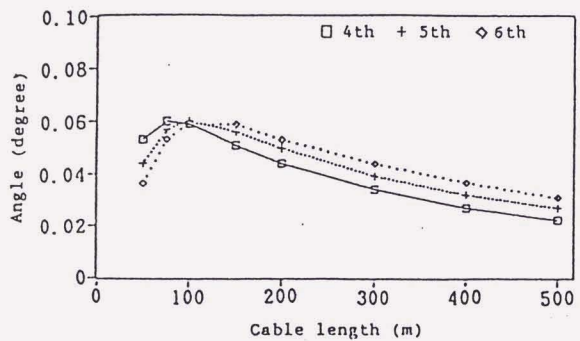
Fig.6.39 Bending angles of cables caused by vibration
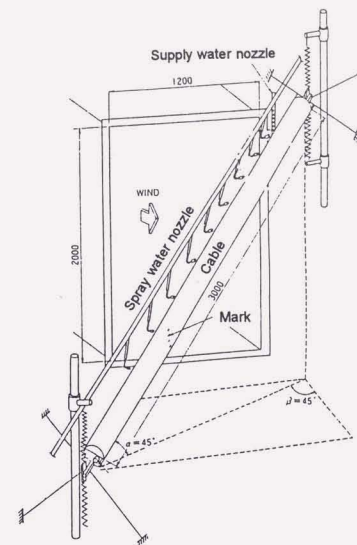
Fig.6.40 General view of wind tunnel test
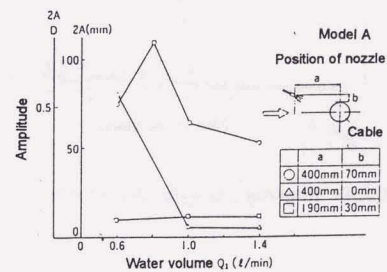
Fig.6.41 Effect of water nozzle location

Table 6.5 Dimensions of cable models

	Model	Mass (kgf・s²/m²)	Frequency (Hz)	Logarithmic damping (δ)
A	Circular (covered with PE)	2.14	1.83	0.0034
B	Circular (scraped surface)	2.14	1.83	0.0032
C	Twisted hexagon (covered with PE)	1.92	1.88	0.0043
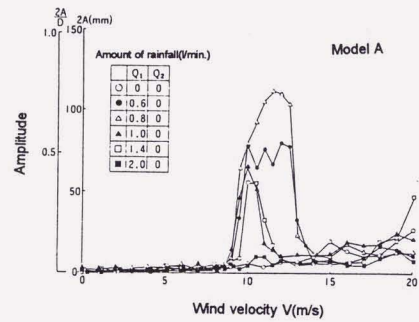
Fig.6.42 Response characteristics of cable model
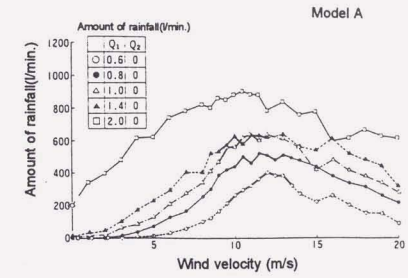
Fig.6.43 Amount of water rivulets on cable model
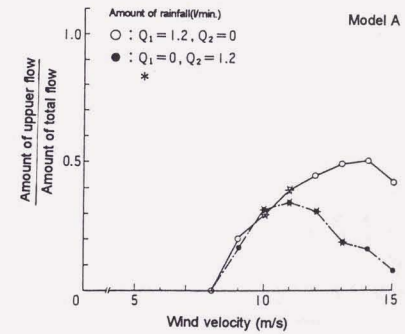
Fig.6.44 Comparison of upper and lower water rivulets on cable model
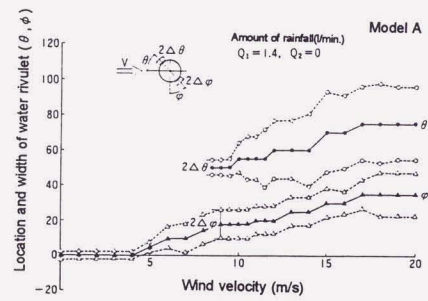
Fig.6.45 Location and width of water rivulets on cable model
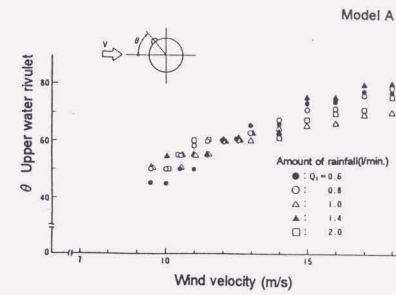
Fig.6.46 Location of upper water rivulets
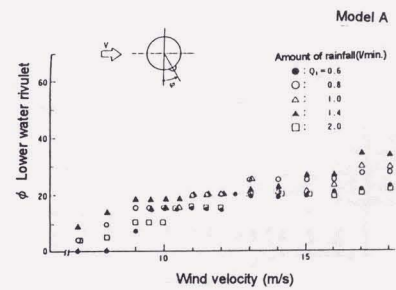
Fig.6.47 Location of lower water rivulets
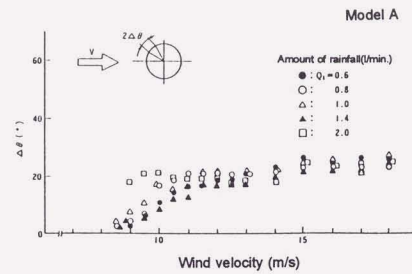
Fig.6.48 Width of upper water rivulets
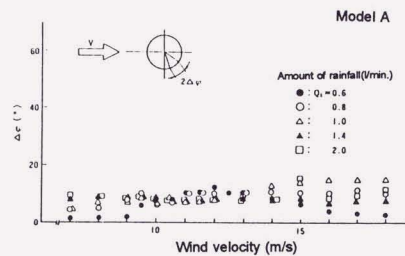
Fig.6.49 Width of lower water rivulets
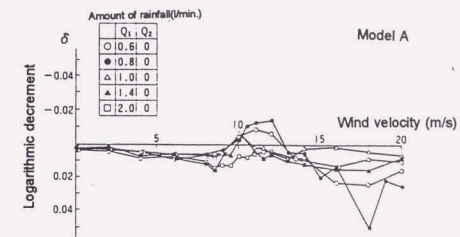
Fig.6.50 Logarithmic decrement of cable model

Table 6.6 Dimensions of cable models

Model	Diameter D (m)	Surface roughness (μm)	Relative surface roughness (k/D)	Remarks
A_1	0.1315	3	2.3×10^{-5}	Smooth
B_1	0.1465	200	1.6×10^{-3}	Grid-like pattern all over the surface
B_2	0.1465	600	4.1×10^{-3}	"
B_3	0.1490	1,200	8.1×10^{-3}	"
C_1	0.140	3	2.1×10^{-5}	Smooth
C_2	0.140	1,500	1.1×10^{-2}	Discrete concave pattern
C_3	0.140	1,500	1.1×10^{-2}	Discrete convex pattern
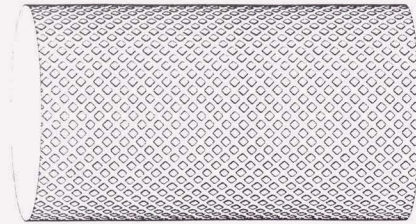
Fig.6.51 Cable model B3
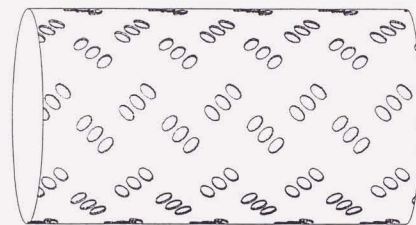
Fig.6.52 Cable model C2
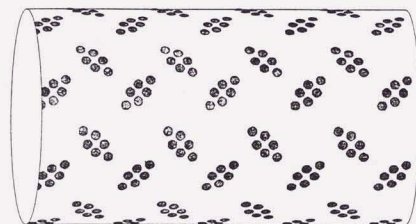
Fig.6.53 Cable model C3
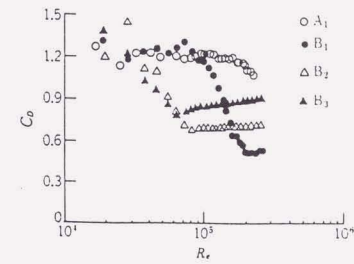
Fig.6.54 Drag coefficient of models B1—B3
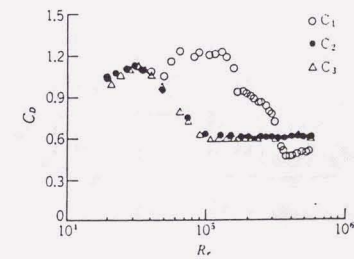
Fig.6.55 Drag coefficient of models C1—C3
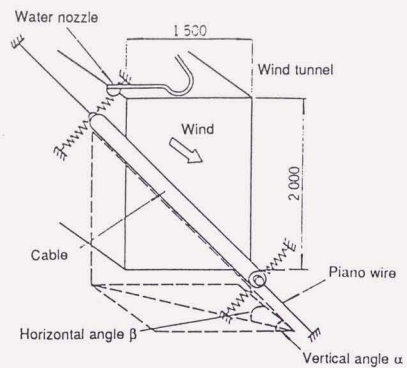
Fig.6.56 Rain vibration experimental apparatus

Fig.6.57 Vibration response characteristics

Table 6.7 Dimensions of cable models

Model	Weight per length (kgf/m)	Frequency (Hz)	Logarithmic decrement δ	Remarks
C_1	6.6	1.8	0.0035	Smooth
C_2	6.6	1.8	0.0039	Discrete concave pattern
C_3	6.6	1.8	0.0032	Discrete convex pattern
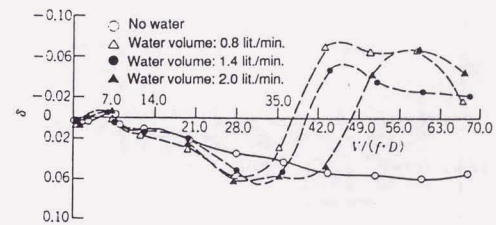
Fig.6.58 Damping characteristics of model C1
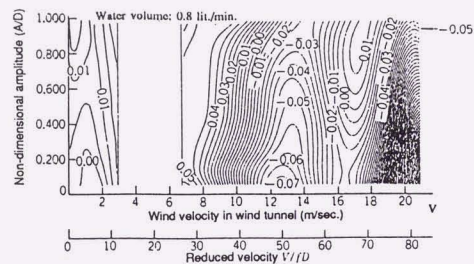
Fig.6.59 V−A− δ curve of model C1

Fig.6.61 Location of water rivulets on upper surface

Fig.6.60 Damping characteristics of models C2 and C3
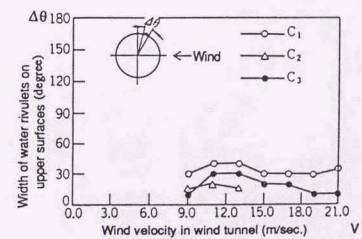
Fig.6.62 Width of water rivulets on upper surface
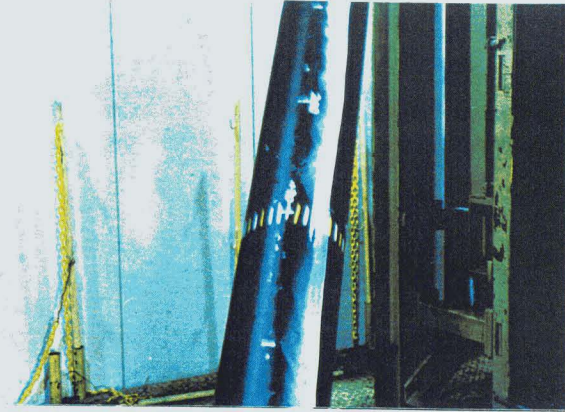
Photo.6.4   Water rivulets on upper surface of model C1

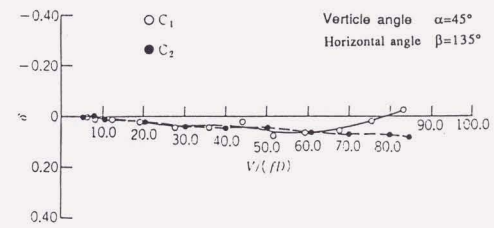Photo.6.5   Water rivulets on upper surface of model C2

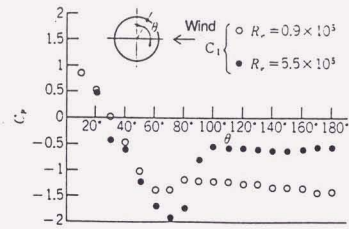Fig.6.63   Damping characteristics of models C1 and C2 (without rain)

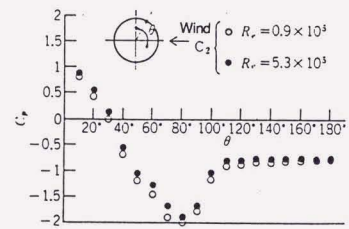Fig.6.64　Pressure distribution of model C1

Fig.6.65　Pressure distribution of model C2

Table 6.8　Analyzed results of surface patterns

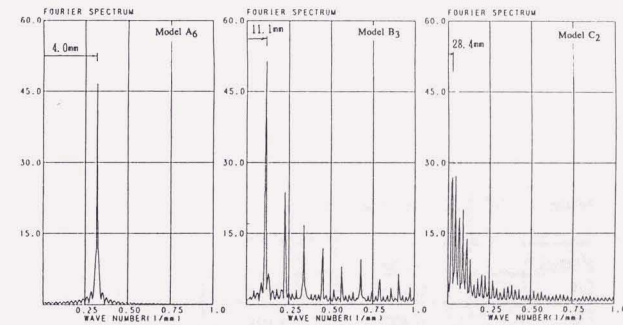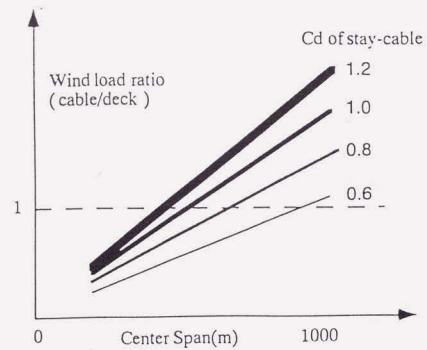| Model number	Relative surface roughness, k/D	Average arithmetic mean deviation of the roughness, R_a (mm)	Wavelength, L (mm)
A_6	1.2×10^{-2}	0.45	4.0
B_3	8.1×10^{-3}	0.41	11.1
C_2	1.1×10^{-2}	0.18	28.4

Fig.6.66　Fourier spectrum of cable surface patterns

Fig.6.67 Relation between span length and wind load ratio

Table 6.9 Dimensions of cable models

Model	Diameter D (m)	Surface roughness(μm)	Relative surface roughness (k/D)	Remarks in roughness
Normal	0.150	3	2×10^{-5}	Smooth
D1	0.150	1500	1×10^{-2}	Lumped
D2	0.150	1500	1×10^{-2}	Lumped
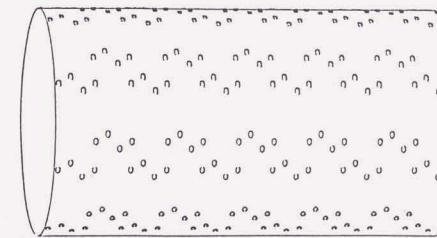
Cable model D1
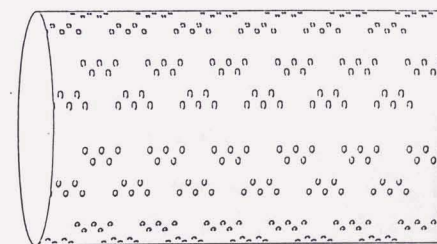
Cable model D2

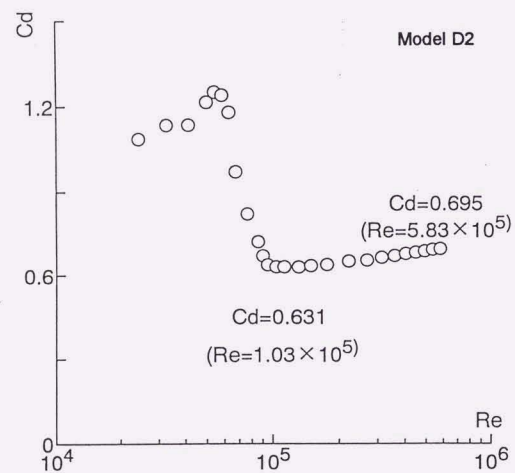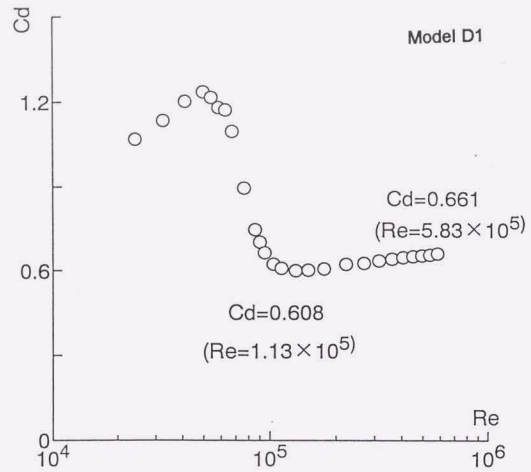Fig.6.68 Two examples of improved models with lumped roughness

Fig.6.69 Drag coefficient of models D1 and D2

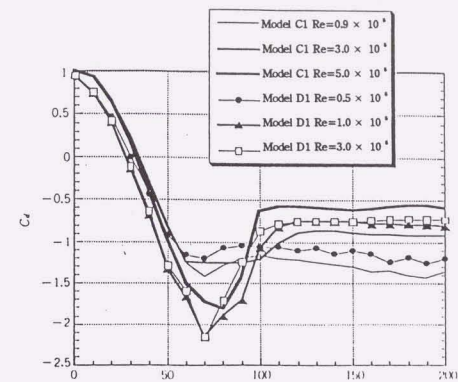Fig.6.70 Pressure distribution of model D1

Table 6.10 Parameters in vibration test

Model	Weight (kg/m)	Frequency (Hz)	Logarithmic decrement	Sc of the experiment
Normal	7.8	0.45-1.25	0.003	almost 2
D1	7.8	0.45-1.25	0.003	almost 2
D2	7.8	0.45-1.25	0.003	almost 2

f =0.45Hz

f =0.73Hz
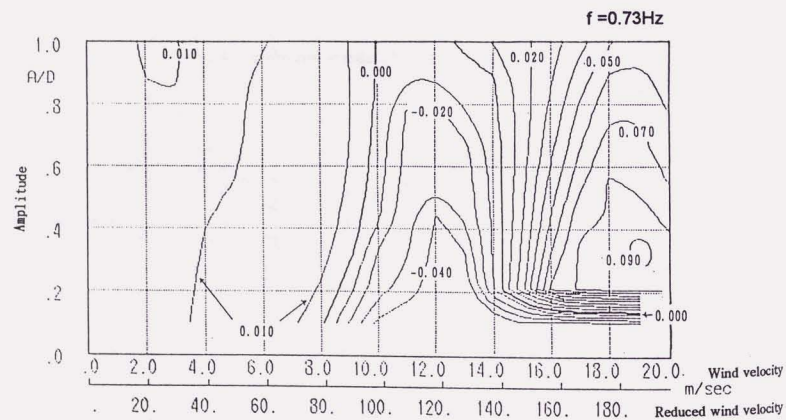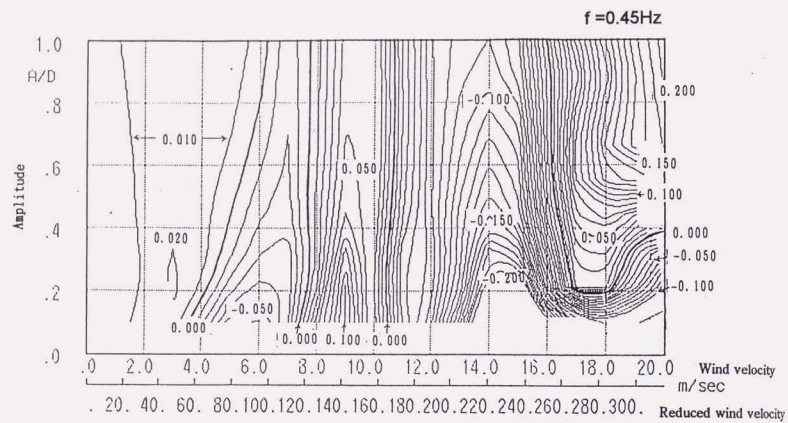
Fig.6.71(1) V－A－ δ curves of normal cable (Sc=2)

f =0.46Hz

f =0.74Hz
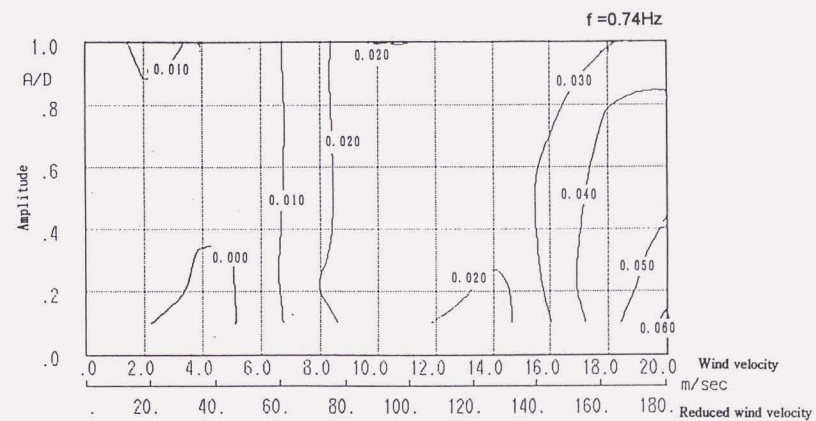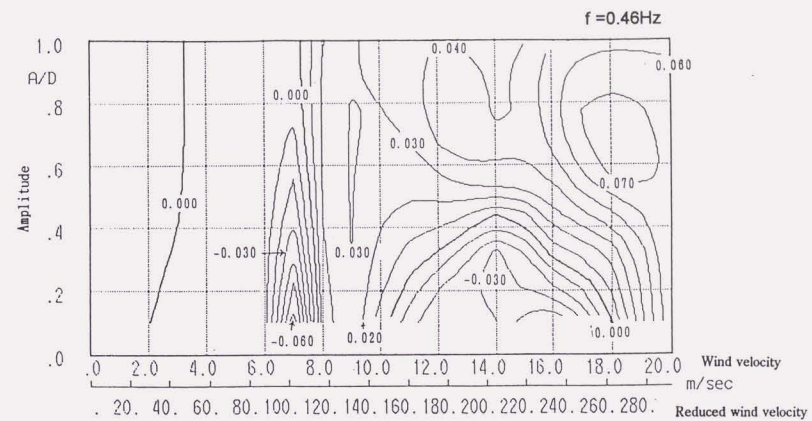
Fig.6.71(2) V－A－ δ curves of model D1 (Sc=2)

f =0.46Hz
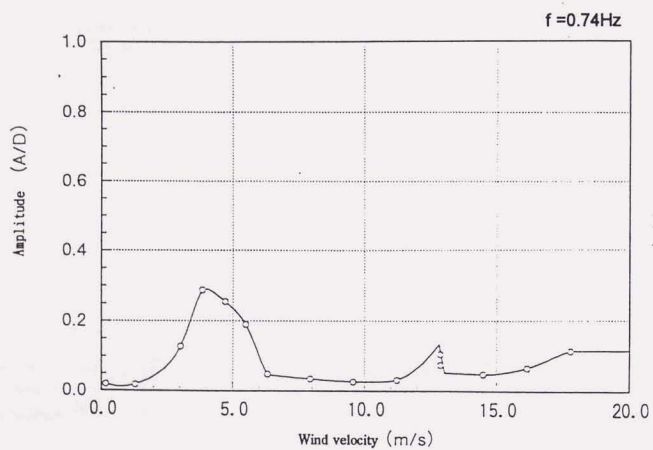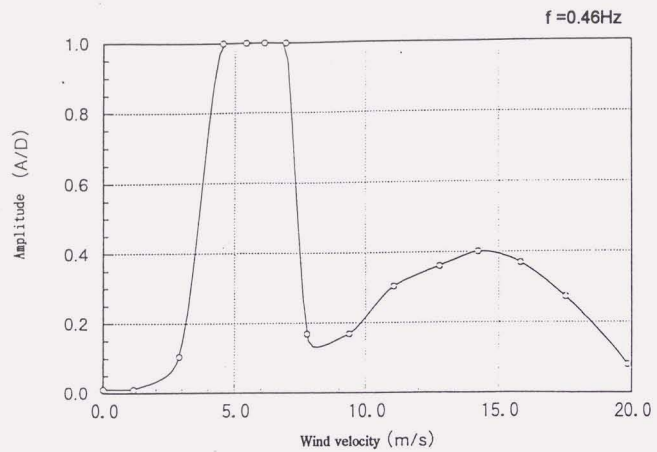
Fig.6.72 Response of model D1 under simulated rainfall(Sc=2)

f =0.74Hz

f =0.43Hz
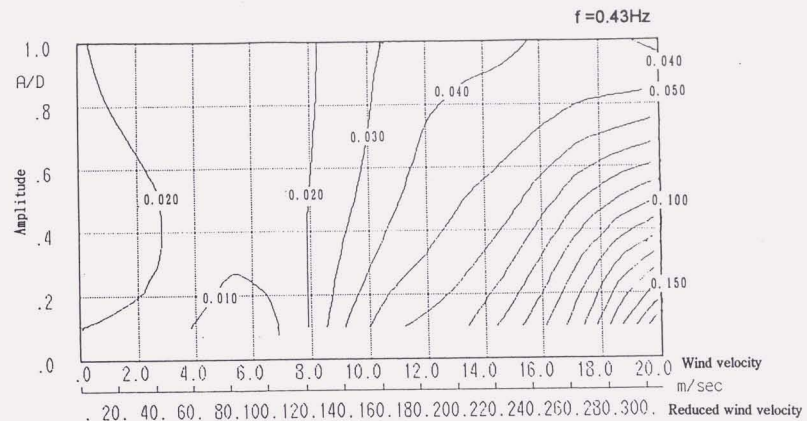
Fig.6.73 V−A− δ curves of model D1 (Sc=21)

f =0.43Hz
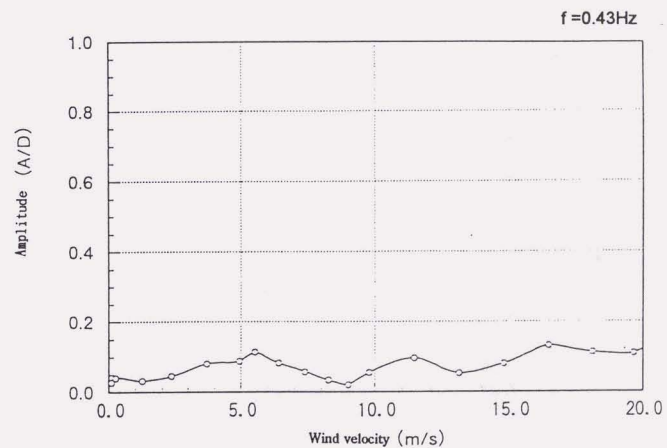
Fig.6.74 Response of model D1 under simulated rainfall (Sc=21)
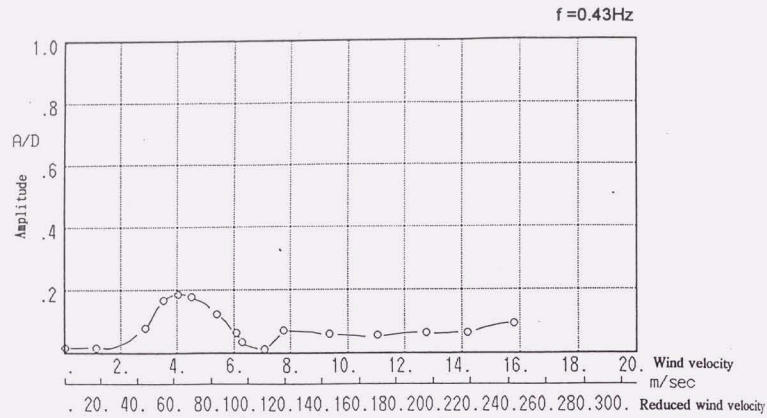
Fig.6.75   Response of model D1 under simulated rainfall in turbulent flow (Sc=21)
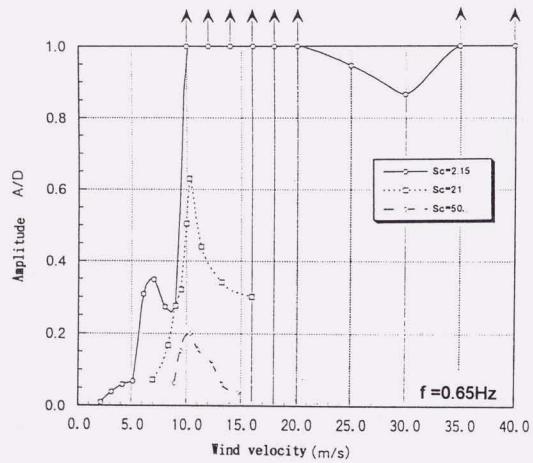
Fig.6.76   Response of model D1 under no-rainfall

* Dots configuration in one lumped roughness

Dense pattern   Medium pattern   Coarse pattern
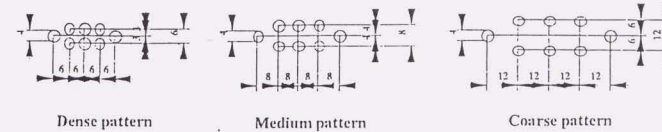
* Arrangemnet of the lumped roughness
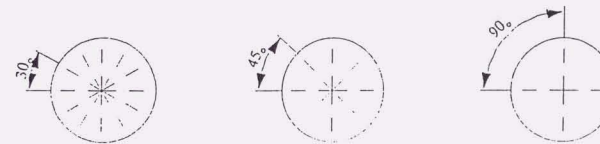
* Pitch of the lumped roughness in longitudinal diretion

     every 100mm and staggered arrangement

Fig.6.77   Configuration of patterned roughness
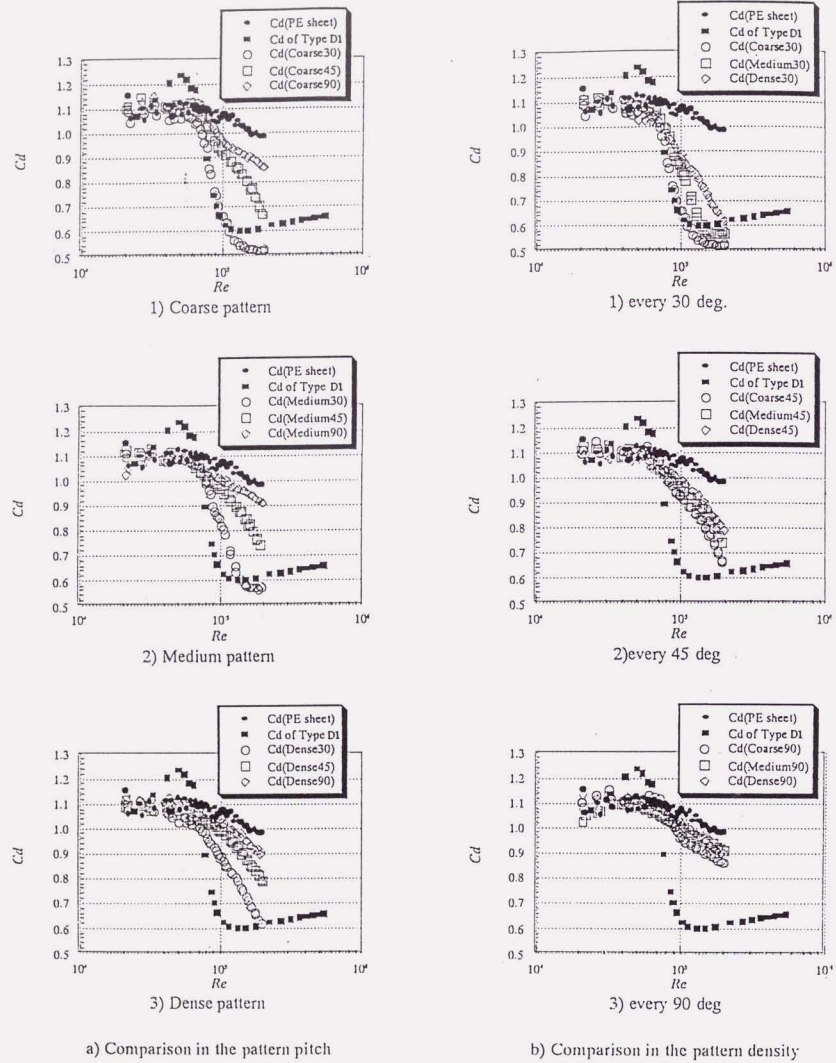
Fig.6.78 Comparison of C_D behavior of patterned roughness
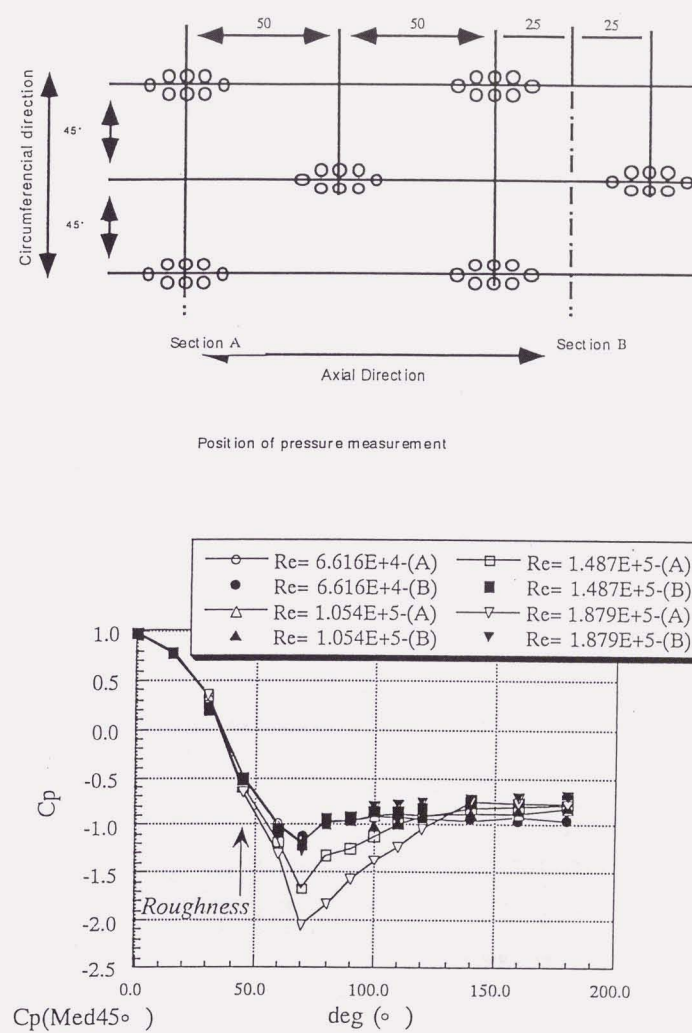
Fig.6.79 Comparison of pressure distribution at two sections
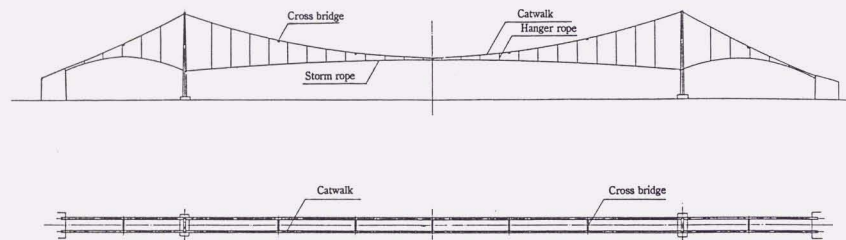
Fig.6.80 General view of catwalk

Table 6.11 Dimensions of test models

| MODEL | DIMENSIONS (mm) | | | SOLIDITY RATIO (%) | |
	WIDTH (b)	HEIGHT (h)	LENGTH (l)	FLOOR ϕ_f	SIDE ϕ_S
I	200	65	1100	47.1	36.5
II	300	65	1100	54.9	38.0
III	400	65	1100	50.6	37.7
IV	400	65	1050	50.5	41.0

Subject area $= h \times l \times y_s$
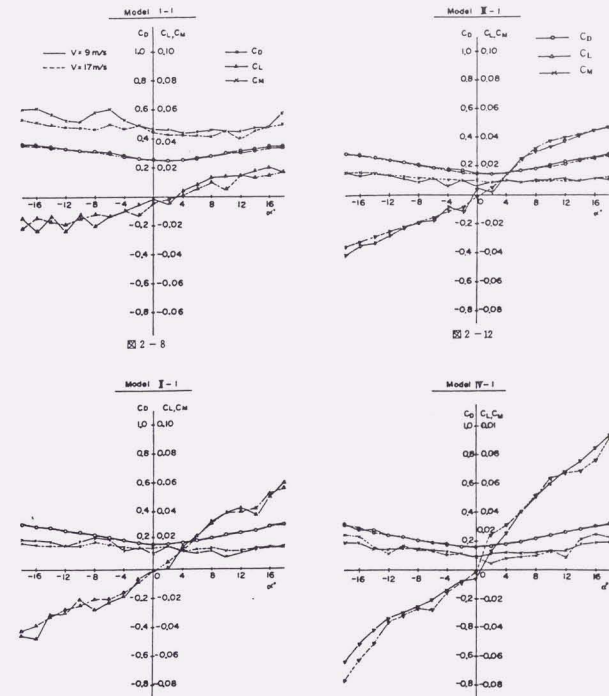
Fig.6.81 Aerodynamic coefficients of catwalk
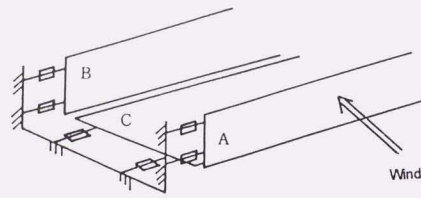
Fig.6.82   Test model of drag force measurement

Table 6.12   Test results of drag force measurement

Model	Surface A	Surface C	Surface B	Overall	B/A	C_w
I	149 (1.26)	47 (0.11)	70 (0.59)	266	0.47	2.25
II	149 (1.26)	62 (0.10)	67 (0.57)	278	0.45	2.34
IV	148 (1.25)	79 (0.09)	66 (0.56)	293	0.45	2.47
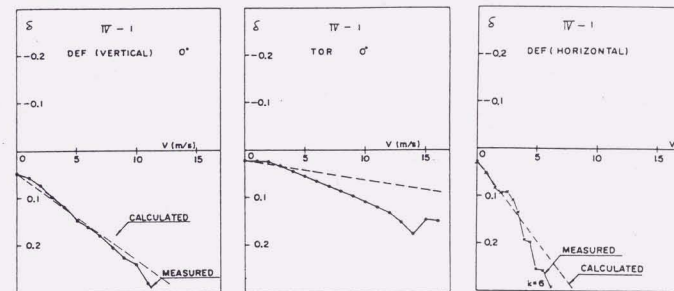
Fig.6.83   Damping characteristics of catwalk

$$0.238 \frac{(556.7 \, f/\bar{U})}{(1+(556.7 \, f/\bar{U})^2)^{5/6}}$$

Power Spectrum

$$0.245 \frac{(471.1 \, f/\bar{U})}{(1+(471.1 \, f/\bar{U})^2)^{5/6}}$$

Power Spectrum

Fig.6.84   Power spectrum of fluctuating wind

Power Spectrum

Fig.6.85   Power spectrum of displacement

Table 6.13 Measurement results of catwalk displacement

AVERAGE WIND SPEED (M/S)	STATIC DEFORMA-TION Z (M)	R.M.S. σ (m)	σ/Z (%)	$\sqrt{u^2}\Big/U$
13.3	1.61	0.134	8.3	6.2
12.9	1.51	0.144	59	7.0
12.8	1.49	0.142	9.5	7.3
12.5	1.39	0.120	8.6	6.4
11.7	1.27	0.105	8.3	12.3
11.4	1.37	0.103	7.5	12.3
11.1	1.38	0.073	5.3	16.4
10.7	1.24	0.063	5.1	10.1
10.5	1.41	0.145	10.3	11.0
10.4	1.22	0.088	6.9	9.5
10.3	1.28	0.178	13.9	13.7
10.1	1.21	0.139	11.5	10.5
9.2	1.21	0.065	5.4	9.5
8.7	0.90	0.089	10.5	14.4
8.2	0.60	0.029	4.8	5.8
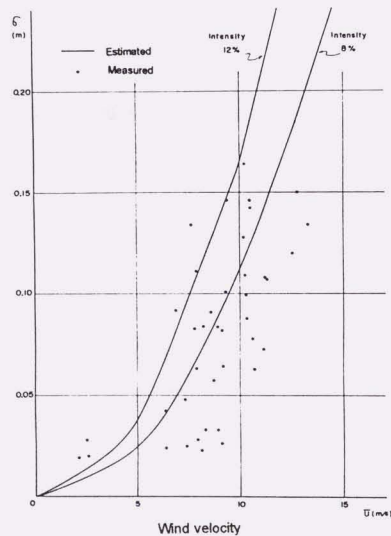
Fig.6.86 Static displacement of catwalk

CHAPTER 7 CABLE MATERIALS FOR A SUPER–LONG CABLE–SUPPORTED BRIDGES

7.1 Introduction

Recently, remarkable progress has been seen in the field of long cable–supported bridges. In Japan, the Akashi Kaikyo Bridge, a suspension bridge having a 1,990 m main span, and the Tatara Bridge, a cable–stayed bridge having a 890 m main span, are now under construction. Further, suspension bridges with a main span of 2,500 m are currently being studied. Overseas projects include suspension bridges at the planning stage which will have a main span of over 3,000 m, such as those planned to cross the Strait of Messina and the Strait of Gibraltar. Lengthening bridge spans are a global trend [1].

As spans increase, the dead load acting on the suspension structure rises. Improved material strength is an effective way to reduce the effect of these rising dead loads, and in this respect the development of cable materials with a super–high tensile strength would be a great advantage.

In this chapter, first the development process of 180 kgf/mm^2 (1,765 MPa) steel wires, which were adopted in the Akashi Kaikyo Bridge, is introduced. Then, the present situation as regards to the strength of various cable materials for suspension bridges is summarized, considering the relationship between suspension bridge span and cable strength. Also problems which will have to be solved are identified.

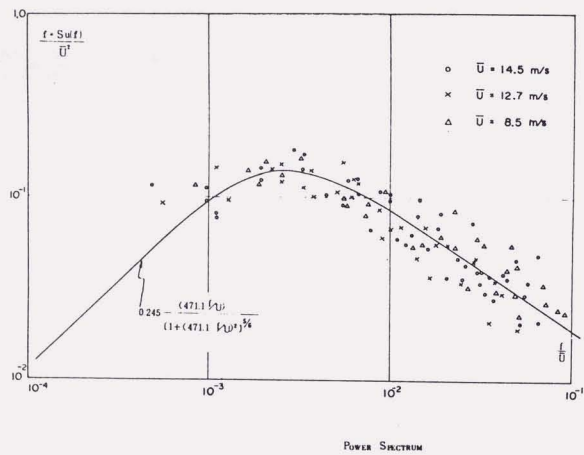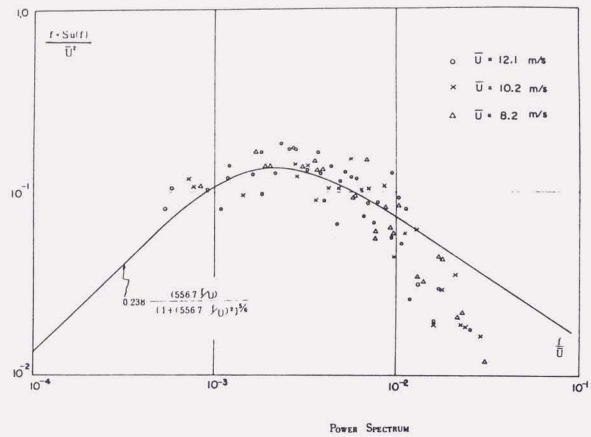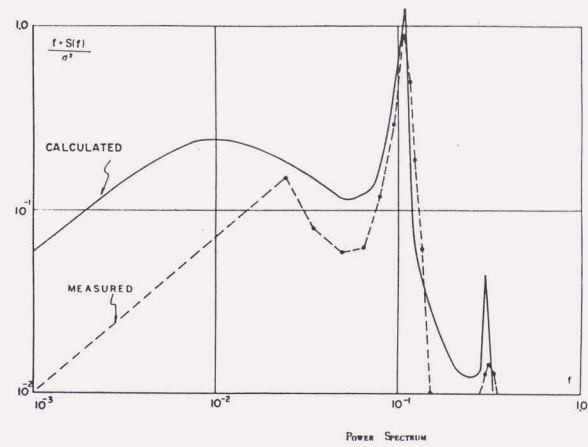## 7.2 Discussion on Cable Materials for Super–Long Suspension Bridges

(1) Development process of 180 kgf/mm^2 steel wire [2,3]

The galvanized steel wire used for bridge cable is given the necessary strength by heat treatment (patenting) using high carbon steel, then it is drawn and finally galvanized, as mentioned in Chapter 2. Three means to increase the strength of galvanized steel wire were considered, namely;

a) Increasing the degree of the drawing process.

b) Adding other elements.

c) Controlling strength loss due to heat reaction.

After examining these measures, it was found that increasing the silicon (Si) content from

conventional $0.12 \sim 0.32$ % to $0.80 \sim 1.00$ %, is effective in raising strength to about 20 kgf//mm^2 (196MPa). Characteristics of high—strength galvanized steel wire are shown in Table 7.1.

Before putting a steel wire of a 180 kgf/mm^2 (1,765 MPa) class into practical use in a suspension bridge cable, the following characteristics should be examined: a) the mechanical properties, b) fatigue, creep, delayed fracture and stress corrosion cracking, c) corrosion resistance, d) effect of side pressure, bending, etc. All these characteristics were investigated by various tests, it was confirmed that a high—strength steel wire (180 kgf/mm^2 class) with a Si low—alloy steel had the equivalent or superior properties to those of a conventional one. About 51,000 tons of the high—strength steel wire have already been produced and installed as parallel strand wires for the Akashi Kaikyo Bridge. In practice, this means that a suitable supply of 180 kgf/mm^2 steel wire is now available in Japan for any purpose.

(2) Suspension bridge span and cable strength

The main cable will have to support greater dead loads as suspension bridge spans increase further. It is important to know what the sectional area of a main cable needs to be in order to support such super—long suspension bridges. Therefore, the effect of increasing the dead load on the main cables was analyzed to estimate the sectional areas required [4]. The effect of improving cable strength was also studied.

Table 7.2 and Fig.7.1 both show the relationship between span length and free—hanging tension due to cable dead load as well as the ratio of free—hanging tension to allowable cable stress. The sag ratios adopted are 1/9, 1/10, and 1/11. These results indicate that as the span length increases, the stress due to the cable dead load increases and accounts for a larger proportion of allowable cable stress. This means that the cable has less capacity to carry the live or dead loads imposed by structural members other than the main cable itself as the span length increases.

Assuming that both the dead and live loads imposed by suspended structural members other than the main cables are constant regardless of span length, the relationship between span length and the required cable sectional area is shown in Fig.7.2. The cable strength and sag ratio used in this calculation are 180 to 220 kgf/mm^2 (1,765 to 2,156 MPa) and 1/10, respectively. The figure indicates that with a span length over 3,000 or 4,000 m, the required cable area increases rapidly. Considering that the largest practical cable diameter is currently about 1.2 m due to limitation of workability, such as problems of squeeze, the required number of cables per bridge can be calculated by assuming a cable diameter of 1.2 m. The

relationship between center span length and required number of cables is shown in Table 7.3. For a steel wire with a tensile strength in the 180 kgf/mm^2 (1,765 MPa) class, four or more cables per one side will be necessary for a bridge with a span of over 4,000 m.

This means that as suspension bridge spans increase further, it will be necessary to a) develop a steel wire of much higher tensile strength or a new materials offering high strength and lower dead weight, and b) reduce the dead load imposed by suspended structural sections of the stiffening girder. Making breakthroughs in these two factors are the key to the feasibility of super—long suspension bridges.

If spans reach 5,000 m, four cables will be required per one side even if a 220 kgf/mm^2 (2,156 MPa) steel wire is used. This means that innovations not only in materials but also in the area of design and construction are required.

7.3 Cable Materials in Future

Future super—long suspension bridges are going to require steel wire with a tensile strength greater than the 180 kgf/mm^2 material used for the Akashi Kaikyo Bridge. In addition to the steel material, the so—called "new materials" offer promising possibilities for high—strength materials applicable to suspension bridge cables. The steel wires and new materials currently being developed or studied are summarized below to help clarify the problems which will have to be solved in the future.

(1) Super—high tensile strength steel wire

Certain materials which have been classified as a super—high tensile strength steel wire have already reached strength of 200 to 300 kgf/mm^2 (1,960 to 2,940 MPa). These have been designed for limited applications, such as steel wire for ropes and reinforcing wires for transmission lines (ACSR), as shown in Table 6.4. However, all of these are less than 3 mm in diameter. The strongest 5 mm galvanized steel wire suitable for suspension bridge cables is the recently attained 180 kgf/mm^2, and stronger versions of this type of material are yet to reach commercialization. For a steel wire of less than 5 mm in diameter, recent technological developments, including an improved patenting process and controlling strength loss during galvanization, have led to prototype steel wires of the 200 kgf/mm^2 (1,960 MPa) level at around 4.5 mm in diameter. In fact, this material was used for the catwalk rope of the Akashi Kaikyo Bridge. A 200 kgf/mm^2 class galvanized steel wire for use in suspension bridge cables has almost reached commercialization.

Beyond this, the commercialization of a super—high tensile strength steel wire will require further studies on the basic characteristics of steel wire and the technology for producing it [5]. Delayed fracture is expected to be one of the major issues to concentrate on. Improvements in cable strength are usually accompanied by a reduction in sectional area. This has the following effects; a) increasing susceptibility to rusting, so requiring more effective corrosion protection than previously, and b) causing a reduction in the longitudinal rigidity of the cable, changing the deformation characteristics of a suspension bridge. Therefore, greater attention to both structural design and durability will be required.

(2) Cables made of new materials

Increases in suspension bridge spans can effectively be facilitated either by enhancing material strength or by reducing the cable weight. One popular subject of research and development in this respect is the investigation of composite materials consisting of carbon fibers, aramid fibers and glass fibers (or fiber—reinforced plastic; FRP) [6]. As is apparent from the characteristics of the fibers given in Table 7.4, these materials offer a high tensile strength and elasticity for their weight. The fibers themselves are quite small, 5 to 20 microns in diameter, and are usually bound with epoxy resin or a similar material and hardened into a wire. For this reason, FRP cables have much poorer quality characteristics than the original pure fiber. It is difficult to generalize the strength characteristics of FRP cables, since they depend on the type of fiber, the binder, the fiber ratio, and the sectional shape, etc. For now, the range of tensile strengths and moduli of elasticity achievable with FRP cables is 50 to 200 kgf/mm ^{2} (490 to 1,960 MPa), and 3,000 to 15,000 kgf/mm ^{2} (29 to 147 GPa), respectively.

A carbon fiber cable that has successfully been brought to the commercialization stage was used as the basis of a calculation to clarify the relationship between span length and required cable section, as shown in Fig.7.3. In this calculation, the cable strength was 180 kgf/mm ^{2} (1,765 MPa). Other conditions were the same as described in previous calculations. The figure indicates that the weight of the cable and its tensile strength both have as much effect on increasing suspension bridge span.

There are many problems to be solved before they can actually be applied to long span suspension bridges, because there is a shortage of data regarding the use of such new materials as construction materials. It includes the following problems;

a) Innovative structures for saddles and hanger clamps have to be developed, since the bending and shear strength of these materials are so low compared with their tensile strength.

b) New design methods will be required, because elongation at the time of fracture is about 1%, less than that of a steel wire.

c) New materials are generally more susceptible to external damage and heat.

d) There have not been sufficient studies of their long—term durability.

It is hoped that these problems will be overcome. It is clear from this overview that materials with improved strength and reduced weight are essential to the realization of super—long suspension bridges [7]. Future studies in this field will have to be multi—faced investigations of materials, structural issues such as wind resistance, and other matters related to construction methods.

7.4 References

[1] T.Hojo and M.Akiyama, Cable Materials for Super—Long Suspension Bridges, Proc. of Workshop on Super Long Span Bridges, International Engineering Consultants Association, Tokyo, 1994, pp.52—57.

[2] Honshu—Shikoku Bridge Authority, Technical Report on Development of High—Strength Galvanized Wire (180 kg/mm ^{2}) for Bridge Cable * , 1988, pp.6—20.

[3] T.Takahashi, S.Konno, H.Sato, I.Ochiai, Y.Noguchi, O.Serikawa and Y.Tawaraya, Development of High—Strength Galvanized Wire * , Seitetsu Kenkyu, No.332, 1989, pp.53—58.

[4] T.Mitamura, H.Nakai, E.Watanabe and K.Sugii, Recent Topics on Bridge Cables and Future Prospects * , Proc. of JSCE, No.444, VI —16, 1992, pp.97—106.

[5] T.Takahashi, S.Ohashi, T.Tarui and Y.Asano, Mechanism of Delamination Cracking in Ultra—High Tensile Strength Wire, Shin—Nittetsu Gihou * , No.347, 1992, pp.22—26.

[6] Japan Society of Civil Engineers, Application of Continuous Fiber—Reinforced Materials to Concrete Structures * , 1992.

[7] J.Tajima, Development of the Cable Material and Suspended Bridges, Kawada Technical Report * , Vol.6, 1987, pp.5—8.

* Published in Japanese

Table 7.1   Characteristics of galvanized steel wire

Item	1569 MPa Grade	1765 MPa Grade
Chemical composition of steels		
C (%)	0.75 ~ 0.80	0.80 ~ 0.85
Si (%)	0.12 ~ 0.32	0.80 ~ 1.00
Mn (%)	0.60 ~ 0.90	0.60 ~ 0.90
Mechanical properties		
Tensile Strength(MPa)	1569 ~ 1765	1765 ~ 1961
0.7% Proof Strength(MPa)	≥ 1158	≥ 1378 *
Elongation (%)	≥ 4	≥ 4
Wrapping Test	Good	Good
Torsion Test(Turns)	≥ 14	≥ 14
Plating properties		
Weight of Plating(g/m²)	≥ 300	≥ 300
Appearance	Good	Good
Die. of Freeing Coil(m)	≥ 4	≥ 4

* 0.8% Proof Strength

Table 7.2   Ratio of cable free—hanging stress to cable allowable stress

Ratio of sag S span	Length of center span	Stress of freehung cable		Ratio of cabel freehung stress S cable allowable stress %		
I/L	m	kgf/mm2	(MPa)	1765MPa Grade	1960MPa Grade	2156MPa Grade
1/9	5,000	49.2	(483)	60%	55%	49%
	4,000	39.4	(386)	48%	44%	39%
	3,000	29.5	(290)	36%	33%	30%
	2,000	19.7	(193)	24%	22%	20%
1/10	5,000	53.6	(526)	65%	60%	54%
	4,000	42.9	(421)	52%	48%	43%
	3,000	32.2	(315)	39%	36%	32%
	2,000	21.5	(210)	26%	24%	22%
1/11	5,000	58.1	(570)	71%	65%	58%
	4,000	46.5	(456)	57%	52%	47%
	3,000	34.9	(342)	43%	39%	35%
	2,000	23.3	(228)	28%	26%	23%

Safety Facter : 2.2
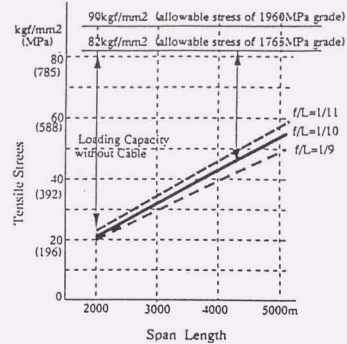
Fig.7.1 Loading capacity without cable
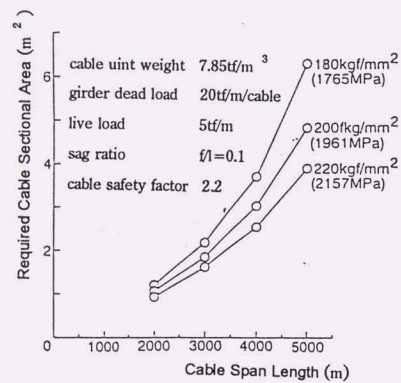
Fig.7.2 Cable strength and required cable sectional area

Table 7.3 Center span length and required number of cable

	2.000m	3.000m	4.000m	5.000m
180kgf/mm² Grade (1765MPa)	2	4	8	12
200kgf/mm² Grade (1960MPa)	2	4	6	10
220kgf/mm² Grade (2156MPa)	2	4	6	8

Table 7.4 Present status of steel wire strength

	Type	Diameter (mm)	Strength (kgf/mm²)
Small diameter (1mm or less)	Steel cord	0.2	340
	Hose wire	0.6	290
Medium diameter (1 to 4mm)	ACSR wire	2.4	200
	Rope (galvanized)	2.5	200
	Rope (exposed)	2.5	210
Large diameter (5 to 7mm)	PWS wire	5.0	180
	PWS wire	7.0	160
	PC strand	5.1	190

1 kgf/mm² = 9.807 MPa

Table 7.5 Characteristics of fiber materials

Type of Fiber	Tensile Strength kgf/mm²	Elastic Modulus kgf/mm²	Elongation %	Density g/cm³
Carbon fiber (Pan)	300 ～ 400	20,000 ～ 35,000	1.3 ～ 1.8	1.8 ～ 2.0
Carbon fiber (Pitch)	200 ～ 350	20,000 ～ 80,000	0.4 ～ 1.5	1.9 ～ 2.1
Aramid	280 ～ 350	7,400 ～ 17,000	2.0 ～ 4.5	1.4 ～ 1.5
Glass	180 ～ 450	7,000 ～ 7,600	2.0 ～ 5.0	2.3 ～ 2.6
Steel wire	180 ＊	20,000	4	7.85

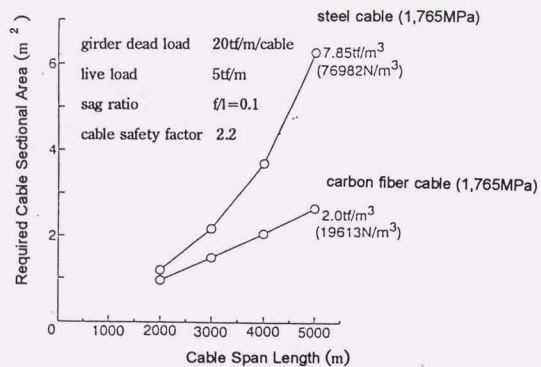＊ 160 to 340 as a material

1 kgf/mm ' = 9.807 MPa

Fig.7.3 Cable weight and required cable sectional area

CHAPTER 8 SUMMARY AND CONCLUSIONS

This thesis described the study on fundamental development of a pre—coated parallel wire cable, and application subjects for higher performance, such as a colored cable or a low drag aerodynamically stable cable. In this chapter, the results obtained by each chapter are summarized in order, and concluding remarks are mentioned.

In Chapter 1, the progress in cables for cable—supported bridges and types of cables particularly used in cable—stayed bridges were introduced. It was pointed out that the development of a new—type cable was essentially required to make progress in cable—stayed bridges. Problems caused by elongating the span of cable—stayed bridges and by applying cables to some bridges were analyzed and classified into five main subjects; a large—sized fabricated cable, higher static and fatigue strength for a cable socket, corrosion—protective coat for a cable, coloring a cable, and aerodynamic measures against cable vibration. Finally, the purpose and scope of the study was mentioned.

In Chapter 2, the basic static characteristics of a newly developed pre—coated parallel wire cable were discussed based on the experimental studies. The wires of the cable were given a slight twist at a pitch designed to maintain the optimum tensile strength and the modulus of elasticity. From the experimental analysis, it was indicated that the cable had the same static characteristics as those of a parallel wire strand when the twisting angle of a cable was less than 3.5°. The influence of the twisting angle on the time dependent characteristics, such as creep and relaxation of the pre—coated parallel wire cable, was investigated. It was shown that the twisting angle had little effect on the time dependent characteristics when the twisting angle of a cable was less than 3.5°. Finally, the tensile test was carried out by using full—size cable models and it was confirmed that a pre—coated parallel wire cable with a breaking load of a 3,000 tonf (29,400 kN) class could be put into practical use.

In Chapter 3, the experimental studies on the development of the socket for the cable were discussed. First, the mechanical properties of large sockets filled with zinc—copper alloy were studied based on the results of tensile tests and analysis. A new method in socket design for a large cable, introducing the concept of rigidity for ultimate strength, was investigated. Then, fatigue strength and bending fatigue strength of the newly developed socket were studied. In this study, the socket casted by zinc—copper alloy and epoxy resin

was developed in order to improve fatigue resistance of a socket, and it was shown that it had a higher fatigue strength of about 25 kgf/mm^2 (245 MPa). Tensile fatigue tests were also carried out by using cables twisted by several different angles. It was confirmed that the twisting angle had no effect on the fatigue strength of the socket when the twisting angle of a cable was less than 3.5°. Next, bending fatigue tests were carried out relating to a bending angle to examine the bending fatigue strength that the cable possessed. Experimental results and analysis indicated that the pre—coated parallel wire cable with the sockets had a bending fatigue strength of about 0.6° and the socket using epoxy resin also had an effect on decreasing the secondary stress at the entrance of a socket.

In Chapter 4, studies on corrosion protective layer, which is an important component to maintain the durability of the cable, were discussed. An extrusion process was applied directly to the bundled cable in the manufacturing plant, which eliminated the need for corrosion protective coating work at the site. A high—density polyethylene was selected as the optimum protective coating material. According to the accelerated weathering test results, it was confirmed that the polyethylene showed no deterioration when 1% carbon black was added. Its' mechanical properties and many other characteristics were studied. The properties of a polyethylene coated cable were analyzed, and installation characteristics of the cable such as unreeling and clamping were examined using full—size cable models. It was indicated that this protection system was a great advantage in the erection of stay cables of cable—stayed bridges, especially long ones.

In Chapter 5, the development of a colored cable (shop—coloring a black cable by covering with a colored fluoropolymer) was indicated. The material properties of the fluoropolymer, especially the weathering durability, were investigated by using various weathering test methods. It became obvious that the fluoropolymer had excellent weathering durability, which could be estimated to last for more than 100 years if the thickness were 1 mm or more. It was also confirmed that a colored fluoropolymer had excellent weathering resistance ability with regard to color change and gloss retention. Structural characteristics of the fluoropolymer—coated cable were examined, and it was indicated that the cable had the same installation properties as those of a polyethylene—coated cable. These characteristics of the fluoropolymer showed that it could be used for various structures, elongated service life and added aesthetic aspects. Finally, it was shown that the colored cable was applied not only to a stay cable of long cable—stayed bridges but also to hangers of long suspension bridges.

In Chapter 6, the vibration problems of a stay cable were surveyed and experimental studies on cable vibration and its suppressing method for a long cable—stayed bridge were discussed. First, the past works on cable aerodynamics were briefly reviewed. Responses of stay cables by vortex—induced vibration in natural wind were measured at an actual cable—stayed bridge with a main span of 490 m. The factors affecting this vibration such as surface roughness and structural damping were examined by using a wind tunnel test and analysis. It was shown that the response amplitude could be estimated at various damping levels, and that the bending angle of a cable caused by vortex—induced vibration was less than 0.1°, which had little effect on the secondary stress and bending fatigue strength of cables.

Next, aerodynamic measures for a stay cable against rain vibration were investigated using wind tunnel tests. First, it was pointed out that development of not only aerodynamically stable but also low drag cable was of great importance for a super—long cable—stayed bridge.

Various experiments on rain vibration of cables with a surface roughness were carried out and the suppressing effect of the surface—roughened cable was discussed. It was found that a cable with a surface roughness had a vibration suppressing effect when the relative surface roughness of 1% of the cable diameter was given discretely on the surface. It was also indicated that the drag coefficient of the cable with a discretely roughened surface was lower than that of cables with the same degree of uniform surface roughness at a design wind velocity range. Measurement of the pressure distribution showed that cables with a lumped pattern roughness made it possible to reproduce a supercritical state for a low wind velocity range where rain vibration occurred.

Based on the results, a new aerodynamic measured cable with indented pattern, having both a low drag force and suppression effects on rain vibration, was developed. To understand further the aerodynamic characteristics of the surface configuration of the cable, various patterned roughnesses were examined in terms of the Reynolds Numbers. It was found that density and arrangement of lumped roughness were the key factors in controlling the drag characteristics of cables and that optimization of the drag coefficient—Reynolds number relationship could enable adjusting those two factors.

In Chapter 7, cable materials in the future for a super—long cable supported bridge were described. It was shown that the development of cable material was inevitable in order to lengthen a bridge span. The present status of cable materials including steel wire and various new materials was surveyed and future problems to overcome were pointed out. As a future prospect, a high strength steel material and a light weight material such as carbon fiber were shown to be possible for use in super—long cable supported bridges.

In Chapter 8, the results of this study are summarized.

The study mentioned above showed that the development of the pre−coated parallel wire cable was essential in the improvement of a long cable−stayed bridge. In the developmental process of the new−type cable, basic characteristics relating to material and structure were investigated and valuable data for the design of a cable−stayed bridge were acquired. In addition to the development of the new−type cable, further investigations were carried out to give a higher−performance ability to the cable. Through the development of a colored cable, a greater freedom of color selection was given to bridge cables that matched the surrounding environment. And a new aerodynamically measured cable having both a low drag force and a suppressing effect on rain vibration was developed, thus making it possible to lengthen cable−stayed bridge spans. Various technical problems of a cable for large cable−supported structures have been solved by this study. As a result, the pre−coated parallel wire cable was applied to many cable−supported bridges, such as the Yokohama Bay Bridge, the Meiko−Central Bridge, the Tatara Bridge and the Akashi Kaikyo Bridge.

Bridge cables are usually required to maintain initial structural performance for a long period. However, damages have been seen in stay cables of some cable−stayed bridges constructed recently. It is quite necessary to examine the structural performance of time dependent properties, such as fatigue strength or weathering durability. A non−destructive inspection system for mechanical properties or deterioration of materials is considered to be one of the effective ways to diagnose the durability of the cables.

As for wind resistant problems, suppression effects have not been investigated in actual bridges but in the wind tunnel tests. Therefore, observations of cable behavior in actual bridges are essential to estimate suppressing effects. The relationship between the results of wind tunnel tests and those of observations in actual bridges is a further study to be examined. Accumulation of observation data could make it possible to make a step forward in wind resistant design of large cable−supported structures. New material cables having high performances, including super high strength steel wires or carbon fibers, are also expected to be studied further in order to be applied to large cable−supported structures.

The author firmly believes that this study has contributed a great deal to the advancement of cable−supported structures.